Probabilistic fracture mechanics by boundary element method

by

Xiyong Huang

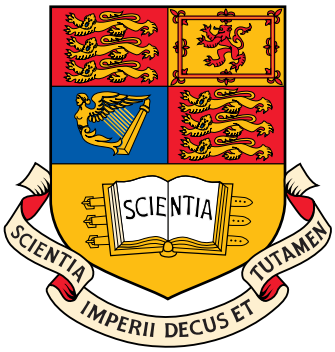

Department of Aeronautics
Imperial College London
London SW7 2AZ
U.K.

This thesis is submitted for the degree of Doctor of Philosophy of the Imperial College London

2010

Acknowledgments

First and foremost I would like to thank my supervisor Prof. Ferri M.H.Aliabadi for his excellent scientific guidance throughout this research in which I learned to share his scientific passion and ideology. Thank you Ferri, for you always understanding what I meant even when I was not able to phrase it.

A special thanks to Dr. P.M.Baiz for teaching me several cool programming tricks and helping me with the numerous technical obstacles I encountered during this eventful journey. I had enjoyed the friendship of colleagues like Silvestre, Sid, Vicky, Supriyono, George, Alessandro, Koen, Albert, Luis, Vincenzo, thank you for the laughter and fun experiences we've shared. And more recently Zahra, Luyun, Omar, Ivano, Miguel, thanks for reminding me to have a sense of humor about my work. As well as of those people of Imperial College with whom i enjoyed numerous football games. In addition, I have lucky enough to have the support of many good friends. Life would not have been the same without them, i'll always remember those memorable time we spent together. I wish I could mention each individually, but will throw a large party instead.

I want to thank my parents Muli Zhuang and Mouyuan Huang, and my brother Guohui Huang for all their love and continuously supporting me throughout my life. Thanks also to my parents in-law for their encouragement and support throughout the duration of my research. I must mention my dear grandpa, Jianxiang Huang and my uncle, Moushun Huang, whose presence always my inspiration.

Very special thanks to my wife Shanhong Wu for showing me the beauty and opposite side of life and making my mind relax during the hard times of my research. My thanks to my two children, Lili and Yongyu, who joined us during my research, for giving me unlimited happiness and pleasure.

Abstract

In this work, a new boundary element method is presented for the Probabilistic Fracture Mechanics analysis. The method developed allows the probabilistic analysis of cracked structure accomplished by the dual boundary element method (DBEM), in which the traction integral equation is used on one of the crack faces as opposed to the usual displacement integral equation. The stress intensity factors and their first order derivatives are evaluated for mode-I and mixed-mode fracture problems.

A new boundary element formulation is derived and implemented to evaluate the design variables sensitivities. This method involves the solution of matrix systems formed by the direct differentiation of the discretised dual boundary element equations with respect to the each random parameter. The derivatives of fracture parameters with respect to design variables are calculated using implicit differentiation method (IDM) in DBEM for mode-I and mixed-mode fracture problems. The gradient of performance function is determined analytically and the total derivative method (TDM) is used in probabilistic fatigue crack growth problems. The randomness in the geometry, material property and the applied stress are considered in 2-D fracture problems; while initial crack size, final crack size, material property and applied stress are considered in fatigue crack growth. Uncertainties in other aspects of the problem can be included. First-Order Reliability Method (FORM) is used for predicting the reliability of cracked structures. The Hasofer–Lind–Rackwitz–Fiessler algorithm is used to find the most probable point, referred as reliability index.

Finally, the validation and applications of the stochastic boundary element coupled with FORM are presented. Numerical calculations are shown to be in good agreement either with the analytical solution or Monte Carlo Simulation.

Contents

Abstract **i**

List of Figures **vi**

List of Tables **xii**

Nomenclature **xiii**

1 Introduction **1**

1.1 General 1

1.2 The boundary element method 4

1.3 Overview of the thesis 8

2 Fundamental concepts in probabilistic structural analysis **11**

2.1 Introduction 11

2.2 Basic approach 13

2.3 Statistically characterized design variables 14

2.3.1 Continuous random variables 14

2.3.2 Discrete random variables 25

2.4 Probabilistic analysis methods 30

2.4.1 Integration 31

2.4.2 Monte Carlo Simulation 32

2.4.3 Limit state approximation 36
2.5 Summary 39

3 The dual boundary element method 41
3.1 Introduction 41
3.2 The boundary element method for elastostatics 42
3.2.1 Basic equations of elasticity 42
3.2.2 Formulation of the internal displacement integral equation 43
3.2.3 The displacement boundary integral equation 48
3.2.4 Formulation of the dual boundary integral equations . . . 50
3.2.5 Dual boundary integral equations 51
3.3 Numerical implementation in two dimensions 58
3.3.1 Boundary elements 58
3.3.2 Discretised equations 62
3.3.3 Implementation of the dual boundary element method . . 63
3.3.4 Rigid body condition 65
3.3.5 Analytical integration of crack elements 66
3.4 Fracture mechanics 69
3.5 Fatigue crack growth 76
3.6 Summary 78

4 Boundary element method for stochastic elastostatics problems 79
4.1 Introduction 79
4.2 Formulations of derivative boundary integral equations 81
4.2.1 Derivatives of fundamental solutions 86
4.3 Accuracy of sensitivity analysis 90
4.4 Reliability analysis 91

4.4.1 Random variables and response 91
4.4.2 Reliability analysis by FORM 91
4.4.3 Analytical sensitivities 92
4.5 Examples: 94
4.5.1 Cylinder under external pressure 94
4.5.2 Plate with a hole under tension 105
4.6 Summary 113

5 Stochastic dual boundary element method for LEFM 114

5.1 Introduction 114
5.2 Boundary integral formulations for displacement and traction derivatives 116
5.2.1 Derivative of fundamental solutions 118
5.2.2 Analytic integration 119
5.3 Derivatives of stress intensity factor 128
5.4 Analytical gradient for LEFM 132
5.5 Examples 135
5.5.1 Sensitivity analysis of centre crack specimen 135
5.5.2 Sensitivity analysis of single edge crack specimen 140
5.5.3 Sensitivity analysis of Mixed-mode problem 145
5.5.4 Reliability analysis of double edge crack specimen 151
5.6 Summary 159

6 Stochastic dual boundary element method for fatigue crack growth 160

6.1 Introduction 160
6.2 Stochastic process in fatigue crack growth 162
6.2.1 Random parameters in fatigue crack growth 163

6.2.2 Randomness of crack propagation 163
6.3 Formulation of fatigue crack growth reliability 165
6.3.1 Explicit expressions for derivatives of the crack growth law 165
6.3.2 Approximation formula for fatigue life and its derivative . 168
6.4 Analytical gradient for fatigue crack growth 169
6.5 Examples 171
6.5.1 Fatigue crack growth reliability analysis of double edge crack specimen 171
6.5.2 Fatigue crack growth reliability analysis of single edge crack specimen 186
6.6 Summary 195

7 Conclusions and future research 196
7.1 Introduction 196
7.2 Summary and Conclusions 196
7.3 Future research 199

Bibliography 201

A Table of the CDF of the standard normal distribution 214

B Rosenblatt Transformation 217

C Treatment of singularity 221
C.1 Weakly singular integration 221
C.2 Strong singular integration 222
C.3 Hyper singular integration 223

List of Figures

2.1 Fundamental of failure evaluation 13

2.2 PDF and CDF of a random variable 15

2.3 PDF of normal random variable 17

2.4 PDF of Lognormal random variable 18

2.5 PDF of Beta random variable 20

2.6 PDF of uniform distribution 21

2.7 PDF of Type-I Extreme Value Distribution 22

2.8 PDF of Type-II Extreme Value Distribution 24

2.9 PDF of three parameter Weibull random variable 25

2.10 PDF of two parameter Weibull random variable 26

2.11 PDF of Binomial random variable 27

2.12 PDF of Poisson random variable 29

2.13 PDF of Exponential random variable 30

2.14 Limit state concept 31

2.15 Generating random numbers 34

2.16 Linear performance function 37

2.17 Nonlinear performance function 38

3.1 Boundary condition for elastostatics analysis 44

3.2 Components of the distance and normal vector 47

3.3 The augmented boundary at the source node 48
3.4 The augmented boundaries on the crack faces 52
3.5 Boundary elements and internal points 59
3.6 Type of quadratic boundary elements 60
3.7 Crack modelling with discontinuous quadratic boundary elements 64
3.8 Straight boundary elements 66
3.9 Crack deformation modes 70
3.10 Crack tip 72
3.11 J-integral 73
3.12 Coordinate reference system and contour path for J-integral . . . 76

4.1 Cylinder under external pressure 94
4.2 Boundary conditions and discretisation with 40 quadratic elements 96
4.3 Normalised radial displacement on AB 97
4.4 Normalised tangential stress on AB 97
4.5 Normalised first order derivatives of radial displacement on AB . 98
4.6 Normalised first order derivatives of tangential stress on AB . . . 98
4.7 Normalised second order derivatives of radial displacement on AB 99
4.8 Normalised second order derivatives of $\sigma_{\theta\theta}$ on AB 99
4.9 First order derivative percentage errors 100
4.10 Second order derivative percentage errors 101
4.11 Reliability by FORM and simulation with $V_a = 0.1$ 102
4.12 Reliability by FORM and simulation with $V_a = 0.2$ 102
4.13 Reliability by FORM and simulation with $V_a = 0.3$ 103
4.14 Reliability by FORM and simulation with $V_a = 0.4$ 103
4.15 Comparison of reliability by FORM and simulation 104
4.16 Plate with a hole under far field stress 105

4.17 Boundary conditions and discretisation with 40 quadratic elements 106
4.18 Reliability by FORM and simulation with $V_a = 0.1$ 108
4.19 Reliability by FORM and simulation with $V_a = 0.2$ 108
4.20 Reliability by FORM and simulation with $V_a = 0.3$ 109
4.21 Reliability by FORM and simulation with $V_a = 0.4$ 109
4.22 Comparison of reliability by FORM and simulation 110
4.23 Reliability by FORM and simulation with $V_a = 0.1$ 111
4.24 Reliability by FORM and simulation with $V_a = 0.2$ 111
4.25 Reliability by FORM and simulation with $V_a = 0.3$ 112
4.26 Reliability by FORM and simulation with $V_a = 0.4$ 112

5.1 Change to node A of a straight crack 120
5.2 Change to node B of a straight crack 121
5.3 Flowchart of algorithm 134
5.4 Geometry and loads of centre crack specimen 135
5.5 Boundary conditions and discretisation of centre crack specimen . 136
5.6 Sensitivity errors for centre crack specimen 137
5.7 Normalised mode I stress intensity factor for centre crack specimen 138
5.8 Normalised derivatives of mode I stress intensity factor with respect to crack length 138
5.9 Geometry and loads of single edge crack specimen 140
5.10 Boundary conditions and discretisation of single edge crack specimen 141
5.11 Sensitivity errors for single edge crack specimen 142
5.12 KI for single edge crack specimen 143
5.13 dKI/da for single edge crack specimen 143
5.14 Geometry and loads of Mixed-mode specimen 145

5.15 Boundary conditions and discretisation of Mixed-mode specimen 146
5.16 dKI/da for single edge crack under shear stress 149
5.17 dKII/da for single edge crack under shear stress 150
5.18 Geometry and loads of double edge crack specimen 151
5.19 Boundary conditions and discretisation of double edge crack specimen 153
5.20 POF and simulation with Va/w=0. 155
5.21 POF and simulation with Va/w=0.1 155
5.22 POF and simulation with Va/w=0.2 156
5.23 POF and simulation with Va/w=0.3 156
5.24 POF and simulation with Va/w=0.4 157
5.25 POF for various uncertainties in crack size 157
5.26 Probabilistic sensitivity factor for $\frac{a}{W} = 0.3$ 158
5.27 Probabilistic sensitivity factor for $\frac{a}{W} = 0.5$ 159

6.1 Random crack path 164
6.2 Geometry and loads of double edge crack specimen 171
6.3 Boundary conditions and discretisation of double edge crack specimen 173
6.4 Normalised K_I with crack growth size $\frac{\triangle a}{W} = 0.06$ 174
6.5 Normalised K_I with crack growth size $\frac{\triangle a}{W} = 0.03$ 175
6.6 Normalised K_I with crack growth size $\frac{\triangle a}{W} = 0.02$ 175
6.7 Normalised K_I with crack growth size $\frac{\triangle a}{W} = 0.015$ 176
6.8 Normalised $\frac{\partial K_I}{\partial a}$ with crack growth size $\frac{\triangle a}{W} = 0.06$ 176
6.9 Normalised $\frac{\partial K_I}{\partial a}$ with crack growth size $\frac{\triangle a}{W} = 0.03$ 177
6.10 Normalised $\frac{\partial K_I}{\partial a}$ with crack growth size with IDM $\frac{\triangle a}{W} = 0.02$ 177
6.11 Normalised $\frac{\partial K_I}{\partial a}$ with crack growth size $\frac{\triangle a}{W} = 0.015$ 178

6.12 Normalised K_I with different crack increment sizes for total 46 boundary elements 179
6.13 Normalised $\frac{\partial K_I}{\partial a}$ with different crack increment sizes for total 46 boundary elements 180
6.14 Normalised K_I with different crack increment sizes for total 96 boundary elements 180
6.15 Normalised $\frac{\partial K_I}{\partial a}$ with different crack increment sizes for total 96 boundary elements 181
6.16 Reliability index with various uncertainty 182
6.17 Reliability index with random initial crack length 183
6.18 Reliability index with random final crack length 183
6.19 Reliability index with random fatigue parameter C 184
6.20 Reliability index with random fatigue parameter m 184
6.21 Reliability index with random stress 185
6.22 Comparison of random parameters 185
6.23 Geometry and loads of single edge crack specimen 186
6.24 Boundary conditions and discretisation of single edge crack specimen 187
6.25 Normalised K_I with different crack increment sizes 188
6.26 Normalised $\frac{\partial K_I}{\partial a}$ with different crack increment sizes 189
6.27 Normalised K_I with different crack increment sizes 189
6.28 Normalised $\frac{\partial K_I}{\partial a}$ with different crack increment sizes 190
6.29 Reliability index with various uncertainty 191
6.30 Reliability index with random initial crack length 191
6.31 Reliability index with random final crack length 192
6.32 Reliability index with random fatigue parameter C 192

6.33 Reliability index with random fatigue parameter m 193

6.34 Reliability index with random stress 193

6.35 Comparison with different distribution 194

A.1 Standard normal distribution 214

List of Tables

4.1 Statistical properties of random input for cylinder 95

4.2 Statistical properties of random input for plate with a hole 106

5.1 Normalised derivative of Mode I stress intensity factor with respect to crack length by the proposed and analytical methods for centre crack specimen 139

5.2 Normalised derivative of Mode I stress intensity factor with respect to crack length by the proposed and analytical methods for single edge crack specimen 144

5.3 Mode-I SIF 147

5.4 Mode-II SIF 147

5.5 First-order derivative of mode-I SIF 148

5.6 First-order derivative of mode-II SIF 148

5.7 Statistical properties of random input for double edge crack specimen 152

6.1 Statistical properties of random parameters 172

Nomenclature

α, β	Parameters of beta distribution
β	Reliability index
β	Shape parameter
β^*	Euler-Mascheroni constant
$\triangle$	Dirac delta function
δ_{ij}	Kronecker delta function
δ_Z	Coefficent of variation
$\mathbf{Z}$	N-dimensional random vector
Γ	Boundary of the problem
γ	Location parameter
γ_s	Surface energy of the material
λ_Z, ζ_Z	Parameters of lognormal distribution
μ	Shear modulus
μ_Z	Mean of random variable distribution

ν	Poisson's ratio
Ω	Domain of the problem
ϕ	Cumulative distribution funtion
Π	Potential energy
σ	Stress
σ_{ij}	Stress tensor
σ_Z	Standard deviation of random variable distribution
θ	Scale parameter
ε_{ij}	Strain tensor
ξ, η	Local Cartesian coordinates
$\xi\prime, \xi$	Source point and field point in local coordinate
A	Area
A	Coefficient system matrix
a^t	Transpose of the gradient vector
b_i	Components of the body force
C_{ij}	Jump terms
D_{kij}, S_{kij}	Fundamental solution for traction integral equaiton
E	Modulus of elasticity
e_i	Cartesian direction vectors

f_σ Stress probability density function

f_R Strength probability density function

G Energy release rate

$g()$ Limit state function

J J-integral

$J^\gamma(\xi)$ Jacobian of transformation

J_{cp} Jacobian of crack path

K_{Ic} Critical mode-I stress intensity factor

K_I, K_{II}, K_{III} Stress intensity factors for mode I, II and III

$M^n(\xi)$ Shape function for the boundary element

N Fatigue life

N_e Total number of elements

N_s Number of simulation

N_{cp} Number of crack increment

N_s Service life

N_v Number of variable

P_r Reliability

r Absolute distance between the source and the field points

R_s Fatigue life

T_{ij} 2-D traction fundamental solutions

$U_{ij,k}, T_{ij,k}$ Derivatives of the fundamental solution with respect to the source node

U_{ij} 2-D displacement fundamental solutions

W Strain energy density

W_i Integration weight for crack incement step

W_s Work required to create new surface

X Vector of unknown values

x, X Field points

x', X' Source point

Z_m Random variable

R Strength

Chapter 1

Introduction

1.1 General

As most observable physical phenomena contain a certain degree of uncertainty, the repeated measurements of those phenomena could generate multiple outcomes. Among them, some are more frequently observed than others. The occurrence of those outcomes without any pattern is described by terms such as randomness, uncertainty and stochasticity. All the parameters of interest in engineering analysis and design have some degree of uncertainty and thus can be treated as random variables.

The need to address the uncertainties in engineering has received worldwide acceptance from the engineering professions. Traditionally, a safety factor is used to provide the confidence level. However, the safety factor approach is based on past experience and usually does not take into account the underlying probability distributions. For consistent reliability analysis, it is important to determine the probability distributions for the structural performance functions. The evaluation of such probability distribution involves complicated numerical computations which is a difficult task, that prohibits the use of the Monte Carlo

simulation method. For problems that involve multiple random variables, the Monte Carlo simulation could became impractical by treating those variables as statistically independent. Probabilistic structural analysis can provide more information about the system or component behaviour, the influence of different random variables on the system or component performance, also interactions between different components within the system.

The earliest study of the mechanical and structural failure data can be found in the work of Weibull [111] who presented a statistical function derived from a weakest link probabilistic characterization of the breaking strengths of materials. Since then, the Weibull function has been extended to many other problems. In 1956, Freudenthal [43] introduced the concept of risk-based design which was later summarized by Freudenthal et al. [44]. In view of the uncertainties in structural analysis, satisfactory performance cannot be absolutely ensured; it can only be associated with satisfying some performance criterion. This probability of successful performance is termed as *Reliability*. An alternative way is to consider unsatisfactory performance of the structure which is termed as *risk* or *Probability of failure*.

It is well recognised that most mechanical failures of the structure result from fracture, fatigue, corrosion and material degradation process. These events fall within the framework of Fracture Mechanics and Fatigue. Each such failure phase may be termed as a performance criterion. The study of structural reliability is concerned with the calculation and prediction of the probability of performance criteria for a structural system at any stage during its life. In fact, all the necessary inputs to fracture mechanics are rarely accurate to a high degree of certainty. *Probabilistic Fracture Mechanics* (PFM) covers the application of mechanistic and stochastic aspects of the fracture problem; it provides a compre-

hensive tool to describe the actual behaviour and reliability of a cracked structure. The theory of fracture mechanics provides a relationship between the mechanics of cracks and material properties. The probability theory analyses the randomness in crack size, loading and material properties affect the integrity of cracked structures. In PFM, the derivatives of *stress intensity factor* (SIF) or *J-integral* are often required for probabilistic analysis [14, 15, 18, 36, 46, 66, 90]. Those two fracture parameters are required for obtaining the gradient of performance criterion with respect to random variable in most probabilistic analysis [90]. Due to the complexity in crack geometry, external loads, and material behavior, several numerical tools have been employed to provide the necessary computational framework for analysis of general cracked structures.

The *Finite Difference Method* (FDM) has been successfully applied to many areas of science; although FDM is simple and versatile, problems arise with irregular geometries and with rapidly changing variables. Currently most researchers have focused on advanced probabilistic algorithms coupled with the *finite element method* (FEM) as the structural analysis tool because of its generality. FEM has been coupled with the first-order-reliability-method (FORM) and second-order-reliability-method (SORM) by Der Kiureghian and Ke [36] for linear structural problems. Lin and Abel [66] introduced a direct-integration approach of the virtual crack extension technique that employs variational formulation and the FEM to calculate the first-order derivative of SIF for a structure containing a single crack. Chen et al. [28] used continuum-based shape sensitivity and reliability analysis of a crack in a homogeneous, isotropic, and linear-elastic body subject to mode-I loading. In his study, Chen et al. [28] implied the material derivative concept of continuum mechanics, domain integral representation of the J-integral and direct differentiation to obtain the derivatives of fracture parameters with

respect to random parameters.

Early application of probabilistic analysis to fatigue crack growth can be found in the work of Ortiz and Kiremidjian [81], Kozin and Bogdanoff [62], Besterfield et al. [15], Schall et al. [98], Harkness et al. [51], Zhu et al. [117]. A probabilistic finite element method in conjunction with FORM has been developed by Besterfield et al. [15], Harkness et al. [51] for the reliability analysis of the fatigue crack growth. Meanwhile, Schall et al. [98] has linked a finite element analysis with the reliability calculation through a response surface program using Hermite polynomials for the fatigue reliability of marine structures. Zhu et al. [117] assumed the material resistance to fatigue crack growth and the time-history of the stress are random to obtain the analytical expressions for a randomized Paris-Erdogan law. Peng et al. [84] combined the stochastic finite element method with a second-order three-moment reliability analytical model to investigate the fatigue strength reliability of a gear teeth subjected to bending.

However, there are disadvantages with FEM such as: required discretisation of the entire domain, not only is the system of equations large, but the data preparation is time consuming. The difficulty and inaccurate calculation of the derivatives of fracture parameters lead to the need of an alternative method. There are other numerical methods that could provide better solutions to such problem, among them the *Boundary Element Method* (BEM) can be highlighted.

1.2 The boundary element method

The BEM is a numerical method for solving partial differential equations which have been transformed into integral equations. These integrals are numerically evaluated over the boundary which is divided into boundary elements. BEM

can be applied in many areas of engineering and science including fluid mechanics, acoustics, electromagnetism, fracture mechanics, plasticity, stability and etc. Over the years, many contributions to BEM have been made in different fields of applications. More detailed introductions related to implementation and application of the BEM can be found in the text books, such as Aliabadi [5], Becker [12], Brebbia [19], Brebbia and Dominguez [20], Fenner [42], Wrobel [113].

The boundary element method has its roots in the Betti's reciprocal work theorem [16] and Somigliana [103] identity of the mid 1800's. However, the application of the method to engineering problems began in the 1960's when two classic papers were published by Jaswon [57] and Symm [104]. Their approach consisted of discretizing the integral equations of two-dimensional potential problems governed by Laplace's equation into straight line elements over which potential functions are assumed constant over each element. The elements were described in terms of nodal points and integrations performed using Simpson's rule except for some singular integrals which were integrated analytically. Jaswon and Symm's approach can be classified as 'in-direct' because the functions used to formulate the problem are fictitious and can be differentiated or integrated to calculate physical quantities.

The first paper to use the direct approach of using displacements and tractions in an integral equation applicable over the boundary was published by Rizzo [94] in 1967. Rizzo's work was the first to exploit the strong analogy between potential theory and classical elasticity theory, which lead to a numerical approach of solving the problem. Straight line elements were used by Rizzo to discretise the boundary where the functions are assumed constant over each element. He then applied Simpson's rule for all but the singular integrals. In 1969, Cruse [33] extended Rizzo's works to three-dimensional problems. In his work, the surface

was discretised into flat triangular elements with the displacements and tractions assumed constant over each element. Cruse's work [33, 35] also made a major contribution to the development and application of the boundary element method to elasticity problems and fracture mechanics both theoretically and computationally. Lachat and Watson [63] developed an isoparametric formulation that has extended the method to solve complex problems.

The attraction of BEM can be largely attributed to the reduction in the dimensionality of the problem. This means that, compared to FEM, a boundary analysis results in a substantial reduction in data preparation and a much smaller system of equations to be solved. Furthermore, this simpler description of the body means that regions of high stress concentration can be modelled more efficiently as the necessary high concentration of grid points is confined to one less dimension. This ability to model high stress gradients efficiently has been the main reason for the method's success in fracture mechanics applications. Early BEM applications to fracture mechanics can be found in the works of Cruse and Vanburen [35], Cruse [34], Tan and Fenner [106], Blandford et al. [17], Becker and Fenner [13], Aliabadi [2]. Comprehensive reviews of the application of BEM to fracture mechanics can be found in review articles by Aliabadi [3, 4].

It is worthy to mention that the BEM is especially effective in random boundary geometry modelling, so that it is used in stochastic shape design sensitivity [80, 116, 23, 75]. In the work of Mellings and Aliabadi [75], Moghaddasi-Tafreshi and Fenner [80], Zhang and Mukherjee [116], who all presented a method with direct differentiation of the governing boundary element formulation to obtain the design sensitivities in elastic bodies. In the view of probabilistic analysis with BEM, earlier publications can be found in the study of Burczynski [22], Drewniak [37], Ettouney et al. [40], Kaljevic and Saigal [58], Roy and Grilli [96]. Most of

the reported researches were dealing with random external loads and boundary conditions. Potential flow problems were analysed in the work of Burczynski [22], Cheng and Lafe [29] and Kaljević and Saigal [59]. The problems defined by a differential equation with a random operator, termed as the random operator problems, were analysed by Ettouney et al. [40], who developed a simple perturbation procedure for the treatment of two-dimensional problems in elastostatics. A general perturbation procedure for random operator problems in elastostatics involving a random geometry or material property was presented by Kaljevic and Saigal [58]. Groundwater flow problems were analysed in the work of Cheng and Lafe [29], El Harrouni et al. [38], Roy and Grilli [96] and Satish [97]. A stochastic heat conduction problem was analysed by Drewniak [37]. Dynamic problems were reported by Burczynski and John [24]. More recently, Honda [54] applied the spectral stochastic approach to the BEM for the two-dimensional elastostatics and elastodynamic problems with geometric uncertainty.

The application of BEM to fatigue crack growth is widely used since the early 90s. For example, Portela et al. [87] and Mi and Aliabadi [77, 78] presented an application of the Dual Boundary Element Method (DBEM) to the analysis of mixed-mode crack growth in 2D and 3D linear elastic fracture mechanics, where the crack growth processes were simulated with an incremental crack extension analysis based on the maximum principal stress criterion for 2D and minimum strain energy density criterion for 3D. As for probabilistic fatigue crack growth analysis, Lua et al. [70] combines the mixed boundary integral equations with first order reliability method (FORM) for probabilistic crack growth analysis; in their work, the least-squares fitting routine was used to obtain the first-order response-surface model of the random parameters.

1.3 Overview of the thesis

The aim of this thesis is to develop the dual boundary element formulations for probabilistic analysis in *Linear-elastic Fracture Mechanics* (LEFM). The deviation and implementation of Dual Boundary Element formulations presented in chapter 3 can be found in the textbook of Aliabadi [5]. The method developed by the author is presented and implemented from chapter 4 to 6 in this thesis. A chapter-by-chapter overview of the thesis is presented as follows:

- Chapter 2: Fundamental concepts in probabilistic structural analysis

The fundamental theory and concepts behind probabilistic methods are presented. Some of the commonly used continuous and discrete random variables are presented along with their *Probability density function* (PDF) and *cumulative density function* (CDF) property. The three main approaches to probabilistic analysis (integration, Monte Carlo simulation and limit state approximation) are explained. The essential elements of the Monte Carlo simulation are also presented. The ideology and implementation of First Order Reliability Methods (FORM) are presented. The Newton-Raphson type recursive algorithm which is used to find the most probable point or failure point are also briefly introduced.

- Chapter 3: The Dual Boundary Element Method

The formulation of the equations used in both the boundary and dual boundary element methods are presented, along with their numerical implementation in two dimensions. The basic principles of fracture mechanics are presented and applied to two-dimensional (2D) example; *J-integral* is used to evaluate fracture

parameters. At the end fatigue crack growth and fatigue life estimation methods are presented.

- Chapter 4: Stochastic Boundary Element Method for elastostatics

The derivative boundary integral equations are formulated to compute the derivatives of boundary response. These equations are then used to form a system of equations for each design variable in the problem. For each analysis, a comparison of the derivatives obtained using this method is made with a series of finite difference approximations and analytical expressions when possible. A BEM coupled with FORM is implemented for probabilistic analysis in elastostatics problems, comparison of results with Monte Carlo simulation are also investigated.

- Chapter 5: Stochastic Boundary Element Method for LEFM

The derivative forms of the dual boundary element equations are formulated to compute the derivatives of boundary response. The Finite difference approximation method is used to study the sensitivity error. *J-integral* and its derivatives are implemented in the post-processing to evaluate the SIFs and their derivatives. The stress intensity factors and their first order derivatives are evaluated for mode-I and mixed-mode fracture problems. Comparison of the derivatives of stress-intensity factors with respect to crack size calculated using this method is made with the reference solutions obtained either analytically (mode I) or using finite-difference (mixed mode) method. In order to evaluate the singular integrals, a new assumption is made for source nodes situated on the crack faces. A convergence study is also carried out to assess the accuracy for the calculation of the derivative of fracture parameters with respect to crack size. The probabilistic

analysis method is studied with a numerical example. Results from simple examples are compared with available references and the Monte Carlo simulation results.

- Chapter 6: Stochastic Boundary Element Method for fatigue crack growth

The DBEM is extended to stochastic fatigue crack growth problems. The probabilistic analysis method of the fatigue crack growth is introduced. The total derivative method is used to obtain the derivative of fatigue life with respect to random parameters. The random crack path is mapped to a local coordinate system using linear interpolation to evaluate the derivatives of fracture parameters with respect to random crack size. Finally, the randomness in initial and final crack size; material property and loading are considered in the numerical examples.

- Chapter 7: Conclusions and future research

At the end conclusions are presented along with some suggestions for future research.

Chapter 2

Fundamental concepts in probabilistic structural analysis

2.1 Introduction

In 1949, Weibull proposed a *probability density function* (PDF) to represent the fatigue data. Since then, the application of this failure distribution has been applied to many other engineering problems. Several other researchers have followed Weibull's work [111, 112] and proposed several other statistical models. The most popular models are the Normal, Lognormal, Beta, Uniform, Binomial, Poisson, Exponential and two Extreme Values distribution [1, 32, 41, 82].

The Normal distribution is the least conservative distribution method; however it is frequently used in the probability analysis in correlation to the complexity of calculations. This is due to the dropping of function values in a quick manner as they move away from the mean in comparison to the Weibull distribution's or Lognormal's skewed tail. Initially the Lognormal distribution was applied to the fields of small-particle physics, economics and biology. Gumbel [47, 48] extended the Weibull's work to the study of floods, aeronautics, geology

and naval engineering. Although there are many applications of Weibull distribution across engineering industries, it is particularly popular in the aerospace industry [90, 41, 73, 50]. It has been frequently suggested on empirical grounds as a time to failure model and satisfactory representations have been reported by Lieblein and Zelen [65] and Perry [85] in their studies of ball-bearing and transistors, respectively. The Exponential law was mathematically assessed as a failure law for complex equipment by several researchers [108, 64, 11].

All of the above distributions are probabilistic assessments about a variable, which is expressed in terms of its probability density function. In contrast to the deterministic approach, the random variables are taken into account explicitly in probabilistic analysis. In 1967, Cornell [31] proposed a second-moment approach for structure analysis. In his work, the variable distribution's means and variances were used to determine the *safety index*, which as a reliability measurement, was used as a replacement for numerical integration of the joint probability density function to assess the probability of failure. In 1972, Lind [67] established the use of Cornell's safety index to obtain safety factors on applied loads and resistance. Further fine-tuning by Hasofer and Lind [53] led to the methods which have come to be recognized as the cornerstone of *probabilistic design theory*. In early 1980s, researchers have derived and experimentally investigated a new reliability distribution based on probabilistic micromechanics concepts applied to the fatigue of polycrystalline metals. Extensive researches on computational tools for quantifying the reliability of complex structures have been reported since late 80s. There has been considerable development in formulation of efficient probabilistic algorithms to reduce the computational costs.

In this chapter, some of the commonly used random variable models are presented along with their property. The fundamental theory and concepts behind

probabilistic methods in engineering are presented. The essential elements of the Monte Carlo simulation are presented. The ideology and implementation of first order reliability method are also presented.

2.2 Basic approach

The basic probabilistic approach can be expressed as the statistical classification for the input variables necessary for structural analysis. The statistical description of the resultant applied stress σ and the strength of the structure R each is described by a known probability density function denoted by $f_{\sigma}()$ and $f_{R}()$ respectively, where σ can be obtained through a structural analysis of applied loading (either deterministic or random components). However, the same scale should be used to express σ and R. The structural element will be treated as a failure in the event where σ, the resultant stress greater than R, its resistance; as illustrated by Figure 2.1 [8, 10, 100, 41, 73, 50].

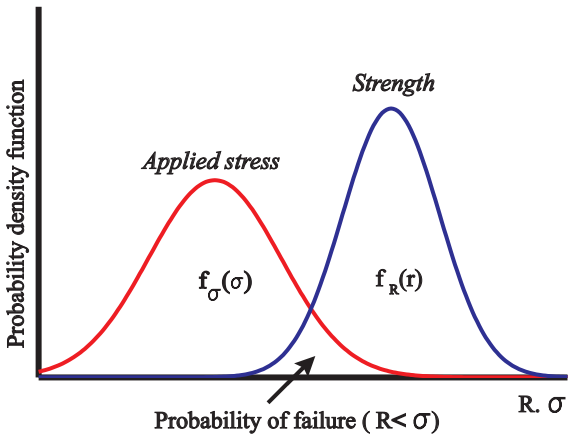

Figure 2.1: Fundamental of failure evaluation

The probability of failure of structural element, P_f can be denoted by

$$P_f = P(R - \sigma \leq 0) \tag{2.1}$$

or

$$P_f = P\left[g(R,\sigma) \leq 0\right] \tag{2.2}$$

with the *limit state function* termed as $g()$ can be defined as:

$$g() = R - \sigma \tag{2.3}$$

where R and σ are independent variables. For any random variable vector $\mathbf{Z}$, equation for P_f can be written in the single integral form as:

$$P_f = P(R - \sigma \leq 0) = \int_{-\infty}^{\infty} F_R(Z_m) f_\sigma(Z_m) dZ_m,\ Z_m \epsilon \mathbf{Z} \tag{2.4}$$

This is known as a *Convolution Integral*, $F_R(Z_m)$ denotes the probability where $R \leq Z_m$ or the probability when Z_m being greater than R, the actual resistance.

2.3 Statistically characterized design variables

2.3.1 Continuous random variables

When a random variable Z_m is defined in the interval of (Z_1, Z_2), the variable Z_m can be assumed as an unlimited number of possible values ranging between Z_1 to Z_2. The graph in Figure 2.2 denotes the *probability density function* (PDF) denoted by $f_{\mathbf{Z}}(Z_m)$. This defines the distribution of all such probabilities as a function of Z_m. It does not directly provide information on probability but only indicates the nature of the randomness.

The calculation of the probability of Z_m having any value in the range of Z_1 to Z_2 is undertaken by finding out the area under the PDF within these limits. This can be expressed as:

$$P(Z_1 \leq Z_m \leq Z_2) = \int_{Z_1}^{Z_2} f_{\mathbf{Z}}(Z_m) dZ_m \tag{2.5}$$

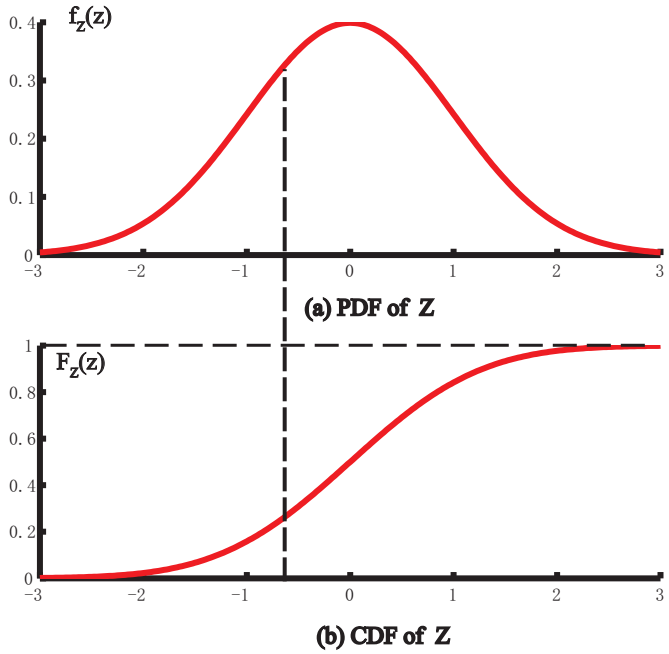

Figure 2.2: PDF and CDF of a random variable

The calculation of $P(\mathbf{Z} \leq Z_m)$, written as $F_{\mathbf{Z}}(Z_m)$ also known as *cumulative distribution function* (CDF). Theoretically, the integral is required to be moved from $-\infty$ to Z_m which can be depicted as

$$F(Z_m) = P(\mathbf{Z} \leq Z_m) = \int_{-\infty}^{Z_m} f_{\mathbf{Z}}(Z_m) dZ_m \tag{2.6}$$

The probability of random variables with a value less than or equal to a specific value is determined directly through CDF. Some of the most commonly used continuous random variables are described next with their property and applications.

Normal distribution $N(\mu_{\mathbf{Z}}, \sigma_{\mathbf{Z}})$

Gaussian or Normal distribution is the most widely known and used probability distribution in engineering industrial. The PDF of the distribution can be expressed as

$$f_{\mathbf{z}}(Z_m) = \frac{1}{\sigma_{\mathbf{Z}}\sqrt{2\pi}} \exp\left[-\frac{1}{2}\left(\frac{Z_m - \mu_{\mathbf{Z}}}{\sigma_{\mathbf{Z}}}\right)^2\right], \quad -\infty < Z_m < +\infty \tag{2.7}$$

where mean $\mu_{\mathbf{z}}$ and standard deviation $\sigma_{\mathbf{z}}$ are the two parameters of the distribution. The corresponding CDF can be expressed as

$$F_{\mathbf{z}}(Z_m) = \int_{-\infty}^{Z_m} \frac{1}{\sigma_{\mathbf{Z}}\sqrt{2\pi}} \exp\left[-\frac{1}{2}\left(\frac{Z_m - \mu_{\mathbf{z}}}{\sigma_{\mathbf{z}}}\right)^2\right] dZ_m \tag{2.8}$$

The first two moments are

$$E(x) = \mu_{\mathbf{z}} \tag{2.9}$$

$$\mathrm{Var}(\mathbf{Z}) = E(Z_m - \mu_{\mathbf{z}}) = \sigma_{\mathbf{z}}^2 \tag{2.10}$$

This distribution is symmetric about its mean and has dispersion represented by its standard deviation. Figure 2.3 shows three normal distributions with the same mean but different standard deviations. It is applicable for any value of a random variable from $-\infty$ to $+\infty$. As $\sigma_{\mathbf{z}}$ decreases, PDF moves toward to the mean. The distance between the mean and the points of inflection denotes the standard deviation of the PDF. However, it is not simple to estimate the probability by integrating equation (2.8). The problem can be addressed by transforming the original random variable Z_m into a standard normal variable with zero mean and unit standard deviation, as

$$S = \frac{Z_m - \mu_{\mathbf{z}}}{\sigma_{\mathbf{z}}} \tag{2.11}$$

Using equation (2.8) and the variable transformation technique, we can ex-

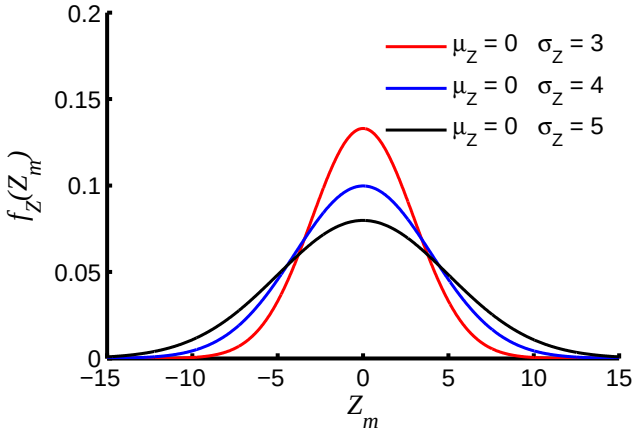

Figure 2.3: PDF of normal random variable

press the PDF of S as

$$f_S(s) = \frac{1}{\sqrt{2\pi}} \exp\left[-\frac{1}{2}s^2\right], \quad -\infty < s < +\infty \tag{2.12}$$

and the corresponding CDF of S is

$$F_S(s) = \int_{-\infty}^{s} \frac{1}{\sqrt{2\pi}} \exp\left[-\frac{1}{2}s^2\right] ds \tag{2.13}$$

The standard normal distribution is denoted as $N(0,1)$, and its CDF is denoted as $\Phi(s)$, that is, $\Phi(s) = F_S(s)$, given by equation (2.13). The CDF of the standard normal distribution is widely available in tabulated form, as shown in Appendix A.

Lognormal distribution $LN(\lambda_{\mathbf{Z}}, \zeta_{\mathbf{Z}})$

In many engineering problems, a random variable cannot have negative values due to the physical meaning of the problems. A random variable is Lognormal distributed when the natural logarithm of random variables is normally distributed. In the studies of reliability, Lognormal distribution arises naturally by considering a physical process where the failure is due to the fatigue crack growth. The

PDF and CDF of Lognormal variables are given by

$$f_{\mathbf{z}}(Z_m) = \frac{1}{Z_m \zeta_{\mathbf{z}} \sqrt{2\pi}} \exp\left[-\frac{1}{2}\left(\frac{\ln Z_m - \lambda_{\mathbf{z}}}{\zeta_{\mathbf{z}}}\right)^2\right], \quad 0 \leq Z_m < +\infty \tag{2.14}$$

and

$$F_{\mathbf{z}}(Z_m) = \frac{1}{\zeta_{\mathbf{z}} \sqrt{2\pi}} \int_{-\infty}^{Z_m} \exp\left[-\frac{1}{2}\left(\frac{\ln Z_m - \lambda_{\mathbf{z}}}{\zeta_{\mathbf{z}}}\right)^2\right] \tag{2.15}$$

where λ_Z and ζ_Z are the two parameters of the Lognormal distribution.

The PDF of three typical Lognormal distributions with 0.2, 0.6 and 1.0 as the mean along with a standard deviation of 1 is shown in Figure 2.4. The Lognormal variable has values between 0 and $+\infty$. In Figure 2.4, the Lognormal distribution is skewed to the right. The degree of skewness increases with the increasing standard deviation for a given mean value. For the same standard deviation, the skewness also increases as the mean increase.

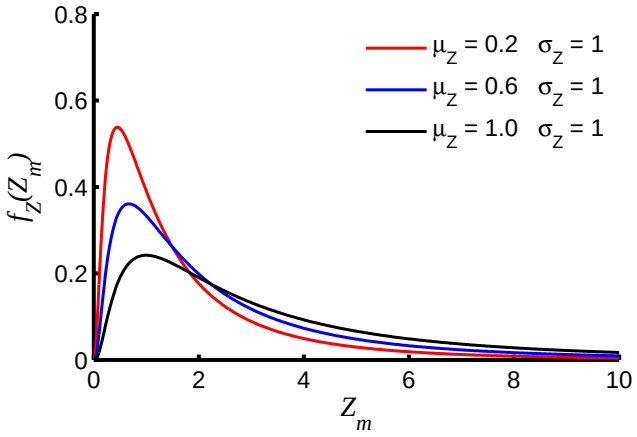

Figure 2.4: PDF of Lognormal random variable

Comparing equation (2.7) and (2.15), the similarities between the Normal and

Lognormal distributions can be observed. In fact, the information on the two parameters of the Normal distribution, the mean $\mu_{\mathbf{Z}}$ and the standard deviation $\sigma_{\mathbf{Z}}$, is used to calculate the two parameters of the Lognormal distribution. It can be shown that

$$\lambda_{\mathbf{Z}} = \ln(\mu_{\mathbf{Z}}) - \frac{1}{2}\zeta_{\mathbf{Z}}^2 \tag{2.16}$$

$$\zeta_{\mathbf{Z}} = \mathrm{Var}(\ln \mathbf{Z}) = \ln\left[1 + \left(\frac{\sigma_{\mathbf{Z}}}{\mu_{\mathbf{Z}}}\right)^2\right] = \ln(1 + \delta_{\mathbf{Z}}^2) \tag{2.17}$$

where $\delta_{\mathbf{Z}}$ is the *coefficient of variation* (COV) defined as

$$\delta_{\mathbf{Z}} = \frac{\sigma_{\mathbf{Z}}}{\mu_{\mathbf{Z}}} \tag{2.18}$$

and the first two moments are

$$E(\mathbf{Z}) = \mu_{\mathbf{Z}} = \exp(\lambda_{\mathbf{Z}} + \frac{1}{2}\zeta_{\mathbf{Z}}^2) \tag{2.19}$$

$$\mathrm{Var}(\mathbf{Z}) = \sigma_{\mathbf{Z}}^2 = \exp(2\lambda_{\mathbf{Z}} + \zeta_{\mathbf{Z}}^2)\left[\exp(\zeta_{\mathbf{Z}}^2) - 1\right] \tag{2.20}$$

Beta distribution

The PDF of a beta distribution is represented as:

$$\begin{aligned} f_{\mathbf{Z}}(Z_m) &= \frac{1}{B(\alpha,\beta)} \frac{(Z_m - a)^{\alpha-1}(b - Z_m)^{\beta-1}}{(b-a)^{\alpha+\beta-1}}, \quad a \le Z_m \le b \\ &= 0 \qquad\qquad \text{elsewhere} \end{aligned} \tag{2.21}$$

where α and β are the parameters of the beta distribution and $B(\alpha, \beta)$ is the beta function. The first two moments are:

$$E(\mathbf{Z}) = \mu_{\mathbf{z}} = a + \frac{\alpha}{\alpha+\beta}(b-a) \tag{2.22}$$

$$\mathrm{Var}(\mathbf{Z}) = \sigma_{\mathbf{z}}^2 = \frac{\alpha\beta}{(\alpha+\beta)^2(\alpha+\beta+1)}(b-a)^2 \tag{2.23}$$

As seen in Figure 2.5, a finite interval from 0 to 1 defines this distribution. In equation (2.21), the beta function can be shown to be

$$B(\alpha,\beta) = \int_0^1 Z_m^{\alpha-1}(1-Z_m)^{\beta-1}dZ_m \tag{2.24}$$

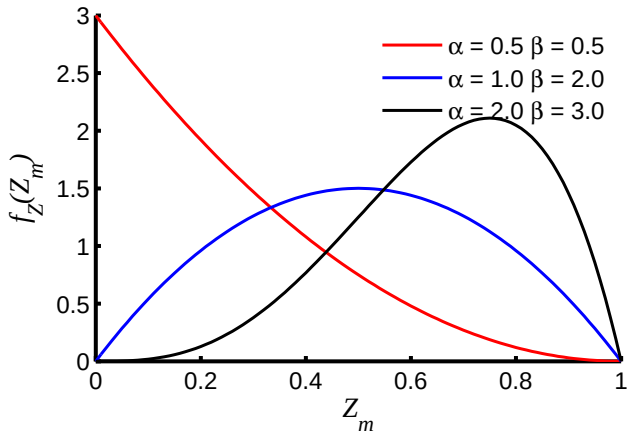

Figure 2.5: PDF of Beta random variable

Uniform distribution $U(a,b)$

The uniform distribution $U(a,b)$, is applicable when the only information available about a parameter Z_m is it varies between the limits a to b. In Figure 2.6, all values falling within the range between 0 and 1 will have equal probability of occurrences.

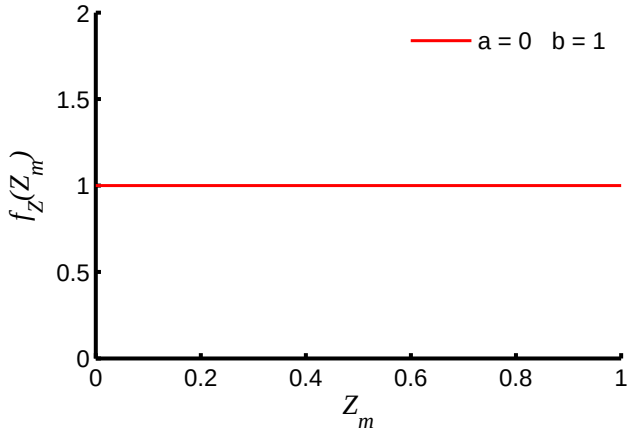

Figure 2.6: PDF of uniform distribution

The Type-I extreme value distribution

The failure of components may frequently be related to the causes that depend directly on either the smallest or the largest value is a particular sample distribution. Since this distribution was extensively used by Gumbel [48] in his study of extreme phenomena, Gumbel Distribution is another name by which it is referred.

In Type I asymptotic form, the PDF and CDF for the maximum value is shown as:

$$f_{\mathbf{z}}(Z_m) = \frac{1}{\theta}\left[-\frac{(Z_m-\gamma)}{\theta} - \exp\left(\frac{Z_m-\gamma}{\theta}\right)\right], \quad -\infty < Z_m < +\infty \tag{2.25}$$

and

$$F_{\mathbf{z}}(Z_m) = \exp\left[-\exp\left(\frac{Z_m-\gamma}{\theta}\right)\right] \tag{2.26}$$

where γ is location parameter and θ is scale parameter. This distribution satisfied by most of the reliability distribution. The maximum value of Type-I extreme distribution (Figure 2.7) is often used for modelling environmental loads such as winds and floods. Another use of the maximum value of Type-I extreme distribution is for the case when the maximum load determines the component

failure.

The first two moments are:

$$E(\mathbf{Z}) = \mu_{\mathbf{z}} = \gamma - \beta^* \theta \tag{2.27}$$

$$\mathrm{Var}(\mathbf{Z}) = \sigma_{\mathbf{z}}^2 = \frac{1}{6}\pi^2\theta^2 \tag{2.28}$$

where β^* is the Euler-Mascheroni constant$\simeq$0.57722.

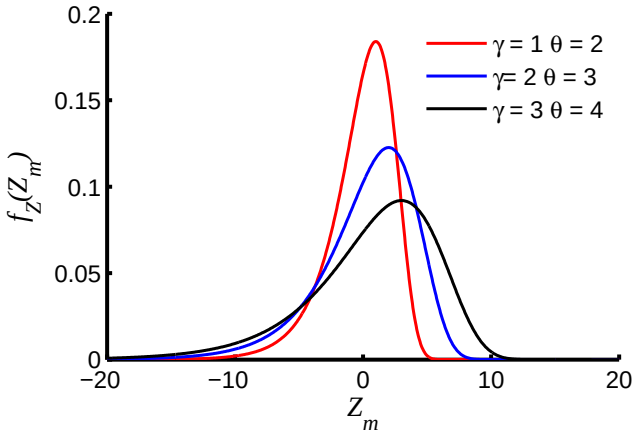

Figure 2.7: PDF of Type-I Extreme Value Distribution

Figure 2.7 shows three different distributions with the different location parameter γ and scale parameter θ. In the context of reliability modelling, there are frequent encounters of the minimum in Type-I extreme distribution. For instance, if a system consist n identical components in series, and the system fails when the first of these components fails, then the system failure times will be the minimum of n random component failure times. The PDF and CDF of the Type I asymptotic form for the minimum value is shown as:

$$f_{\mathbf{z}}(Z_m) = \frac{1}{\theta}\exp\left[\frac{(Z_m - \gamma)}{\theta} - \exp\left(\frac{Z_m - \gamma}{\theta}\right)\right], \quad -\infty < Z_m < +\infty \tag{2.29}$$

and

$$F_{\mathbf{z}}(Z_m) = 1 - \exp\left[-\exp\left(\frac{Z_m - \gamma}{\theta}\right)\right] \tag{2.30}$$

The Type-II extreme value distribution

The type-II asymptotic form, also referred to as *Frechet Distribution*. The PDF and CDF for the maximum value of a Frechet Distribution are shown as:

$$f_{\mathbf{z}}(Z_m) = \frac{\beta}{\theta}\left[\frac{\theta}{Z_m - \gamma}\right]^{\beta+1} \exp\left[-\left(\frac{\theta}{Z_m - \gamma}\right)\right]^{\beta}, \quad -\infty < Z_m < +\infty \tag{2.31}$$

and

$$F_{\mathbf{z}}(Z_m) = \exp\left[-\left(\frac{Z_m - \gamma}{\theta}\right)^{-\beta}\right] \tag{2.32}$$

where is γ location parameter, θ is scale parameter and β shape parameter. The first two moments are:

$$E(\mathbf{Z}) = \mu_{\mathbf{z}} = \gamma\Gamma(1 - \frac{1}{\beta}), \quad \beta > 1 \tag{2.33}$$

$$\mathrm{Var}(\mathbf{Z}) = \sigma^2_{\mathbf{z}} = \gamma\left[\Gamma(1 - \frac{2}{\beta}) - \Gamma^2(1 - \frac{1}{\beta})\right], \quad \beta > 2 \tag{2.34}$$

Figure 2.8 shows three different distributions with the same location parameter γ and scale parameter θ, but different shape parameter β.

Weibull distribution

The great versatility of Weibull distribution stems from the possibility to adjust it to fit the many cases where the failure rate either increases or decreases. It is also known as the Type III asymptotic distribution of the smallest extreme. Furthermore, of all statistical distributions that are available the Weibull dis-

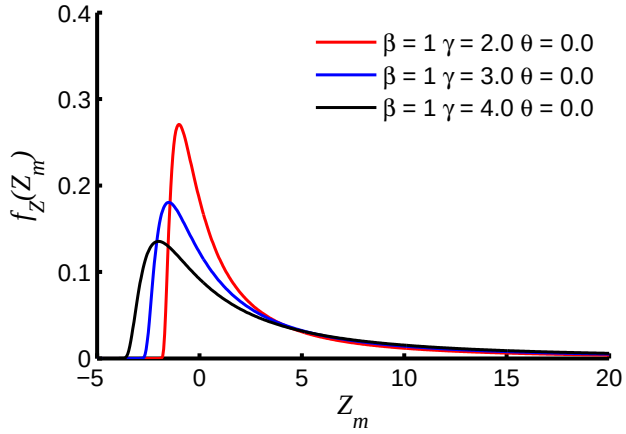

Figure 2.8: PDF of Type-II Extreme Value Distribution

tribution can be regarded as the most valuable, because it describes the life to failure when the initial strength distribution is not normal and embraces a great variety of forms including one that closely approximates the normal.

- The three-parameter Weibull distribution

The CDF of the Weibull distribution can be expressed as

$$F_{\mathbf{z}}(Z_m) = 1 - \exp\left[-\left(Z_m - \frac{\gamma}{\theta}\right)^{\beta}\right] \tag{2.35}$$

with $F_{\mathbf{z}}(Z_m)$ being the probability of failure and γ, θ and β being its three parameters of location parameter, scale parameter and shape parameter respectively. The PDF of the distribution can be expressed as

$$f_{\mathbf{z}}(Z_m) = \frac{\beta(Z_m - \gamma)^{\beta-1}}{\theta^{\beta}} \exp\left[-\left(\frac{Z_m - \gamma}{\theta}\right)^{\beta}\right], \quad -\infty < Z_m < +\infty \tag{2.36}$$

Figure 2.9 shows three different Weibull distributions with the same scale parameter θ but different location parameterγ, and shape parameter β. If $\beta < 1$ then the rate of failure decreases with time and if $\beta = 1$ the rate of failure is constant over time. More detail study of failure rate can be found in [90].

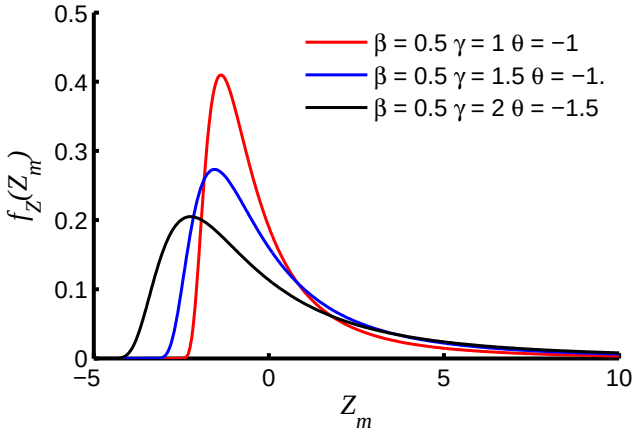

Figure 2.9: PDF of three parameter Weibull random variable

- The two-parameter Weibull distribution

For certain phenomena, it can be assumed that the lower bound of the associate random variable is equal to zero. For this case the Weibull PDF and CDF are depicted in

$$f_{\mathbf{z}}(Z_m) = \frac{\beta Z_m^{\beta-1}}{\theta^{\beta}} \exp\left[-\left(\frac{Z_m}{\theta}\right)^{\beta}\right], \quad Z_m > 0; \quad \beta, \theta > 0 \tag{2.37}$$

and

$$F_{\mathbf{z}}(Z_m) = 1 - \exp\left[\left(-\frac{Z_m}{\theta}\right)^{\beta}\right] \tag{2.38}$$

where the scale parameter is denoted by θ and the shape parameter is denoted by β . The three different values of shape parameters β with the same scale parameter are shown in Figure 2.10.

2.3.2 Discrete random variables

Some random variables are used while conducting engineering reliability analysis which are only measurable as integers; as such they are treated as discrete random

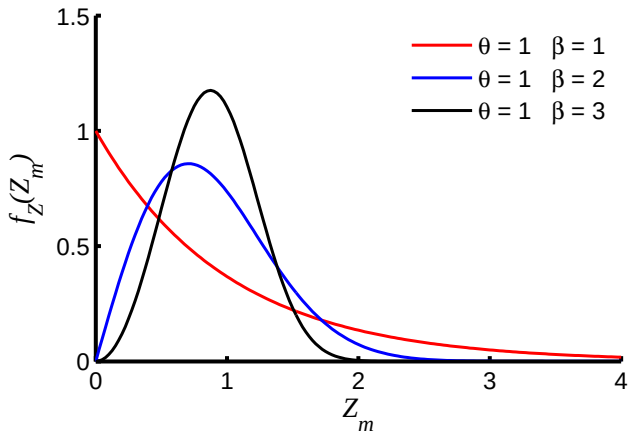

Figure 2.10: PDF of two parameter Weibull random variable

variables. Since a distinct random variable only occurs at distinct points, its relative frequency of occurrence can be evaluated only at these discrete points, which is called *probability mass function* (PMF). PMF is similar to PDF; however, it is not a continuous function, and it consists of a series of spikes. Some common discrete random variables are described next.

Binomial distribution

The binomial distribution gives the probability of Z_m exact occurrence in n trials. Its PMF is given by

$$P(\mathbf{Z} = Z_m) = P_{\mathbf{Z}}(Z_m) = \binom{n}{Z_m} p^{Z_m}(1-p)^{n-Z_m}, \quad Z_m = 0, 1, 2, \ldots n \tag{2.39}$$

and the CDF is given by

$$P(\mathbf{Z} \leq Z_m) = F_{\mathbf{Z}}(Z_m) = \sum_{y=0}^{Z_m} \binom{n}{y} p^{y}(1-p)^{n-y}, \quad Z_m = 0, 1, 2, \ldots n \tag{2.40}$$

where p, the probability of occurrence in each trial, is the parameter of the distribution, and

$$\binom{n}{Z_m} = \frac{n!}{Z_m!(n-Z_m)!} \tag{2.41}$$

is the binomial coefficient, indicating the number of ways that Z_m occurrence out of total n trails are possible.

The moments are

$$E(Z) = \mu_{\mathbf{z}} = np \tag{2.42}$$

$$\text{var}(Z) = \sigma_{\mathbf{z}}^2 = np(1-p) \tag{2.43}$$

The binomial distribution is applicable where there are only two discrete alternatives per independent trial, with probability p and $1-p$ respectively. Figure 2.11 shows a typical binomial distribution with 100 trails and probability of 0.4.

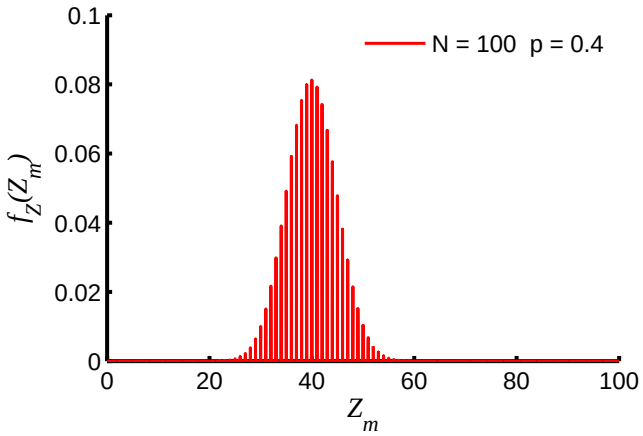

Figure 2.11: PDF of Binomial random variable

Poisson distribution

Poisson distribution gives the probability of a number of occurrences Z_t of a random event in a given (time) interval t, given that the mean rate of occurrences is known.

The probability mass function and cumulative distribution function are:

$$P(Z_t = Z_m) = P_{\mathbf{z}}(Z_m) = \frac{(\nu t)^{Z_m}}{Z_m!} e^{\nu t} \tag{2.44}$$

and

$$P(Z_t \leq Z_m) = F_{\mathbf{z}}(Z_m) = \sum_{k=0}^{Z_m} \frac{(\nu t)^r}{Z_t!} e^{-\nu t} \tag{2.45}$$

The parameters are the mean occurrence rate (per unit time or space units) ν, the time or space interval t, the average number $\lambda(= \nu t)$ of events in t, and the number Z_t of occurrences in t.

The moments are

$$E(\mathbf{Z}) = \mu_{\mathbf{z}} = \nu t \tag{2.46}$$

$$\mathrm{var}(\mathbf{Z}) = \sigma_{\mathbf{z}}^2 = \nu t \tag{2.47}$$

Figure 2.12 shows three distributions with the different average number $\lambda(= \nu t)$ of events in t.

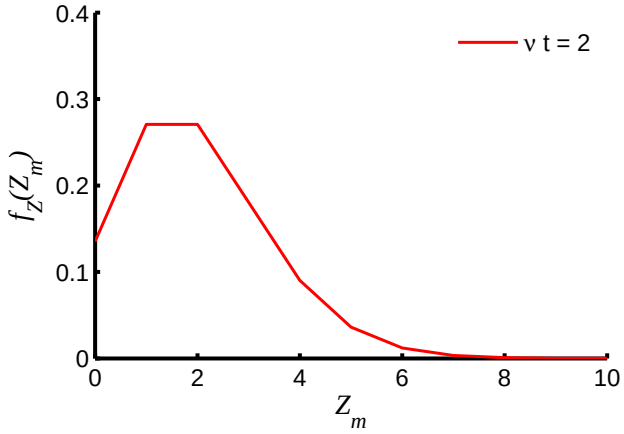

Figure 2.12: PDF of Poisson random variable

Exponential distribution $EX(\nu)$

The probability density and the cumulative distribution functions of exponential distribution are:

$$P(T = t) = f_{_T}(t) = \nu e^{-\nu t} \tag{2.48}$$

$$P(T \leq t) = F_{_T}(t) = 1 - e^{-\nu t} \tag{2.49}$$

The moments are

$$E(T) = \mu_{\mathbf{z}} = \frac{1}{\nu} = \overline{\Delta t} \tag{2.50}$$

$$\text{var}(T) = \sigma_{\mathbf{z}}^2 = \left(\frac{1}{\nu}\right)^2 = \left(\overline{\Delta t}\right)^2 \tag{2.51}$$

where $\overline{\Delta t}$ is the average time between the mean life. Figure 2.13 shows three distributions with the different rate parameters $\lambda(= \nu t)$.

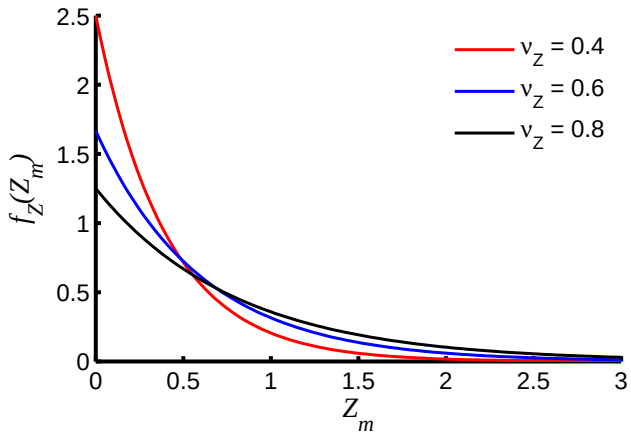

Figure 2.13: PDF of Exponential random variable

2.4 Probabilistic analysis methods

The essential steps in the evaluation of the reliability of the structure is to choose a specific performance criterion and the related resistance and load parameters, referred to as the basic random variables Z_m, $(m = 1....N_v)$, with N_v being the total number of random variables, with the functional relationship among them corresponding to each performance criterion. Mathematically, this performance function can be termed as:

$$g = g(Z_1, Z_2, ..., Z_n) \tag{2.52}$$

The limit state surface is then defined by $g() = 0$, which is the boundary between the safe and unsafe regions in the designing parameters space. Assuming R and σ are the two basic random variables, the limit state surface and the safe and unsafe regions can be defined in terms of R and σ as shown in Figure 2.14. The definition of limit state equation is a fundamental step in the development of structural reliability analysis methods. The limit state can either be an explicit or an implicit function of the basic random variable, which can be present in

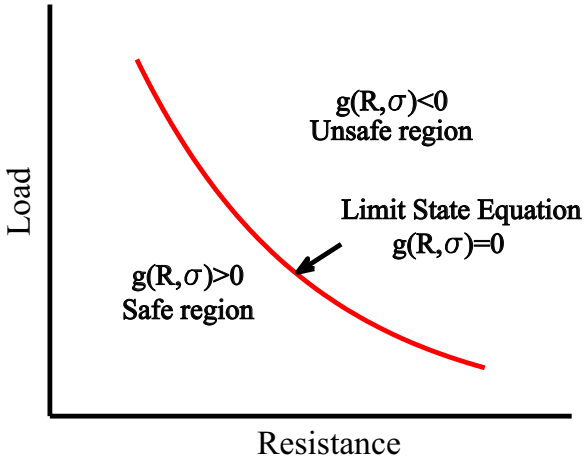

Figure 2.14: Limit state concept

simple or complicated forms. In equation (2.52), failure occurred when $g() < 0$. Therefore, the probability of failure P_f , is denoted by the integral

$$P_f = \int \dots \int_{g()<0} f_{\mathbf{Z}}(Z_1, Z_2, \dots, Z_n) dZ_1, dZ_2, \dots, dZ_n \tag{2.53}$$

where $f_{\mathbf{Z}}(Z_1, Z_2, \dots, Z_n)$ depicts the joint probability density function for the basic random variables $Z_1, Z_2, \dots, Z_n$ and the integration is carried out over the failure region, meaning, $g() < 0$. When the random variables are statistically independent, the joint probability density function can be replaced by the product of the individual probability density functions.

2.4.1 Integration

Analytical integration of the convolution integral (2.4) or the integral (2.53) is possible only for some very special cases of limited practical interest. Numerical solution of the convolution integral (2.4) is easily obtained through the use of the Trapezoidal Rule. The Polynomial based formula and other methods like

the Simpson's Rule can also applied. When the load σ and the resistance R in the convolution integral (2.4) are not independent, or there are more than two variables, the probability of failure must be obtained from the general formulation (2.53). The computation of this probability cannot be achieved in closed form.

In practice, limit state functions usually are more general form in equation (2.53) than linear functions in equation (2.3). Usually the performance function is not even known. In the meantime, there will be more than two random variables involved, which make it very difficult to obtain the resulting joint probability density function. Also, the random variables $\mathbf{Z}$ are unlikely to be normally distributed which require different methodologies to tackle them accordingly. Because of the rapidly increasing computational demands as the number of dimensions increase, numerical integration of the classic variety has not found great favour in reliability analysis. Instead, other alternative methods have been developed for the large integration problems.

2.4.2 Monte Carlo Simulation

The early probabilistic analysis relied primarily on simulation techniques like the Monte Carlo method. It comprises of selecting a value for each input variable randomly from its known statistical distribution, and then substitute into the underlying deterministic model. For the structural reliability analysis, the random variable Z_m is randomly chosen from its known statistical distribution to assign a simple value $\hat{Z_m}$, then the limit state function $g(\hat{\mathbf{Z}}) = 0$ is verified. If the conditions of the limit state function are violated, that is, $g(\hat{\mathbf{Z}}) \leq 0$, it shows the component or the structure has failed. This exercise is repeated many times with randomly chosen vector $\hat{\mathbf{Z}}$ of $\hat{Z_m}$ values, which lead to the conclusion that for a total number of simulations N_s conducted, the probability of failure, P_f , is

approximately evaluated by [9, 27, 76, 89]

$$P_f = \frac{n\left[g(\hat{\mathbf{Z}})\right] \leq 0}{N_s} \tag{2.54}$$

where $n\left[g(\hat{Z}_m)\right] \leq 0$ denotes the number of simulation n for which $g(\hat{Z}_m) \leq 0$.

The probability of failure P_f can be obtained with N_s simulation. Therefore a single Monte Carlo simulation is equivalent to a single application of the corresponding fracture mechanics analysis with the exception that some of the input values have been selected randomly.

Accuracy and number of simulations required

The accuracy of P_f in equation (2.54) depends on the total number of simulations N_s conducted. The estimated P_f will near its true value as N_s approaches infinity. The error of computational margin can be estimated by the rule that it is proportional to the square root of the quantity $(\frac{1}{N_s})$[102, 73]. Therefore, in order to reduce the error margin by 10, the total number of simulations will have to be increased by 100[102]. Shooman [100] derived the following formula to evaluate the percentage error:

$$\%\ \text{error} = \sqrt{\frac{1 - P_f}{N_s}} \tag{2.55}$$

This equation was developed using a 95% confidence level, which means there is a 95% chance that the error in the estimated probability of failure will be less than the error generated by this equation.

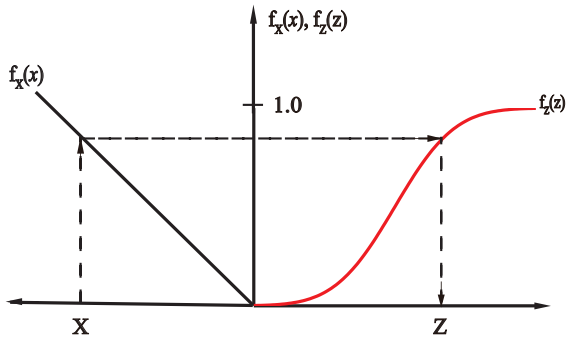

Figure 2.15: Generating random numbers

Generating random numbers from PDFs

The random numbers generated from PDFs values of each input are selected in such a manner that they represent the probability characteristics of that variable. The ability to generate random numbers from a *uniform distribution* between 0 and 1 becomes the fundamental step in Monte Carlo simulation. All values within 0 and 1 have equal probability of being selected and once a random number is selected from $U(0,1)$, a corresponding random PDF value of interest is generated. Assuming the CDF value of the random variable **Z** is denoted $F_{\mathbf{Z}}(Z_m)$ and **X** is the randomly generated number, the corresponding value of the variable **Z** is $Z_m = F_{\mathbf{Z}}^{-1}(x)$. Figure 2.15 shows the CDF of the random variable **Z** on the right and CDF of **X** on the left.

Correlated random variables

When some or all the variables are correlated, it is incorrect to sample from each PDF by treating them independently. In general, the correlated variables are difficult to generate, therefore a processes which transforms the correlated variables into uncorrelated variables is needed. A classical method developed by Rosenblatt [95] is shown in Appendix B.

Simulation efficiency improvement approaches

The Monte Carlo Simulation is very useful for number of applications; however, it is extremely time consuming in numerical analysis tools like FEM and BEM for practical problems. With the small probability of structural failure expected, a huge amount of simulations would be required. Several methodologies have been employed to increase simulation efficiency, including [50, 72]:

- *Importance sampling* It is the technique for modelling sample points within the region which mainly contributes to the probability of failure. Instead of spreading the sample points evenly across the entire range of values, generating a huge amount of simulations where the performance function $g(\hat{\mathbf{Z}}) > 0$, this technique generates only a few simulations; most of them result in a failure. This method is applied by modification of every variable's PDF to generate those important samples; the modifications are taken into account while computing the failure probability. *Adaptive importance sampling* has been developed for the increase of efficiency by focusing on sampling in the probability critical regions.

- *Stratified sampling* It is based on the number of simulations N_s which has been calculated, with the expected failure probability, the domains of the random variables are then divided into regions of equal probability, such that the sum of regions adds up to N_s. After this, one random sample is generated from each region, and the g-function is evaluated for each sample. The probability of failure is then calculated from the ratio of the number of failures over the total number of simulations.

Monte Carlo simulation can be used for validating the analytical methods and solving large, complex systems where other methods are not feasible, for instance,

when the performance function, $g(\mathbf{Z})$ is a function of many variables or it cannot be represented in terms of the random variables $\mathbf{Z}$. In that case, $g(\mathbf{Z})$ can only be evaluated numerically through a structural analysis such as FEM or BEM for sets of input variables. Monte Carlo simulation can provide input to perform multiple numerical analysis of the system and then assesses the number of times successes and failures occurred. Monte Carlo simulation is treated as a benchmark for other methodologies because it does not restrict the way in which the analysis must be structured.

2.4.3 Limit state approximation

The probability of failure, P_f, is defined by equation (2.53); however, it is practically impossible to obtain the joint probability density function of random variables. Even if this information is available, it is very difficult to evaluate the multiple integrals. One approach is to use analytical approximations of this integral that are simpler to compute. A *First Order Reliability Method* (FORM) suggested by Rackwitz and Fiessler [91] has been successfully applied to the probabilistic structural analysis. In their study, the performance function is linearized at each iteration point. A Newton-Raphson type recursive algorithm is used to define the design point or the most probable point. Rather than solving the limit state equation explicitly, it uses the gradient of performance function to find the next iteration point.

The algorithm can be best explained with the help of Figures 2.16 and 2.17. Consider the linear performance function shown in Figure 2.16, where the close form expression for limit state is not available. The starting point $\mathbf{Z}_0$, which usually is the vector of the mean values of the random variables, may not be on the limit state $g(Z_1, Z_2) = 0$, but on a parallel line $g(Z_1, Z_2) = k$. Thus the

optimization algorithm starts from $\mathbf{Z}_0$ and converges to the minimum distance point $\mathbf{Q}_f$ on the limit state. The limit state performance function $g(\mathbf{Z})$ can be expressed as

$$g(\mathbf{Z}) = b + \mathbf{a}^t\mathbf{Z} \tag{2.56}$$
$$= b + a_1 Z_1 + a_2 Z_2 \tag{2.57}$$

where $\mathbf{a}^t = (a_1, a_2)$ is the transpose of the gradient vector of the performance function. The magnitudes of the vectors $\mathbf{Q}_0$ and $\mathbf{Q}_f$ denote the distance from the origin to the starting point and to the limit state $g(\mathbf{Z}) = 0$, respectively.

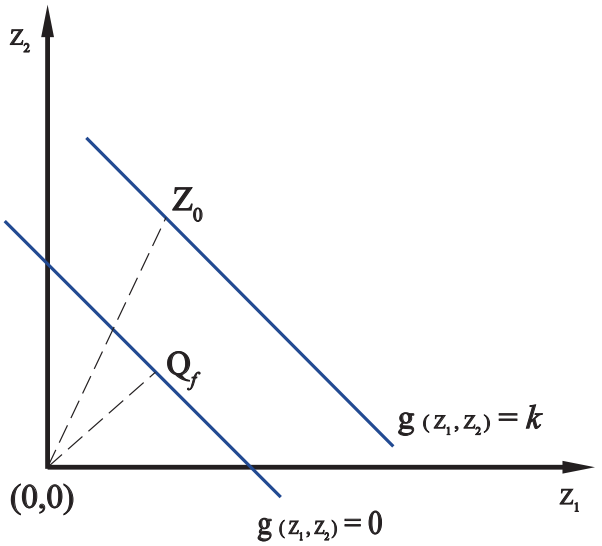

Figure 2.16: Linear performance function

Using geometry, vector $\mathbf{Q}_f$ can be expressed in terms of $\mathbf{Q}_0$ as

$$\mathbf{Q}_f = \frac{1}{|\mathbf{a}|^2}\left[\mathbf{a}^t\mathbf{Q}_0 - g(\mathbf{Q}_0)\right]\{\mathbf{a}\} \tag{2.58}$$

Expanding equation (2.58) in terms of the components of all the vectors result in

$$\begin{Bmatrix} Q_{f1} \\ Q_{f2} \end{Bmatrix} = \frac{1}{a_1^2 + a_2^2}\left[a_1 Q_{01} + a_2 Q_{02} - g(Q_{01}, Q_{02})\right]\begin{Bmatrix} a_1 \\ a_2 \end{Bmatrix} \tag{2.59}$$

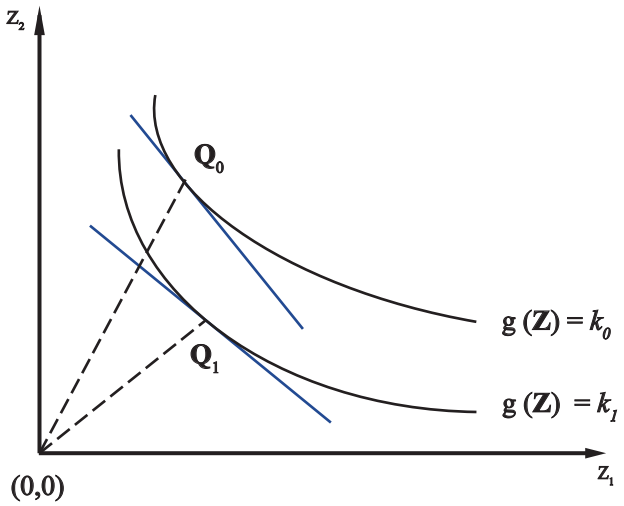

Figure 2.17: Nonlinear performance function

Since the performance function is linear in this case, its gradient is constant; hence the distance to the limit state from the origin is obtained in one step.

Equation (2.58) can be generalized for a nonlinear performance function as shown in Figure 2.17 as

$$\mathbf{Q}_{k+1} = \frac{1}{|\bigtriangledown g(\mathbf{Q}_k)|^2} \left[\bigtriangledown g(\mathbf{Q}_k)^t \mathbf{Q}_k - g(\mathbf{Q}_k)\right] \bigtriangledown g(\mathbf{Q}_k) \tag{2.60}$$

where $\bigtriangledown g(\mathbf{Q}_k)$ is the gradient vector of the performance function at $\mathbf{Q}_k$, the k_{th} iteration point. Therefore $\mathbf{Q}_k$ is a vector with component $\{Q_{k1}, Q_{k2}, \ldots, Q_{kn}\}^t$, where n is the number of random variables and $\mathbf{Q}_k$ has similar connotation.

The nonlinear nature of the performance function means that the gradient is not constant, but varies from point to point. Therefore, instead of a one-step solution in the case of a linear performance function, the point of minimum distance has to be searched through the recursive formula in equation (2.60). This formula can be geometrically interpreted using Figure 2.17. At each iteration point, the performance function is approximated by the tangent at the point, that is, the performance function is linearized with $g(\mathbf{Q}_k)$ and $\bigtriangledown g(\mathbf{Q}_k)$ corresponding

to $g(\mathbf{Q}_0)$ and $\mathbf{a}$, respectively, in equation (2.59). The next iteration point $\mathbf{Q}_{k+1}$ is computed in a way similar to the linear performance function. When the performance function is linear, $\mathbf{Q}_{k+1}$ would be identical to $\mathbf{Q}_k$, for $k > 0$. However, since the performance function is nonlinear, its value and gradient at $\mathbf{Q}_{k+1}$ are different from those at $\mathbf{Q}_k$. Therefore it is again linearized at $\mathbf{Q}_{k+1}$ and another iteration point $\mathbf{Q}_{k+2}$ is computed. The algorithm is repeated until convergence, satisfying the following two criteria:

$$\begin{array}{lll} \text{If} & \left|\mathbf{Q}_k - \mathbf{Q}_{k-1}\right| \leq \delta & \text{Stop} \\ \text{If} & |g(\mathbf{Q}_k)| \leq \epsilon & \text{Stop} \end{array} \tag{2.61}$$

Both δ and ϵ are small values, commonly assumed to be 0.001.

From this discussion, it is obvious that the recursive formula in equation (2.60) results from the linearisation of the performance function. Consider a First-order Taylor series approximation of the performance function as

$$g(\mathbf{Q}_{k+1}) = g(\mathbf{Q}_k) + \bigtriangledown g(\mathbf{Q}_k)(\mathbf{Q}_{k+1} - \mathbf{Q}_k) \tag{2.62}$$

Thus, the limit state function $g(\mathbf{Q}_{k+1}) = 0$ becomes

$$g(\mathbf{Q}_k) + \bigtriangledown g(\mathbf{Q}_k)(\mathbf{Q}_{k+1} - \mathbf{Q}_k) = 0 \tag{2.63}$$

Rearrangement of the terms in this equation gives equation (2.60) as the solution for the minimum distance point on the linearized limit state.

2.5 Summary

The fundamental theory and concepts in probabilistic analysis were presented. Some of the commonly used continuous and discrete random variable distributions are presented. The PMF or PDF and CDF of those distributions were presented along with their properties. The three approaches techniques of probabilistic

structural analysis which include Direct Integration; Monte Carlo Simulation and Limit state approximation were explained. The implementation of Monte Carlo Simulation and First Order Reliability Method (FORM) are explained extensively. In comparison to the other nonlinear optimization algorithms, the Newton-Raphson type requires least computations with the subsequent iteration point calculated through a single recursive formula that only requires the gradient and value of the performance function. The algorithm was also found to converge fast in many cases. For these reasons, this algorithm has been adopted in author's work.

Chapter 3

The dual boundary element method

3.1 Introduction

In this chapter, the application of boundary elements to linear elastostatics problem is described. The basic equations of linear elastostatics are presented. The standard boundary and dual boundary integral equations will be formulated for elastostatics analysis. The fundamental solutions associated with those formulations will be presented. The integral equation for internal displacements will be derived from the basic elastostatics equilibrium equations, and will then be transformed to a point on the boundary. The internal stress equation will be derived and transferred to a smooth crack boundary. These equations will be implemented into the dual boundary element method in the subsequent section. The special analytical integration used to evaluate integrals on the crack boundary will be presented. The fundamental concepts of fracture mechanics and fatigue crack growth for 2D elastic analysis are also described.

3.2 The boundary element method for elastostatics

3.2.1 Basic equations of elasticity

The basic equilibrium equations of a linear elastic body can be written as

$$\sigma_{ij,j} + b_i = 0 \qquad \text{in} \quad \Omega \tag{3.1}$$

where σ_{ij} represents the stress tensor, subscript $,_j$ denotes differentiation with respect to x_j, b_i is the body force vector and Ω represents the domain of the problem.

The strain tensor can be written in terms of the displacement derivatives using

$$\varepsilon_{ij} = \frac{1}{2}\left(\frac{\partial u_i}{\partial x_j} + \frac{\partial u_j}{\partial x_i}\right) \tag{3.2}$$

Stresses at a point can be given by the stress-strain relationships,

$$\sigma_{ij} = \frac{2\mu\nu}{1-2\nu}\varepsilon_{kk}\delta_{ij} + 2\mu\varepsilon_{ij} \tag{3.3}$$

where ε_{ij} represents the strain tensor; ν is the Poisson's ratio and μ is the shear modulus defined as follows:

$$\mu = \frac{E}{2(1+\nu)} \tag{3.4}$$

where E is the Young's Modulus, and the term δ_{ij} in equation (3.3) represents the Kronecker Delta, defined by

$$\delta_{ij} = \begin{cases} 1 & \text{if} \quad i = j \\ 0 & \text{if} \quad i \neq j \end{cases} \tag{3.5}$$

By substituting the strain-displacements of equation (3.2) into the stress-

strain equation (3.3), the stress-displacement equation can be obtained as:

$$\sigma_{ij} = \frac{2\mu\nu}{1-2\nu}\left(\frac{\partial u_m}{\partial x_m}\right)\delta_{ij} + \mu\left(\frac{\partial u_i}{\partial x_j} + \frac{\partial u_j}{\partial x_i}\right) \tag{3.6}$$

The governing equations of elasticity, known as Navier's equations, are the conditions of equilibrium expressed in terms of displacements. They can be obtained by substituting the stress-displacement relationship (3.6) into equations of equilibrium (3.1) to, gives

$$\frac{\partial^2 u_i}{\partial x_i \partial x_j} + \left(\frac{1}{1-2\nu}\right)\frac{\partial^2 u_j}{\partial x_i \partial x_j} = -\frac{b_i}{\mu} \tag{3.7}$$

which can be solved by a complementary function and a particular integral.

Boundary conditions are required to solve the problem and these usually take the form

$$\begin{aligned} u_i =& \bar{u}_i \\ t_i =& \sigma_{ij} n_j = \bar{t}_i \end{aligned} \tag{3.8}$$

The terms $\bar{u}_i$ and $\bar{t}_i$ are known values of displacement and traction on the boundary sections Γ_1 and Γ_2 respectively, as shown in Figure 3.1.

3.2.2 Formulation of the internal displacement integral equation

The derivation of BEM can be found in many text books on the subject. Here, the formulation presented in [5] is adopted. The boundary element method for elasticity can be formed from a boundary integral representation of the equilibrium equations (3.1). Assume that an approximation is made to the stress σ_{ij} in equation (3.1), it is possible to write the following relationship:

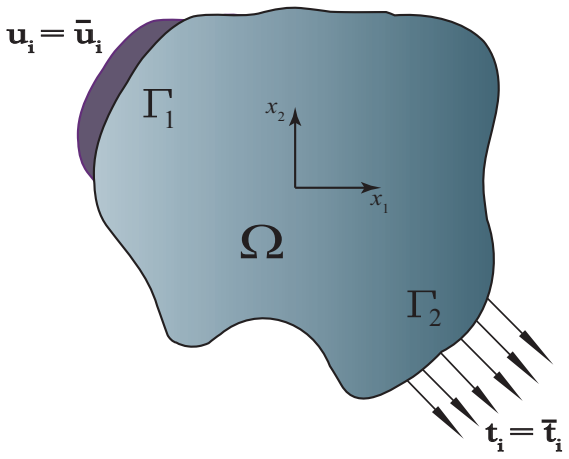

Figure 3.1: Boundary condition for elastostatics analysis

$$\int_{\Omega} (\sigma_{ij,j} + b_i) u_i^* d\Omega = 0 \tag{3.9}$$

Integrating by parts for equation (3.9) will result in

$$\int_{\Gamma} \sigma_{ij} n_j u_i^* d\Gamma - \int_{\Omega} \sigma_{ij} u_{i,j}^* d\Omega + \int_{\Omega} b_i u_i^* d\Omega = 0 \tag{3.10}$$

Using the relations from equation (3.3), the above equation can be written as follow:

$$\int_{\Gamma} \sigma_{ij} n_j u_i^* d\Gamma - \int_{\Omega} \left(\frac{2\mu\nu}{1-2\nu} \varepsilon_{kk} \delta_{ij} + 2\mu\varepsilon_{ij} \right) u_{i,j}^* d\Omega + \int_{\Omega} b_i u_j^* d\Omega = 0 \tag{3.11}$$

Integrating by parts for the second integral of equation (3.11) and with property of strain and displacement defined in equation (3.2):

$$\begin{aligned} &\int_{\Gamma} \sigma_{ij} n_j u_i^* d\Gamma - \int_{\Gamma} \left(\frac{2\mu\nu}{1-2\nu} u_k n_k \delta_{ij} + \mu(u_i n_j + u_i n_i) \right) u_{i,j}^* d\Gamma \\ &+ \int_{\Omega} \left(\frac{2\mu\nu}{1-2\nu} u_k \delta_{ij} u_{i,jk}^* + \mu(u_i u_{i,jj}^* + u_j u_{i,ij}^*) \right) d\Omega + \int_{\Omega} b_i u_j^* d\Omega \\ =&0 \end{aligned} \tag{3.12}$$

Using again the stress-displacement equation (3.6) and the property of Kronecker Delta function in equation (3.5), it can be shown that [5]:

$$\int_{\Gamma}\left(\frac{2\mu\nu}{1-2\nu}u_k n_k \delta_{ij}+\mu(u_i n_j+u_i n_i)\right)u^*_{i,j}d\Gamma=\int_{\Gamma}u_i T^*_i d\Gamma \tag{3.13}$$

and

$$\int_{\Omega}\left(\frac{2\mu\nu}{1-2\nu}u_k \delta_{ij}u^*_{i,jk}+\mu(u_i u^*_{i,jj}+u_j u^*_{i,ij})\right)d\Omega=\int_{\Gamma}u_i \sigma^*_{ij,j}d\Omega \tag{3.14}$$

Now introducing the above equations into equation (3.12) gives:

$$\int_{\Gamma}t_i u^*_i d\Gamma-\int_{\Gamma}u_i T^*_i d\Gamma+\int_{\Omega}u_i \sigma^*_{ij,j}d\Omega+\int_{\Omega}b_i u^*_i d\Omega=0 \tag{3.15}$$

The fundamental state $(\cdot)^*$ is defined for concentrated generalized loads, at an arbitrary point $\mathbf{X}'$, $\mathbf{X}' \in \Omega$. After introducing the direction of the load j in equation (3.15):

$$\begin{aligned}&\int_{\Gamma}t_i(\mathbf{x})u^*_{ij}(\mathbf{X}',\mathbf{x})d\Gamma(\mathbf{x})-\int_{\Gamma}u_i(x)T^*_{ij}(\mathbf{X}',\mathbf{x})d\Gamma(\mathbf{x})\\&+\int_{\Omega}u_i(\mathbf{X})\sigma^*_{ijj,j}(\mathbf{X}',\mathbf{X})d\Omega(\mathbf{X})+\int_{\Omega}b_i(\mathbf{X})u^*_{ij}(\mathbf{X}',\mathbf{X})d\Omega(\mathbf{X})\\=&0\end{aligned} \tag{3.16}$$

The fundamental state $(\cdot)^*$ is chosen such that:

$$\sigma^*_{ijj,j}(\mathbf{X}',\mathbf{X})+\triangle(\mathbf{X}',\mathbf{X})e_{ij}=0 \tag{3.17}$$

where $\triangle(\mathbf{X}',\mathbf{X})$ is known as the Dirac Delta function, with a property as:

$$\int_{\Omega}g(\mathbf{X})\triangle(\mathbf{X}',\mathbf{X})d\Omega=g(\mathbf{X}') \tag{3.18}$$

and the unit vector component e_{ij} in equation (3.17) corresponds to a unit positive force in the j direction applied at $\mathbf{X}'$ and $\mathbf{X}$. The displacement and traction fields corresponding to the point force solution can be written as

$$u_i^* = U_{ij}(\mathbf{X}', \mathbf{x})e_j \tag{3.19}$$

and

$$t_i^* = T_{ij}(\mathbf{X}', \mathbf{x})e_j \tag{3.20}$$

Equation (3.15) can be written for an internal source point $\mathbf{X}'$ as follows:

$$\begin{aligned} u_i(\mathbf{X}') = &\int_\Gamma U_{ij}(\mathbf{X}', \mathbf{x})t_j(\mathbf{x})d\Gamma(\mathbf{x}) - \int_\Gamma T_{ij}(\mathbf{X}', \mathbf{x})u_j(\mathbf{x})d\Gamma(\mathbf{x}) \\ &+ \int_\Omega U_{ij}(\mathbf{X}', \mathbf{X})b_j(\mathbf{X})d\Omega(\mathbf{X}) \end{aligned} \tag{3.21}$$

The above equation is known as Somigliana's identity for displacements, where $U(\mathbf{X}', \mathbf{x})$ and $T_{ij}(\mathbf{X}', \mathbf{x})$, are the fundamental solutions. They represent displacements or tractions at the field point $\mathbf{x}$ or $\mathbf{X}$ in the direction i due to unit load applied at the source point $\mathbf{X}'$ in the direction j, and are given by:

$$U_{ij}(\mathbf{X}', \mathbf{x}) = \frac{1}{8\pi\mu(1-\nu)} \left\{ r_{,i}r_{,j} - (3-4\nu)\ln(\frac{1}{r})\delta_{ij} \right\} \tag{3.22}$$

$$\begin{aligned} T_{ij}(\mathbf{X}', \mathbf{x}) = &\frac{-1}{4\pi(1-\nu)r} \left\{ \frac{\partial r}{\partial \mathrm{n}} \left[(1-2\nu)\delta_{ij} \right.\right. \\ &\left.\left. + 2r_{,i}r_{,j} - (1-2\nu)(\mathrm{n}_j r_{,i} - \mathrm{n}_i r_{,j}) \right] \right\} \end{aligned} \tag{3.23}$$

where the distance r , from the source point $\mathbf{X}'$ to the field point $\mathbf{x}$, as shown in Figure 3.2, is given by:

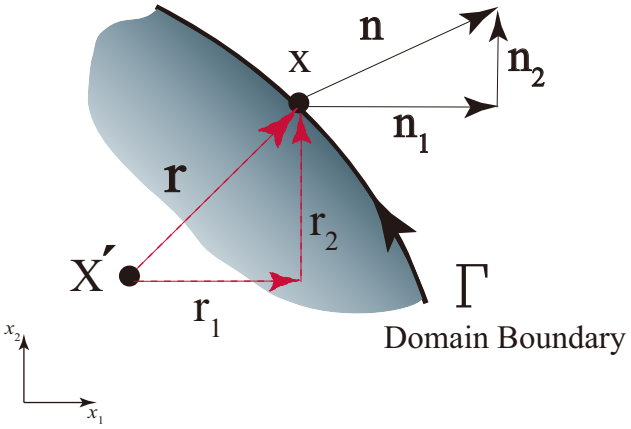

Figure 3.2: Components of the distance and normal vector

$$r = \sqrt{r_i r_i} \tag{3.24}$$

where the Cartesian components are defined by

$$r_i = x_i(\mathbf{x}) - x_i(\mathbf{X}') \tag{3.25}$$

The normal derivatives of this distance, used in the equation (3.23), are defined to be

$$\frac{\partial r}{\partial \mathbf{n}} = \frac{\partial r}{\partial x_i} \mathrm{n}_i = r_{,i} \mathrm{n}_i \tag{3.26}$$

where the terms n_i are the coordinate components of the unit outward normal $\mathbf{n}$, as shown in Figure 3.2 and

$$r_{,i} = \frac{\partial r}{\partial x_i} = \frac{x_i}{r} \tag{3.27}$$

Somigliana's identity (3.35) gives the displacement at an internal point in terms of boundary displacement and traction values.

3.2.3 The displacement boundary integral equation

A boundary equation can be obtained from Somigliana's identity by moving the source point $\mathbf{X}'$ to the boundary Γ. This can be achieved by considering the limiting process as $\mathbf{X}' \rightarrow \mathbf{x}' \in \Gamma$. Replacing the domain at the boundary source point, with a small circular or spherical region of radius ϵ, as shown in Figure 3.3, the boundary Γ may be written as

$$\Gamma = \lim_{\epsilon \rightarrow 0}(\Gamma - \Gamma_\epsilon^* + \Gamma_\epsilon) \tag{3.28}$$

where Γ_ϵ^* is the portion of the boundary removed by the augmented region.

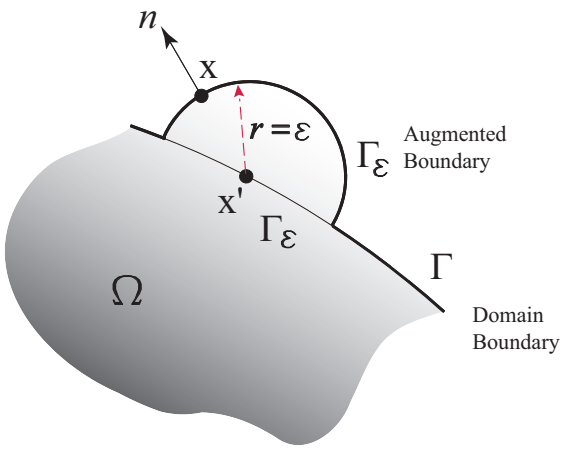

Figure 3.3: The augmented boundary at the source node

Using this boundary expression in the integral containing T_{ij} term gives

$$\begin{aligned}\int_\Gamma T_{ij}(\mathbf{x}', \mathbf{x}) u_j(\mathbf{x}) d\Gamma(\mathbf{x}) =& \lim_{\epsilon \rightarrow 0} \left\{ \int_{\Gamma - \Gamma_\epsilon^*} T_{ij}(\mathbf{x}', \mathbf{x}) u_j(\mathbf{x}) d\Gamma(\mathbf{x}) \right\} \\ &+ \lim_{\epsilon \rightarrow 0} \left\{ \int_{\Gamma_\epsilon} T_{ij}(\mathbf{x}', \mathbf{x}) \left[u_j(\mathbf{x}) - u_j(\mathbf{x}') \right] d\Gamma(\mathbf{x}) \right\} \\ &+ u_j(\mathbf{x}') \lim_{\epsilon \rightarrow 0} \left\{ \int_{\Gamma_\epsilon} T_{ij}(\mathbf{x}', \mathbf{x}) d\Gamma(\mathbf{x}) \right\} \\ =& \mathrm{I}^1 + \mathrm{I}^2 + \mathrm{I}^3 \end{aligned} \tag{3.29}$$

Integral (I^2) is regular, assuming that the displacements satisfy Hölder continuity,

$$|u_i(X') - u_i(x')| < Ar^n; A = constant > 1,\ 0 < n \leq 1$$

and it vanishes in the limiting process. The first integral in the expansion (I^1) can be integrated in the Cauchy principle value sense, ie:

$$\lim_{\epsilon \to 0} \left\{ \int_{(\Gamma - \Gamma_\epsilon^*)} T_{ij}(\mathbf{x}', \mathbf{x}) u_j(\mathbf{x}) d\Gamma(\mathbf{x}) \right\} = \fint_\Gamma T_{ij}(\mathbf{x}', \mathbf{x}) u_j(\mathbf{x}) d\Gamma(\mathbf{x}) \tag{3.30}$$

Finally, (I^3) can be integrated analytically by transformation to a local polar coordinate system centered on the source node $\mathbf{x}'$, giving:

$$I^3 = u_j(\mathbf{x}') \lim_{\epsilon \to 0} \left\{ \int_{\Gamma_\epsilon} T_{ij}(\mathbf{x}', \mathbf{x}) d\Gamma(\mathbf{x}) \right\} = \alpha_{ij}(\mathbf{x}') u_j(\mathbf{x}') \tag{3.31}$$

where $\alpha_{ij}(\mathbf{x}') = -\frac{1}{2}$ for a point $\mathbf{x}'$ on a smooth boundary.

A similar procedure can be carried out for the second integral in Somigliana's Identity, i.e. the integral containing the U_{ij} kernel. Here however, there is no jump term produced in the limiting process. Thus the basic boundary displacement equation can be written as [5]:

$$\begin{aligned} &C_{ij}(\mathbf{x}') u_j(\mathbf{x}') + \fint_\Gamma T_{ij}(\mathbf{x}', \mathbf{x}) u_j(\mathbf{x}) d\Gamma(\mathbf{x}) \\ &= \int_\Gamma U_{ij}(\mathbf{x}', \mathbf{x}) t_j(\mathbf{x}) d\Gamma(\mathbf{x}) + \int_\Omega U_{ij}(\mathbf{x}', \mathbf{X}) b_i(\mathbf{X}) d\Omega(\mathbf{X}) \end{aligned} \tag{3.32}$$

where $\fint_\Gamma$ stands for Cauchy principle value integral, $C_{ij}(\mathbf{x}')$ is a tensor, dependent on the boundary shape at the source point $\mathbf{x}'$ and is known as the jump term. Equation (3.32) is the basic boundary element equation of elasticity, giving an implicit relationship for the boundary displacement and tractions values.

3.2.4 Formulation of the dual boundary integral equations

In the analysis of crack domain, Blandford et al. [17] proposed a method based on a multi-region formulation which was used extensively up to early 1990s. They sub-divided the domain along the crack boundary, in order to avoid a singular system of equations. BEM analysis would then be performed in each-domain separately and a system of equations formed from combining these sub-regions. This sub-division is used in order to avoid duplicate equations being formed on the crack faces, see Aliabadi and Rooke [6]. However, using these sub-domains, extra unknowns are introduced into the system along the subdivision, thus increasing the matrix size.

The Dual Boundary Element Method (DBEM) has been developed to overcome the problems created by the analysis of crack domains without the need to use sub-regions [86]. The usual displacement equation is now replaced with the traction equation on one of the crack surfaces. In order to formulate this traction equation, initially the internal stress equation will be derived. Then this equation, with the displacement equation, will be evaluated for a source point $\mathbf{x}'$ on a smooth crack boundary to give the DBEM equations.

Differentiation of Somigliana's identity (3.21), with respect to the source point $\mathbf{X}'$ gives:

$$u_{i,k}(\mathbf{X}') = \int_\Gamma U_{ij,k}(\mathbf{X}', \mathbf{x}) t_j(\mathbf{x}) d\Gamma(\mathbf{x}) - \int_\Gamma T_{ij,k}(\mathbf{X}', \mathbf{x}) u_j(\mathbf{x}) d\Gamma(\mathbf{x}) + \int_\Omega U_{ij,k}(\mathbf{X}', \mathbf{X}) b_j(\mathbf{X}) d\Omega(\mathbf{X}) \tag{3.33}$$

where $U_{ij,k}$ and $T_{ij,k}$ are derivatives of the fundamental solution, also taken with respect to the source point $\mathbf{X}'$. The stress at a point $\mathbf{x}$ was given in equation (3.3) by:

$$\sigma_{ij}(\mathbf{x}) = \frac{2\mu\nu}{(1-2\nu)}\delta_{ij}\frac{\partial u_l(\mathbf{x})}{\partial x_l(\mathbf{x})} + \mu\left(\frac{\partial u_i(\mathbf{x})}{\partial x_j(\mathbf{x})} + \frac{\partial u_j(\mathbf{x})}{\partial x_i(\mathbf{x})}\right) \tag{3.34}$$

Substitution of equation (3.34) into (3.33), allow the stress at internal points to be written as:

$$\begin{aligned}\sigma_{ij}(\mathbf{X}') = &\int_\Gamma D_{kij}(\mathbf{X}', \mathbf{x}) t_k(\mathbf{x}) d\Gamma(\mathbf{x}) - \int_\Gamma S_{kij}(\mathbf{X}', \mathbf{x}) u_k(\mathbf{x}) d\Gamma(\mathbf{x}) \\ &+ \int_\Omega D_{kij}(\mathbf{X}', \mathbf{X}) b_k(\mathbf{X}) d\Omega(\mathbf{X})\end{aligned} \tag{3.35}$$

For two dimensional problems, the terms D_{kij} and S_{kij} are formed from the derivatives terms $U_{ij,k}$ and $T_{ij,k}$, and are given by:

$$D_{kij}(\mathbf{X}', \mathbf{x}) = \frac{1}{4\pi(1-\nu)r}\left\{(1-2\nu)(\delta_{ik}r_{,j} + \delta_{jk}r_{,i} - \delta_{ij}r_{,k}) + 2r_{,i}r_{,j}r_{,k}\right\} \tag{3.36}$$

$$\begin{aligned}S_{kij}(\mathbf{X}', \mathbf{x}) = &\frac{E}{4\pi(1-\nu^2)r^2}\left\{2\frac{\partial r}{\partial \mathbf{n}}\left[(1-2\nu)\,\delta_{ij}r_{,k} + \nu\left(\delta_{ik}r_{,j} + \delta_{jk}r_{,i}\right) - 4r_{,i}r_{,j}r_{,k}\right]\right. \\ &+ \left[2\nu r_{,j}r_{,k} + (1-2\nu)\,\delta_{jk}\right]\mathrm{n}_i + \left[2\nu r_{,i}r_{,k} + (1-2\nu)\,\delta_{ik}\right]\mathrm{n}_j \\ &\left.+ \left[2\,(1-2\nu)\,r_{,i}r_{,j} - (1-4\nu)\,\delta_{ij}\right]\mathrm{n}_k\right\}\end{aligned} \tag{3.37}$$

3.2.5 Dual boundary integral equations

In order to use the dual boundary integral equations, it is necessary to transfer equations (3.21) and (3.35) to the crack boundary. Consider that the boundary at a point $\mathbf{x}'$ is augmented by a circle region of radius ϵ and the boundary Γ'_ϵ , and at the opposite node $\mathbf{x}''$ by another region of radius ϵ and the boundary Γ''_ϵ, as shown in Figure 3.4. Then the boundary Γ can be written as:

$$\Gamma = \lim_{\epsilon\to 0}\left[\Gamma - \Gamma'^{*}_\epsilon - \Gamma''^{*}_\epsilon + \Gamma'_\epsilon + \Gamma''_\epsilon\right] \tag{3.38}$$

where Γ'^{*}_{ϵ} and Γ''^{*}_{ϵ} are shown in Figure 3.4. The effect of letting the source point approach the boundary will be investigated for the displacement equation and then subsequently for the stress equations.

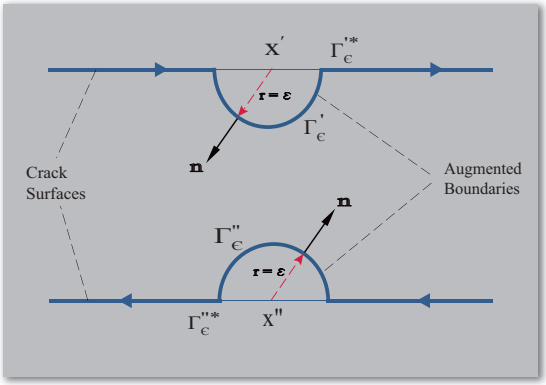

Figure 3.4: The augmented boundaries on the crack faces

Displacement equation on the crack

In the displacement equation, the jump terms are only produced by the integral containing $T_{ij}(\mathbf{x}', \mathbf{x})$ kernel, giving the jump terms as the source point $\mathbf{X}'$ approaches the boundary Γ. This integral may be written for a source point on a crack, as

$$\begin{aligned}\int_{\Gamma} T_{ij}(\mathbf{x}', \mathbf{x}) u_j(\mathbf{x}) d\Gamma(\mathbf{x}) =& \lim_{\epsilon \to 0} \left\{ \int_{(\Gamma - \Gamma'^{*}_{\epsilon} - \Gamma''^{*}_{\epsilon})} T_{ij}(\mathbf{x}', \mathbf{x}) u_j(\mathbf{x}) d\Gamma(\mathbf{x}) \right\} \\ &+ \lim_{\epsilon \to 0} \left\{ \int_{\Gamma'_{\epsilon}} T_{ij}(\mathbf{x}', \mathbf{x}) \left[u_j(\mathbf{x}) - u_j(\mathbf{x}') \right] d\Gamma(\mathbf{x}) \right\} \\ &+ u_j(\mathbf{x}') \lim_{\epsilon \to 0} \left\{ \int_{\Gamma'_{\epsilon}} T_{ij}(\mathbf{x}', \mathbf{x}) d\Gamma(\mathbf{x}) \right\} \\ &+ \lim_{\epsilon \to 0} \left\{ \int_{\Gamma''_{\epsilon}} T_{ij}(\mathbf{x}', \mathbf{x}) \left[u_j(\mathbf{x}) - u_j(\mathbf{x}'') \right] d\Gamma(\mathbf{x}) \right\} \\ &+ u_j(\mathbf{x}'') \lim_{\epsilon \to 0} \left\{ \int_{\Gamma''_{\epsilon}} T_{ij}(\mathbf{x}', \mathbf{x}) d\Gamma(\mathbf{x}) \right\} \\ =& \mathrm{I}^1 + \mathrm{I}^2 + \mathrm{I}^3 + \mathrm{I}^4 + \mathrm{I}^5 \end{aligned} \tag{3.39}$$

Integrals (I^2) and (I^4) are regular and vanish in the limiting process. The first integral (I^1) can be evaluated in the Cauchy principle value sense, ie:

$$\lim_{\epsilon\to 0}\left\{\int_{(\Gamma-\Gamma'^{*}_{\epsilon}-\Gamma''^{*}_{\epsilon})} T_{ij}(\mathbf{x}',\mathbf{x})u_j(\mathbf{x})d\Gamma(\mathbf{x})\right\} = \cancel{\int_{\Gamma}} T_{ij}(\mathbf{x}',\mathbf{x})u_j(\mathbf{x})d\Gamma(\mathbf{x}) \tag{3.40}$$

Integral (I^3) and (I^5) can be computed analytically around the circular boundary to give the jump terms on the boundary. A coordinate transformation is made to a local system of polar coordinates and use of analytical integration gives the terms (I^3) and (I^5) to be

$$I^3 = u_j(\mathbf{x}')\lim_{\epsilon\to 0}\left\{\int_{\Gamma'_{\epsilon}} T^{*}_{ij}(\mathbf{x}',\mathbf{x})d\Gamma(\mathbf{x})\right\} = -\frac{1}{2}u_i(\mathbf{x}') \tag{3.41}$$

$$I^5 = u_j(\mathbf{x}'')\lim_{\epsilon\to 0}\left\{\int_{\Gamma''_{\epsilon}} T^{*}_{ij}(\mathbf{x}',\mathbf{x})d\Gamma(\mathbf{x})\right\} = \frac{1}{2}u_i(\mathbf{x}'') \tag{3.42}$$

The stress equation on the boundary

$$\begin{aligned}\int_{\Gamma} D_{kij}(\mathbf{x}',\mathbf{x})t_k(\mathbf{x})d\Gamma(\mathbf{x}) = &\lim_{\epsilon\to 0}\left\{\int_{(\Gamma-\Gamma'^{*}_{\epsilon}-\Gamma''^{*}_{\epsilon})} D_{kij}(\mathbf{x}',\mathbf{x})t_k(\mathbf{x})d\Gamma(\mathbf{x})\right\}\\ &+\lim_{\epsilon\to 0}\left\{\int_{\Gamma'_{\epsilon}} D_{kij}(\mathbf{x}',\mathbf{x})\left[t_k(\mathbf{x})-t_k(\mathbf{x}')\right]d\Gamma(\mathbf{x})\right\}\\ &+t_k(\mathbf{x}')\lim_{\epsilon\to 0}\left\{\int_{\Gamma'_{\epsilon}} D_{kij}(\mathbf{x}',\mathbf{x})d\Gamma(\mathbf{x})\right\}\\ &+\lim_{\epsilon\to 0}\left\{\int_{\Gamma''_{\epsilon}} D_{kij}(\mathbf{x}',\mathbf{x})_l\left[t_k(\mathbf{x})-t_k(\mathbf{x}'')\right]d\Gamma(\mathbf{x})\right\}\\ &+t_k(\mathbf{x}'')\lim_{\epsilon\to 0}\left\{\int_{\Gamma''_{\epsilon}} D_{kij}(\mathbf{x}'',\mathbf{x})d\Gamma(\mathbf{x})\right\}\\ &=J^1+J^2+J^3+J^4+J^5\end{aligned} \tag{3.43}$$

In the same way the S_{kij} integral can also be expanded, using a Taylor expansion of the displacement about the source point, namely

$$\begin{aligned}\int_\Gamma S_{kij}(\mathbf{x}',\mathbf{x})u_k(\mathbf{x})d\Gamma(\mathbf{x}) =& \lim_{\epsilon\to 0}\left\{\int_{(\Gamma-\Gamma'^{*}_{\epsilon}-\Gamma''^{*}_{\epsilon})} S_{kij}(\mathbf{x}',\mathbf{x})u_k(\mathbf{x})d\Gamma(\mathbf{x})\right\}\\ &+\lim_{\epsilon\to 0}\left\{\int_{\Gamma'_\epsilon} S_{kij}(\mathbf{x}',\mathbf{x})\left[u_k(\mathbf{x})-u_k(\mathbf{x}')\right.\right.\\ &\left.\left.-u_{k,l}(\mathbf{x}')(\mathbf{x}_l-\mathbf{x}'_l)\right]d\Gamma(\mathbf{x})\right\}\\ &+u_k(\mathbf{x}')\lim_{\epsilon\to 0}\left\{\int_{\Gamma'_\epsilon} S_{kij}(\mathbf{x}',\mathbf{x})d\Gamma(\mathbf{x})\right\}\\ &+u_{k,l}(\mathbf{x}')\lim_{\epsilon\to 0}\left\{\int_{\Gamma'_\epsilon} S_{kij}(\mathbf{x}',\mathbf{x})(\mathbf{x}_l-\mathbf{x}'_l)d\Gamma(\mathbf{x})\right\}\\ &+\lim_{\epsilon\to 0}\left\{\int_{\Gamma''_\epsilon} S_{kij}(\mathbf{x}'',\mathbf{x})\left[u_k(\mathbf{x})-u_k(\mathbf{x}'')\right.\right.\\ &\left.\left.-u_{k,l}(\mathbf{x}'')(\mathbf{x}_l-\mathbf{x}''_l)\right]d\Gamma(\mathbf{x})\right\}\\ &+u_k(\mathbf{x}'')\lim_{\epsilon\to 0}\left\{\int_{\Gamma''_\epsilon} S_{kij}(\mathbf{x}',\mathbf{x})d\Gamma(\mathbf{x})\right\}\\ &+u_{k,l}(\mathbf{x}'')\lim_{\epsilon\to 0}\left\{\int_{\Gamma''_\epsilon} S_{kij}(\mathbf{x}',\mathbf{x})(\mathbf{x}_l-\mathbf{x}''_l)d\Gamma(\mathbf{x})\right\}\\ =&\mathrm{I}^1+\mathrm{I}^2+\mathrm{I}^3+\mathrm{I}^4+\mathrm{I}^5+\mathrm{I}^6+\mathrm{I}^7 \end{aligned} \tag{3.44}$$

In these equations, integrals (J^2), (J^4), (I^2) and (I^5) are regular under the basic assumptions about the continuity of the traction and displacement fields. These integrals will all vanish in the limit as $\epsilon \to 0$. The first term in the expansion of the D_{kij} integral can be evaluated in the Cauchy principal value sense. This is written as:

$$\int\!\!\!\!\!\!-_\Gamma D_{kij}(\mathbf{x}',\mathbf{x})t_k(\mathbf{x})d\Gamma(\mathbf{x}) = \lim_{\epsilon\to 0}\left\{\int_{(\Gamma-\Gamma'^{*}_{\epsilon}-\Gamma''^{*}_{\epsilon})} D_{kij}(\mathbf{x}',\mathbf{x})t_k(\mathbf{x})d\Gamma(\mathbf{x})\right\} \tag{3.45}$$

In the expansion of the S_{kij} integral, the terms (I^3) and (I^6) can be written in the form,

$$u_k(\mathbf{x}')\lim_{\epsilon\to 0}\left\{\int_{\Gamma'_\epsilon} S_{kij}(\mathbf{x}',\mathbf{x})d\Gamma(\mathbf{x})\right\} = u_k(\mathbf{x}')\lim_{\epsilon\to 0}\left\{\frac{\zeta'_{kij}}{\epsilon}\right\} \tag{3.46}$$

$$u_k(\mathbf{x}'')\lim_{\epsilon\to 0}\left\{\int_{\Gamma''_\epsilon} S_{kij}(\mathbf{x}',\mathbf{x})d\Gamma(\mathbf{x})\right\} = u_k(\mathbf{x}'')\lim_{\epsilon\to 0}\left\{\frac{\zeta''_{kij}}{\epsilon}\right\} \tag{3.47}$$

where

$$\zeta'_{kij} = -\zeta''_{kij} = \frac{E}{4\pi(1-\nu^2)r^2}\int_0^\pi (\delta_{ij}r_{,k} + \delta_{ik}r_{,j} + \delta_{jk}r_{,i} - 4r_{,i}r_{,j}r_{,k})d\theta \tag{3.48}$$

Terms (3.46) and (3.47) are unbounded but may be considered with the integral (I^1) in the Hadamard principal value sense and are written as

$$\begin{aligned}\neq\!\!\!\!\!\!\int_\Gamma S_{kij}(\mathbf{x}',\mathbf{x})u_k(\mathbf{x})d\Gamma(\mathbf{x}) = \lim_{\epsilon\to 0}\Bigg\{&\int_{(\Gamma-\Gamma'^*_\epsilon-\Gamma''^*_\epsilon)} S_{kij}(\mathbf{x}',\mathbf{x})u_k(\mathbf{x})d\Gamma(\mathbf{x}) \\ &+u_k(\mathbf{x}')\frac{\zeta'_{kij}}{\epsilon}+u_k(\mathbf{x}'')\frac{\zeta''_{kij}}{\epsilon}\Bigg\}\end{aligned} \tag{3.49}$$

These terms will be considered together in the analytical integration in the next section. Integrals (J^3), (J^5), (I^4) and (I^7) can be computed analytically around the circular boundary. This is done by transformation of the coordinate to the local system. (J^3) integral is given by

$$\begin{aligned}\mathrm{J}^3 =&\sigma_{kl}(\mathbf{x}')\lim_{\epsilon\to 0}\left\{\int_{\Gamma'_\epsilon} D_{kij}(\mathbf{x}',\mathbf{x})\mathrm{n}_l(\mathbf{x})d\Gamma(\mathbf{x})\right\} \\ =&\frac{1}{16(1-\nu)}\begin{bmatrix} (5-4\nu)\sigma_{11}(\mathbf{x}') - (1-4\nu)\sigma_{22}(\mathbf{x}') & 2(1-4\nu)\sigma_{12}(\mathbf{x}') \\ 2(1-4\nu)\sigma_{12}(\mathbf{x}') & -(1-4\nu)\sigma_{11}(\mathbf{x}') + (5-4\nu)\sigma_{22}(\mathbf{x}') \end{bmatrix}\end{aligned} \tag{3.50}$$

In the same way, on the opposite crack face (J^5) is given by

$$\begin{aligned} J^5 =& \sigma_{kl}(\mathbf{x}'') \lim_{\epsilon \to 0} \left\{ \int_{\Gamma''_\epsilon} D_{kij}(\mathbf{x}', \mathbf{x}) n_l(\mathbf{x}) d\Gamma(\mathbf{x}) \right\} \\ =& \frac{-1}{16(1-\nu)} \Bigg[\\ & \begin{matrix} (5-4\nu)\sigma_{11}(\mathbf{x}') - (1-4\nu)\sigma_{22}(\mathbf{x}') & 2(1-4\nu)\sigma_{12}(\mathbf{x}') \\ 2(1-4\nu)\sigma_{12}(\mathbf{x}') & -(1-4\nu)\sigma_{11}(\mathbf{x}') + (5-4\nu)\sigma_{22}(\mathbf{x}') \end{matrix} \Bigg] \end{aligned} \tag{3.51}$$

Similarly, the terms in the S_{kij} integral expansion, (I^4) and (I^7), can also be computed analytically using the transformation of coordinates.

$$\begin{aligned} I^4 &= u_{k,l}(\mathbf{x}') \lim_{\epsilon \to 0} \left\{ \int_{\Gamma'_\epsilon} S_{kij}(\mathbf{x}', \mathbf{x})(\mathbf{x}_l - \mathbf{x}'_l) d\Gamma(\mathbf{x}) \right\} \\ &= -\frac{E}{16(1-\nu^2)} \begin{bmatrix} 3u_{1,1}(\mathbf{x}') + u_{2,2}(\mathbf{x}') & u_{1,2}(\mathbf{x}') + u_{2,1}(\mathbf{x}') \\ u_{1,2}(\mathbf{x}') + u_{2,1}(\mathbf{x}') & u_{1,1}(\mathbf{x}') + 3u_{2,2}(\mathbf{x}') \end{bmatrix} \end{aligned} \tag{3.52}$$

On the opposite crack face the term is given by

$$\begin{aligned} I^7 &= u_{k,l}(\mathbf{x}'') \lim_{\epsilon \to 0} \left\{ \int_{\Gamma''_\epsilon} S_{kij}(\mathbf{x}'', \mathbf{x})(\mathbf{x}_l - \mathbf{x}''_l) d\Gamma(x) \right\} \\ &= \frac{E}{16(1-\nu^2)} \begin{bmatrix} 3u_{1,1}(\mathbf{x}') + u_{2,2}(\mathbf{x}') & u_{1,2}(\mathbf{x}') + u_{2,1}(\mathbf{x}') \\ u_{1,2}(\mathbf{x}') + u_{2,1}(\mathbf{x}') & u_{1,1}(\mathbf{x}') + 3u_{2,2}(\mathbf{x}') \end{bmatrix} \end{aligned} \tag{3.53}$$

Summing these four integrals and making use of the stress-strain relationships (3.3) gives the jump terms on the crack to be

$$d_{ij}(\mathbf{x}') = I^4 - J^3 = \frac{1}{2}\sigma_{ij}(\mathbf{x}') \tag{3.54}$$

$$d_{ij}(\mathbf{x}'') = I^7 - J^5 = -\frac{1}{2}\sigma_{ij}(\mathbf{x}'') \tag{3.55}$$

The dual boundary integral equation

The preceding analysis allows the two equations (3.15) and (3.35) to be written for a source point $\mathbf{x}'$ on a smooth crack boundary. This gives the displacement equation, in the absence of body force on a smooth crack, to be

$$\begin{aligned}&\frac{1}{2}u_i(\mathbf{x}') + \frac{1}{2}u_i(\mathbf{x}'') + \int\!\!\!\!\!\!-_{\Gamma} T_{ij}(\mathbf{x}', \mathbf{x})u_j(\mathbf{x})\, d\Gamma(\mathbf{x}) \\ &= \int_{\Gamma} U_{ij}(\mathbf{x}', \mathbf{x})t_j(\mathbf{x})\, d\Gamma(\mathbf{x})\end{aligned} \tag{3.56}$$

and the boundary stress equation for the at the source point $\mathbf{x}'$ on crack face is given by

$$\begin{aligned}&\frac{1}{2}\sigma_{ij}(\mathbf{x}') + \frac{1}{2}\sigma_{ij}(\mathbf{x}'') + \int\!\!\!\!\!\!=_{\Gamma} S_{kij}(\mathbf{x}', \mathbf{x})u_k(\mathbf{x})\, d\Gamma(\mathbf{x}) \\ &= \int\!\!\!\!\!\!=_{\Gamma} D_{kij}(\mathbf{x}', \mathbf{x})t_k(\mathbf{x})\, d\Gamma(\mathbf{x})\end{aligned} \tag{3.57}$$

Multiplication of the stress equation by the normal components at the source point gives the required boundary traction equation

$$\begin{aligned}&\frac{1}{2}t_i(\mathbf{x}') - \frac{1}{2}t_i(\mathbf{x}'') + \mathrm{n}_j(\mathbf{x}') \int\!\!\!\!\!\!=_{\Gamma} S_{kij}(\mathbf{x}', \mathbf{x})u_k(\mathbf{x})\, d\Gamma(\mathbf{x}) \\ &= \mathrm{n}_j(\mathbf{x}') \int\!\!\!\!\!\!=_{\Gamma} D_{kij}(\mathbf{x}', \mathbf{x})t_k(\mathbf{x})\, d\Gamma(\mathbf{x})\end{aligned} \tag{3.58}$$

Equations (3.57) and (3.58) are the two equations used in the DBEM to analyse crack boundaries.

3.3 Numerical implementation in two dimensions

In this section, the dual boundary element method implemented for the two dimensional analysis of crack problems as presented by Portela et al. [86] will be reviewed. The boundary elements that will be used are shown and the discretisation of the boundary integral equations using these boundary elements is presented. The use of these equations is described and the linear system of equations is derived. Finally, analytical integration which is used to evaluate the singular integrals on the crack boundaries will be presented.

3.3.1 Boundary elements

The boundary integral equations, formulated in the preceding sections, are valid for a domain Ω, with boundary Γ. In order to evaluate these equations it is generally necessary to use a numerical integration procedure. The first step required is to divide the boundary, Γ, into a number of line segments, known as boundary elements, see Figure 3.5. The geometry on each of these boundary elements is defined by a set of points or nodes and the variation of function over an element is assumed to satisfy some simple relationship. The simplest type of element, a constant element with a single node at the centre of the element, is found by keeping the function values constant over the entire element. A more sophisticated scheme is produced with a linear variation in the functions with two element nodes used, one at either end of the element.

In this work, the variation in the geometry and unknown functions over the boundary element is assumed to be quadratic. The elements are described by three element nodes, one placed at each end of the element and with the other at the center, as in Figure 3.6. Then, using a univariate, dimensionless variable,

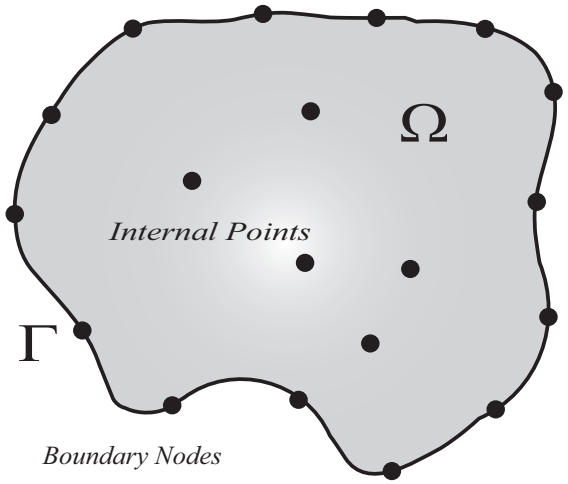

Figure 3.5: Boundary elements and internal points

$\xi(\xi \in [-1,+1])$, to define a point on the element, the global coordinates of the point can be expressed as

$$x_i = M^1(\xi)x_i^1 + M^2(\xi)x_i^2 + M^3(\xi)x_i^3 = \sum_{n=1}^{3} M^n(\xi)x_i^n \tag{3.59}$$

In this equation, the term x_i^n represents the global coordinate of node n in direction i. The expressions $M^n(\xi)$ are known as shape (or interpolation) functions, and for the continuous quadratic element are given by (see Figure 3.6 (a))

$$\begin{aligned} M^1(\xi) &= \frac{\xi(\xi-1)}{2} \\ M^2(\xi) &= (1-\xi)(1+\xi) \\ M^3(\xi) &= \frac{\xi(\xi+1)}{2} \end{aligned} \tag{3.60}$$

In elastostatics analyses, the displacement and traction functions can be written in the local coordinate system as:

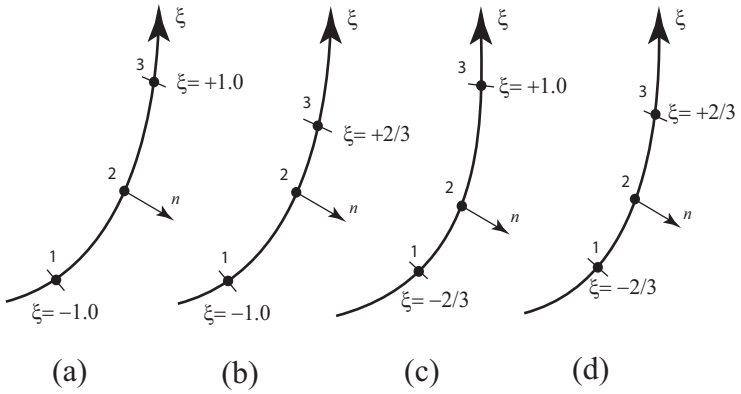

Figure 3.6: Type of quadratic boundary elements

$$u_i(\xi) = \sum_{n=1}^{3} M^n(\xi) u_i^n \tag{3.61}$$

$$t_i(\xi) = \sum_{n=1}^{3} M^n(\xi) t_i^n \tag{3.62}$$

where u_i^n and t_i^n represent the nodal displacement and traction values. These boundary elements enable the integrals to be split into manageable sections. It is also necessary to transform the integrals to the local coordinate system using

$$d\Gamma(\mathbf{x}) = J(\xi) d\xi \tag{3.63}$$

In this expression, $J^\gamma(\xi)$ is the *Jacobian of Transformation* given by

$$J^\gamma(\xi) = \sqrt{\left(\frac{dx_1(\xi)}{d\xi}\right)^2 + \left(\frac{dx_2(\xi)}{d\xi}\right)^2} \tag{3.64}$$

where $\frac{dx_1(\xi)}{d\xi}$ and $\frac{dx_2(\xi)}{d\xi}$ are the derivatives of the global coordinates x_1 and x_2 with respect to the local coordinate ξ, and are given as:

$$\frac{dx_i(\xi)}{d\xi} = \sum_{n=1}^{3} \frac{dM^n(\xi)}{d\xi} x_i^n \tag{3.65}$$

For effective implementation of the dual boundary integral equations (3.56) and (3.58), discontinuous and semi-discontinuous quadratic elements are used for interpolating the displacement and traction fields over the crack surfaces. These are elements where the end nodes, normally placed at $\xi = \pm 1$, are moved inside the element and are at $\xi = \pm\frac{2}{3}$ as in Figure 3.6 (d). This allows the boundary at a crack node to be smooth for any crack shape. The shape functions used for this type of element are given as:

$$\begin{aligned} M^1(\xi) =& \frac{\frac{3}{2}\xi(\frac{3}{2}\xi - 1)}{2} \\ M^2(\xi) =& (1 - \frac{3}{2}\xi)(1 + \frac{3}{2}\xi) \\ M^3(\xi) =& \frac{\frac{3}{2}\xi(\frac{3}{2}\xi + 1)}{2} \end{aligned} \tag{3.66}$$

When bodies with edge cracks are to be analysed, a semi-discontinuous boundary element is used for points where the crack joins the external boundary. These elements are discontinuous along the crack edge only. The shape functions used for this type of element are given as (see Figure 3.6 (b) and (c)):

$$\begin{aligned} M^1(\xi) &= \frac{9}{10}\xi(\xi - 1) & M^1(\xi) &= \frac{3}{5}\xi(\xi - \frac{2}{3}) \\ M^2(\xi) &= -\frac{3}{2}(\xi - 1)(\xi + \frac{2}{3}) & M^2(\xi) &= -\frac{3}{2}(\xi + 1)(\xi - \frac{2}{3}) \\ M^3(\xi) &= \frac{3}{5}\xi(\xi + \frac{2}{3}) & M^3(\xi) &= \frac{9}{10}\xi(\xi + 1) \end{aligned} \tag{3.67}$$

The components of the unit outward normal vector are:

$$\mathrm{n}_1(\xi) = \frac{1}{J^\gamma(\xi)} \frac{dx_2(\xi)}{d\xi} \tag{3.68}$$

$$\mathrm{n}_2(\xi) = -\frac{1}{J^\gamma(\xi)}\frac{dx_1(\xi)}{d\xi} \tag{3.69}$$

3.3.2 Discretised equations

Use of boundary elements enables the boundary integral equations to be written in a discretised form. These discretised equations contain integrals, in the local variable ξ, that may be evaluated using a standard Gaussian quadrature technique. The elastostatics equations can be discretised using quadratic boundary elements. The displacement equation (3.32) on a regular boundary, is written as

$$\begin{aligned} &C_{ij}(\mathbf{x}')u_j(\mathbf{x}') + \sum_{\gamma=1}^{N_e}\sum_{n=1}^{3} u_j^n(\mathbf{x}) \int_{-1}^{+1} T_{ij}(\mathbf{x}', \mathbf{x}(\xi)) M^n(\xi) J^\gamma(\xi) d\xi \\ =&\sum_{\gamma=1}^{N_e}\sum_{n=1}^{3} t_j^n(\mathbf{x}) \int_{-1}^{+1} U_{ij}(\mathbf{x}', \mathbf{x}(\xi)) M^n(\xi) J^\gamma(\xi) d\xi \end{aligned} \tag{3.70}$$

where N_e is the total number of elements, $J^\gamma(\xi)$ is the Jacobian of Transformation and M^n is the shape functions used for this type of element. The displacement equation on a smooth crack, equation (3.56), can be rewritten as:

$$\begin{aligned} &\frac{1}{2}u_i(\mathbf{x}') + \frac{1}{2}u_i(\mathbf{x}'') + \sum_{\gamma=1}^{N_e}\sum_{n=1}^{3} u_j^n(\mathbf{x}) \int_{-1}^{+1} T_{ij}(\mathbf{x}', \mathbf{x}(\xi)) M^n(\xi) J^\gamma(\xi) d\xi \\ =&\sum_{\gamma=1}^{N_e}\sum_{n=1}^{3} t_j^n(\mathbf{x}) \int_{-1}^{+1} U_{ij}(\mathbf{x}', \mathbf{x}(\xi)) M^n(\xi) J^\gamma(\xi) d\xi \end{aligned} \tag{3.71}$$

Finally, the discretised form of traction equation (3.58) on the crack, is given by

$$\frac{1}{2}t_i(\mathbf{x}') - \frac{1}{2}t_i(\mathbf{x}'') + \mathrm{n}_j(\mathbf{x}')\sum_{\gamma=1}^{N_e}\sum_{n=1}^{3} u_k^n(\mathbf{x})\int_{-1}^{+1} S_{kij}(\mathbf{x}', \mathbf{x}(\xi))M^n(\xi)J^\gamma(\xi)d\xi$$

$$=\mathrm{n}_j(\mathbf{x}')\sum_{\gamma=1}^{N_e}\sum_{n=1}^{3} t_k^n(\mathbf{x})\int_{-1}^{+1} D_{kij}(\mathbf{x}', \mathbf{x}(\xi))M^n(\xi)J^\gamma(\xi)d\xi \tag{3.72}$$

In elastostatics, the crack is usually assumed to be traction free. Such assumption aid the computation since the right hand terms are not required for any collocation node, $\mathbf{x}'$, on the crack boundary.

3.3.3 Implementation of the dual boundary element method

The discretised equations (3.70) to (3.72) above can now be used to analyse the relevant elastostatics problems. Using the modelling strategy described earlier, the boundary Γ is discretised giving a series of nodes. At each of these nodes one of the above equations is evaluated. On the outer boundary, the common displacement equation (3.70) is used as in the standard boundary element method. On one of the crack boundaries the second form of the displacement equation (3.71), for a point $\mathbf{x}'$ on a smooth crack, is used. Finally for the source point $\mathbf{x}''$ on the opposite crack face, the traction equation (3.72) is used. Figure 3.7 shows a typical example of crack modelling with discontinuous quadratic boundary elements and the implementation of relevant formulations.

Each of the boundary element equations contains unknown displacement and tractions values. However, from boundary conditions given for each system, one of the values at each node can be found, giving a linear system of equations which may be solved using a standard method. The system can be written in matrix form as

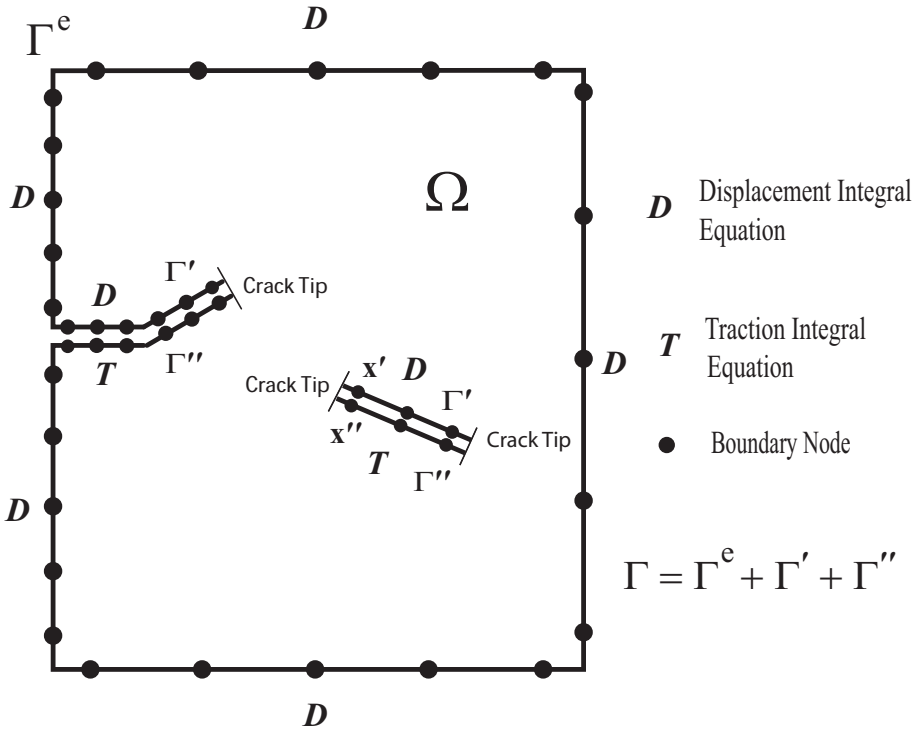

Figure 3.7: Crack modelling with discontinuous quadratic boundary elements

$$\mathbf{A}\ \mathbf{X} = \mathbf{F} \tag{3.73}$$

In this equation, the vector $\mathbf{F}$ is evaluated from the application of the known boundary conditions to the system of equation, $\mathbf{X}$ is the vector of unknown values and $\mathbf{A}$ is the coefficient matrix. Although any standard linear algebraic routine can be used to solve the above system, the *LU Decomposition* method is used here. In this method, the matrix $\mathbf{A}$, is decomposed into two matrices, a lower and an upper triangular matrix such that

$$\mathbf{A} = \mathbf{L}\ \mathbf{U} \tag{3.74}$$

The system can then be decomposed into two problems as

$$\mathbf{L}\ \mathbf{Y} = \mathbf{F}$$
$$\mathbf{U}\ \mathbf{X} = \mathbf{Y} \tag{3.75}$$

which is solved in two stages. Firstly, the vector $\mathbf{Y}$ is evaluated using forward substitution in the first equation; this vector is then used in the second equation and $\mathbf{X}$ is evaluated using backward substitution. This method is used in this work because only the forward and backward substitution will be required for obtaining the derivatives of boundary response with respect to random variables, a more detailed study can be found in Chapter 4 to 6.

3.3.4 Rigid body condition

In the dual boundary element method, special care is needed in order to evaluate certain integrals. If the integration element or field element contains either the source node $\mathbf{x}'$ or the corresponding node on the opposite crack face $\mathbf{x}''$, the integrals become singular. This singularity is due to the kernel containing terms of the form $\frac{1}{r^\alpha}$, where $\alpha > 0$.

With the standard boundary element equation (3.70), a simple numerical technique can be used to evaluate the singular integrals. This technique is obtained by applying a constant displacement field to the entire domain. Using the rigid body condition, traction function values would be zero at all points in the body. Hence, the boundary displacement equation reduces to

$$C_{ij}(\mathbf{x}')u_j(\mathbf{x}') + \sum_{\gamma=1}^{N_e}\sum_{n=1}^{3} u_j^n(\mathbf{x}) \int_{-1}^{+1} T_{ij}(\mathbf{x}', \mathbf{x}(\xi)) M^n(\xi) J^\gamma(\xi) d\xi = 0 \tag{3.76}$$

In this equation the singular integral, i.e. terms when $\mathbf{x}' = \mathbf{x}$, can be computed (with the C_{ij} term) by summation of the remaining terms. This is known as a row sum technique.

However, when the source node $\mathbf{x}'$ is on the crack surface, this technique cannot be used. Since in each equation there are two singular terms, one at $\mathbf{x}' = \mathbf{x}$ and the other at $\mathbf{x}'' = \mathbf{x}$. These terms have the same values, with opposite signs and therefore in the row summation they cancel out each other. This is true for all equations on the crack surface, hence alternative methods of computing these integrals must be used. In two dimensional analyses this integration can be performed analytically if the elements used to model the crack are assumed to be flat.

3.3.5 Analytical integration of crack elements

In two dimensional analyses, the singular integrals are computed analytically with the elements on the crack assumed to be straight, as in Figure 3.8. This allows relationships in the elements to be simplified so that the integrals may be integrated analytically [86, 74, 5].

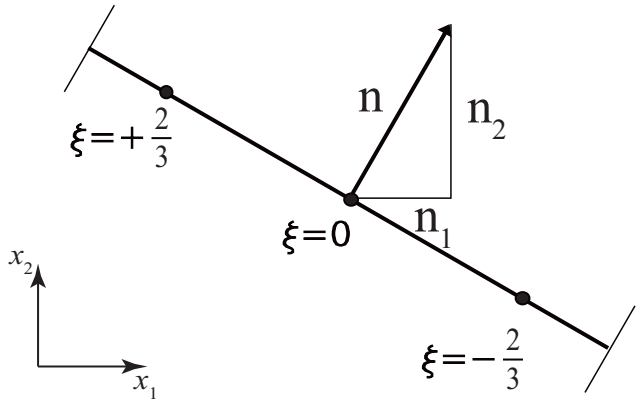

Figure 3.8: Straight boundary elements

On a flat, discontinuous element

$$\begin{aligned} \mathrm{n}_1 = \frac{\partial r}{\partial x_2} &= r_{,2} \\ \mathrm{n}_2 = -\frac{\partial r}{\partial x_1} &= -\, r_{,1} \end{aligned} \tag{3.77}$$

giving

$$\begin{aligned} \mathrm{n}_1^2 + \mathrm{n}_2^2 &= 1 \\ \frac{\partial r}{\partial \mathrm{n}} &= 0 \end{aligned} \tag{3.78}$$

Also the Jacobian $J^\gamma(\xi)$ and the distance term r can be written in terms of the length of the element (l) and the local coordinates of the source and field nodes, ξ' and ξ.

$$J^\gamma(\xi) = \frac{l}{2} \qquad \text{and} \qquad r = \frac{l(\xi - \xi')}{2} \tag{3.79}$$

In elastostatics analyses, since the crack is traction free, the integrals required analytically arise from the T_{ij} and S_{kij} terms in the displacement and traction equation. Using a flat, discontinuous boundary element, the T_{ij} integral can be written as [5]:

$$u_j^n(\mathbf{x}) \int_{-1}^{+1} T_{ij}(\mathbf{x}', \mathbf{x}(\xi)) M^n(\xi) J^\gamma(\xi) d\xi = \frac{1-2\nu}{4\pi(1-\nu)} h_{ij}^n u_j^n \int_{-1}^{+1} \frac{M^n(\xi)}{\xi - \xi'} d\xi \tag{3.80}$$

where $h^n = (h_{ij}^n)$ is given by

$$h = \begin{bmatrix} 0 & -1 \\ 1 & 0 \end{bmatrix} \tag{3.81}$$

The analytical forms of the integral relating to the three discontinuous shape

functions are given by

$$\begin{aligned}
\int_{-1}^{+1} \frac{M^1(\xi)}{\xi - \xi'} d\xi =& \frac{3}{4}\left[\frac{\xi'(3\xi'-2)}{2}\ln\left|\frac{1-\xi'}{1+\xi'}\right| + (3\xi'-2)\right] \\
\int_{-1}^{+1} \frac{M^2(\xi)}{\xi - \xi'} d\xi =& \frac{1}{2}\left[\frac{(3\xi'+2)(3\xi'-2)}{2}\ln\left|\frac{1-\xi'}{1+\xi'}\right| - 9\xi'\right] \\
\int_{-1}^{+1} \frac{M^3(\xi)}{\xi - \xi'} d\xi =& \frac{3}{4}\left[\frac{\xi'(3\xi'+2)}{2}\ln\left|\frac{1-\xi'}{1+\xi'}\right| + (3\xi'+2)\right]
\end{aligned} \tag{3.82}$$

In the same way, the S_{kij} integral can be written as [5]:

$$u_k^n(\mathbf{x}) \int_{-1}^{+1} S_{kij}(\mathbf{x}', \mathbf{x}(\xi)) M^n(\xi) J^\gamma(\xi) d\xi = \frac{E}{4\pi l(1-\nu^2)} h_{kij}^n u_k^n \int_{-1}^{+1} \frac{M^n(\xi)}{(\xi - \xi')^2} d\xi \tag{3.83}$$

where the terms h_{kij}^n are given by

$$h = \begin{bmatrix} h_{111}^n & h_{211}^n \\ h_{122}^n & h_{222}^n \\ h_{112}^n & h_{221}^n \end{bmatrix} = \begin{bmatrix} n_1(2n_2^2+1) & -n_2(-2n_2^2+1) \\ n_1(2n_1^2-1) & -n_2(-2n_1^2-1) \\ -n_2(2n_1^2-1) & n_1(-2n_2^2+1) \end{bmatrix} \tag{3.84}$$

The analytical forms of the S_{kij} integral relating to the three discontinuous shape functions are given by

$$\begin{aligned}
\int_{-1}^{+1} \frac{M^1(\xi)}{(\xi - \xi')^2} d\xi =& \frac{3}{4}\left[(3\xi'-1)\ln\left|\frac{1-\xi'}{1+\xi'}\right| + \frac{6\xi'^2 - 2\xi' - 3}{\xi'^2 - 1}\right] \\
\int_{-1}^{+1} \frac{M^2(\xi)}{(\xi - \xi')^2} d\xi =& \frac{1}{2}\left[9\xi'\ln\left|\frac{1-\xi'}{1+\xi'}\right| - \frac{18\xi'^2 - 13}{\xi'^2 - 1}\right] \\
\int_{-1}^{+1} \frac{M^3(\xi)}{(\xi - \xi')^2} d\xi =& \frac{3}{4}\left[(3\xi'+1)\ln\left|\frac{1-\xi'}{1+\xi'}\right| + \frac{6\xi'^2 + 2\xi' - 3}{\xi'^2 - 1}\right]
\end{aligned} \tag{3.85}$$

3.4 Fracture mechanics

The theory of fracture mechanics provides the link between the strength of the materials, and the analysis of the stresses and strains distribution in the body under the guideline of the mathematical theory of elasticity. A general fracture approach in terms of energy is due to the pioneering work of Griffith [45]. In his early work he postulated that the potential energy (Π) supplied by the strain field and external force when the crack advances a small quantity dA, balances the energy required to form the new surface:

$$\frac{dW_s}{dA} = 2\gamma_s \tag{3.86}$$

where dA is the incremental area, dW_s is the work required to create new surface and $2\gamma_s$ is the surface energy of the material.

In 1956, Irwin [55] modified Griffith's work to deal with practical engineering problem more conveniently. In his work *Energy Release Rate* (G) is used to characterize crack behaviour, which is defined as:

$$G = -\frac{d\Pi}{dA} \tag{3.87}$$

Irwin [56] then proposed three modes of fracture based on the relative movement of the crack faces, as shown in Figure 3.9. Figure 3.9(a) shows the opening mode or mode I, where the crack faces separate along the normal to the crack faces; Figure 3.9(b) corresponds to the sliding mode or mode II, in which the crack faces slide in the plane of the crack; and tearing mode or mode III given in Figure 3.9(c) that corresponds to crack faces sliding in a way which is perpendicular to that of mode II.

It has been demonstrated that the stress field at the crack tip can be expressed

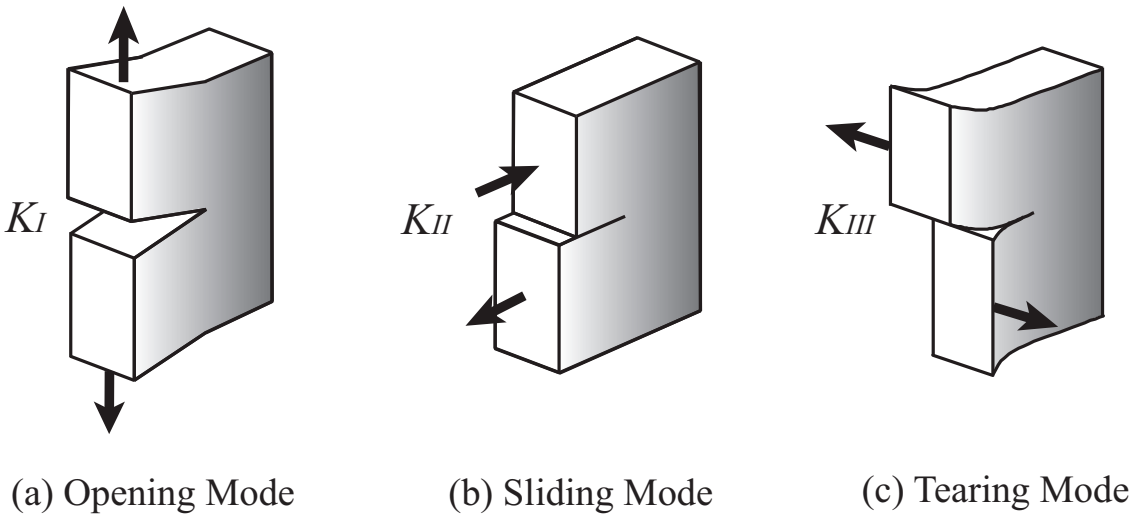

Figure 3.9: Crack deformation modes

in terms of Stress Intensity Factors (SIFs). The 2D analysis was given by Irwin [56] and by Hartranft and Sih [52], for 3D analysis. Taking a coordinate system, centered on the crack tip as shown in Figure 3.10, the stress field at the crack tip can be written as follows:

$$\begin{aligned}\sigma_{11} =& \frac{1}{\sqrt{2\pi r}}\left[K_I \cos\frac{\theta}{2}(1-\sin\frac{\theta}{2}\sin\frac{3\theta}{2})\right.\\ &\left.+K_{II}\sin\frac{\theta}{2}(-2-\cos\frac{\theta}{2}\cos\frac{3\theta}{2})\right]\end{aligned} \tag{3.88}$$

$$\begin{aligned}\sigma_{22} =& \frac{1}{\sqrt{2\pi r}}\left[K_I \cos\frac{\theta}{2}(1+\sin\frac{\theta}{2}\sin\frac{3\theta}{2})\right.\\ &\left.+K_{II}\sin\frac{\theta}{2}\cos\frac{\theta}{2}\cos\frac{3\theta}{2}\right]\end{aligned} \tag{3.89}$$

$$\sigma_{33} = \frac{3-\nu-\kappa(1+\nu)}{4\nu}(\sigma_{11}+\sigma_{22}) \tag{3.90}$$

$$\sigma_{12} = \frac{1}{\sqrt{2\pi r}}\left[K_I \sin\frac{\theta}{2}\cos\frac{\theta}{2}\cos\frac{3\theta}{2}) + K_{II}\cos\frac{3\theta}{2}(1-\sin\frac{\theta}{2}\sin\frac{3\theta}{2})\right] \tag{3.91}$$

$$\sigma_{23} = \frac{1}{\sqrt{2\pi r}} K_{III}\cos\frac{\theta}{2} \tag{3.92}$$

$$\sigma_{13} = \frac{-1}{\sqrt{2\pi r}} K_{III}\sin\frac{\theta}{2} \tag{3.93}$$

and for the displacement field:

$$u_1 = \frac{\sqrt{2\pi r}}{8\pi\mu}\left\{K_I\left[(2\kappa-1)\cos\frac{\theta}{2} - \cos\frac{3\theta}{2}\right] + K_{II}\left[(2\kappa+3)\sin\frac{\theta}{2} + \sin\frac{3\theta}{2}\right]\right\} \tag{3.94}$$

$$u_2 = \frac{\sqrt{2\pi r}}{8\pi\mu}\left\{K_I\left[(2\kappa+1)\sin\frac{\theta}{2} - \sin\frac{3\theta}{2}\right] + K_{II}\left[(3-2\kappa)\cos\frac{\theta}{2} - \cos\frac{3\theta}{2}\right]\right\} \tag{3.95}$$

$$u_3 = \frac{2\sqrt{2\pi r}}{\pi\mu} K_{III}\sin\frac{\theta}{2} \tag{3.96}$$

where r is the distance from the crack tip, θ is the angle measured anticlockwise from the plane of expected crack growth, μ is the shear modulus and $\kappa = 3-4\nu$ for plane stain and $\kappa = (3-\nu)/(1+\nu)$ for plane stress, respectively. K_I,K_{II} and K_{III} are stress intensity factor (SIFs) for fracture mode I, II and III.

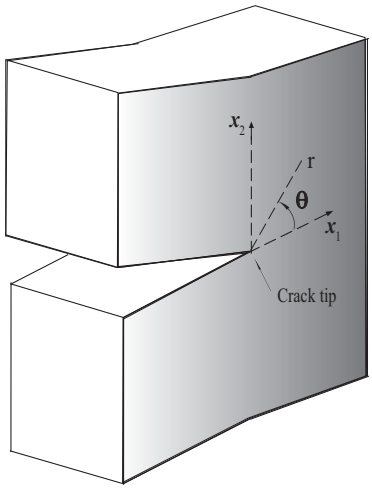

Figure 3.10: Crack tip

The evaluation of SIFs plays a fundamental role in understanding the crack behaviour in the material. There are several methods that can perform accurate SIFs calculation, a comprehensive study of the evaluation of SIFs can be found in Aliabadi and Rooke [6].

The J-integral

One of the most popular path independent integrals is the *J-integral.* Application of the *J-integral* to two-dimensional symmetrical crack problems can be found in Kishitani et al. [61], Karami and Fenner [60]. Aliabadi [2] applied the *J-integral* and BEM to mixed-mode crack problems and decoupled the *J-integral* into its symmetrical and anti-symmetrical components. In his work, it was shown that accurate values of mode I and II stress intensity factors can be obtained from the *J-integral [2].*

Consider a body with a crack of length a, subject to mode-I loading. Using an arbitrary counter-clockwise path around the crack tip, as shown in Figure 3.11, a formal definition of *J-integral* under mode-I condition is [93]

$$J = \int_{\Gamma} \left(W dy - t_j \frac{\partial u_i}{dx} ds \right) \tag{3.97}$$

where Γ is the arbitrary contour, ds is the length increment along contour Γ, U_i and $t_j = \sigma_{ij} n_j$ are the components of the displacement and traction vectors, W is the strain energy density per unit area, defined as

$$W = \int_{0}^{\varepsilon_{ij}} \sigma_{ij} d\varepsilon_{ij} \tag{3.98}$$

where $\sigma_{ij}$and ε_{ij} are the stress and strain tensors, respectively.

$$\varepsilon_{ij} = \frac{1}{2} \left(\frac{\partial u_i}{\partial x_j} + \frac{\partial u_j}{\partial x_i} \right) \tag{3.99}$$

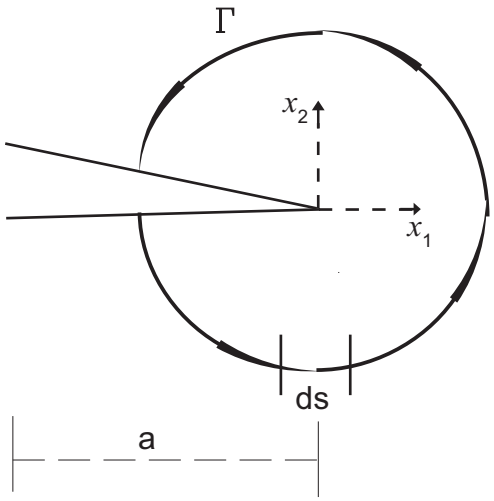

Figure 3.11: J-integral

It has been shown by Rice [93] that the value of the *J-integral* is independent of the path of integration around the crack. Since $n_1 ds = dy$, the *J-Integral* in equation (3.97) can be written as

$$J = \int_{\Gamma} (W \mathrm{n}_1 - t_j u_{j,1})\, ds \tag{3.100}$$

where $u_{j,1}$ is the differentiation of displacement u_j with respect to x_1. In a linear elastic material the variation of the potential energy for a virtual crack extension (J) is equal to the energy release rate (G) which is related to the SIFs as follows:

$$J = G = \frac{K_I^2 + K_{II}^2}{E'} \tag{3.101}$$

where E' is the elastic modulus for plane stress and $E' = E/(1-\nu^2)$ for plane strain condition. In equation (3.101), the *J-integral* is related to the a combination of the value of K_I and K_{II}. Thus, it is necessary to decouple it, a simple procedure implemented by Aliabadi [2] can be used to evaluate the values of K_I and K_{II}.

Consider two points $P(x_1, x_2)$ and $P^*(x_1, x_2)$, symmetrical with respect to crack axis, as shown in Figure 3.12. The displacement at these points can be expressed in terms of their symmetric components u_j^I and anti-symmetric components u_j^{II} as [5, 86]:

$$\left\{ \begin{array}{c} u_1^I \\ u_2^I \end{array} \right\} = \frac{1}{2} \left\{ \begin{array}{c} u_1 + u_1' \\ u_2 - u_2' \end{array} \right\}, \qquad \left\{ \begin{array}{c} u_1^{II} \\ u_2^{II} \end{array} \right\} = \frac{1}{2} \left\{ \begin{array}{c} u_1 - u_1' \\ u_2 + u_2' \end{array} \right\} \tag{3.102}$$

and, similarly for stress σ_{ij}^I and σ_{ij}^{II},

$$\left\{ \begin{array}{c} \sigma_{11}^I \\ \sigma_{22}^I \\ \sigma_{12}^I \end{array} \right\} = \frac{1}{2} \left\{ \begin{array}{c} \sigma_{11} + \sigma_{11}' \\ \sigma_{22} + \sigma_{22}' \\ \sigma_{12} - \sigma_{12}' \end{array} \right\}, \qquad \left\{ \begin{array}{c} \sigma_{11}^{II} \\ \sigma_{22}^{II} \\ \sigma_{12}^{II} \end{array} \right\} = \frac{1}{2} \left\{ \begin{array}{c} \sigma_{11} - \sigma_{11}' \\ \sigma_{22} - \sigma_{22}' \\ \sigma_{12} + \sigma_{12}' \end{array} \right\} \tag{3.103}$$

Using the equations (3.102) and (3.103), the *J-integral* components can be defined as:

$$J^m = \int_\Gamma \left(W^m \mathrm{n}_1 - t_j^m u_{j,1}^m \right) ds \tag{3.104}$$

where $m = I$ or $m = II$.

The integral J is represented by the sum of two integrals as :

$$J = J^I + J^{II} \tag{3.105}$$

where the superscript indicate their mode. The relationship between *J-integral* components and SIFs at each mode becomes:

$$J^I = \frac{K_I^2}{E'} \qquad\qquad J^{II} = \frac{K_{II}^2}{E'} \tag{3.106}$$

The *J-integral* is an effective method in the Boundary Element Method, because the interior elastic field can be determined accurately along the contour path, since the exact variation of the interior elastic field is built into the fundamental solution. The integration along the contour path is performed by the Trapezoidal rule. For traction free cracks, the contribution of the integration over the part of crack surface included in the contour is equal to zero, and therefore does not need to be computed. Crack growth, life expectancy and residual strength of engineering structures can be determined with the accurate evaluation of the SIFs.

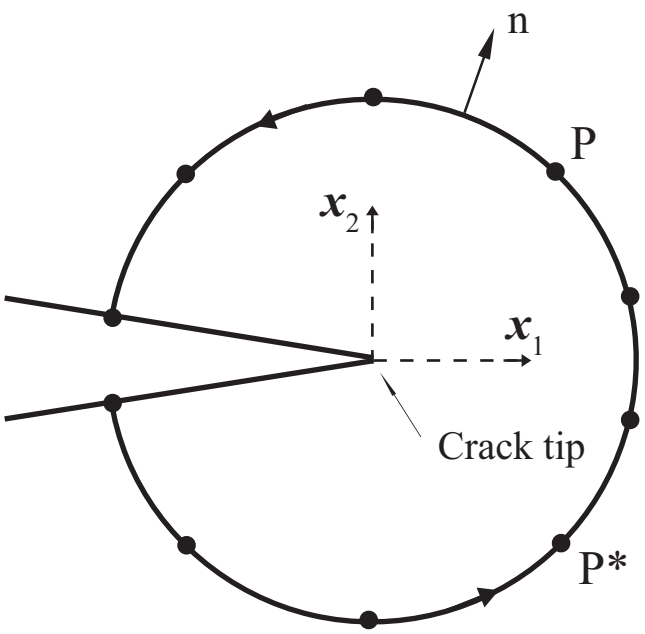

Figure 3.12: Coordinate reference system and contour path for J-integral

3.5 Fatigue crack growth

In general, fatigue crack-growth is driven by the variation of amplitude loading. It is also well known that fatigue crack propagation could be affected by many other parameters: loading, type of product, heat treatment, temperature, manufacture, environment, etc. The analysis of fatigue crack life envisages the problem of showing the relation between the number of cycles of loading and the increments of cracks to obtain the final life of the cracked structure.

The growth of cracks under fatigue loading, can be described following Paris's postulate [83] which relates the rate of growth per cycle (da/dN) to the stress intensity range ($\Delta K = K_{max} - K_{min}$):

$$\frac{da}{dN} = f(\Delta K, R_s) \tag{3.107}$$

where a is the crack length, N is the number of load cycles, ΔK is the stress

intensity range which depends on the stress ratio R_s, which is defined as:

$$\begin{aligned} R_s =& \frac{K_{max}}{K_{min}} \\ =& \frac{\sigma_{max}}{\sigma_{min}} \end{aligned} \tag{3.108}$$

where K_{max} is the maximum stress intensity factor corresponding to the maximum load. Under linear elastic assumptions, after the SIFs have been evaluated for the maximum load, the value for any load can be related by R_s using equation (3.108). Under general mixed-mode loadings, this is replaced by an equivalent mode I stress intensity factor K_{Ieq}. In a mixed-mode analysis, an equivalent mode I stress intensity factor is defined as [87]:

$$K_{Ieq} = K_I \cos^3 \frac{\theta_t}{2} - 3K_{II} \cos^2 \frac{\theta_t}{2} \sin \frac{\theta_t}{2} \tag{3.109}$$

In order to show the variation in the number of loading cycles as a function of crack length, in the present work the fatigue life N is determined from the empirical Paris model defined as [83]:

$$\frac{da}{dN} = C(\triangle K_{eff})^m \tag{3.110}$$

where a is the crack length, C, m are the material constants that are determined through experiment, and ΔK_{eff} is the range of the effective stress intensity factor. The model of Tanaka [107] is used, in which $\triangle K_{eff}$ is evaluated by [87]:

$$\triangle K_{eff} = \sqrt{\triangle K_I^2 + 2\triangle K_{II}^2} \tag{3.111}$$

Thus, although $\triangle K_{eff} = \triangle K_{Ieq}$ when the maximum principal stress criterion is

used, the model of Tanaka was applied in the present work.

Several criteria have been proposed to describe the local direction of mixed-mode crack growth. Among them, one of the most commonly used is based on the maximum principal stress at the crack tip [39]. The maximum principal stress criterion postulates that the growth of the crack will occur in a direction perpendicular to the maximum principal stress. Therefore, the local crack growth direction θ_t is determined by the condition that local shear stress is zero, which is [39]:

$$K_I \sin\theta_t + K_{II}(3\cos\theta_t - 1) = 0 \tag{3.112}$$

where θ_t is the angular coordinate of the tangent to the crack path, centered at the crack tip and measured from the crack axis ahead of the crack tip.

3.6 Summary

In this chapter, the boundary and dual boundary integral equations have been reviewed for elastostatics analysis. The implementation of equations has been presented in 2D elastostatics. The special analytical integration used in [86] to evaluate integrals on the crack boundary has been presented. Fracture mechanics and fatigue crack growth concepts for 2D elastic analysis were briefly reviewed.

In the following chapters, the formulation presented here will be further extended to obtain the derivatives of boundary value with respect to random variables in 2D elastostatic problem, as well as to Linear-Elastic Fracture-Mechanics (LEFM).

Chapter 4

Boundary element method for stochastic elastostatics problems

4.1 Introduction

The concept of sensitivity analysis is to quantify the impact of randomness in random variables on the uncertainty of the outputs. It reveals how the all random variable affect the reliability of structure or component; this allows the variation of random variables to produce acceptable reliability at minimum weight in the context of aerospace design. Sensitivity analysis can be performed once the probabilistic analysis model has been established. There are several methods that can perform sensitivity analysis. The derivatives of boundary response with respect to random variables are required for probabilistic analysis in elastostatic problems [10, 36, 40, 58]. For example in the limit state approximation adopted here, the gradient of performance function with respect to random variable is required.

There are three methods to compute the derivatives of boundary response with respect to random variables; finite difference method (FDM), the material derivative method and implicit (or direct) differentiation method (IDM) [49, 110]. The

first of these three uses the well known finite difference approximation to compute the derivatives. A typical example is the forward difference approximation given by:

$$\frac{\partial f(Z)}{\partial Z_m} = \lim_{\delta Z_m \to 0} \frac{f(Z + \delta Z_m) - f(Z)}{\delta Z_m} \tag{4.1}$$

where δZ_m is a small value. Using this method, the accuracy of the derivatives theoretically increases as the step size decrease. Although this method is computationally expensive, it is easy to implement and by taking a range of different step sizes, an accurate approximation for the derivatives can be obtained.

In the second method, material derivatives of the variational state equations are used in conjunction with the adjoint variable technique. The adjoint variable method employs an adjoint system to obtain an explicit sensitivity expression in terms of design variables. The adjoint generally corresponds to a high concentrated force solution which is very difficult to implement in the boundary element method analysis as they lead to unbounded integrals. Application of material derivative method can be found in the work of Burczynski et al. [26], Burczynski and Skrzypczyk [25], Choi and Haug [30], Longo et al. [69], Chen et al. [28], Haftka and Adelman [49].

In the third method, the derivatives of boundary response are obtained directly by the differentiation of the boundary and dual boundary element equations with respect to the random variable Z_m. There have been several applications of this method reported [80, 74, 99, 58]. Moghaddasi-Tafreshi and Fenner [80] used an Hermitian cubic splines in their study of shape optimization with BEM. Mellings and Aliabadi [75] used an implicit differentiation method for flaw identification. In their work the coordinate of the end points of each element on the crack surface were used as design variables. Recently, Sfantos and Aliabadi [99]

have extended the same method to contact problems where the design variables are defined in terms of the normal gap between the contact bodies.

In this chapter, the direct differentiation method is further extended to probabilistic analysis for elastostatic problems. First and second order boundary response derivatives with respect to random variables are obtained. The accuracy of the computed derivatives is compared with the result obtained either from analytical solutions or finite difference methods. Finally, the proposed method is implemented for the reliability analysis in elastostatics problems and compared with results obtained using the Monte Carlo simulation.

4.2 Formulations of derivative boundary integral equations

In this approach, direct differentiation of the system equations is to be used. Consider an arbitrary random variable vector $\mathbf{Z}$ with components Z_m $(m = 1....N_v)$, where N_v is the number of random variables. These parameters may represent the random geometry, load and material properties. It is assumed that the prescribed boundary conditions are deterministic, and do not depend on the random parameters. Differentiating equation (3.32) with respect to the design variable Z_m in the absence of body force, gives

$$\begin{aligned} & C_{ij,m}(\mathbf{x}')u_j(\mathbf{x}') + C_{ij}(\mathbf{x}')u_{j,m}(\mathbf{x}') \\ & + \int\!\!\!\!\!\!-_{\Gamma} T_{ij,m}(\mathbf{x}', \mathbf{x})u_j(\mathbf{x})d\Gamma(\mathbf{x}) + \int\!\!\!\!\!\!-_{\Gamma} T_{ij}(\mathbf{x}', \mathbf{x})u_{j,m}(\mathbf{x})d\Gamma(\mathbf{x}) \\ & = \int_{\Gamma} U_{ij,m}(\mathbf{x}', \mathbf{x})t_j(\mathbf{x})d\Gamma(\mathbf{x}) + \int_{\Gamma} U_{ij}(\mathbf{x}', \mathbf{x})t_{j,m}(\mathbf{x})d\Gamma(\mathbf{x}) \end{aligned} \tag{4.2}$$

where $()_{,m}$ indicates the first order derivatives with respect to the design variable

Z_m. Differentiating the above equation (4.2) with respect to the design variable Z_m gives:

$$\begin{aligned}
&C_{ij,mm}(\mathbf{x}')u_j(\mathbf{x}') + 2C_{ij,m}(\mathbf{x}')u_{j,m}(\mathbf{x}') + C_{ij}(\mathbf{x}')u_{j,mm}(\mathbf{x}') \\
&+ \int\!\!\!\!\!\!-_{\Gamma} T_{ij,mm}(\mathbf{x}',\mathbf{x})u_j(\mathbf{x})d\Gamma(\mathbf{x}) + 2\int\!\!\!\!\!\!-_{\Gamma} T_{ij,m}(\mathbf{x}',\mathbf{x})u_{j,m}(\mathbf{x})d\Gamma(\mathbf{x}) \\
&+ \int\!\!\!\!\!\!-_{\Gamma} T_{ij}(\mathbf{x}',\mathbf{x})u_{j,mm}(\mathbf{x})d\Gamma(\mathbf{x}) \\
=&\int_{\Gamma} U_{ij,mm}(\mathbf{x}',\mathbf{x})t_j(\mathbf{x})d\Gamma(\mathbf{x}) + 2\int_{\Gamma} U_{ij,m}(\mathbf{x}',\mathbf{x})t_{j,m}(\mathbf{x})d\Gamma(\mathbf{x}) \\
&+ \int_{\Gamma} U_{\Gamma ij}(\mathbf{x}',\mathbf{x})t_{j,mm}(\mathbf{x})d\Gamma(\mathbf{x})
\end{aligned} \tag{4.3}$$

where $()_{,mm}$ indicates the second order derivatives with respect to the design variable Z_m. The above equations are discretised in a similar manner to equation (3.32) on a regular boundary to give the discretised first order derivatives boundary element equation as:

$$\begin{aligned}
&C_{ij,m}(\mathbf{x}')u_j(\mathbf{x}') + C_{ij}(\mathbf{x}')u_{j,m}(\mathbf{x}') + \sum_{\gamma=1}^{N_e}\sum_{n=1}^{3} u^n_{j,m}(\mathbf{x}) \int_{-1}^{+1} T_{ij}M^n J^\gamma d\xi \\
&+ \sum_{\gamma=1}^{N_e}\sum_{n=1}^{3} u^n_j(\mathbf{x}) \int_{-1}^{+1} T_{ij,m}M^n J^\gamma d\xi + \sum_{\gamma=1}^{N_e}\sum_{n=1}^{3} u^n_j(\mathbf{x}) \int_{-1}^{+1} T_{ij}M^n J^\gamma_{,m} d\xi \\
=&\sum_{\gamma=1}^{N_e}\sum_{n=1}^{3} t^n_{j,m}(\mathbf{x}) \int_{-1}^{+1} U_{ij}M^n J^\gamma d\xi + \sum_{\gamma=1}^{N_e}\sum_{n=1}^{3} t^n_j(\mathbf{x}) \int_{-1}^{+1} U_{ij,m}M^n J^\gamma d\xi \\
&+ \sum_{\gamma=1}^{N_e}\sum_{n=1}^{3} t^n_j(\mathbf{x}) \int_{-1}^{+1} U_{ij}M^n J^\gamma_{,m} d\xi
\end{aligned} \tag{4.4}$$

where the integrals in the local variable ξ, use the following expressions:

$$T_{ij}M^nJ^\gamma \Leftrightarrow T_{ij}(\mathbf{x}', \mathbf{x}(\xi))M^n(\xi)J^\gamma(\xi) \tag{4.5}$$

and

$$U_{ij}M^nJ^\gamma \Leftrightarrow U_{ij}(\mathbf{x}', \mathbf{x}(\xi))M^n(\xi)J^\gamma(\xi) \tag{4.6}$$

and the discretised second order derivatives boundary element equation can be written as:

$$\begin{aligned}
&C_{ij,mm}(\mathbf{x}')u_j(\mathbf{x}') + 2C_{ij,m}(\mathbf{x}')u_{j,m}(\mathbf{x}') + C_{ij}(\mathbf{x}')u_{j,mm}(\mathbf{x}') \\
&+ \sum_{\gamma=1}^{N_e}\sum_{n=1}^{3} u^n_{j,mm}(\mathbf{x}) \int_{-1}^{+1} T_{ij}M^nJ^\gamma d\xi + 2\sum_{\gamma=1}^{N_e}\sum_{n=1}^{3} u^n_{j,m}(\mathbf{x}) \int_{-1}^{+1} T_{ij,m}M^nJ^\gamma d\xi \\
&+ 2\sum_{\gamma=1}^{N_e}\sum_{n=1}^{3} u^n_{j,m}(\mathbf{x}) \int_{-1}^{+1} T_{ij}M^nJ^\gamma_{,m} d\xi + 2\sum_{\gamma=1}^{N_e}\sum_{n=1}^{3} u^n_{j}(\mathbf{x}) \int_{-1}^{+1} T_{ij,m}M^nJ^\gamma_{,m} d\xi \\
&+ \sum_{\gamma=1}^{N_e}\sum_{n=1}^{3} u^n_{j}(\mathbf{x}) \int_{-1}^{+1} T_{ij,mm}M^nJ^\gamma d\xi + \sum_{\gamma=1}^{N_e}\sum_{n=1}^{3} u^n_{j}(\mathbf{x}) \int_{-1}^{+1} T_{ij}M^nJ^\gamma_{,mm} d\xi \qquad (4.7) \\
=&\sum_{\gamma=1}^{N_e}\sum_{n=1}^{3} t^n_{j,mm}(\mathbf{x}) \int_{-1}^{+1} U_{ij}M^nJ^\gamma d\xi + 2\sum_{\gamma=1}^{N_e}\sum_{n=1}^{3} t^n_{j,m}(\mathbf{x}) \int_{-1}^{+1} U_{ij,m}M^nJ^\gamma d\xi \\
&+ 2\sum_{\gamma=1}^{N_e}\sum_{n=1}^{3} t^n_{j,m}(\mathbf{x}) \int_{-1}^{+1} U_{ij}M^nJ^\gamma_{,m} d\xi + 2\sum_{\gamma=1}^{N_e}\sum_{n=1}^{3} t^n_{j}(\mathbf{x}) \int_{-1}^{+1} U_{ij,m}M^nJ^\gamma_{,m} d\xi \\
&+ \sum_{\gamma=1}^{N_e}\sum_{n=1}^{3} t^n_{j}(\mathbf{x}) \int_{-1}^{+1} U_{ij,mm}M^nJ^\gamma d\xi + \sum_{\gamma=1}^{N_e}\sum_{n=1}^{3} t^n_{j}(\mathbf{x}) \int_{-1}^{+1} U_{ij}M^nJ^\gamma_{,mm} d\xi
\end{aligned}$$

In these derivative equations, derivatives of fundamental solutions with respect to design variable Z_m are required. The details of first and second order derivatives of fundamental solutions $T_{ij,m}$, $U_{ij,m}$, $T_{ij,mm}$ and $U_{ij,mm}$; Jacobian of Transformation $J_{,m}$ and $J_{,mm}$ are shown in the section 4.2.1.

Substitution of the known displacement and traction values in equations (4.4) and (4.7) gives a linear system of equations for the unknown displacement and traction derivatives $u^n_{k,m}(\mathbf{x})$, $t^n_{k,m}(\mathbf{x})$, $u^n_{k,mm}(\mathbf{x})$ and $t^n_{k,mm}(\mathbf{x})$. A set of boundary conditions for equation (4.4) can be prescribed by consideration of the original boundary conditions given in equation (3.8), i.e:

$$\begin{aligned} u_i(\mathbf{x}) =& \bar{u}_i(\mathbf{x}) && \mathbf{x} \text{ on } \Gamma_1 \\ t_i(\mathbf{x}) =& \sigma_{ij}(\mathbf{x})n_j(\mathbf{x}) = \bar{t}_i(\mathbf{x}) && \mathbf{x} \text{ on } \Gamma_2 \end{aligned} \tag{4.8}$$

In order to use the derivatives system of equation to evaluate the boundary response derivatives it is necessary to prescribe a new set of boundary conditions for the derivatives. Since the known displacements and tractions of the boundary nodes are independent of the boundary geometry. Their derivatives with respect to design variable Z_m are equal to 0, i.e:

$$\begin{aligned} u_{i,m}(\mathbf{x}) =& 0 && \mathbf{x} \text{ on } \Gamma_1 \\ t_{i,m}(\mathbf{x}) =& 0 && \mathbf{x} \text{ on } \Gamma_2 \end{aligned} \tag{4.9}$$

After applying the new boundary conditions, a system of linear equations is formed which can be written in matrix form as:

$$\mathbf{A}\mathbf{X}_{,m} = \mathbf{F}_{,m} - \mathbf{A}_{,m}\mathbf{X} \tag{4.10}$$

where $\mathbf{X}_{,m}$ is the first order derivatives of unknown displacement and traction vector, $\mathbf{A}_{,m}$ is the first order derivatives of coefficient matrix, while $\mathbf{X}$ is the vector of known values at this stage. For the derivatives analysis, the same coefficient matrix $\mathbf{A}$ that was used to solve the deterministic problem is reused. Thus there is no need for inverting again the left-hand side matrix as it was already inverted for the solution of the problem. As a result, the computational

cost is considerably reduced and moreover, the derivatives with respect to random variable are evaluated more accurately as they are done analytically. Similarly, the second order derivatives of the system of equation can be written in matrix form as:

$$\mathbf{A}\mathbf{X}_{,mm} = \mathbf{F}_{,mm} - 2\mathbf{A}_{,m}\mathbf{X}_{,m} - \mathbf{A}_{,mm}\mathbf{X} \tag{4.11}$$

where $\mathbf{A}_{,mm}$ is the second order derivatives of coefficient matrix, the second order derivatives of unknown displacement and traction vector $\mathbf{X}_{,mm}$ can be obtained once the deterministic and first order derivatives of unknown displacement and traction vector $\mathbf{X}$ and $\mathbf{X}_{,m}$ are evaluated.

In the first of the derivative equation (4.2), the term $C_{ij,m}(\mathbf{x}')$ is required and this can be evaluated using a derivative form of the rigid body condition. The rigid body condition, as given in equation (3.76), allows both the singular integral and the jump term to be computed for any source point on an external boundary. This equation can be differentiated with respect to the random variable Z_m to give a new equation for the derivative jump term.

$$C_{ij,m}(\mathbf{x}')u_j(\mathbf{x}') + \sum_{\gamma=1}^{N_e}\sum_{n=1}^{3} u_j^n(\mathbf{x}) \int_{-1}^{+1} T_{ij,m}(\mathbf{x}', \mathbf{x}(\xi)) M^n(\xi) J^\gamma(\xi) d\xi$$

$$+ \sum_{\gamma=1}^{N_e}\sum_{n=1}^{3} u_j^n(\mathbf{x}) \int_{-1}^{+1} T_{ij}(\mathbf{x}', \mathbf{x}(\xi)) M^n(\xi) J^\gamma_{,m}(\xi) d\xi = 0 \tag{4.12}$$

In equation (4.12), all terms can be computed easily, except for the singular integral and the derivative jump term $C_{ij,m}(\mathbf{x}')$. Using the same row sum technique as used with the rigid body condition, both of these terms may be evaluated.

In the second order derivative equation (4.3), the term $C_{ij,mm}(\mathbf{x}')$ is required

and this can be evaluated using a derivative form of the rigid body condition. As described above for the first order derivatives. This equation can be differentiated with respect to the random variable Z_m to give a new equation for the derivative jump term, as:

$$C_{ij,mm}(\mathbf{x}')u_j(\mathbf{x}') + \sum_{\gamma=1}^{N_e}\sum_{n=1}^{3} u_j^n(\mathbf{x}) \int_{-1}^{+1} T_{ij,mm}(\mathbf{x}', \mathbf{x}(\xi)) M^n(\xi) J^\gamma(\xi) d\xi$$

$$+2\sum_{\gamma=1}^{N_e}\sum_{n=1}^{3} u_j^n(\mathbf{x}) \int_{-1}^{+1} T_{ij,m}(\mathbf{x}', \mathbf{x}(\xi)) M^n(\xi) J^\gamma_{,m}(\xi) d\xi$$

$$+\sum_{\gamma=1}^{N_e}\sum_{n=1}^{3} u_j^n(\mathbf{x}) \int_{-1}^{+1} T_{ij}(\mathbf{x}', \mathbf{x}(\xi)) M^n(\xi) J^\gamma_{,mm}(\xi) d\xi = 0 \quad (4.13)$$

In equation (4.13), after the computation of first order derivatives, the same row sum technique can be used to compute the second order of singular integral and the derivative jump term $C_{ij,mm}(\mathbf{x}')$.

4.2.1 Derivatives of fundamental solutions

In the derivatives equation, differentiated fundamental solutions are required. These terms are obtained by taking the derivatives of the terms given in equations (3.22) and (3.23) with respect to the design variable Z_m, gives:

$$U_{ij,m}(\mathbf{x}', \mathbf{x}) = \frac{1}{8\pi\mu(1-\nu)r}\left\{r_{,m}r_{,j} + r_{j,m}r_{,i} - [(3-4\nu)\delta_{ij} + 2r_{,i}r_{,j}]r_{,m}\right\} \quad (4.14)$$

$$\begin{aligned} T_{ij,m}(\mathbf{x}', \mathbf{x}) =& \frac{-1}{4\pi(1-\nu)r^2}\left\{2\frac{\partial r}{\partial \mathrm{n}}[r_{i,m}r_{,j} + r_{j,m}r_{,i} - ((1-2\nu)\delta_{ij} + 4r_{,i}r_{,j})r_{,m}]\right. \\ &+ (r_k \mathrm{n}_k)_{,m}[(1-2\nu)\delta_{ij} + 2r_{,i}r_{,j}] + (1-2\nu)(\mathrm{n}_i r_{j,m} + \mathrm{n}_{i,m}r_j \quad (4.15) \\ &\left. -\mathrm{n}_j r_{i,m} - \mathrm{n}_{j,m}r_i) + 2(1-2\nu)(\mathrm{n}_j r_{,i} - \mathrm{n}_i r_{,j})r_{,m}\right\} \end{aligned}$$

and for second order derivatives of fundamental solutions $T_{ij,mm}$ and $U_{ij,mm}$;

$$U_{ij,mm}(\mathbf{x}',\mathbf{x}) = \frac{1}{8\pi\mu(1-\nu)r^2}\Big\{(3-4\upsilon)(r_{,m}^2 - r_{,mm}r)\delta_{ij} + (6r_{,m}^2 - 2r_{,mm}r)r_{,i}r_{,j} + (r_{i,mm}r_j + 2r_{i,m}r_{j,m} + r_i r_{j,mm}) - 4(r_{i,m}r_{,j} + r_{,i}r_{j,m})r_{,m}\Big\} \tag{4.16}$$

$$\begin{aligned} T_{ij,mm}(\mathbf{x}',\mathbf{x}) =& \frac{-1}{4\pi(1-\nu)r^3}\Big\{2(\frac{\partial r}{\partial \mathrm{n}})_{,m}[r_{i,m}r_{,j} + r_{j,m}r_{,i} - ((1-2\nu)\delta_{ij} + 4r_{,i}r_{,j})r_{,m}] \\ &+ 2\frac{\partial r}{\partial \mathrm{n}}[r_{i,mm}r_{,j} + 2r_{i,m}r_{j,m} + r_{,i}r_{j,mm} - ((1-2\nu)\delta_{ij} + 4r_{,i}r_{,j})r_{,mm}r \\ &- (4r_{i,m}r_j + 4r_i r_{j,m})r_{,m}r - 2r_{i,m}r_{,j}r_{,m} - 2r_{,i}r_{j,m}r_{,m} \\ &+ 2((1-2\nu)\delta_{ij} + 4r_{,i}r_{,j})r_{,m}^2] + (r_k \mathrm{n}_k)_{,mm}[(1-2\nu)\delta_{ij} + 2r_{,i}r_{,j}] \\ &+ (r_k \mathrm{n}_k)_{,m}2(r_{,im}r_{,j} + r_{,i}r_{,jm}) + (1-2\nu)(r_{j,mm}\mathrm{n}_i + 2r_{j,m}\mathrm{n}_{i,m} \\ &+ r_j \mathrm{n}_{i,mm} - r_{i,mm}\mathrm{n}_j - 2r_{i,m}\mathrm{n}_{j,m} - r_i \mathrm{n}_{j,mm}) \\ &+ 2(1-2\nu)[(\mathrm{n}_j r_{,i} - \mathrm{n}_i r_{,j})r_{,mm} \\ &+ (\mathrm{n}_j r_{,im} + \mathrm{n}_{j,m}r_{,i} - \mathrm{n}_{i,m}r_{,j} - \mathrm{n}_i r_{,jm})r_{,m}]\Big\} \end{aligned} \tag{4.17}$$

The derivatives of the distance r with respect to random variable Z_m are given as:

$$r_{,m} = r_{,i}r_{i,m} \tag{4.18}$$

where the derivatives of the Cartesian components r_i with respect to random variable Z_m are given as:

$$r_{i,m} = \frac{\partial r_i}{\partial z_m} = x_{i,m}(\mathbf{x}) - x_{i,m}(\mathbf{X}') \tag{4.19}$$

The terms $x_{i,m}$ represent the effects of a change in global coordinate i at x

due to a change in random variable Z_m. The global coordinates x_i are obtained using the interpolation function (3.59). Similarly, the first order derivatives of the global coordinates x_i with respect to the random variable Z_m are given as:

$$x_{i,m} = \sum_{n=1}^{3} M^n(\xi) x_{i,m}^n \tag{4.20}$$

The Jacobian of transformation is given in equation (3.64), and its derivative respect to the random variable Z_m is given as:

$$J_{,m}^{\gamma}(\xi) = \frac{1}{J^{\gamma}(\xi)} \left\{ \frac{dx_1(\xi)}{d\xi} \left[\frac{dx_1(\xi)}{d\xi} \right]_{,m} + \frac{dx_2(\xi)}{d\xi} \left[\frac{dx_2(\xi)}{d\xi} \right]_{,m} \right\} \tag{4.21}$$

The second order derivatives of the radius r with respect to random variable Z_m are given as:

$$r_{,mm} = r_{,im} r_{i,m} + r_{,i} r_{i,mm} \tag{4.22}$$

where the second order derivatives of the Cartesian components r_i with respect to random variable Z_m are given as:

$$r_{i,mm} = \left(\frac{\partial r_i}{\partial z_m} \right)_{,m} = x_{i,mm}(\mathbf{x}) - x_{i,mm}(\mathbf{x}') \tag{4.23}$$

The second order derivatives of the coordinates of the field point with respect to the random variable Z_m are given as:

$$x_{i,mm} = \sum_{n=1}^{3} M^n(\xi) x_{i,mm}^n \tag{4.24}$$

The second order derivative of Jacobian transformation respect to the random variable Z_m are given by:

$$J^{\gamma}_{,mm}(\xi) = \frac{1}{J^{\gamma}(\xi)} \left\{ \left[\frac{dx_1(\xi)}{d\xi} \right]_{,m} \left[\frac{dx_1(\xi)}{d\xi} \right]_{,m} + \frac{dx_1(\xi)}{d\xi} \left[\frac{dx_1(\xi)}{d\xi} \right]_{,mm} + \left[\frac{dx_2(\xi)}{d\xi} \right]_{,m} \left[\frac{dx_2(\xi)}{d\xi} \right]_{,m} + \frac{dx_2(\xi)}{d\xi} \left[\frac{dx_2(\xi)}{d\xi} \right]_{,m} \right\} - \frac{1}{\left(J^{\gamma}(\xi)\right)^3} \left\{ \frac{dx_1(\xi)}{d\xi} \left[\frac{dx_1(\xi)}{d\xi} \right]_{,m} + \frac{dx_2(\xi)}{d\xi} \left[\frac{dx_2(\xi)}{d\xi} \right]_{,m} \right\}^2 \tag{4.25}$$

The components of the unit outward normal vector and their derivatives are:

$$\mathrm{n}_1(\xi) = \frac{1}{J^{\gamma}(\xi)} \frac{dx_2(\xi)}{d\xi} \tag{4.26}$$

$$\mathrm{n}_2(\xi) = -\frac{1}{J^{\gamma}(\xi)} \frac{dx_1(\xi)}{d\xi} \tag{4.27}$$

Differentiating the above equations with respect to the design variable Z_m gives:

$$\mathrm{n}_{1,m} = \frac{1}{J^{\gamma}(\xi)} \left[\left(\frac{dx_2(\xi)}{d\xi} \right)_{,m} - n_1(\xi) J^{\gamma}_{,m}(\xi) \right] \tag{4.28}$$

and

$$\mathrm{n}_{2,m} = -\frac{1}{J^{\gamma}(\xi)} \left[\left(\frac{dx_1(\xi)}{d\xi} \right)_{,m} + n_2(\xi) J^{\gamma}_{,m}(\xi) \right] \tag{4.29}$$

Differentiating the above equations with respect to the random variable Z_m gives:

$$\mathrm{n}_{1,mm} = \frac{1}{J^{\gamma}(\xi)} \left(\frac{dx_2(\xi)}{d\xi} \right)_{,mm} - \frac{1}{\left(J^{\gamma}(\xi)\right)^2} \left[2J^{\gamma}_{,m}(\xi) \left(\frac{dx_2(\xi)}{d\xi} \right)_{,m} + J^{\gamma}_{,mm}(\xi) \frac{dx_2(\xi)}{d\xi} \right] + \frac{2\left(J^{\gamma}_{,m}(\xi)\right)^2}{\left(J^{\gamma}(\xi)\right)^3} \frac{dx_2(\xi)}{d\xi} \tag{4.30}$$

and

$$\mathrm{n}_{2,mm} = -\frac{1}{J^{\gamma}(\xi)} \left(\frac{dx_1(\xi)}{d\xi} \right)_{,mm} + \frac{1}{\left(J^{\gamma}(\xi)\right)^2} \left[2J^{\gamma}_{,m}(\xi) \left(\frac{dx_1(\xi)}{d\xi} \right)_{,m} + J^{\gamma}_{,mm}(\xi) \frac{dx_1(\xi)}{d\xi} \right] - \frac{2\left(J^{\gamma}_{,m}(\xi)\right)^2}{\left(J^{\gamma}(\xi)\right)^3} \frac{dx_1(\xi)}{d\xi} \tag{4.31}$$

4.3 Accuracy of sensitivity analysis

It is essential to verify that the sensitivity values computed by the proposed formulation are accurate. In order to carry out such a task, a comparison of the sensitivity values evaluated with the derivative boundary element method, is made with the computations made using another method. The technique used here to calculate these alternative derivative values is the forward difference approximation method, as described in equation (4.1). In order to achieve a good comparison using the forward difference approximation, it is necessary to choose a range of value for the step size δZ_m. Four step sizes have been chosen in this work, these being 0.1, 0.01, 0.001, 0.0001.

4.4 Reliability analysis

4.4.1 Random variables and response

Consider an elastostatics structure subjected to random loads. Suppose the structure fails when the stress σ is greater or equal to the strength R. This requirement cannot be satisfied with certainty, since σ is dependent on the input vector $\mathbf{Z}$ which is random, and R itself may be a random variable. Hence, the probability of failure P_f is defined as [9]:

$$P_f = \int_{g(\mathbf{Z})<0} f_{\mathbf{Z}}(\mathbf{Z}) d\mathbf{Z} \tag{4.32}$$

where $f_{\mathbf{Z}}(\mathbf{Z})$ is the joint probability density function of $\mathbf{Z}$, and

$$g(\mathbf{Z}) = R - \sigma \tag{4.33}$$

is the performance function, where R is the strength limitation of stress and σ is the equivalent stress of the considered point in the structure.

4.4.2 Reliability analysis by FORM

Equation (4.32) involves the evaluation of multi-dimensional probability integration. In this work, the first-order reliability method (FORM) was used to compute the probability of failure. The FORM is based on linear approximation of the limit state surface $g(\mathbf{Z}) = 0$ tangent to the closest point of the surface to the origin of the space. The determination of this point involves nonlinear constrained optimization and is usually performed in the standard Gaussian image of the original space. The probability of failure P_f in equation (4.32) is thus approximated by [71]:

$$P_f = \Phi(-\beta) \tag{4.34}$$

where

$$\Phi(Z_m) = \frac{1}{\sqrt{2\pi}} \int_{-\infty}^{Z_m} \exp(-\frac{1}{2}\xi^2) d\xi \tag{4.35}$$

is the cumulative probability distribution function of a standard Gaussian random variable, β is the most probable point, referred to as the reliability index. A Hasofer–Lind–Rackwitz–Fiessler algorithm [53, 91] is chosen to find the failure point in this work. The first-order derivatives of performance function with respect to random parameters $\mathbf{Z}$ will be calculated analytically and are described next.

4.4.3 Analytical sensitivities

For the performance function, one must also calculate its derivative with respect to $\mathbf{Z}$ in order to perform the recursive formula in equation (2.60). That is usually performed in the standard Gaussian image of the original space $\mathbf{\Psi}$.

Assume that a transformation of $\mathbf{Z} \in \mathbb{H}^N$ to $\mathbf{\Psi} \in \mathbb{H}^N$, given by

$$\mathbf{Z} = Z(\mathbf{\Psi}) \tag{4.36}$$

exists. The performance function in the $\mathbf{\Psi}$ space can then be expressed as

$$g_{\Psi}(\mathbf{\Psi}) = g(\mathbf{Z}(\mathbf{\Psi})) = R(\mathbf{Z}(\mathbf{\Psi})) - \sigma(\mathbf{Z}(\mathbf{\Psi})) \tag{4.37}$$

Using the chain rule of differentiation, the first-order derivative of $g_{\Psi}(\mathbf{\Psi})$ with respect to Ψ_k , $(k = 1, 2 \dots N_v)$ is

$$\frac{\partial g_{\Psi}(\mathbf{\Psi})}{\partial \Psi_k} = \sum_{m=1}^{N_v} \frac{\partial g}{\partial Z_m} \frac{\partial Z_m}{\partial \Psi_k} = \sum_{m=1}^{N_v} \frac{\partial g}{\partial Z_m} R_{mk} \tag{4.38}$$

where $R_{mk} = \frac{\partial Z_m}{\partial \Psi_k}$ can be obtained from the explicit form of equation (4.36). The partial derivatives in the $\mathbf{Z}$ space are

$$\frac{\partial g}{\partial \mathbf{Z}} = -\frac{\partial \sigma}{\partial \mathbf{Z}} \tag{4.39}$$

and

$$\frac{\partial g}{\partial R} = 1 \tag{4.40}$$

Using the proposed implicit differentiation method, the partial derivative of stress with respect to design variables can be easily calculated. Hence, for a given $\mathbf{\Psi}$ or $\mathbf{Z}$, all gradients of $g_{\Psi}(\mathbf{\Psi})$ can be evaluated analytically. Therefore, FORM or any other gradient-based reliability analysis can be performed efficiently.

4.5 Examples:

4.5.1 Cylinder under external pressure

A hollow cylinder subjected to an external pressure P_o is considered in this example (see Figure 4.1). The inner radius $a = 1$, outer radius $b = 2$, the external load $p_o = 1$, and plane stress condition is assumed. The material properties used were assumed to be $E = 1$ unit and Poisson's ratio $\upsilon = 0.3$. The geometry of the inner radius a and critical tangential stress $\sigma^c_{\theta\theta}$ at point A were treated as statistically independent random variables. Table 4.1 presents the mean, coefficient of variation (COV), and probability distribution for each of these random parameters.

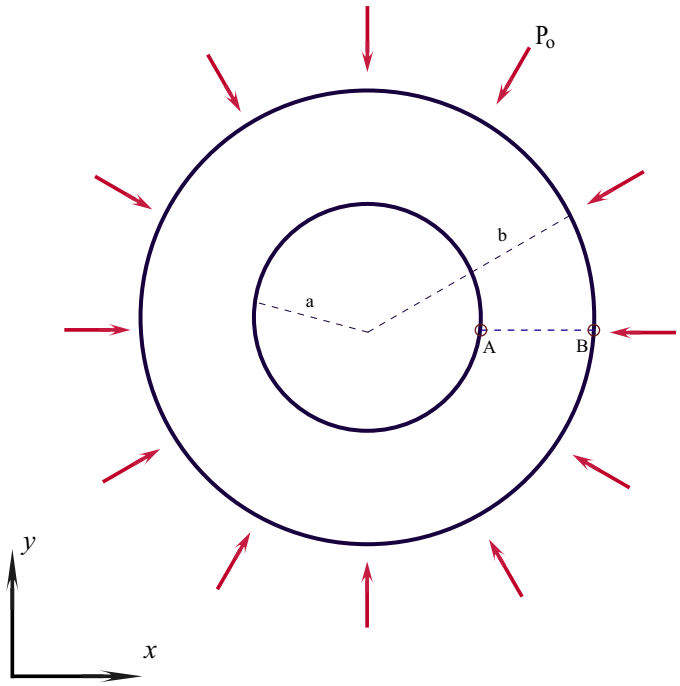

Figure 4.1: Cylinder under external pressure

The well known analytical solution for stress components in polar coordinates can be found in [109].

$$\sigma_{rr} = \frac{p_i a^2 - p_o b^2}{b^2 - a^2} + \frac{a^2 b^2 (p_o - p_i)}{r^2 (b^2 - a^2)} \tag{4.41}$$

$$\sigma_{\theta\theta} = \frac{p_i a^2 - p_o b^2}{b^2 - a^2} - \frac{a^2 b^2 (p_o - p_i)}{r^2 (b^2 - a^2)} \tag{4.42}$$

where the internal pressure P_i is assumed to be 0 in this example. The analytical expression for first and second order derivatives with respect to inner radius a can be derived directly.

Table 4.1: Statistical properties of random input for cylinder

	Mean	COV[a]	Probability distribution
Inner radius (a)	Variable	Variable[b]	Normal
Critical tangential stress ($\sigma^c_{\theta\theta}$)	3	0.1	Normal

[a] Coefficient of variation (COV) = standard deviation/mean.
[b] Arbitrarily varied.

Both inner and the outer contours were discretised with 8, 20, 40 quadratic boundary elements for each derivative calculation, respectively. Figure 4.2 shows the boundary conditions and the discretisation using 40 quadratic elements.

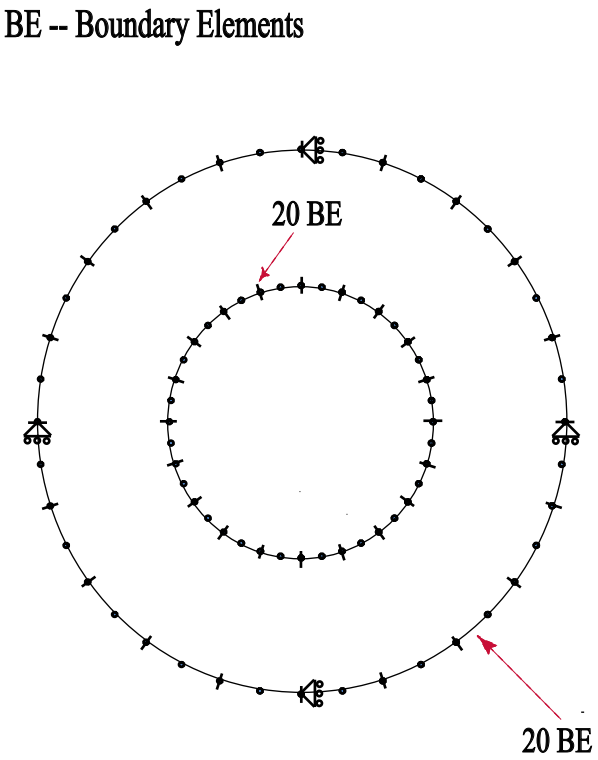

Figure 4.2: Boundary conditions and discretisation with 40 quadratic elements

The deterministic value of radial displacement at selected sample points between points A and B with the comparisons of analytical solution is shown in Figure 4.3. The value of the local tangential stress normalised with respect to the E, between points A and B is shown in Figure 4.4. The value of the first and second order derivatives of the radial displacement and tangential stress with respect to design variable a along segment AB are shown in Figures 4.5 to 4.8. As it can be seen in those Figures, the results obtained by the BEM with implicit differentiation method (BEM-IDM) agree well with the analytical solution.

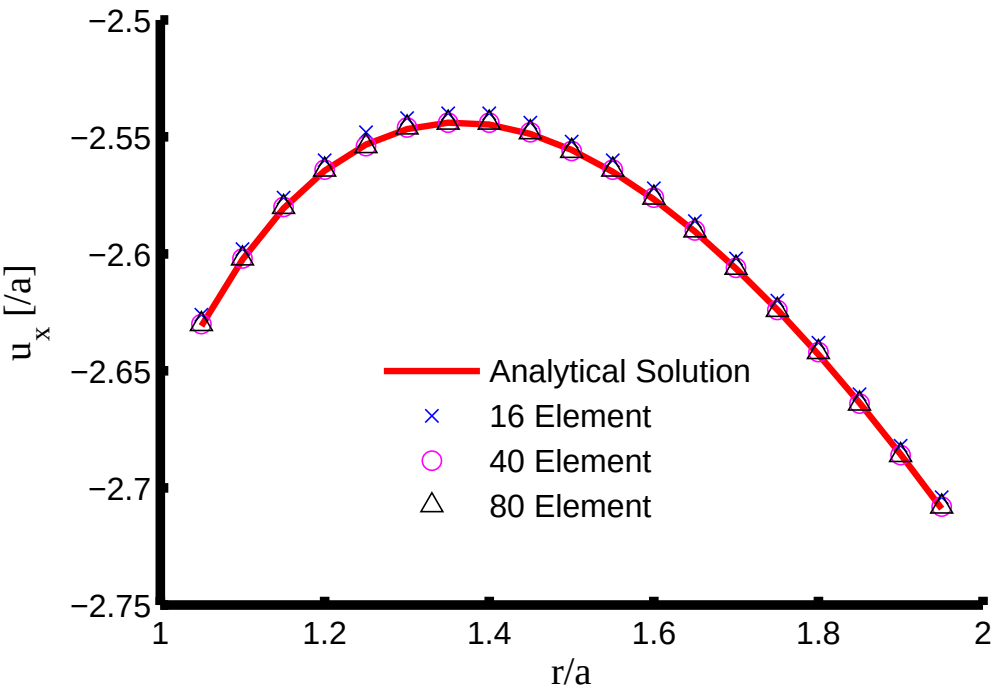

Figure 4.3: Normalised radial displacement on AB

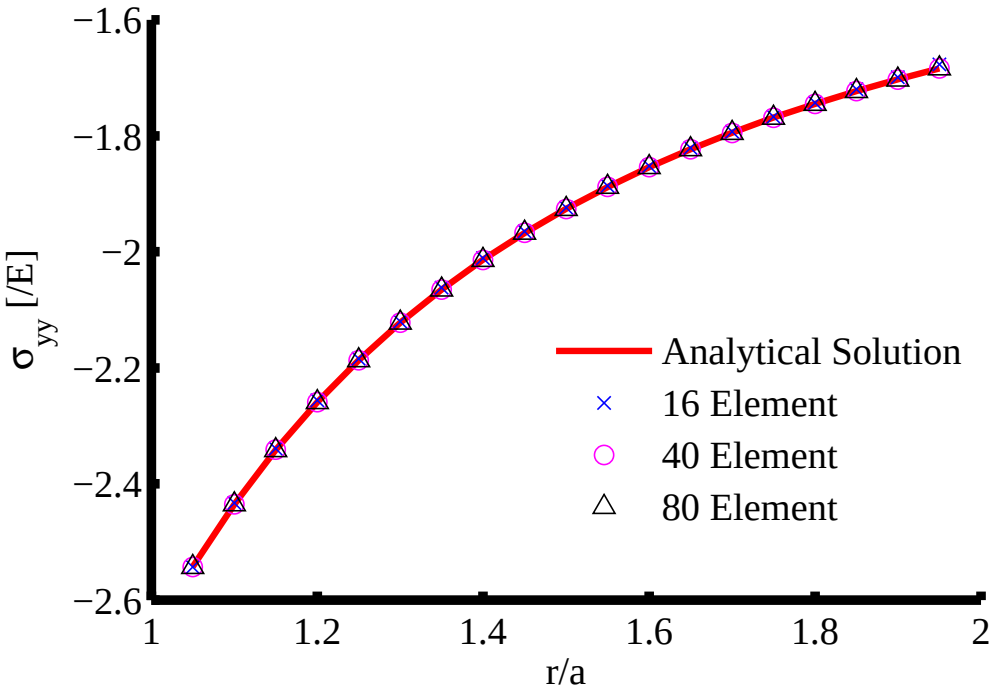

Figure 4.4: Normalised tangential stress on AB

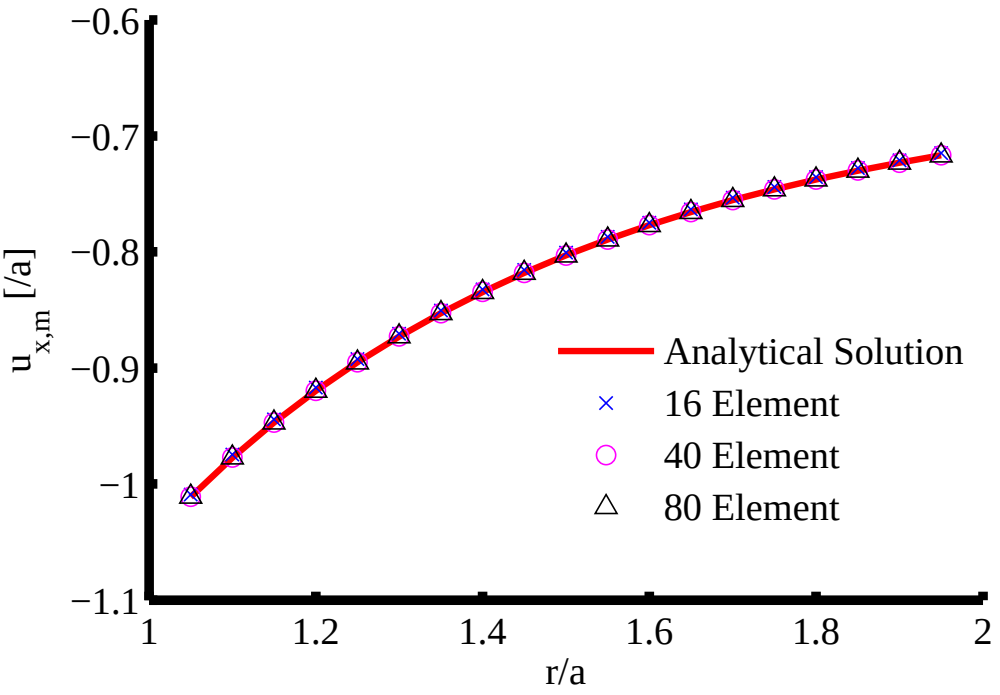

Figure 4.5: Normalised first order derivatives of radial displacement on AB

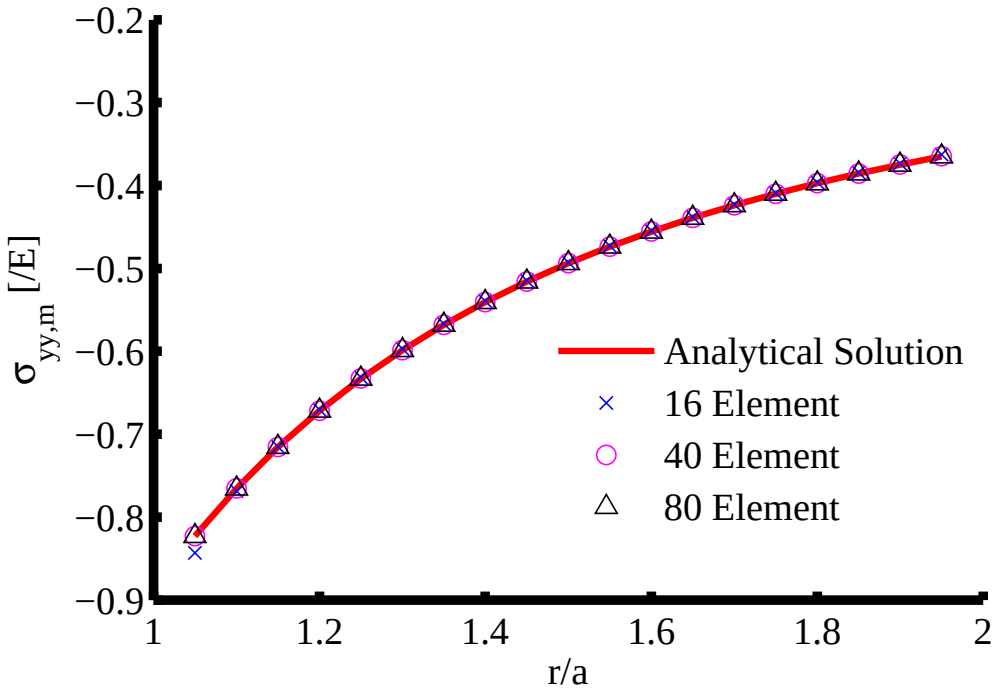

Figure 4.6: Normalised first order derivatives of tangential stress on AB

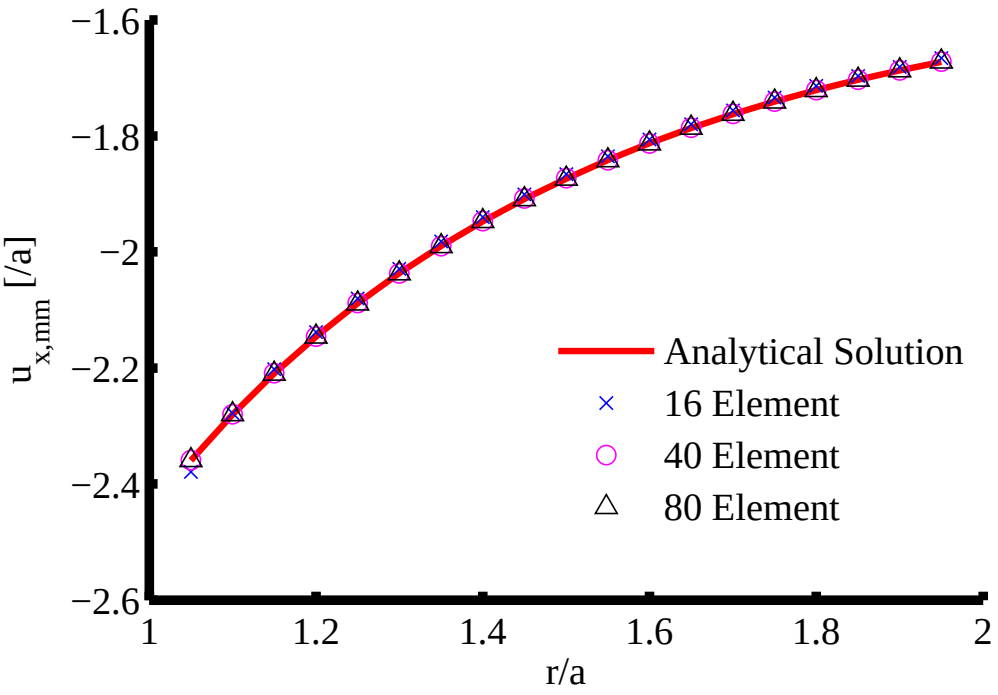

Figure 4.7: Normalised second order derivatives of radial displacement on AB

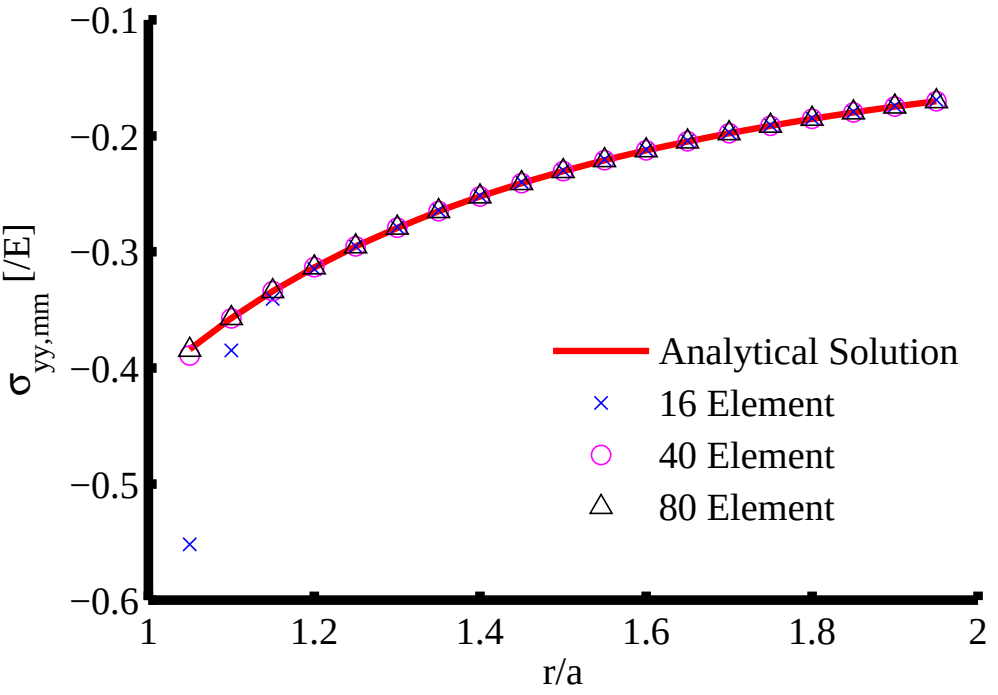

Figure 4.8: Normalised second order derivatives of $\sigma_{\theta\theta}$ on AB

A convergence study is carried out for this particular example to validate the derivative values. As it can be seen in Figures 4.9 and 4.10, for the first and second order derivatives of tangential stress along segment AB, converge to the analytical solution with the increasing number of elements. The results obtained by BEM-IDM with 40 elements agree well with the analytical solution, with a maximum 0.027% of difference over the entire segment AB for the first order derivatives; and with a maximum 1.36% of difference for the second order derivatives.

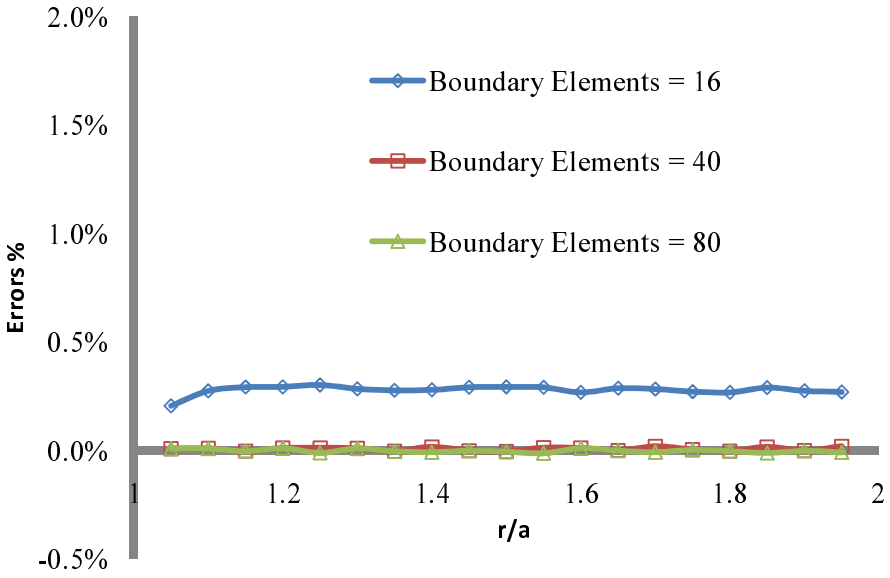

Figure 4.9: First order derivative percentage errors

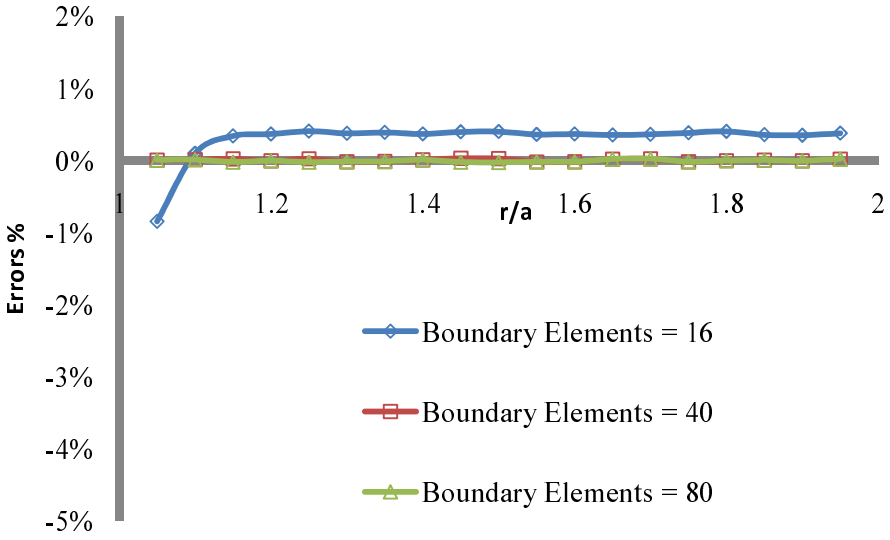

Figure 4.10: Second order derivative percentage errors

Using the method developed here, a number of probabilistic analyses were performed to calculate the reliability of the cylinder, as a function of mean inner radius $E[a]$, where $E[\bullet]$ is the expectation (mean) operator. Both inner and the outer contours of the cylinder were discretised with 20 quadratic boundary elements. Figures 4.11 to 4.14 plot the reliability of cylinder P_r against inner radius a for $V_a = 0.1$, 0.2, 0.3 and 0.4, where V_a is the COV of the inner radius. Figure 4.15 shows the comparison of reliability index β vs. a using FORM for different COV of inner radius a.

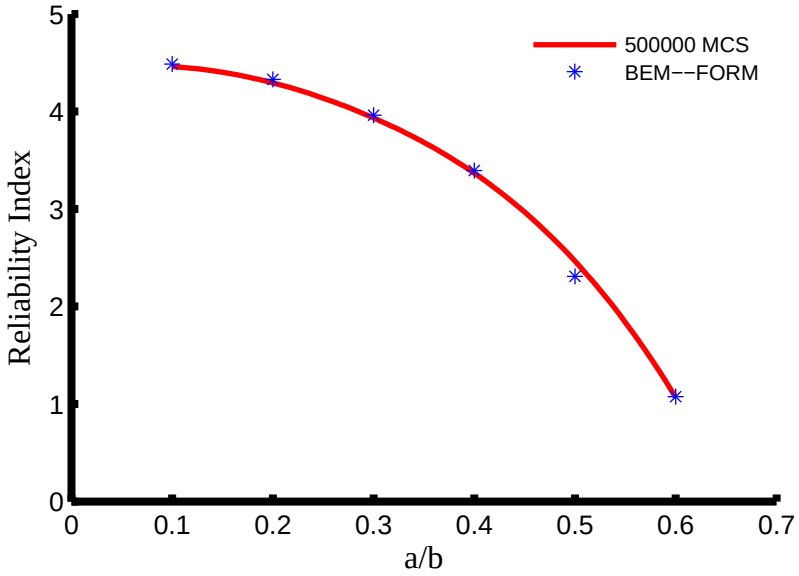

Figure 4.11: Reliability by FORM and simulation with $V_a = 0.1$

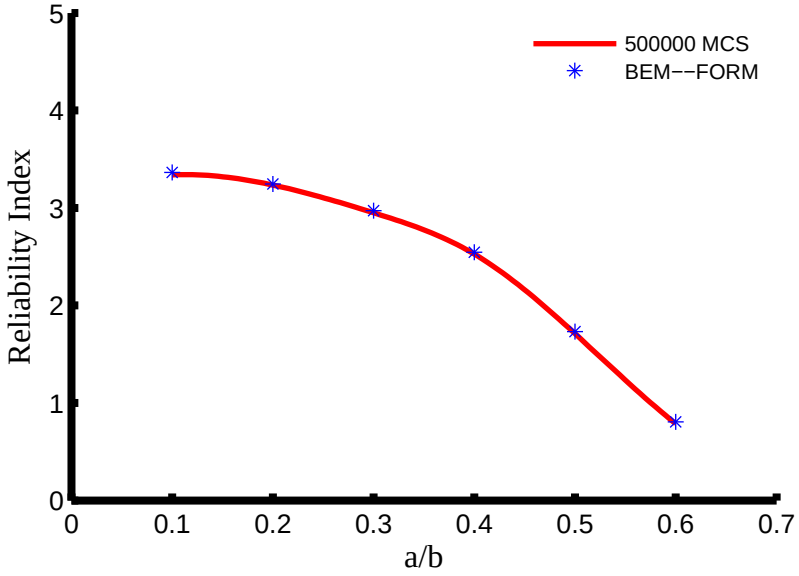

Figure 4.12: Reliability by FORM and simulation with $V_a = 0.2$

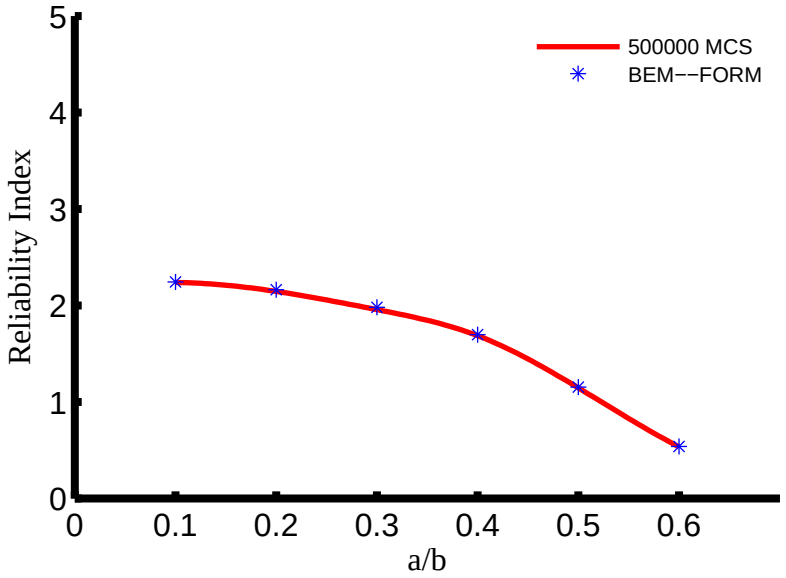

Figure 4.13: Reliability by FORM and simulation with $V_a = 0.3$

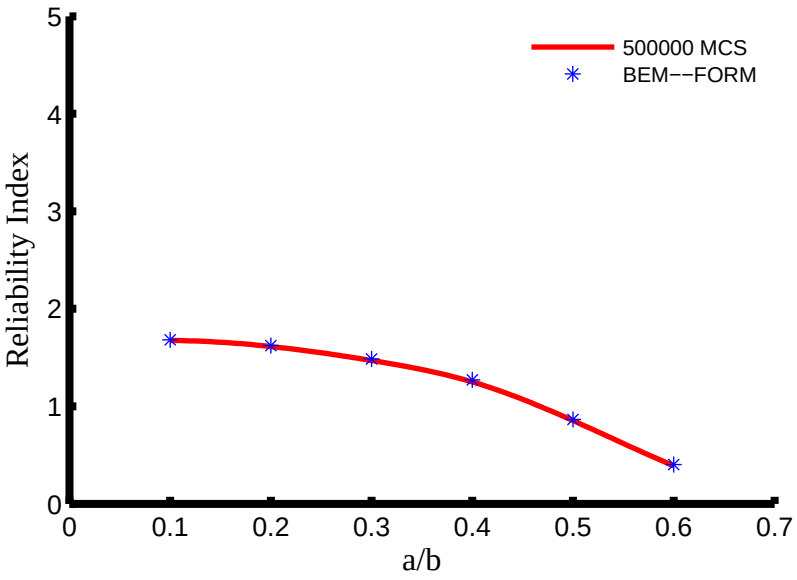

Figure 4.14: Reliability by FORM and simulation with $V_a = 0.4$

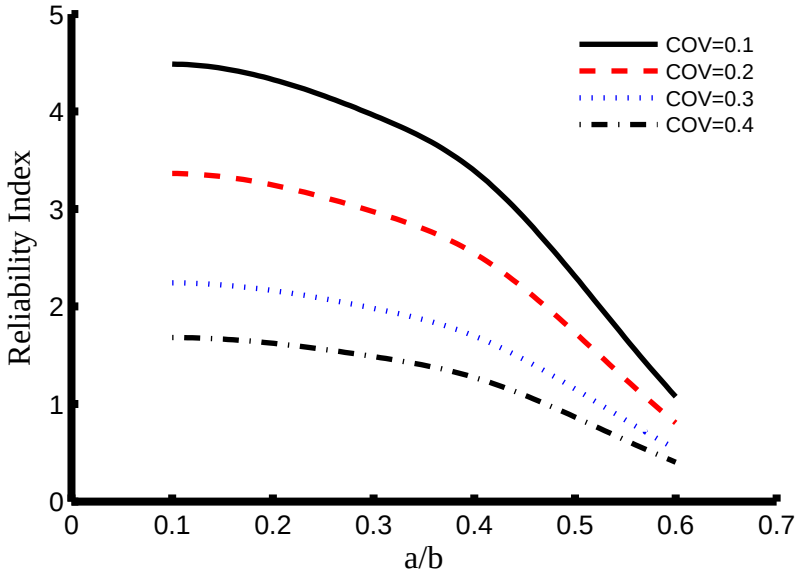

Figure 4.15: Comparison of reliability by FORM and simulation

The reliability was calculated using sensitivity-based FORM and Monte Carlo simulations. For the Monte Carlo simulation, the analytical solution is used with 500,000 simulations performed to estimate the reliability. As can be seen in Figures 4.11 to 4.14, where $\frac{a}{b}$ vary from 0.1 to 0.6, the reliability index by FORM is in good agreement with the simulation results. In Figure 4.15, it shows for the same coefficient of variation V_a, the smaller inner radius certainly has a higher reliability index and vice-versa. As expected, the results indicate that the reliability decreases with the increase of uncertainty in inner radius a. Reliability index β can be very small, particularly when both inner radius and uncertainty of V_a is large.

4.5.2 Plate with a hole under tension

A rectangular plate with a circular hole, as shown in Figure 4.16, was analysed. It was assumed that the outer rectangular contour is deterministic and has the dimensions shown in Figure 4.16. The width of the plate is assumed to be W, length $L = 2W$, and the material properties used were assumed to be $E = 1$ unit and poison ratio $\upsilon = 0.3$, the plate is subjected to a far-field remote tensile stress $\sigma/E = 1$. The geometry of the radius r and critical tangential stress σ^c at point A were treated as statistically independent random variables. Table 4.2 presents the mean, coefficient of variation (COV), and probability distribution for each of these random parameters.

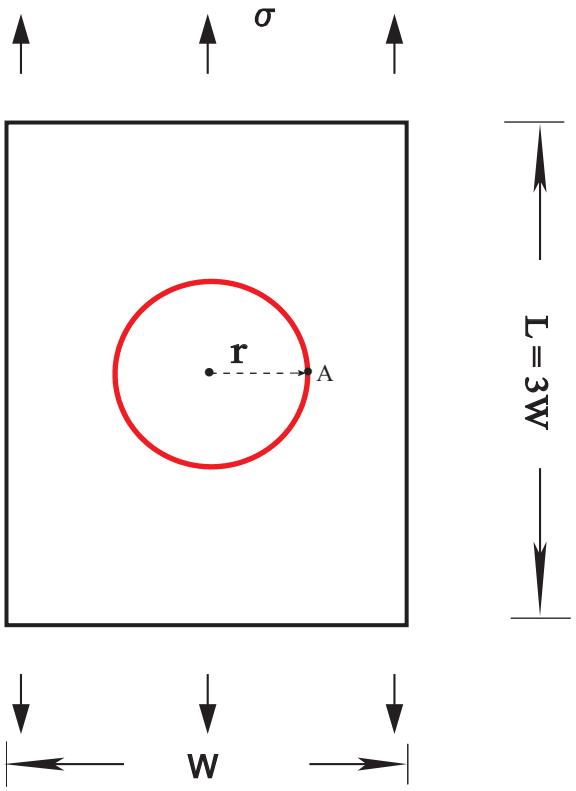

Figure 4.16: Plate with a hole under far field stress

Table 4.2: Statistical properties of random input for plate with a hole

	Mean	COV[a]	Probability distribution
Radius (r)	Variable	Variable[b]	Normal
Critical tangential stress (σ^c)	5	Variable[b]	Normal

[a] Coefficient of variation (COV) = standard deviation/mean.
[b] Arbitrarily varied.

Figure 4.17 shows the boundary conditions and the discretisation using 40 quadratic elements. The outer boundary is discretised with 20 quadratic boundary elements and the inner circle is discretised with 20 quadratic boundary elements for the calculation, respectiely.

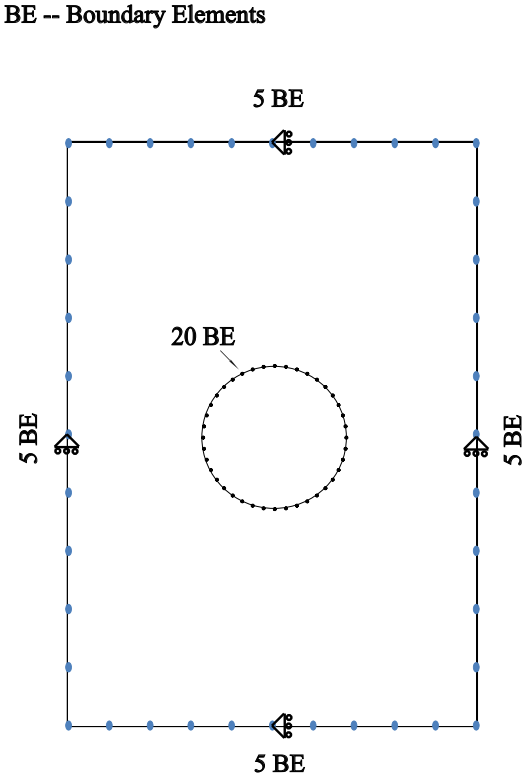

Figure 4.17: Boundary conditions and discretisation with 40 quadratic elements

Using the method developed here, a number of probabilistic analyses were performed to calculate the reliability of the example, as a function of radius r. Firstly, the probability distributions of the both random parameters are assumed to be normally distributed. Figures 4.18 to 4.21 plot the reliability index β of the plate against radius r for $V_r = 0.1$, 0.2, 0.3 and 0.4, where V_r is the COV of the radius. Figure 4.22 shows the comparison of reliability index β vs. r using FORM for different COV of radius r.

The reliability was calculated using sensitivity-based FORM and Monte Carlo simulations. 500,000 Monte Carlo simulations were performed to estimate the reliability. As can be seen in Figures 4.18 to 4.21, where $\frac{r}{W}$ vary from 0.05 to 0.3, the reliability index by FORM is in good agreement with the simulation results. In Figure 4.22, it shows for the same coefficient of variation V_r, the smaller radius certainly has higher reliability index and vice-versa. As expected, the results indicate that the reliability decreases with the increase of uncertainty in inner radius r. Reliability index β can be very small, particularly when both inner radius and uncertainty of V_r is large.

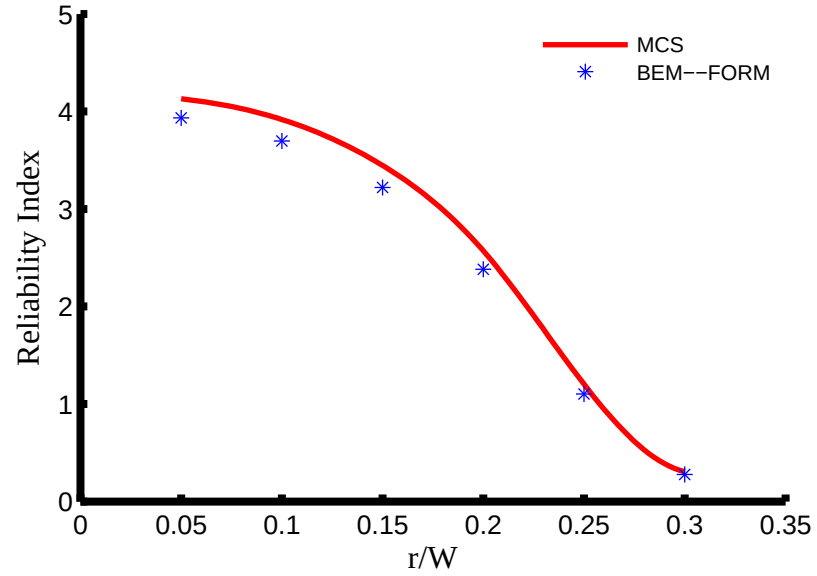

Figure 4.18: Reliability by FORM and simulation with $V_a = 0.1$

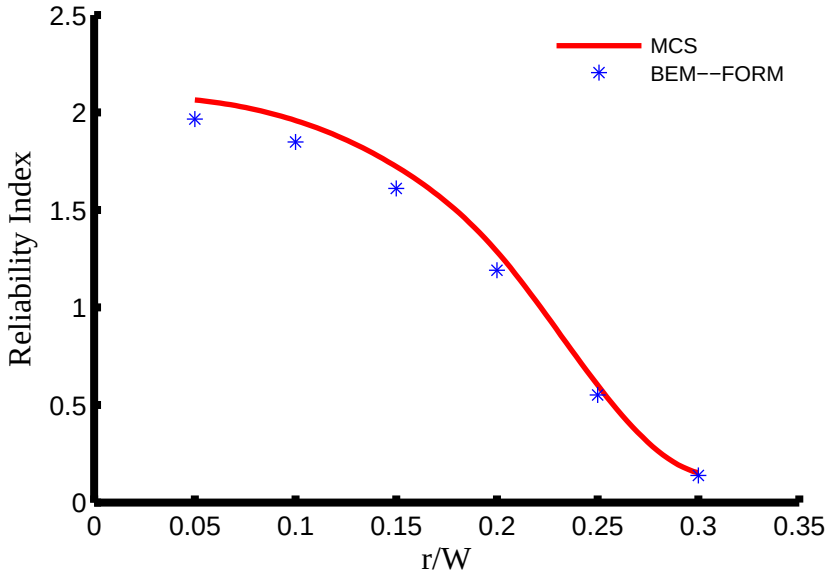

Figure 4.19: Reliability by FORM and simulation with $V_a = 0.2$

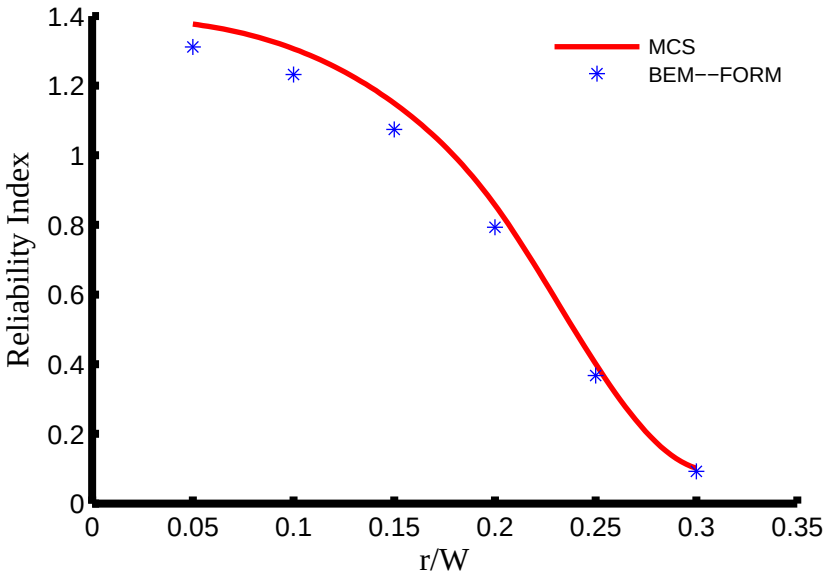

Figure 4.20: Reliability by FORM and simulation with $V_a = 0.3$

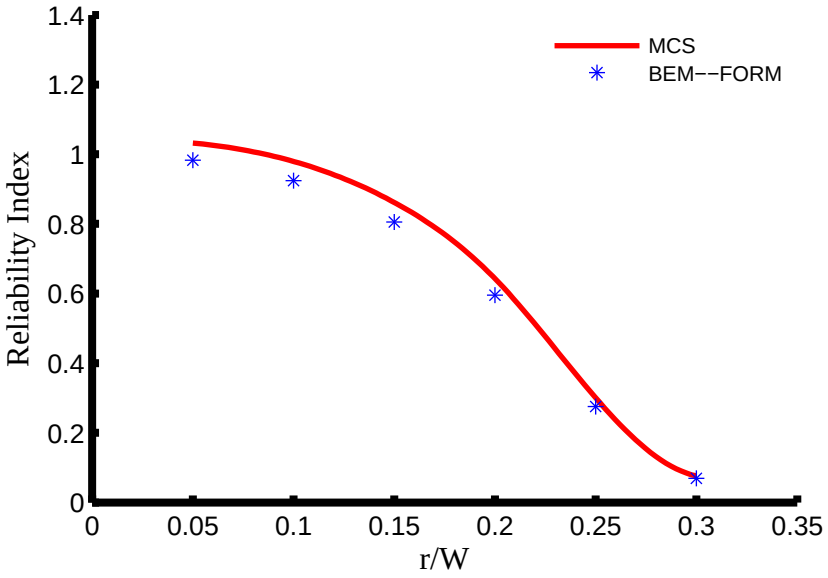

Figure 4.21: Reliability by FORM and simulation with $V_a = 0.4$

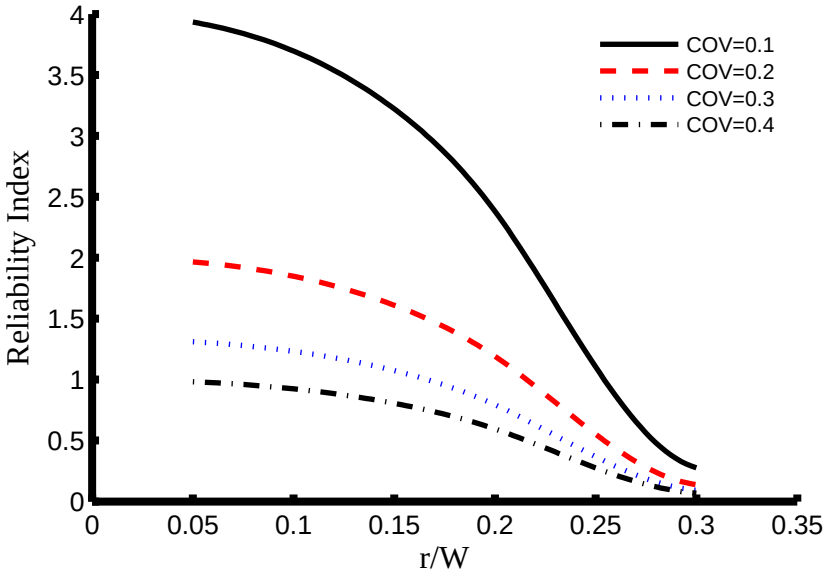

Figure 4.22: Comparison of reliability by FORM and simulation

It is essential to study the effect of different probability distribution functions on the reliability of the structure. For the present analysis, critical tangential stress at point A is assumed to be Lognormal distributed, a different probability distribution function is considered for the radius. Figures 4.23 to 4.26 show the reliability of the plate with hole, as a function of radius with different types of probability distributions, where $\frac{r}{W}$ varies from 0.05 to 0.3. As can be seen from Figs. 4.23 to 4.26, the reliability obtained with Lognormal distribution has a higher value of reliability than the one with Normal distribution when $\frac{r}{W}$ is less than 0.2.

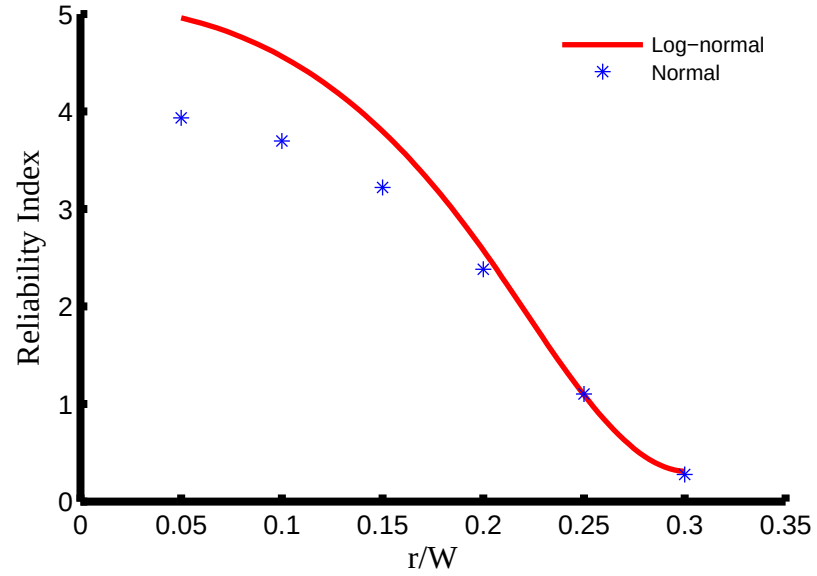

Figure 4.23: Reliability by FORM and simulation with $V_a = 0.1$

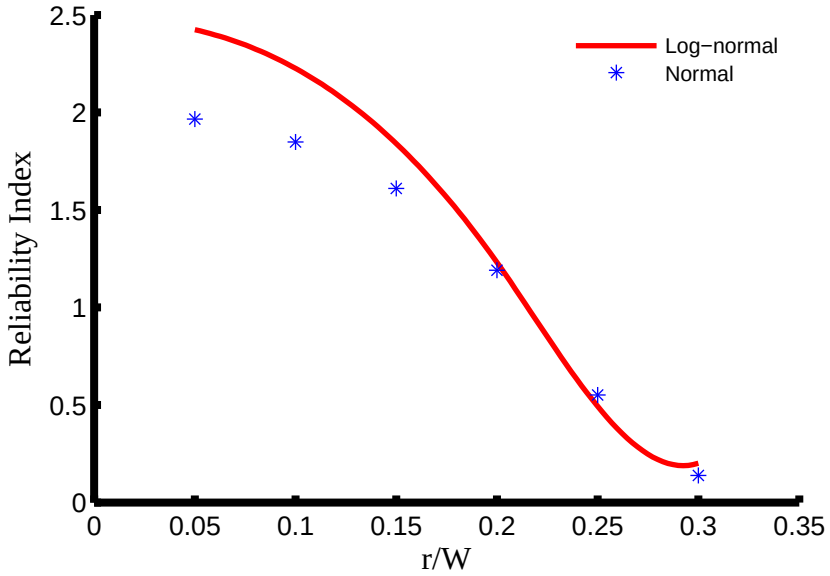

Figure 4.24: Reliability by FORM and simulation with $V_a = 0.2$

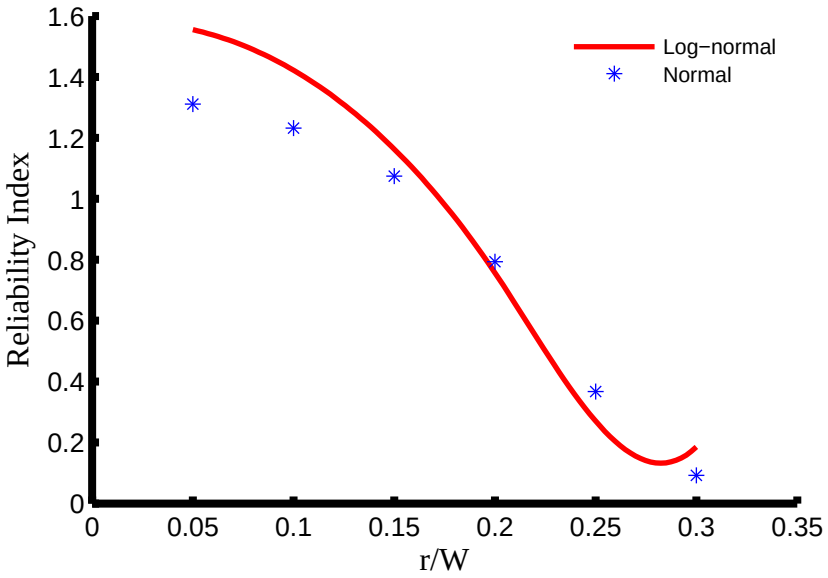

Figure 4.25: Reliability by FORM and simulation with $V_a = 0.3$

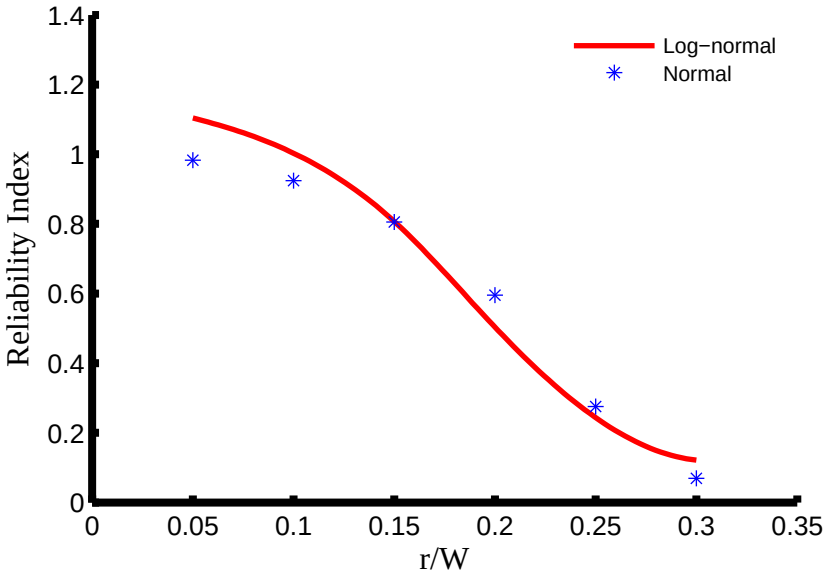

Figure 4.26: Reliability by FORM and simulation with $V_a = 0.4$

4.6 Summary

In this chapter, a formulation of the implicit differentiation method coupled with boundary element method for calculating reliability of the problem in elastostatics was presented. The proposed formulation can be used to evaluate the design sensitivities analysis and probabilistic analysis. Both first and second order derivatives of boundary response with respect to random variables were evaluated accurately and fast, as it does not require the resolution of the system of equations. Comparison was made with the finite difference method for a simple problem that the analytical solution is available. Convergence studies were also carried out with a different boundary mesh to validate the formulation developed. The modified Hasofer-Lind iterative technique was used to find the most probable point. The probabilistic results obtained from proposed method reveal good agreement with the Monte Carlo simulation.

Chapter 5

Stochastic dual boundary element method for LEFM

5.1 Introduction

In probabilistic fracture mechanics, the derivatives of stress intensity factors (SIFs) or *J-integral* with respect to random parameter are often required for probabilistic analysis [14, 15, 18, 36, 46, 66, 90]. Those two fracture parameters are required for obtaining the gradient of performance criterion with respect to random variables in most probabilistic analysis for two dimensional crack problems [90]. As mentioned in Chapter 1, most of the method developed to evaluate the derivatives of stress intensity factors (SIFs) or *J-integral* with respect to random parameter are in conjunction with FEM.

Early application of probabilistic analysis with the BEM for linear elastic fracture mechanics problems can be found in the work of Millwater [79] and Burczynski and Skrzypczyk [25]. The randomness in geometry, loading, material properties and crack parameters were considered in their works. Millwater [79] used finite difference approach to evaluate the derivatives of fracture parameters

with respect to random variables. Burczynski and Skrzypczyk [25] used material derivatives of the variational state equations to evaluate the derivatives of boundary responses. Burczynski and Skrzypczyk [25] also used the path-independent integral approach to obtain the derivatives with respect to internal defects. As demonstrated in Chapter 4, the boundary value and its derivatives with respect to random parameters can be accurately evaluated using direct differentiation method in BEM. The method developed in Chapter 4 can then be extended to DBEM, and the derivative of fracture parameters can be evaluated. Probabilistic analysis with respect to fracture parameters can be carried out.

In this chapter, the probabilistic analysis will be implemented for two dimensional crack problems within the context of linear elastic fracture mechanics. The derivatives of the dual boundary integral equations will be formulated to compute the derivatives of boundary responses. New boundary conditions will be prescribed and implemented into the derivative equations to generate a set of linear equations, which will be solved for the unknown derivatives of displacement and traction with respect to random variables. New assumptions will be made to evaluate the singular integrals for source nodes situated on the crack boundary. The derivative of *J-integral* will be formulated to evaluate the derivatives of fracture parameter with respect to random variables. The derivatives of stress-intensity factors with respect to crack size are evaluated for mode-I and mixed-mode fracture problems. Convergence study is also carried out for the accuracy of the derivative of fracture parameters with respect to random parameters. The first order reliability method will be used to evaluate the reliability index. Numerical examples will be presented to validate the method developed here; comparison will be made with available references and the Monte Carlo simulation to demonstrate the accuracy of the numerical algorithm.

5.2 Boundary integral formulations for displacement and traction derivatives

The boundary response derivatives with respect to random parameters are to be computed using a system of equations created by the direct differentiation of the two displacement equations (3.70) and (3.71) and the traction equation (3.72). The derivative equations for the normal boundary were presented in Chapter 4. The derivatives equations for dual boundary integral equation on a smooth crack are presented here.

For a source point on a smooth crack boundary, differentiating equation (3.71) to with respect to the random variable Z_m gives:

$$\begin{aligned}
&\frac{1}{2}u_{i,m}(\mathbf{x}') + \frac{1}{2}u_{i,m}(\mathbf{x}'') + \sum_{\gamma=1}^{N_e}\sum_{n=1}^{3} u^n_{j,m}(\mathbf{x}) \int_{-1}^{+1} T_{ij} M^n J^\gamma d\xi \\
&+ \sum_{\gamma=1}^{N_e}\sum_{n=1}^{3} u^n_{j}(\mathbf{x}) \int_{-1}^{+1} T_{ij,m} M^n J^\gamma d\xi + \sum_{\gamma=1}^{N_e}\sum_{n=1}^{3} u^n_{j}(\mathbf{x}) \int_{-1}^{+1} T_{ij} M^n J^\gamma_{,m} d\xi \\
=&\sum_{\gamma=1}^{N_e}\sum_{n=1}^{3} t^n_{j,m}(\mathbf{x}) \int_{-1}^{+1} U_{ij} M^n J^\gamma d\xi + \sum_{\gamma=1}^{N_e}\sum_{n=1}^{3} t^n_{j}(\mathbf{x}) \int_{-1}^{+1} U_{ij,m} M^n J^\gamma d\xi \qquad (5.1) \\
&+ \sum_{\gamma=1}^{N_e}\sum_{n=1}^{3} t^n_{j}(\mathbf{x}) \int_{-1}^{+1} U_{ij} M^n J^\gamma_{,m} d\xi
\end{aligned}$$

where for the sake of simplicity, the terms involving local coordinate ξ are expressed in the following forms:

$$U_{ij} M^n J^\gamma \Leftrightarrow U_{ij}(\mathbf{x}', \mathbf{x}(\xi)) M^n(\xi) J^\gamma(\xi) \qquad (5.2)$$

$$T_{ij} M^n J^\gamma \Leftrightarrow T_{ij}(\mathbf{x}', \mathbf{x}(\xi)) M^n(\xi) J^\gamma(\xi) \qquad (5.3)$$

For a source point on a smooth crack boundary, differentiating equation (3.72) with respect to the random variable Z_m gives:

$$\begin{aligned}
&\frac{1}{2}t_{i,m}(\mathbf{x}') - \frac{1}{2}t_{i,m}(\mathbf{x}'') + \mathrm{n}_{j,m}(\mathbf{x}'')\sum_{\gamma=1}^{N_e}\sum_{n=1}^{3} u_k^n(\mathbf{x})\int_{-1}^{+1} S_{kij}M^n J^\gamma d\xi \\
&+ \mathrm{n}_j(\mathbf{x}')\sum_{\gamma=1}^{N_e}\sum_{n=1}^{3} u_{k,m}^n(\mathbf{x})\int_{-1}^{+1} S_{kij}M^n J^\gamma d\xi + \mathrm{n}_j(\mathbf{x}')\sum_{\gamma=1}^{N_e}\sum_{n=1}^{3} u_k^n(\mathbf{x})\int_{-1}^{+1} S_{kij,m}M^n J^\gamma d\xi \\
&+ \mathrm{n}_j(\mathbf{x}')\sum_{\gamma=1}^{N_e}\sum_{n=1}^{3} u_k^n(\mathbf{x})\int_{-1}^{+1} S_{kij}M^n J^\gamma_{,m} d\xi \qquad (5.4) \\
=&\mathrm{n}_{j,m}(\mathbf{x}')\sum_{\gamma=1}^{N_e}\sum_{n=1}^{3} t_k^n(\mathbf{x})\int_{-1}^{+1} D_{kij}M^n J^\gamma d\xi + \mathrm{n}_j(\mathbf{x}')\sum_{\gamma=1}^{N_e}\sum_{n=1}^{3} t_{k,m}^n(\mathbf{x})\int_{-1}^{+1} D_{kij}M^n J^\gamma d\xi \\
&+ \mathrm{n}_j(\mathbf{x}')\sum_{\gamma=1}^{N_e}\sum_{n=1}^{3} t_k^n(\mathbf{x})\int_{-1}^{+1} D_{kij,m}M^n J^\gamma d\xi + \mathrm{n}_j(\mathbf{x}')\sum_{\gamma=1}^{N_e}\sum_{n=1}^{3} t_k^n(\mathbf{x})\int_{-1}^{+1} D_{kij}M^n J^\gamma_{,m} d\xi
\end{aligned}$$

where the expression of the following terms are:

$$D_{kij}M^n J^\gamma \Leftrightarrow D_{kij}(\mathbf{x}', \mathbf{x}(\xi))M^n(\xi)J^\gamma(\xi) \qquad (5.5)$$

$$S_{kij}M^n J^\gamma \Leftrightarrow S_{kij}(\mathbf{x}', \mathbf{x}(\xi))M^n(\xi)J^\gamma(\xi) \qquad (5.6)$$

The equations (4.4), (5.1) and (5.4) contain the required displacement and traction derivatives, $u_{k,m}^n(\mathbf{x})$ and $t_{k,m}^n(\mathbf{x})$, can now be used to analyse the relevant fracture problems. In order to use the derivatives system of equations to evaluate the response derivatives, it is necessary to prescribe a new set of boundary conditions for the derivative values as presented in Chapter 4. A system of equations can be formed from the derivative equations (4.4),(5.1) and (5.4) for

each of the random variables. These systems of linear equations may be written in matrix form as:

$$\mathbf{A}\mathbf{X}_{,m} = \mathbf{F}_{,m} - \mathbf{A}_{,m}\mathbf{X} \tag{5.7}$$

The matrix $\mathbf{A}$ is the same coefficient matrix that was used to solve the displacement and traction value in deterministic problem, $\mathbf{X}_{,m}$ is the first order derivatives of unknown displacement and traction vector, $\mathbf{A}_{,m}$ is the first order derivatives of coefficient matrix, while $\mathbf{X}$ is the vector of known values at this stage. Many terms in the derivative equations will vanish or have already been computed in the standard DBEM analysis and in the derivative equations for the normal boundary. The only terms required in the derivative systems are those when the source point is on the crack boundary.

5.2.1 Derivative of fundamental solutions

In the derivative boundary displacement integral equation (5.1), the differentiated fundamental solutions $U_{ij,m}(\mathbf{x}', \mathbf{x})$ and $T_{ij,m}(\mathbf{x}', \mathbf{x})$ are shown in equations (4.14) and (4.15). For derivative boundary traction integral equation, the differentiated fundamental solutions $D_{kij,m}(\mathbf{x}', \mathbf{x})$ and $S_{kij,m}(\mathbf{x}', \mathbf{x})$ are needed. These terms are obtained by taking the derivatives of the terms given in equations (3.36) and (3.37) with respect to the random variable Z_m, to give

$$\begin{aligned} D_{kij,m}(\mathbf{x}', \mathbf{x}) = & \frac{1}{4\pi(1-\nu)r^2} \Big\{ \left[2r_{,i}r_{,k} + (1-2\nu)\delta_{ik}\right] r_{j,m} \\ & + \left[2r_{,j}r_{,k} + (1-2\nu)\delta_{jk}\right] r_{i,m} + \left[2r_{,i}r_{,j} - (1-2\nu)\delta_{ij}\right] r_{k,m} \\ & 2\left[(1-2\nu)(\delta_{ik}r_{,j} + \delta_{jk}r_{,i} - \delta_{ij}r_{,k}) + 4r_{,i}r_{,j}r_{,k}\right] r_{,m} \Big\} \end{aligned} \tag{5.8}$$

and

$$
\begin{aligned}
S_{kij,m}(\mathbf{x}', \mathbf{x}) = & \frac{E}{4\pi(1-\nu^2)r^3} \Big\{ [2\nu r_{,j} r_{,k} + (1-2\nu)\delta_{jk}]\, \mathrm{n}_{i,m} r \\
& + [2\nu r_{,i} r_{,k} + (1-2\nu)\delta_{ik}]\, \mathrm{n}_{j,m} r \\
& + [2(1-2\nu) r_{,i} r_{,j} - (1-4\nu)\delta_{ij}]\, \mathrm{n}_{k,m} r \\
& - 2\,[(4\nu r_{,j} r_{,k} + (1-2\nu)\delta_{jk}) r_{,m} - \nu(r_{j,m} r_{,k} + r_{k,m} r_{,j})]\, \mathrm{n}_i \\
& - 2\,[(4\nu r_{,i} r_{,k} + (1-2\nu)\delta_{ik}) r_{,m} - \nu(r_{i,m} r_{,k} + r_{k,m} r_{,i})]\, \mathrm{n}_j \\
& - 2\,[(4(1-2\nu) r_{,i} r_{,j} - (1-4\nu)\delta_{ij}) r_{,m} \\
& - (1-2\nu)(r_{j,m} r_{,i} + r_{i,m} r_{,j})\mathrm{n}_k] \Big\}
\end{aligned} \tag{5.9}
$$

In these expressions, the terms $\mathrm{n}_{i,m}$ and $\mathrm{n}_{j,m}$ are the derivative of the normal component with respect to the random variable as given in equation (4.28) and (4.29). The terms $r_{,m}$, $r_{i,m}$ and $r_{j,m}$ are the derivatives of the distance components and the distance respectively and these were given in equations (4.18) and (4.19).

5.2.2 Analytic integration

In the dual boundary element method, the singular integration was performed analytically for source nodes on the crack boundary. It is again possible to perform similar analytical integration for the derivatives formulation as those in deterministic DBEM analysis. Since the crack faces are modelled as straight lines, the random variables are restricted to the coordinates of the end points of one or more crack elements in this work. Both the non-singular and the singular terms of equations (5.1) and (5.4) can be evaluated on the basis of the geometric

derivatives.

Consider a flat, boundary element with the end nodes labeled as A and B, as shown in Figure 5.1. The local coordinates of the end nodes given by $\xi = \eta$. Assume the random variables relate to the coordinates of these end nodes. Then a change in the random variable is a change in one direction of one of the end nodes, with the other end node remaining fixed.

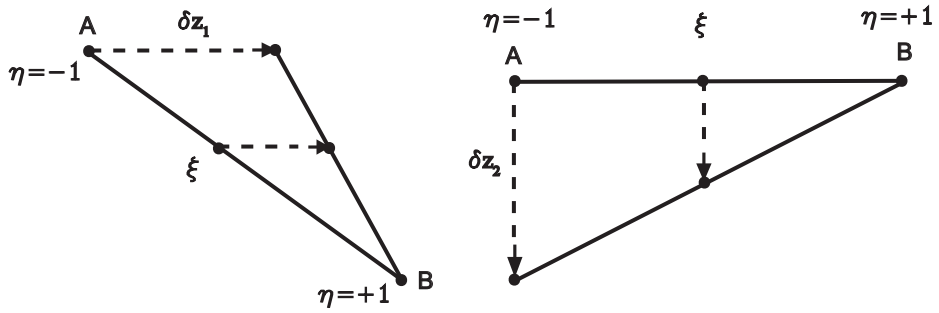

Figure 5.1: Change to node A of a straight crack

Consider first that node A is changed in direction 1 (Figure 5.1), then the new coordinates of a point, with local variable ξ, are given by

$$x_1(x^A + \delta x_1^A) = x_1(x^A) + \frac{(1-\xi)}{2}\delta x_1^A \tag{5.10}$$

$$x_2(x^A + \delta x_1^A) = x_2(x^A) \tag{5.11}$$

Using this change the derivatives, taken with respect to a change in the first coordinate of A, are then given by

$$x_{1,x_1^A} = \frac{(1+\eta\xi)}{2} \quad \text{and} \quad x_{2,x_1^A} = 0 \tag{5.12}$$

where $\eta = -1$ is the local coordinate of the end node A. Similarly, a change in the second coordinate direction at A gives the derivatives as:

$$x_{1,x_2^A} = 0 \quad \text{and} \quad x_{2,x_2^A} = \frac{(1+\eta\xi)}{2} \tag{5.13}$$

The same can be done with node B giving the derivatives with respect to each coordinate direction at B to be (see Figure 5.2)

$$x_{1,x_1^B} = \frac{(1+\eta\xi)}{2} \quad \text{and} \quad x_{2,x_1^B}=0 \tag{5.14}$$

$$x_{1,x_2^B} = 0 \quad \text{and} \quad x_{2,x_2^B} = \frac{(1+\eta\xi)}{2} \tag{5.15}$$

where $\eta = 1$ is the local coordinate of the end node B.

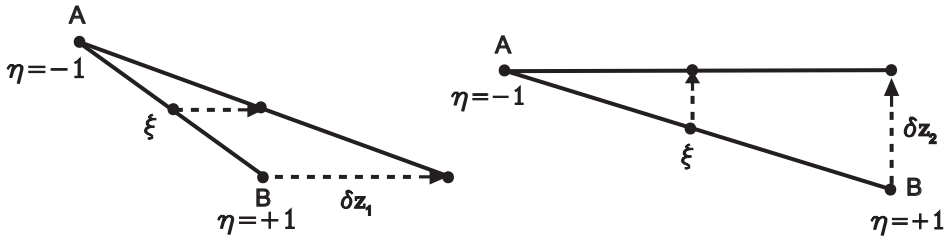

Figure 5.2: Change to node B of a straight crack

Applying simple parametric function, the derivatives of the element node with respect to random parameter Z_m can be written in generalized form as:

$$x_{i,z_m} = \frac{(1+\eta\xi)}{2}\delta_{im} \tag{5.16}$$

where

$$\delta_{im} = \begin{cases} 1 & if\ Z_m\ represents\ a\ change\ in\ direction\ i \\ 0 & otherwise \end{cases}$$

Using the above definitions, the other required derivatives can be simplified. The derivatives of the coordinate distance components are defined by

$$r_{i,m} = \frac{\partial r_i}{\partial z_m} = x_{i,m}(\mathbf{x}) - x_{i,m}(\mathbf{x}') \tag{5.17}$$

On the crack element, this derivative can be written as

$$r_{i,m} = \frac{\eta}{2}(\xi - \xi')\delta_{im} \tag{5.18}$$

where ξ' is the local coordinate of the source node $\mathbf{x}'$. Similarly, the derivative of the distance r can also be written as

$$r_{,m} = r_{i,m}r_{,i} = \frac{\eta}{2}(\xi - \xi')\delta_{im}r_{,i} \tag{5.19}$$

However, since the element is flat, the normal can be written as

$$\begin{aligned} r_{,1} &= -\mathrm{n}_2 \\ r_{,2} &= \mathrm{n}_1 \end{aligned} \tag{5.20}$$

and the derivative of the distance can then be written as

$$\begin{aligned} r_{,m} &= -\frac{\eta}{2}(\xi - \xi')\mathrm{n}_2 \quad \textit{when } Z_m \textit{ represents a change in direction } 1 \\ r_{,m} &= \frac{\eta}{2}(\xi - \xi')\mathrm{n}_1 \quad \textit{when } Z_m \textit{ represents a change in direction } 2 \end{aligned} \tag{5.21}$$

Similarly, the derivatives of the element lengths can be also determined as:

$$l_{i,m} = x_{i,m}(B) - x_{i,m}(A) = \eta\delta_{im} \tag{5.22}$$

$$l_{,m} = -\frac{1}{l}l_i\eta\delta_{im} = \eta\delta_{im}r_{,i} \tag{5.23}$$

Then, since the Jacobian can be written in terms of this length, the derivative of Jacobian transformation can be evaluated as

$$J = \frac{l}{2}$$

$$\Rightarrow J_{,m} = \frac{\eta}{2}\delta_{im}r_{,i} \tag{5.24}$$

and gives

$$J_{,m} = -\frac{\eta}{2}\mathrm{n}_2 \qquad \textit{when } Z_m \textit{ represents a change in direction } 1$$

$$J_{,m} = \frac{\eta}{2}\mathrm{n}_1 \qquad \textit{when } Z_m \textit{ represents a change in direction } 2 \tag{5.25}$$

Using the relationships between the normal components and the distance derivatives (5.20), the normal derivatives can be written as

$$\mathrm{n}_{1,m} = r_{,2m} = \frac{r_{2,m}}{r} - \frac{r_{,2}r_{,m}}{r^2} = \frac{\eta}{l}(\delta_{2m} - r_{,2}r_{,i}\delta_{im}) \tag{5.26}$$

$$\mathrm{n}_{2,m} = -r_{,1m} = \frac{r_{1,m}}{r} - \frac{r_{,1}r_{,m}}{r^2} = -\frac{\eta}{l}(\delta_{1m} - r_{,1}r_{,i}\delta_{im}) \tag{5.27}$$

Using these expressions and the relationships in equation (5.20) again, these derivatives can be written as

$$\mathrm{n}_{1,m} = \frac{\eta}{l}\mathrm{n}_1\mathrm{n}_2 \qquad \mathrm{n}_{2,m} = -\frac{\eta}{l}\mathrm{n}_1^2 \qquad \textit{when } Z_m \textit{ represents a change in direction } 1$$

$$\mathrm{n}_{1,m} = \frac{\eta}{l}\mathrm{n}_2^2 \qquad \mathrm{n}_{2,m} = -\frac{\eta}{l}\mathrm{n}_1\mathrm{n}_2 \qquad \textit{when } Z_m \textit{ represents a change in direction } 2 \tag{5.28}$$

In Chapter 3, the normal derivatives of the distance r was shown to be zero for a flat element, which gives

$$\frac{\partial r}{\partial \mathrm{n}} = r_{,k}\mathrm{n}_{,k} = 0 \tag{5.29}$$

Differentiation of this expression gives

$$(r_{,k}\mathrm{n}_{,k})_{,m} = \frac{(r_k n_{,k})_{,m}}{r} - \frac{2(r_{,k}\mathrm{n}_{,k})r_{,m}}{r} = 0 \tag{5.30}$$

Therefore it can be shown that

$$(r_k \mathrm{n}_{,k})_{,m} = 0 \tag{5.31}$$

Derivative displacement equation

In the displacement equation, since the crack is traction free, the integral with terms involving the U_{ij} and $U_{ij,m}$ kernels are not required. The integrals required are those containing the T_{ij} and $T_{ij,m}$ fundamental solutions. The T_{ij} kernel was considered in Chapter 3, where

$$T_{ij}(\mathbf{x}', \mathbf{x}(\xi)) = \frac{1-2\nu}{4\pi(1-\nu)} \left[\frac{(1-2\nu)}{2\pi l(1-\nu)(\xi-\xi')} h^n_{ij} \right] \tag{5.32}$$

where $h^n = (h^n_{ij})$ is given by

$$h = \begin{bmatrix} 0 & -1 \\ 1 & 0 \end{bmatrix} \tag{5.33}$$

The $T_{ij,m}$ is also required for the derivative analysis and is given by

$$T_{ij,m}(\mathbf{x}', \mathbf{x}) = -\frac{(1-2\nu)}{4\pi(1-\nu)r^2} \Big\{ (n_i r_{j,m} + n_{i,m} r_j - n_j r_{i,m} - n_{j,m} r_i) + 2(n_j r_{,i} - n_i r_{,j}) r_{,m} \Big\} \tag{5.34}$$

Using the derivative expressions for components on a flat crack, this can be reduced to be,

$$T_{ij,m}(\mathbf{x}', \mathbf{x}(\xi)) = -\frac{\eta(1-2\nu)}{2\pi(1-\nu)} \frac{\mathrm{n}_2}{l^2(\xi-\xi')} h^n_{ij} \qquad \textit{for a change in direction } 1 \tag{5.35}$$

$$T_{ij,m}(\mathbf{x}', \mathbf{x}(\xi)) = \frac{\eta(1-2\nu)}{2\pi(1-\nu)} \frac{\mathrm{n}_1}{l^2(\xi-\xi')} h^n_{ij} \qquad \textit{for a change in direction } 1 \tag{5.36}$$

Using these expressions with the Jacobian and its derivative the new integrals in the derivative equation can be evaluated. The integral required for analytical integration then reduces to:

$$\int_{-1}^{+1} \left[T_{ij,m}(\mathbf{x}', \mathbf{x}(\xi))J^{\gamma}(\xi) + T_{ij}(\mathbf{x}', \mathbf{x}(\xi))J^{\gamma}_{,m}(\xi)\right] M^{n}(\xi)d\xi = 0 \tag{5.37}$$

Derivative traction equation

The integrals in the derivative traction equation can be simplified with the expressions for flat crack elements. Since the crack is traction free, only the integrals containing the S_{kij} and $S_{kij,m}$ terms are required analytically and these fundamental solutions are investigated here. The first of these terms, S_{kij} can be written, on a flat element, as

$$\begin{aligned} S_{kij}(\mathbf{x}', \mathbf{x}) =& \frac{E}{4\pi(1-\nu^2)r^2} \Big\{ \left[2\nu r_{,j} r_{,k} + (1-2\nu)\,\delta_{jk}\right] \mathrm{n}_i + \left[2\nu r_{,i} r_{,k} \right. \\ & \left. + (1-2\nu)\,\delta_{ik}\right] \mathrm{n}_j + \left[2\,(1-2\nu)\, r_{,i} r_{,j} - (1-4\nu)\,\delta_{ij}\right] \mathrm{n}_k \Big\} \\ =& \frac{E}{\pi l^2 (1-\nu^2)(\xi-\xi^2)} h^{n}_{kij} \end{aligned} \tag{5.38}$$

where the terms $h^n = h^n_{kij}$ are given by

$$h = \begin{bmatrix} h^n_{111} & h^n_{211} \\ h^n_{122} & h^n_{222} \\ h^n_{112} & h^n_{221} \end{bmatrix} = \begin{bmatrix} n_1(2n_2^2+1) & -n_2(-2n_2^2+1) \\ n_1(2n_1^2-1) & n_2(2n_1^2+1) \\ -n_2(2n_1^2-1) & n_1(-2n_2^2+1) \end{bmatrix} \tag{5.39}$$

Also, the derivative kernel $S_{kij,m}$ is required and this can be written, on a flat crack element as

$$
\begin{aligned}
S_{kij,m}(\mathbf{x}', \mathbf{x}(\xi)) =& \frac{E}{4\pi(1-\nu^2)r^3} \Big\{ \left[2\nu r_{,j} r_{,k} + (1-2\nu)\delta_{jk}\right] \mathrm{n}_{i,m} r \\
&+ \left[2\nu r_{,i} r_{,k} + (1-2\nu)\delta_{ik}\right] \mathrm{n}_{j,m} r \\
&+ \left[2(1-2\nu) r_{,i} r_{,j} - (1-4\nu)\delta_{ij}\right] \mathrm{n}_{k,m} r \\
&- 2\left[\left(4\nu r_{,j} r_{,k} + (1-2\nu)\delta_{jk}\right) r_{,m} - \nu(r_{j,m} r_{,k} + r_{k,m} r_{,j})\right] \mathrm{n}_i \\
&- 2\left[\left(4\nu r_{,i} r_{,k} + (1-2\nu)\delta_{ik}\right) r_{,m} - \nu(r_{i,m} r_{,k} + r_{k,m} r_{,i})\right] \mathrm{n}_j \\
&- 2\left[\left(4(1-2\nu) r_{,i} r_{,j} - (1-4\nu)\delta_{ij}\right) r_{,m}\right. \\
&\left. -(1-2\nu)(r_{j,m} r_{,i} + r_{i,m} r_{,j})\mathrm{n}_k\right] \Big\}
\end{aligned} \tag{5.40}
$$

This term can be divided into three possible cases. The first, written as $S_{iii}$is for $i = j = k$, the second, S_{kii} has $i = j \neq k$, whilst the third, S_{iij} has $i = k \neq j$.

$$
\begin{aligned}
S_{iii,m}(\mathbf{x}', \mathbf{x}(\xi)) =& \frac{E}{4\pi(1-\nu^2)r^3} \Big[(1 + 2r_{,i}^2)\mathrm{n}_{i,m} r \\
&+2\left(2r_{i,m} r_{,i} - (1 + 4r_{,i}^2) r_{,m}\right) \mathrm{n}_i \Big]
\end{aligned} \tag{5.41}
$$

$$
\begin{aligned}
S_{kii,m}(\mathbf{x}', \mathbf{x}(\xi)) =& \frac{E}{4\pi(1-\nu^2)r^3} \Big\{ 4\nu r_{,i} r_{,k} \mathrm{n}_{i,m} r \\
&+ \left[2(1-2\nu) r_{,i}^2 - (1-4\nu)\right] \mathrm{n}_{k,m} r \\
&- 4\nu\left[4 r_{,i} r_{,k} r_{,m} - (r_{i,m} r_{,k} + r_{k,m} r_{,i})\right] \mathrm{n}_i \\
&- 2\left[\left(4(1-2\nu) r_{,i}^2 - (1-4\nu)\right) r_{,m}\right. \\
&\left. -2(1-2\nu) r_{i,m} r_{,i})\mathrm{n}_k\right] \Big\}
\end{aligned} \tag{5.42}
$$

and

$$
\begin{aligned}
S_{iik,m}(\mathbf{x}', \mathbf{x}(\xi)) = & \frac{E}{4\pi(1-\nu^2)r^3}\Big\{2(1-\nu)r_{,i}r_{,k}\mathrm{n}_{i,m}r \\
& + \left[2\nu r_{,i}^2 + (1-2\nu)\right]\mathrm{n}_{j,m}r \\
& - 2(1-\nu)\left[4r_{,k}r_{,i}r_{,m} - (r_{i,m}r_{,i} + r_{i,m}r_{,k})\right]\mathrm{n}_i \\
& -2\left[(4\nu(r_{,i}^2-1)+1)r_{,m} - 2\nu r_{i,m}r_{,i}\right]\mathrm{n}_k\Big\}
\end{aligned}
\tag{5.43}
$$

These terms then give

$$
S_{kij,m}(\mathbf{x}', \mathbf{x}(\xi)) = \frac{E\eta}{\pi l^3(1-\nu^2)(\xi-\xi')^2}h^n_{kij,m} \tag{5.44}
$$

where the terms $h^n_m = h^n_{kij,m}$ are given by

$$
h^n_m = \begin{bmatrix} n_1n_2(10n_2^2-1) & 10n_2^4 - 9n_2^2 + 1 \\ n_1n_2(10n_1^2-3) & 10n_1^4 + 5n_1^2 + 2 \\ 10n_2^4 - 9n_2^2 + 1 & n_1n_2(10n_2^2-3) \end{bmatrix} \quad \begin{matrix} for\ a\ change \\ in\ direction\ 1 \end{matrix} \tag{5.45}
$$

and

$$
h^n_m = \begin{bmatrix} 10n_2^4 - 5n_2^2 - 2 & n_1n_2(-10n_2^2+3) \\ -10n_1^4 + 9n_1^2 - 1 & n_1n_2(-10n_1^2+1) \\ n_1n_2(-10n_2^2+3) & -10n_1^4 + 9n_1^2 - 1 \end{bmatrix} \quad \begin{matrix} for\ a\ change \\ in\ direction\ 2 \end{matrix} \tag{5.46}
$$

Using these representations with the Jacobian and its derivatives, J^γ and $J^\gamma_{,m}$, as given by equations (3.79) and (5.24), the required integral for analytical

integration can be written as

$$\int_{-1}^{+1} \left[S_{kij,m}(\mathbf{x}', \mathbf{x}(\xi)) J^{\gamma}(\xi) + S_{kij}(\mathbf{x}', \mathbf{x}(\xi)) J^{\gamma}_{,m}(\xi) \right] M^{n}(\xi) d\xi$$

$$= \frac{E\eta}{2\pi l^2 (1-\nu^2)} h^{n}_{kij,m} u^{n}_{j} \int_{-1}^{+1} \frac{M^{n}(\xi)}{(\xi - \xi')^2} d\xi \tag{5.47}$$

where the terms $h^{n}_{m} = h^{n}_{kij,m}$ are given by

$$h^{n}_{m} = \begin{bmatrix} 2n_1 n_2 (4n_2^2 - 1) & -8n_2^2 n_1^2 + 1 \\ 2n_1 n_2 (4n_1^2 - 1) & 8n_2^2 n_1^2 - 4n_1^2 + 1 \\ -8n_2^2 n_1^2 + 1 & 2n_1 n_2 (-4n_2^2 + 3) \end{bmatrix} \begin{array}{l} for\, a\, change\, z_m \\ in\, direction\, 1 \end{array} \tag{5.48}$$

and

$$h^{n}_{m} = \begin{bmatrix} -8n_1^2 n_2^2 + 4n_2^2 - 1 & 2n_1 n_2 (-4n_2^2 + 1) \\ 8n_1^2 n_2^2 - 1 & 2n_1 n_2 (-4n_1^2 + 1) \\ 2n_1 n_2 (4n_1^2 - 3) & 8n_2^2 n_1^2 - 1 \end{bmatrix} \begin{array}{l} for\, a\, change\, z_m \\ in\, direction\, 2 \end{array} \tag{5.49}$$

5.3 Derivatives of stress intensity factor

The derivatives of *J-Integral*

The *J-integral* in equation (3.100) can be written as

$$J = \int_{\Gamma} \left(W n_1 - t_1 \varepsilon_{11} - t_2 \frac{\partial u_2}{\partial x_1} \right) ds \tag{5.50}$$

where W is the strain energy density per unit area, defined in equation (3.98). Expanding the terms in equation (3.99) gives

$$W = \frac{1}{2}\left(\sigma_{11}\varepsilon_{11} + \sigma_{22}\varepsilon_{22} + \sigma_{12}\varepsilon_{12}\right) \tag{5.51}$$

The stress tensors, σ_{ij}, and strain tensors ε_{ij} are defined in equation (3.3) and (3.99), respectively. The components of the traction vectors $t_j = \sigma_{ij}n_j$ are given as

$$\begin{aligned} t_1 &= \sigma_{11}n_1 + \sigma_{12}n_2 \\ t_2 &= \sigma_{12}n_1 + \sigma_{22}n_2 \end{aligned} \tag{5.52}$$

For plane strain, the strain tensors ε_{ij} are given as

$$\begin{aligned} \varepsilon_{11} &= \frac{1-\nu^2}{E}\left(\sigma_{11} - \frac{\upsilon}{1-\upsilon}\sigma_{22}\right) \\ \varepsilon_{22} &= \frac{1-\nu^2}{E}\left(\sigma_{22} - \frac{\upsilon}{1-\upsilon}\sigma_{11}\right) \\ \varepsilon_{12} &= \frac{1+\nu}{E}\sigma_{12} \end{aligned} \tag{5.53}$$

and for plane stress

$$\begin{aligned} \varepsilon_{11} &= \frac{1}{E}\left(\sigma_{11} - \nu\sigma_{22}\right) \\ \varepsilon_{22} &= \frac{1}{E}\left(\sigma_{22} - \nu\sigma_{11}\right) \\ \varepsilon_{12} &= \frac{1+\nu}{E}\sigma_{12} \end{aligned} \tag{5.54}$$

Direct differentiation of J in equation (5.50) with respect to random variable Z_m gives

$$J_{,m} = \int_{\Gamma} \Big[W_{,m} \mathrm{n}_1 + W \mathrm{n}_{1,m} - t_{1,m}\varepsilon_{11} \\ -t_1 \varepsilon_{11,m} - t_{2,m} \frac{\partial u_2}{\partial x_1} - t_2 \left(\frac{\partial u_2}{\partial x_1} \right)_{,m} \Big] ds$$

Assuming the crack length a to be the variable of interest, since the crack faces are modelled as straight lines, therefore, a change in crack length is restricted to the coordinates of the end node of the crack elements in the x_1 direction only, induced $\frac{\partial u_2}{\partial x_{1,m}} = 0$. $J_{,m}$ then becomes

$$J_{,m} = \int_{\Gamma} \Big[W_{,m} n_1 + W n_{1,m} - t_{1,m}\varepsilon_{11} \\ -t_1 \varepsilon_{11,m} - t_{2,m} \frac{\partial u_2}{\partial x_1} - t_2 \frac{\partial u_{2,m}}{\partial x_1} \Big] ds \tag{5.55}$$

where $W_{,m}$, $t_{1,m}$ and $t_{2,m}$ can be obtained by direct differentiation of equations (5.51) and (5.52), to give

$$W_{,m} = \frac{1}{2} \Big(\sigma_{11,m}\varepsilon_{11} + \sigma_{11}\varepsilon_{11,m} + \sigma_{22,m}\varepsilon_{22} \\ +\sigma_{22}\varepsilon_{22,m} + \sigma_{12,m}\varepsilon_{12} + \sigma_{12}\varepsilon_{12,m} \Big) \tag{5.56}$$

and the derivatives of traction components with respect to the random variable Z_m give

$$t_{1,m} = \sigma_{11,m} n_1 + \sigma_{11} n_{1,m} + \sigma_{12,m} n_2 + + \sigma_{12} n_{2,m} \tag{5.57}$$

and

$$t_{2,m} = \sigma_{12,m} n_1 + \sigma_{12} n_{1,m} + \sigma_{22,m} n_2 + \sigma_{22} n_{2,m} \tag{5.58}$$

For plane strain conditions, the derivative of strain tensors ε_{ij} with respect to random variable Z_m are given as

$$\begin{aligned}
\varepsilon_{11,m} =& \frac{1-\nu^2}{E}\left(\sigma_{11,m} - \frac{\upsilon}{1-\upsilon}\sigma_{22,m}\right) \\
\varepsilon_{22,m} =& \frac{1-\nu^2}{E}\left(\sigma_{22,m} - \frac{\upsilon}{1-\upsilon}\sigma_{11,m}\right) \\
\varepsilon_{12,m} =& \frac{1+\nu}{E}\sigma_{12,m}
\end{aligned} \tag{5.59}$$

and for plane stress conditions

$$\begin{aligned}
\varepsilon_{11,m} =& \frac{1}{E}\left(\sigma_{11,m} - \nu\sigma_{22,m}\right) \\
\varepsilon_{22,m} =& \frac{1}{E}\left(\sigma_{22,m} - \nu\sigma_{11,m}\right) \\
\varepsilon_{12,m} =& \frac{1+\nu}{E}\sigma_{12,m}
\end{aligned} \tag{5.60}$$

The integral in equation (5.55) is also independent of the domain size Γ; a more detail study on the path independent property of the derivative of *J-integral* can be found in Anderson [7]. The derivative of *J-integral* can be calculated also by the Trapezoidal rule. For the implementation in the DBEM, the derivative of stress intensity factor with respect to random variables can be obtained by the same decomposition method illustrated in Chapter 3. The derivatives of integral $J_{,m}$ with respect to random variable Z_m can then be represented by the sum of two derivative integrals as:

$$J_{,m} = J^I_{,m} + J^{II}_{,m} \tag{5.61}$$

The relationship between the derivative of *J-integral* components and derivative of SIFs with respect to random variable Z_m at each mode becomes:

$$J^I_{,m} = \frac{(K^2_I)_{,m}}{E'}$$

$$\Rightarrow K_{I,m} = \frac{J^I_{,m} E'}{2K_I} \tag{5.62}$$

and

$$J^{II}_{,m} = \frac{(K^2_{II})_{,m}}{E'}$$

$$\Rightarrow K_{II,m} = \frac{J^{II}_{,m} E'}{2K_{II}} \tag{5.63}$$

where K_I and K_{II} are the values evaluated from the deterministic boundary element analysis.

5.4 Analytical gradient for LEFM

The structure fails when mode I stress intensity factor (SIF) is greater or equal to the critical stress intensity factor $K_I \geq K_{Ic}$. This requirement cannot be satisfied with certainty, since K_I is dependent on the input vector $\mathbf{Z}$ which is random, and K_{Ic} itself may be a random variable. The probability of failure P_f, is defined as in equation 4.32 and the performance function can be defined as:

$$g(\mathbf{Z}) = K_{Ic} - K_I \tag{5.64}$$

where K_{Ic} is the critical stress intensity factor. Using the transformation formula given in 4.36, the performance function in the $\mathbf{\Psi}$ space can then be expressed as

$$g_{\Psi}(\mathbf{\Psi}) = g(\mathbf{Z}(\mathbf{\Psi})) = K_{Ic}(\mathbf{Z}(\mathbf{\Psi})) - K_I(\mathbf{Z}(\mathbf{\Psi})) \tag{5.65}$$

The first-order derivative of $g_{\Psi}(\mathbf{\Psi})$ with respect to Ψ_k is given as equation (4.38). The partial derivatives in the Z_m space are

$$\frac{\partial g}{\partial Z_m} = -\frac{\partial K_I}{\partial Z_m} \tag{5.66}$$

and the derivative of performance function with respect to critical stress intensity factor K_{Ic} is

$$\frac{\partial g}{\partial K_{ic}} = 1 \tag{5.67}$$

The partial derivative of fracture parameters with respect to random variables can be easily calculated. Hence, for a given Ψ or Z_m, all gradients of $g_{\Psi}(\mathbf{\Psi})$ can be evaluated analytically. Figure 5.3 illustrates the algorithm of the probabilistic analysis with BEM.

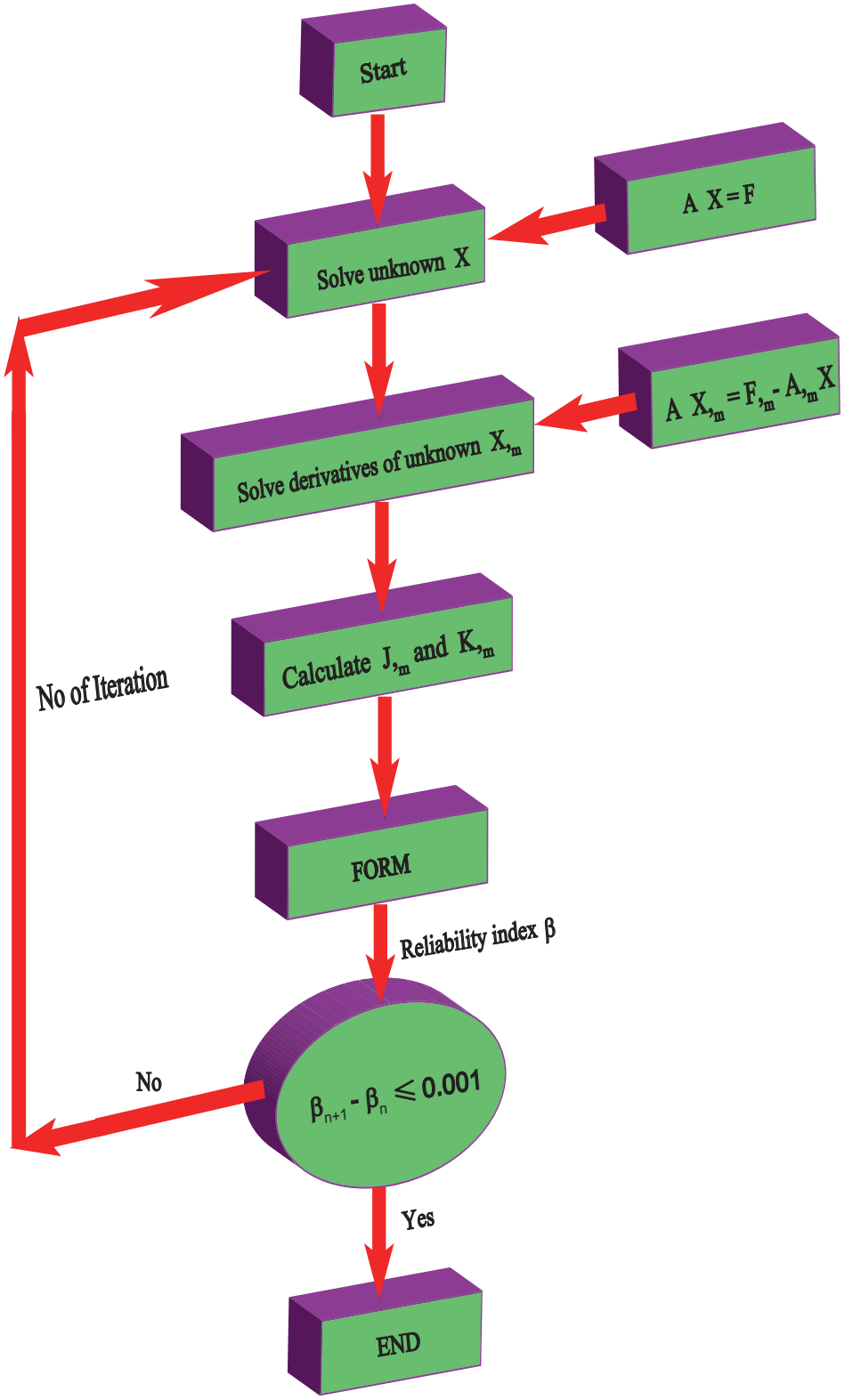

Figure 5.3: Flowchart of algorithm

5.5 Examples

5.5.1 Sensitivity analysis of centre crack specimen

Consider a centre crack panel with width W, length $L = 2W$, crack length a and elastic modulus is E, subjected to a far-field remote tensile stress $\sigma/E = 1$. The Poisson's ratio $\nu = 0.3$. Figure 5.4 illustrates the geometry and loads of the centre crack specimen.

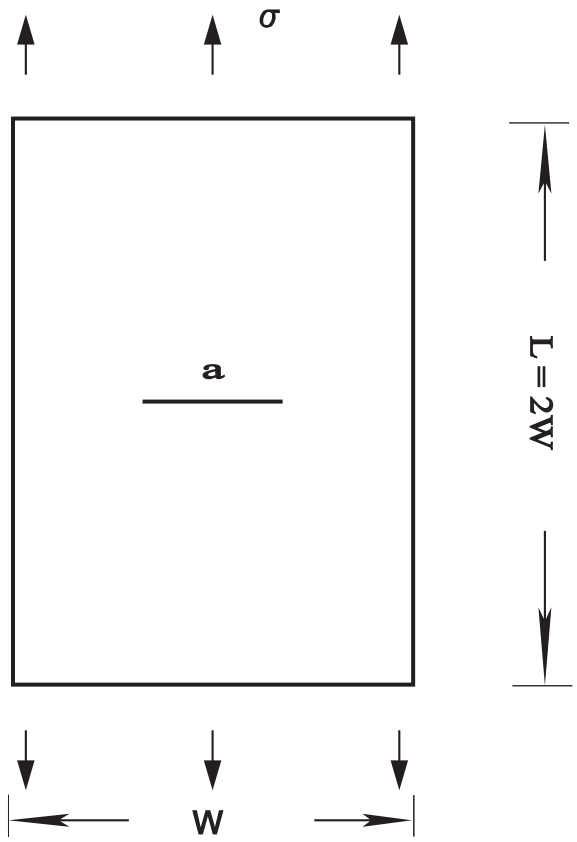

Figure 5.4: Geometry and loads of centre crack specimen

The external boundary is discretised with 20 continuous boundary elements, while the crack face is discretised with three different number of elements with 6, 8, 10 quadratic discontinuous elements for each derivatives calculation, respectively. Plane stress conditions were assumed. The random parameter of interest

is the crack size; the evaluation of derivatives of boundary response with respect to crack size is the key to calculating the fracture parameter's derivative. Subsequently, the evaluation of the gradient of performance functions in probabilistic analysis.

Figure 5.5 shows the boundary conditions and the discretisation using 36 quadratic elements. The external boundary is discretised with 20 continuous boundary elements, while each crack face is discretised with 8 discontinuous elements.

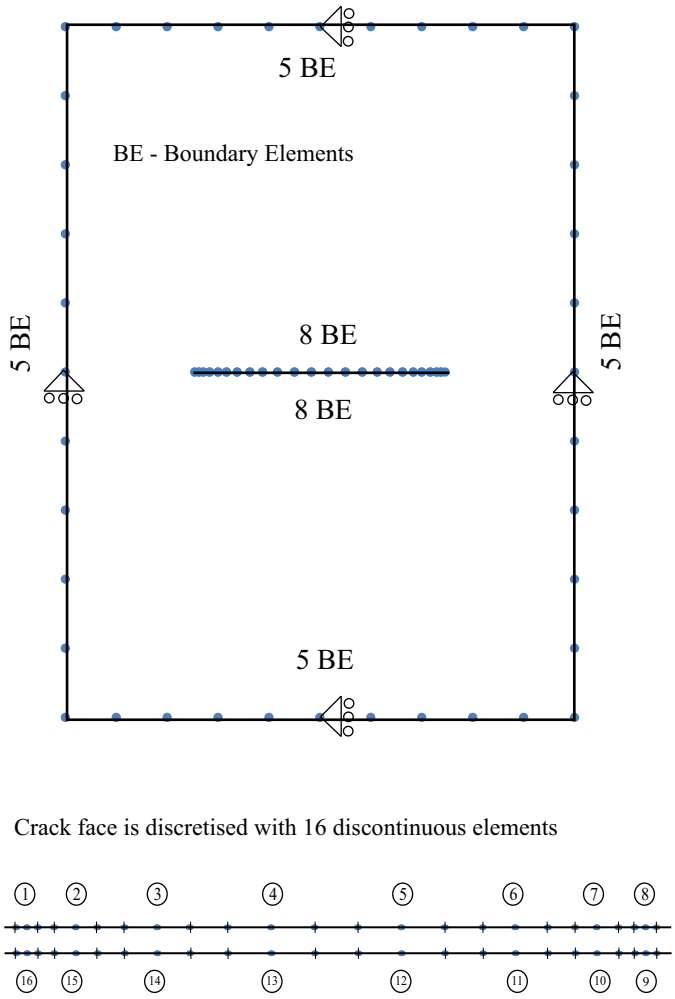

Figure 5.5: Boundary conditions and discretisation of centre crack specimen

Figure 5.6 shows the sensitivity error for the derivatives of boundary displacement compare with forward different approximation with 4 different step size. As can be seen in Figure 5.6, the overall percentage error for the derivatives of boundary displacements are really small. It also demonstrates the step size with 0.01 and 0.001 yield better derivative results for boundary displacement of centre crack specimen than the step size of 0.1 and 0.0001.

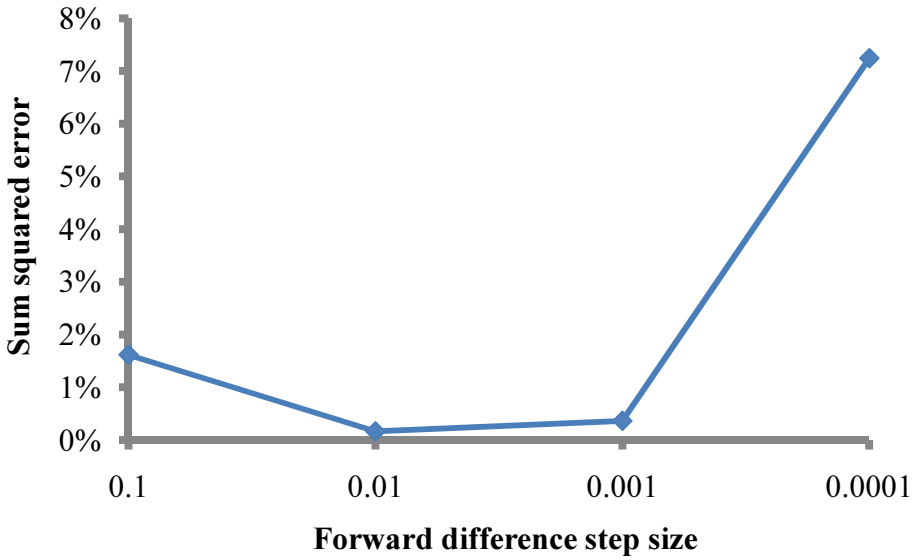

Figure 5.6: Sensitivity errors for centre crack specimen

Different normalised crack lengths are also considered in this example, with a/W varying from 0.1 to 0.7. As can be seen in Figures 5.7 and 5.8, the evaluation of K_I and $\partial K_I/\partial a$ agree well with the available analytical solution from Tada et al. [105]. The increase of the number of elements on the crack face also yielded better accuracy of the evaluation of K_I and $\partial K_I/\partial a$.

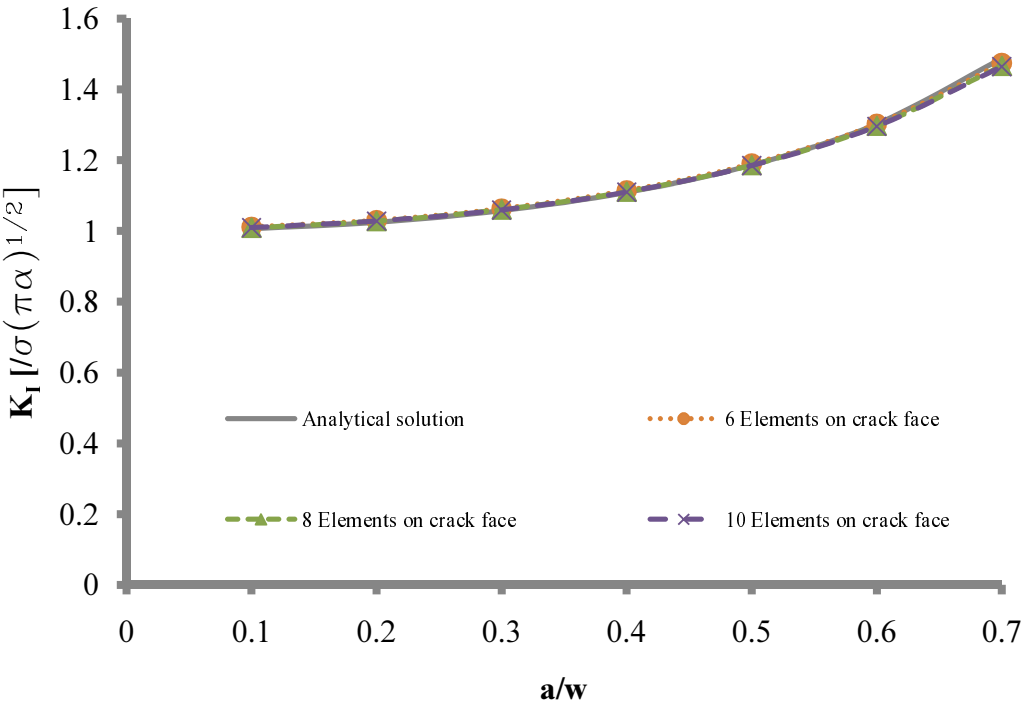

Figure 5.7: Normalised mode I stress intensity factor for centre crack specimen

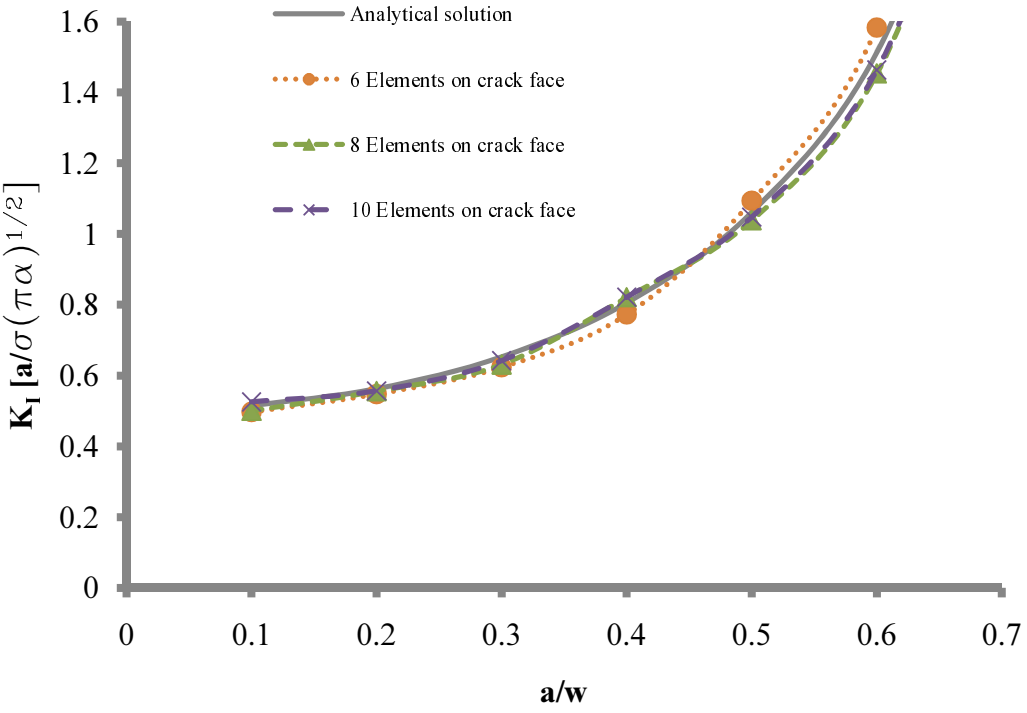

Figure 5.8: Normalised derivatives of mode I stress intensity factor with respect to crack length

Table 5.1 presents analytical solution for an infinite panel for K_I and $\partial K_I/\partial a$ [105], and the numerical results for the center crack problem with a/W equal to 0.2 and 0.5, respectively. Each crack face is modelled with 8 discontinuous elements. The results in Table 5.1 demonstrated the proposed derivative BEM provides very accurate evaluation of $\partial K_I/\partial a$ in comparison with the corresponding results from the analytical solution. The difference between the results of the proposed method and the analytical solution is less than 2%.

Table 5.1: Normalised derivative of Mode I stress intensity factor with respect to crack length by the proposed and analytical methods for centre crack specimen

a/W	K_I			$\partial K_I/\partial a$		
	BEM	Analytical	Difference* (%)	BEM	Analytical	Difference* (%)
0.2	1.0279	1.0245	0.337	0.5561	0.5629	1.21
0.5	1.1862	1.1862	0.002	1.0388	1.0619	2.18

* Difference is defined by (Analytical - BEM)/Analytical

5.5.2 Sensitivity analysis of single edge crack specimen

Consider a single edge crack specimen with width W, length $L = 2W$, crack length a and elastic modulus is E, subjected to a far-field remote tensile stress $\sigma = E$. The Poisson's ratio $\nu = 0.25$. The geometry and loads of the single edge crack specimen are shown in Figure 5.9.

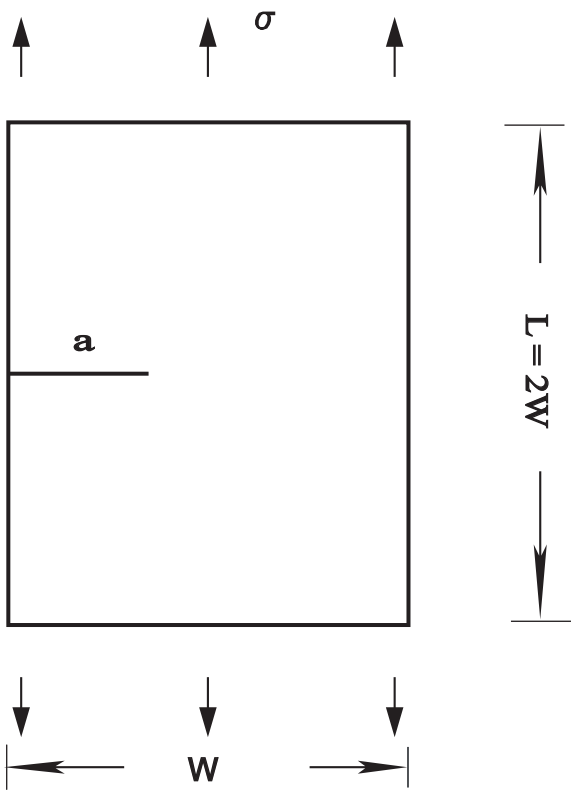

Figure 5.9: Geometry and loads of single edge crack specimen

The external boundary is discretised with 25 continuous elements, while the crack face is discretised using three different number of element with 6, 8, 10 quadratic discontinuous elements for each derivatives calculation, respectively. As before, a plane stress condition was studied.

Figure 5.10 shows the boundary conditions and the discretisation using 41 quadratic elements. The external boundary is discretised with 25 boundary ele-

ments, while each crack face is discretised with 8 discontinuous elements.

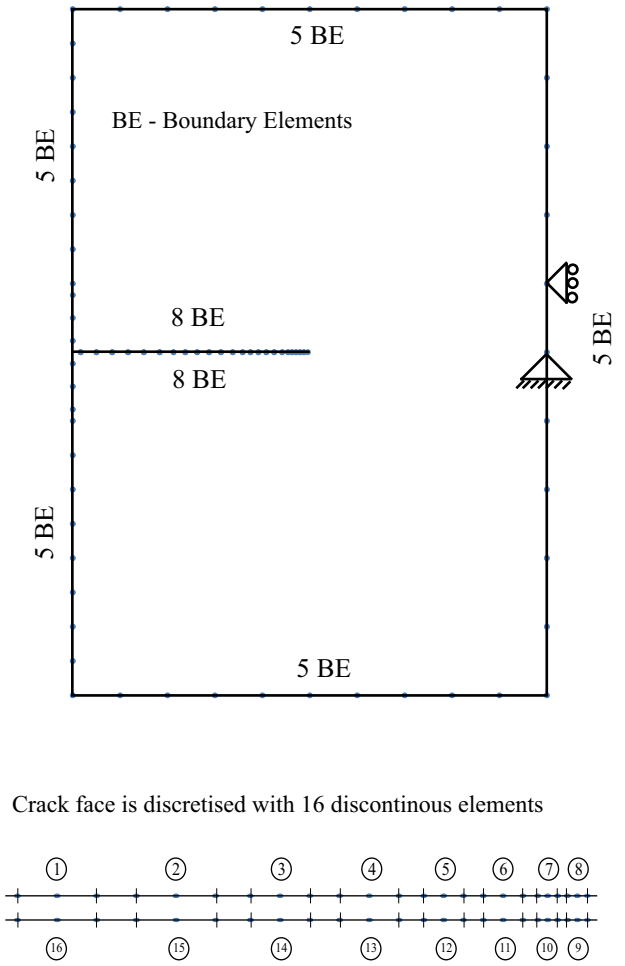

Figure 5.10: Boundary conditions and discretisation of single edge crack specimen

Figure 5.11 investigates the sensitivity error for the derivatives of boundary stress compared with finite difference approximation with 4 different step sizes, where the overall derivatives of boundary stress with respect to crack size are computed accurately. The step size with 0.01 and 0.001 yield better derivative of boundary stress with respect to crack size of single edge crack specimen than the step size of 0.1 and 0.0001.

Different normalised crack lengths were also considered in this example, with

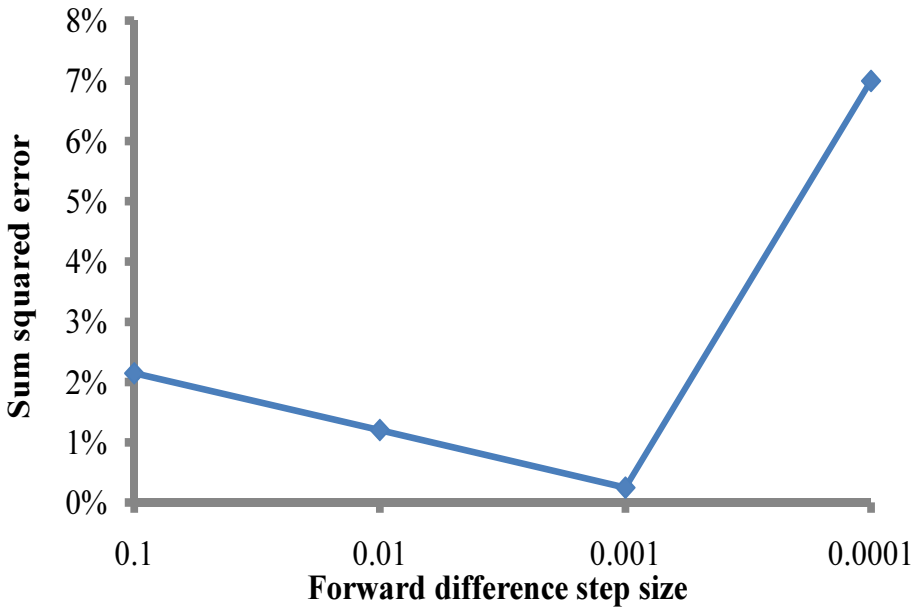

Figure 5.11: Sensitivity errors for single edge crack specimen

a/W varying from 0.1 to 0.7. As can be seen in Figures 5.12 and 5.13, the evaluation of K_I and $\partial K_I/\partial a$ agree well with the available analytical solution from Tada et al. [105]. Table 5.2 presents the numerical results for K_I and $\partial K_I/\partial a$ for the single edge crack problem. Two sets of results are shown for $\partial K_I/\partial a$, the first computed using the proposed method and the second set was calculated using the analytical solution [105]. As in Example 5.5.1, the results in Table 5.2 also demonstrate that the proposed method provides accurate estimates of $\partial K_I/\partial a$ as compared with corresponding results from the analytical solution. The proposed method and the analytical solution agree well with less than 2% difference.

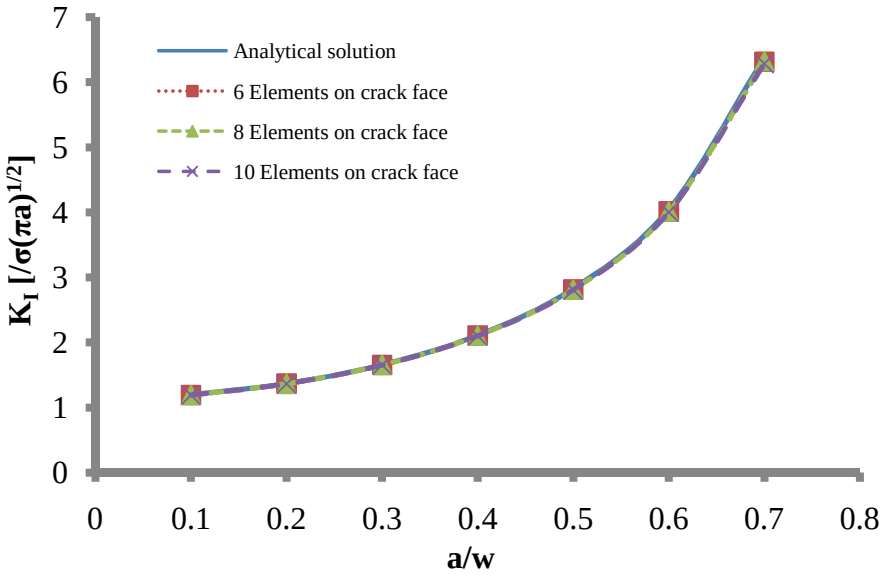

Figure 5.12: KI for single edge crack specimen

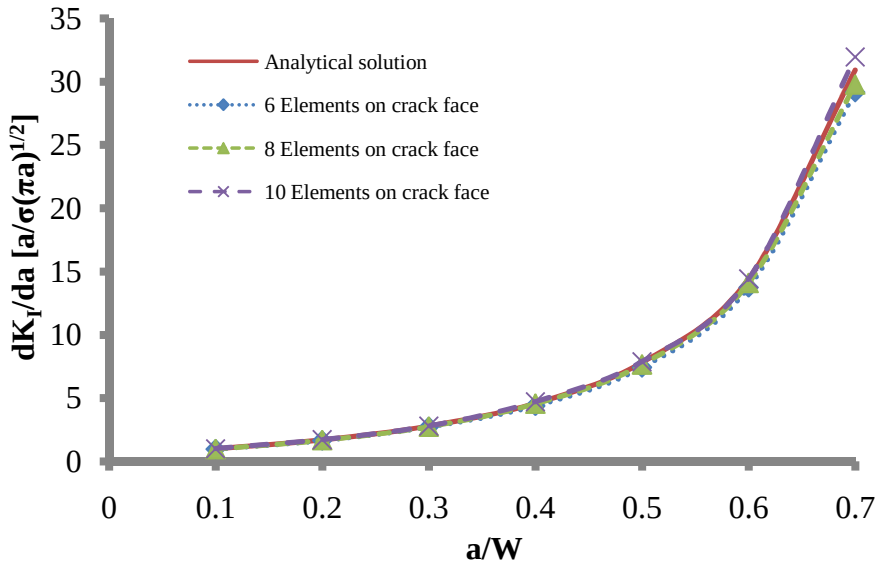

Figure 5.13: dKI/da for single edge crack specimen

Table 5.2: Normalised derivative of Mode I stress intensity factor with respect to crack length by the proposed and analytical methods for single edge crack specimen

a/W	K_I			$\partial K_I/\partial a$		
	BEM	Analytical	Difference* (%)	BEM	Analytical	Difference* (%)
0.2	1.3655	1.3666	0.078	1.6745	1.68	0.333
0.5	2.812	2.8265	0.515	7.6581	7.8027	1.854

* Difference is defined by (Analytical - BEM)/Analytical

5.5.3 Sensitivity analysis of Mixed-mode problem

This mixed-mode example can be found in the work of Rao and Rahman [92]. In this example, an edge-cracked plate is fixed at the bottom and subjected to a shear traction $t = 1$ unit applied on the top, as shown in Figure 5.14. The dimensions of the plate were length $L = 16$ units and width $W = 7$ units. The elastic modulus and Poisson's ratio were 30×10^6 units and 0.25, respectively. A plane strain condition was assumed. The normalised crack lengths $\frac{a}{W}$ of 0.1 to 0.6 are considered.

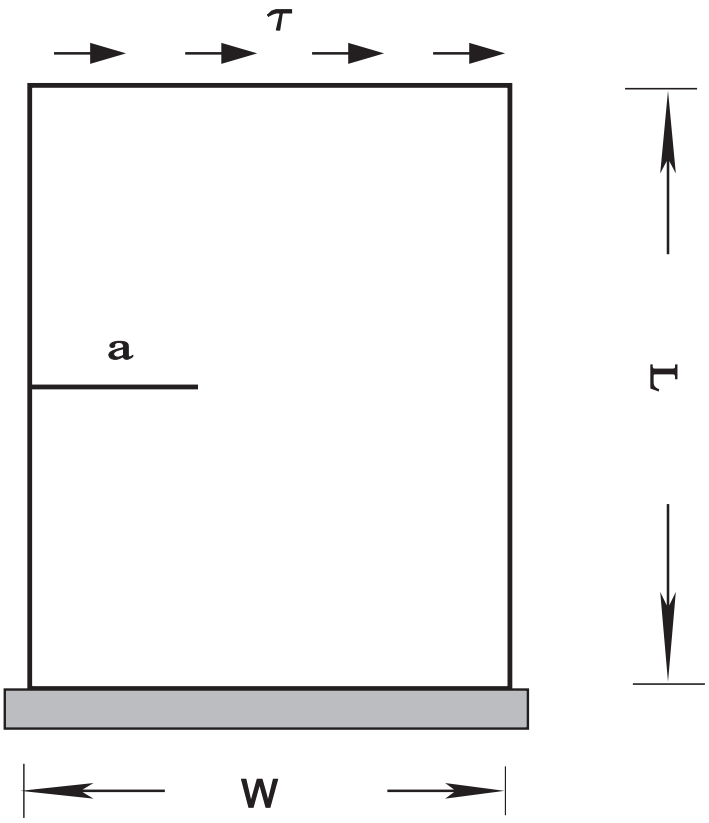

Figure 5.14: Geometry and loads of Mixed-mode specimen

Figure 5.15 shows the boundary conditions and the discretisation using 41 quadratic elements. The BEM model employed 25 continuous elements on the external boundary, while the each crack face is discretised using 8 quadratic

discontinuous elements.

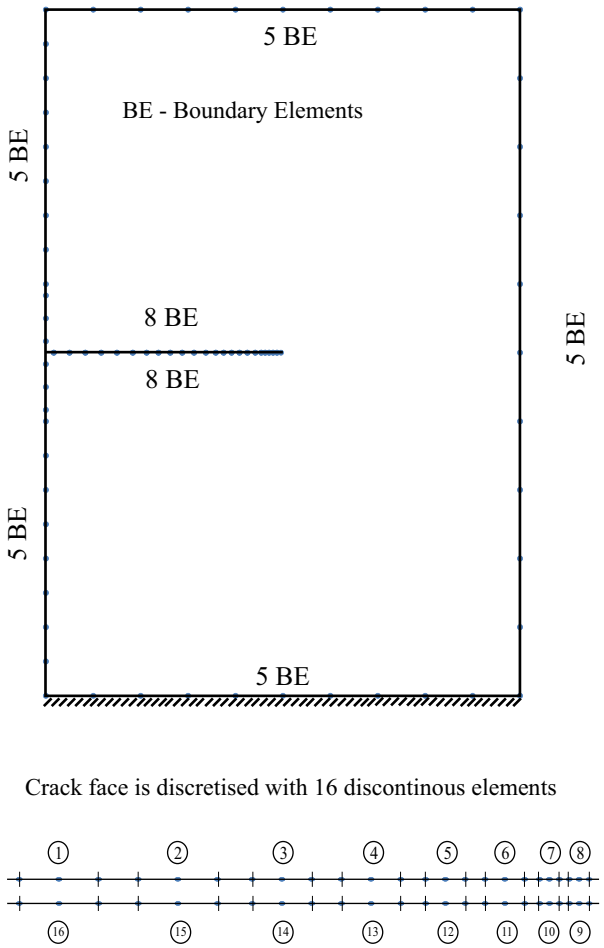

Figure 5.15: Boundary conditions and discretisation of Mixed-mode specimen

Tables 5.3 to 5.6 present the results for mode I and mode II, respectively. The tables compare the results obtained using the BEM Sensitivity, the finite difference approach with the BEM and FEM which is reported in [92]. A step size with 0.01 of crack length is adopted in both finite difference approaches.

Table 5.3: Mode-I SIF

a/W	K_I		
	BEM	FEM[92]	Difference[1] (%)
0.3	19.868	19.82	0.247
0.4	25.732	25.68	0.206
0.5	34.173	34.09	0.244%

Table 5.4: Mode-II SIF

a/W	K_{II}		
	BEM	FEM[92]	Difference[1] (%)
0.3	2.4814	2.46	0.87
0.4	3.5212	3.49	0.89
0.5	4.5771	4.54	0.82

[1] Difference is defined by (FEM - BEM)/FEM

Table 5.5: First-order derivative of mode-I SIF

a/W	$\partial K_I/\partial a$				
	BEM-Sensitivity	BEM-FDM	Difference[2] (%)	FEM-FDM[92]	Difference[3] (%)
0.3	7.3226	7.1	3.14	7.143	2.51
0.4	10.0316	9.87821	1.55	9.643	4.02
0.5	15.2339	14.9376	1.98	15.14	0.62

Table 5.6: First-order derivative of mode-II SIF

a/W	$\partial K_{II}/\partial a$				
	BEM-Sensitivity	BEM-FDM	Difference[2] (%)	FEM-FDM[92]	Difference[3] (%)
0.3	1.4719	1.4582	0.94	1.476	1.205
0.4	1.4982	1.4951	0.21	1.393	7.33
0.5	1.5504	1.5221	-1.86	1.486	4.33

[2] Difference is defined by (FDM - BEM)/FDM
[3] Difference is defined by (FEM - BEM(Sensitivity))/FEM

The results show reasonable agreement between the three methods. The finite difference method coupled with finite element method is reported by Rao and Rahman [92]. The maximum difference between the results of the sensitivity method and the finite difference method coupled with BEM is less than 3.14%, while compare with the results obtained by finite difference method coupled with finite element method has a maximum difference of 7.33%. For $\frac{a}{W}$ equal to 0.4, a smaller percentage of difference than $\frac{a}{W} = 0.3$ arised in the evaluation of first

order derivatives of mode I and mode II of SIF with respect to crack size. Such difference also appeared in the results obtained by the FEM-FDM in the work of Rao and Rahman [92], where the $\frac{a}{W}$ equal to 0.5 has a smaller percentage of difference than $\frac{a}{W} = 0.4$. The cause of such difference is due to the chosen step size is 0.01 of crack length in finite difference approximation for this particular example. The suggestion for this difference is use step size with 0.001 of crack length for $\frac{a}{W} = 0.3$, and use step size with 0.01 of crack length for $\frac{a}{W} = 0.4$.

Figures 5.16 and 5.17 show that the evaluation of $\partial K_I/\partial a$ and $\partial K_{II}/\partial a$ using the sensitivity approach agree well with the finite different method for the normalised crack lengths $\frac{a}{W}$ from 0.1 to 0.6 .

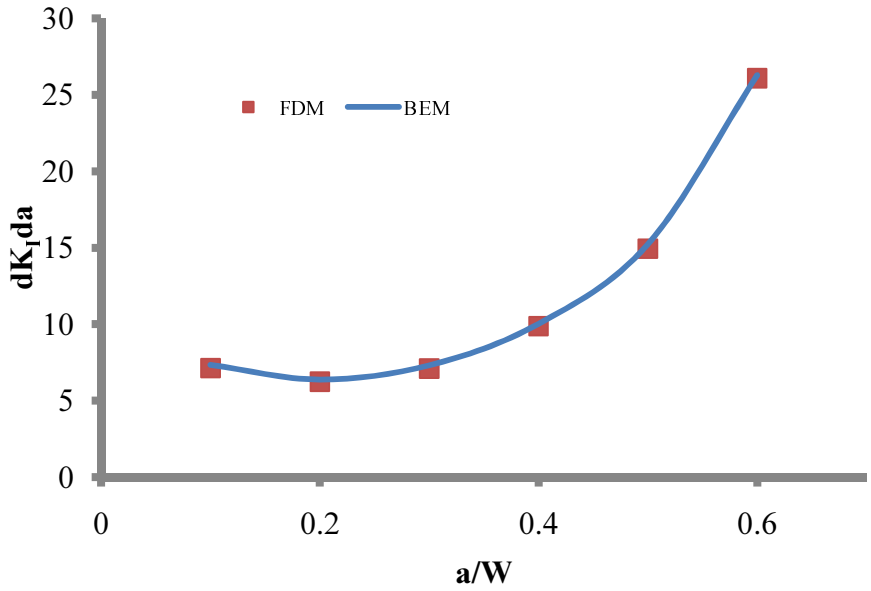

Figure 5.16: dKI/da for single edge crack under shear stress

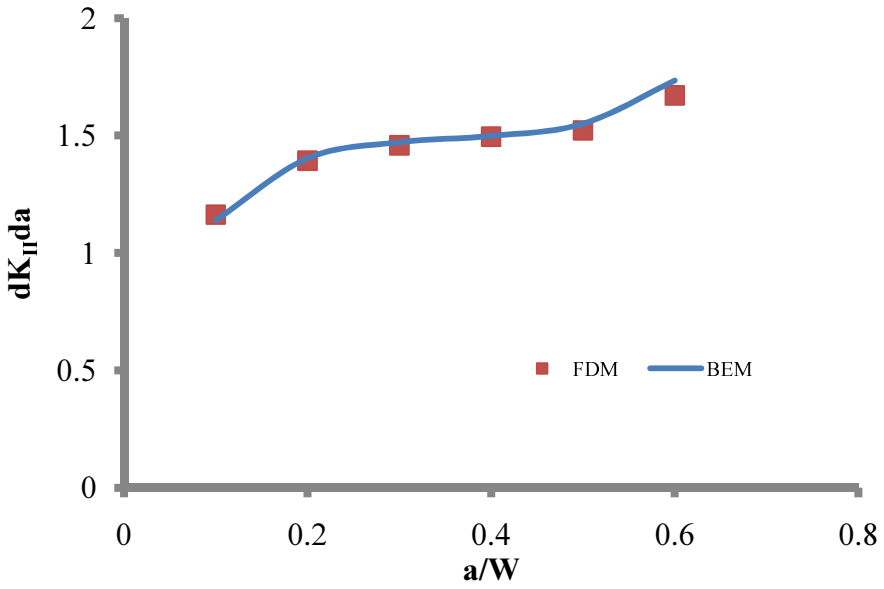

Figure 5.17: dKII/da for single edge crack under shear stress

5.5.4 Reliability analysis of double edge crack specimen

The example presented here can be found in the work of Chen et al. [28]. In their study, the material derivative concept of continuum mechanics, domain integral representation of the J-integral and direct differentiation are used to obtain the derivatives of fracture parameters with respect to random parameters. In the example they stated, a double edge crack tension specimen with crack length a, width $2W$, length $L = 5W$ is subjected to a far-field tensile stress σ, as shown in Figure 5.18. The load, crack size and material properties were treated as statistically independent random variables.

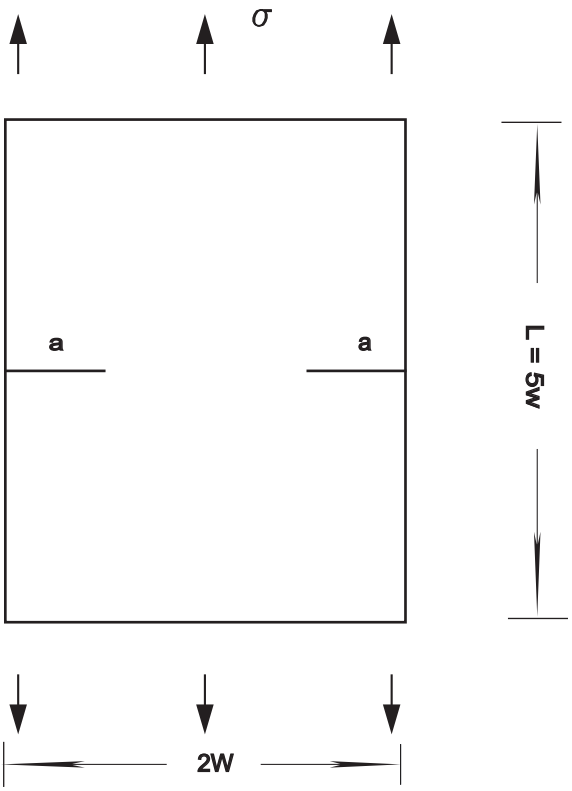

Figure 5.18: Geometry and loads of double edge crack specimen

Table 5.7 presents the mean, coefficient of variation (COV) and probability distribution for each of these random parameters. The Poisson's ratio $\nu = 0.3$

was assumed to be deterministic. The plane stress condition is assumed in this example.

Table 5.7: Statistical properties of random input for double edge crack specimen

	Mean	COV[a]	Probability distribution
Normalised crack length ($\frac{a}{w}$)	0.5	Variable[b]	Lognormal
Elastic modulus(E)	$206.8GPa$	0.05	Normal
Initiation fracture toughness (J_{ic})	1242.6 kJ/m^2	0.47	Lognormal
Far-field tensile stress (σ)	Variable[b]	0.1	Normal

[a] Coefficient of variation (COV) = standard deviation/mean.
[b] Arbitrarily varied.

Half of the plate is modelled due to symmetry. Figure 5.19 shows the boundary conditions and the discretisation using 41 quadratic elements. The BEM model employed 25 continuous elements on the external boundary, while the each crack face is discretised using 8 quadratic discontinuous elements.

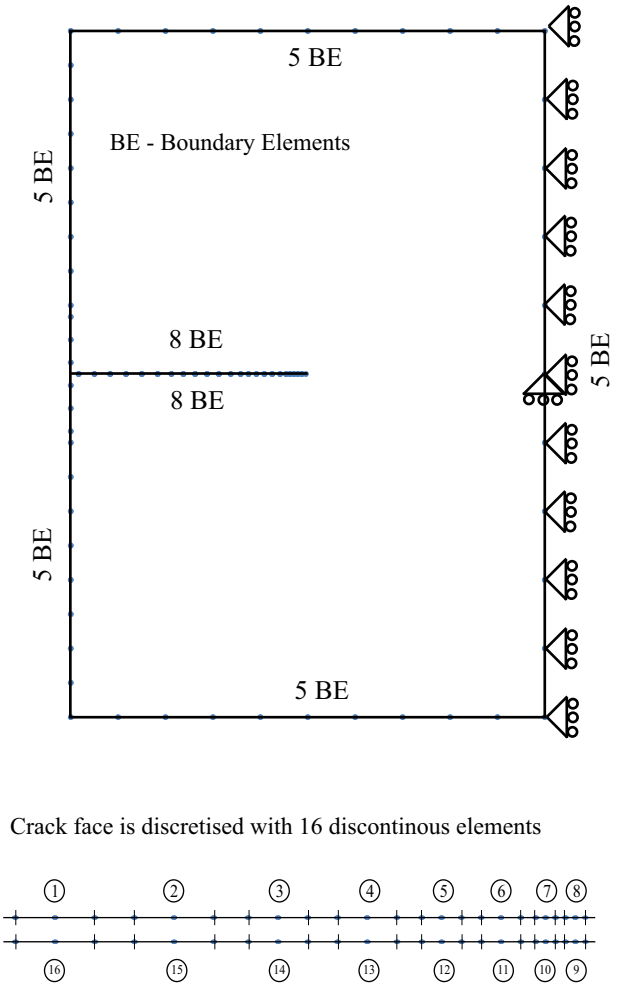

Figure 5.19: Boundary conditions and discretisation of double edge crack specimen

The performance function in this particular example is in terms of fracture toughness which is defined as:

$$g(X) = J_{Ic} - J \tag{5.68}$$

A number of probabilistic analyses were performed to calculate the probability of failure P_f of the double edge crack specimen, as a function of mean far-field tensile stress $E[\sigma]$, where $E[\bullet]$ is the mean operator. Figures 5.20 to 5.24 plot the P_f vs. $E[\sigma]$ results for $V_{a/\mathrm{W}} = 0$; 10; 20; 30 and 40 percent, where $V_{a/\mathrm{W}}$ is the

COV of the normalised crack length a/W.

The probability of failure was calculated using the proposed method and Monte Carlo simulation. For the Monte Carlo simulation, the closed form solution provided in Tada et al. [105] is used to obtain the fracture parameter and its derivatives with respect to crack size. The geometry coefficient in this particular example is calculated using modified Benthem's empirical formula, and is given as [105]:

$$F\left(\frac{a}{W}\right) = \frac{1.122 - 0.561(a/W) - 0.205(a/W)^2 + 0.471(a/W)^3 - 0.19(a/W)^4}{\sqrt{1 - a/W}} \tag{5.69}$$

100000 simulations were carried out to evaluate the probability of failure. As can be seen in Figures 5.20 to 5.24, the probability of failure obtained by the proposed method is in good agreement with Chen et al. [28] and the simulation results. Figure 5.25 indicates that the failure probability increases with the COV (uncertainty) of a/W.

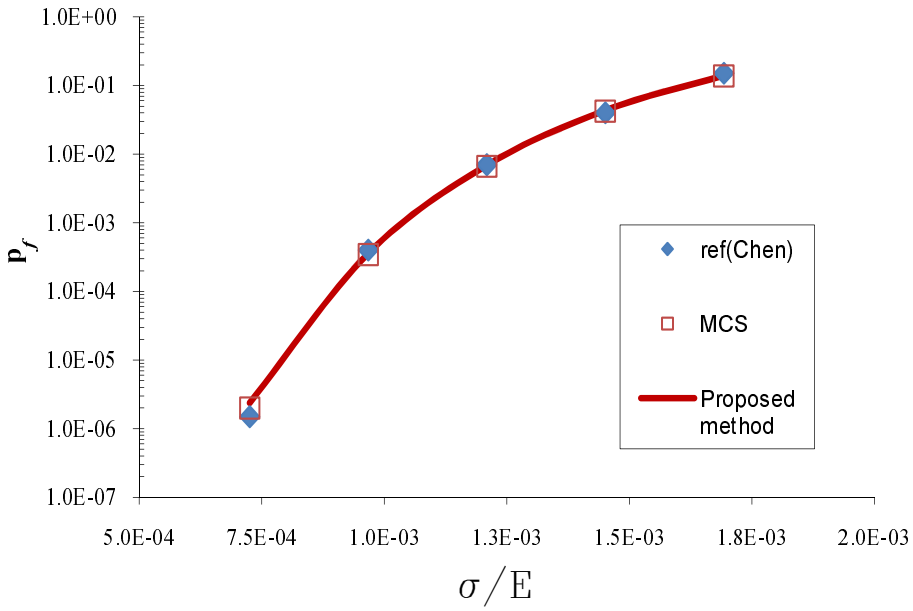

Figure 5.20: POF and simulation with Va/w=0.

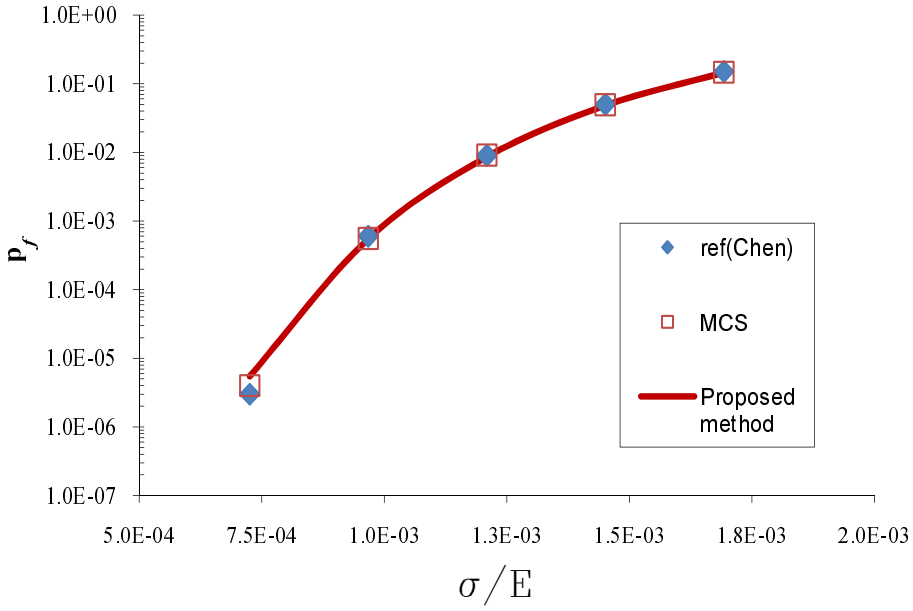

Figure 5.21: POF and simulation with Va/w=0.1

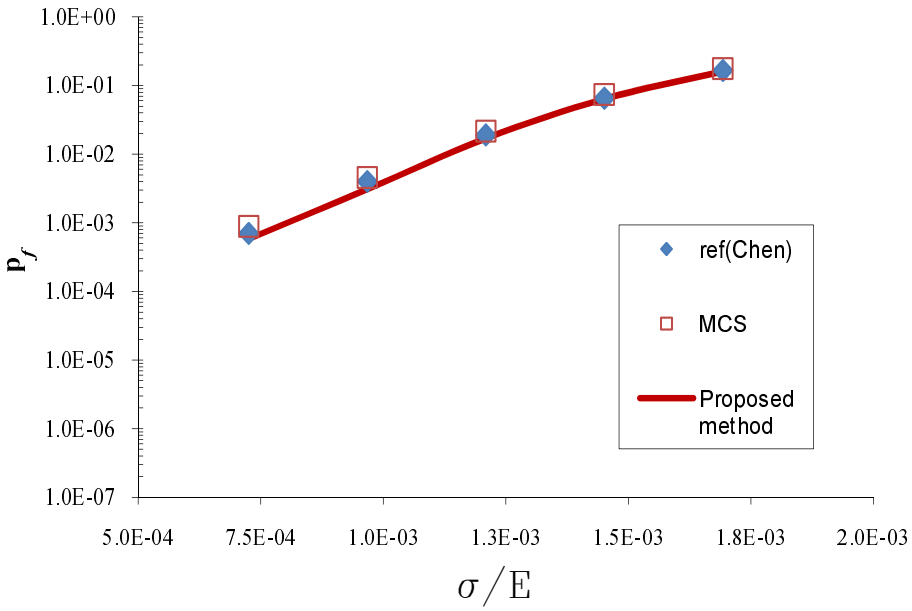

Figure 5.22: POF and simulation with Va/w=0.2

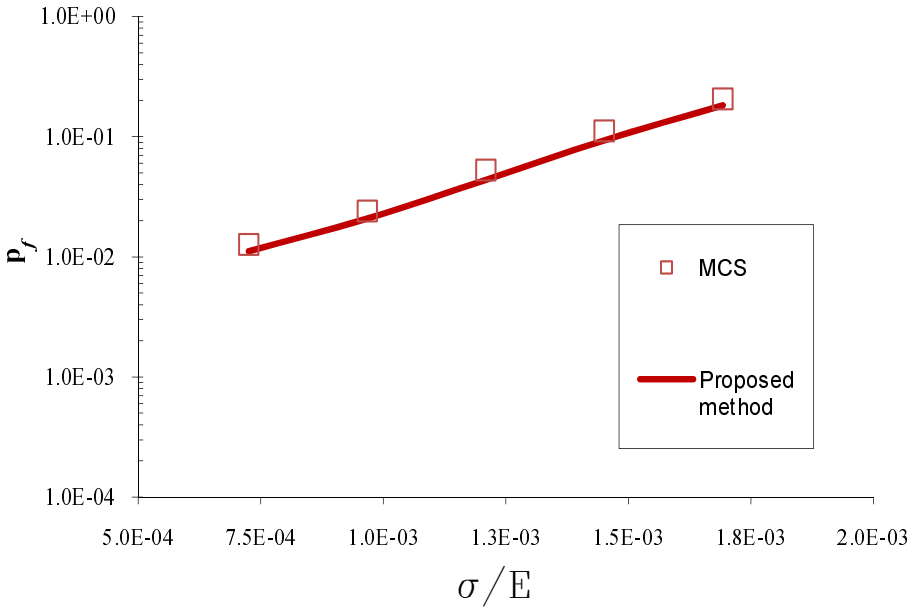

Figure 5.23: POF and simulation with Va/w=0.3

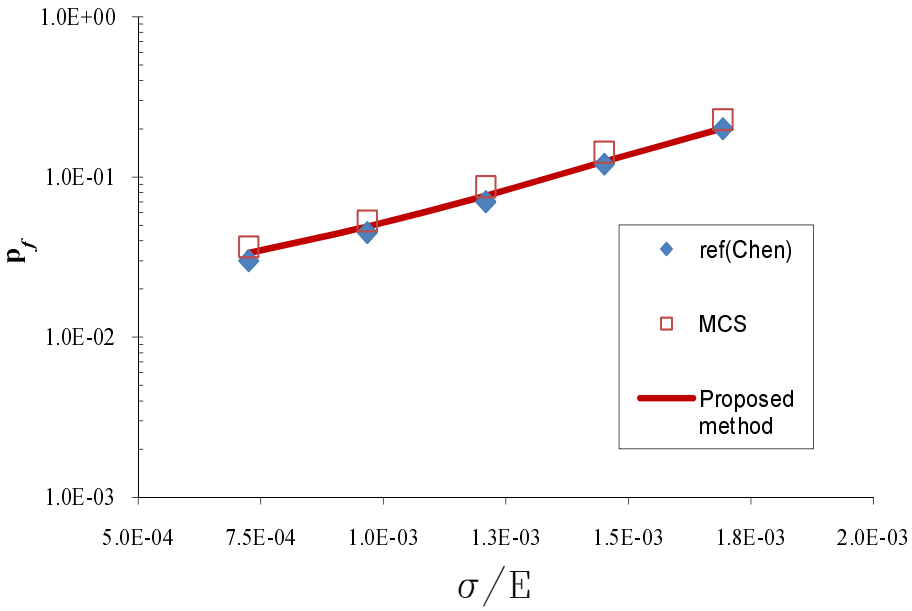

Figure 5.24: POF and simulation with Va/w=0.4

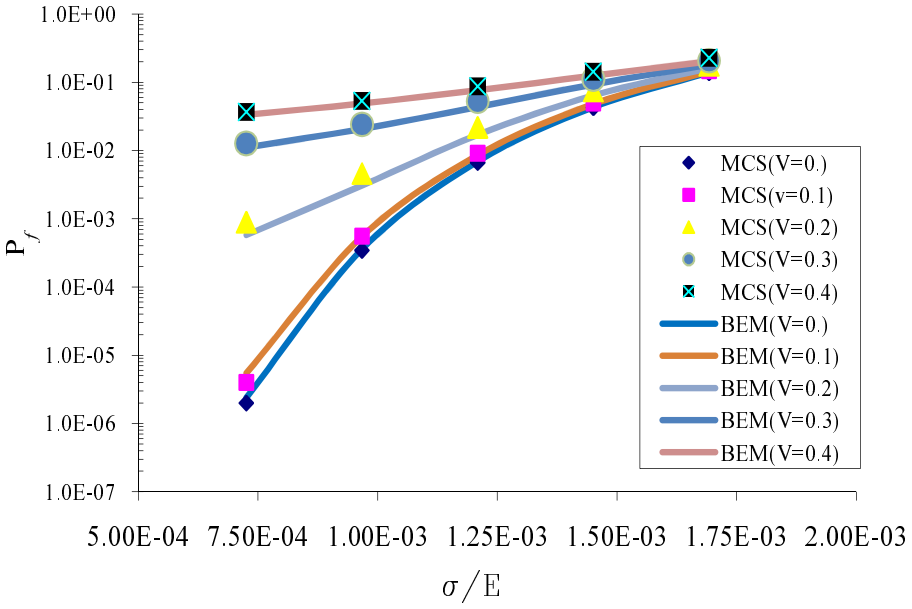

Figure 5.25: POF for various uncertainties in crack size

Sensitivity of random variables is investigated for cases when normalised crack length $a/\mathrm{w} = 0.3$ and $a/\mathrm{w} = 0.5$ with an uncertainty of $V_{a/\mathrm{W}} = 0.1$, as can be seen in Figures 5.26 and 5.27, the fracture toughness contributed more for the

reliability of structure. The normalised crack length a/w and far field tensile stress σ have negative sensitivity factors, meaning the increase of crack length or stress will induce higher probability of failure. Figures 5.26 and 5.27 also display three different levels of far field tensile stress σ normalised with Young Modulus E while other random variables are unchanged, which show how the variation of sensitivity of all random variables relate to the change of stress.

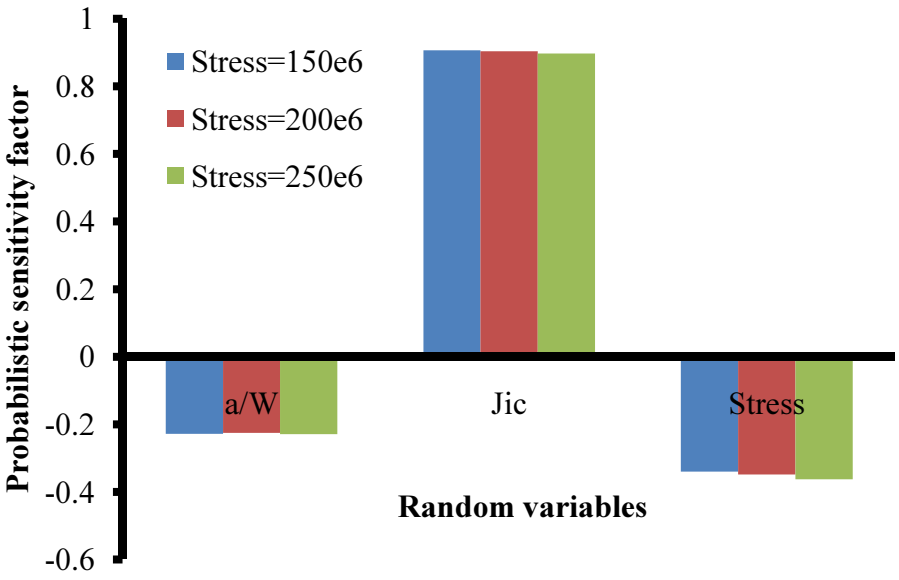

Figure 5.26: Probabilistic sensitivity factor for $\frac{a}{W} = 0.3$

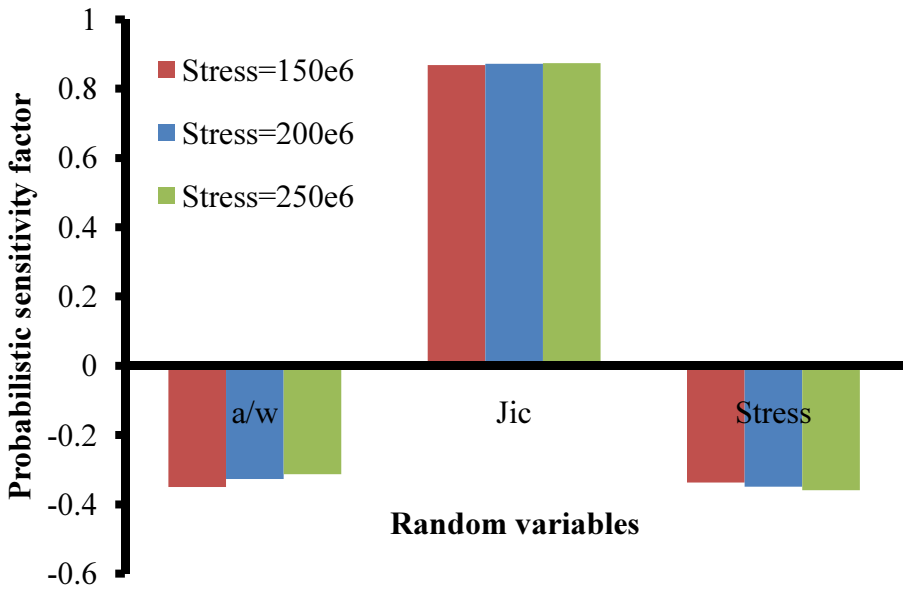

Figure 5.27: Probabilistic sensitivity factor for $\frac{a}{W} = 0.5$

5.6 Summary

In this chapter, the dual boundary element method coupled with FORM for calculating reliability of the problem in LEFM was presented. The proposed method can be used to evaluate the response derivatives with respect to the random parameter in reliability analysis, accurately and fast, as it does not require the resolution of the system of equations. The Hasofer-Lind iterative technique is used to find the failure point. The sensitivity of the random variables affecting the reliability of component was also investigated. The results obtained from the proposed method demonstrated good agreement with the Monte Carlo simulation.

Chapter 6

Stochastic dual boundary element method for fatigue crack growth

6.1 Introduction

Fatigue crack growth is sensitive to many parameters and these parameters can seldom be determined accurately. Uncertainties in the crack geometry, material properties, crack direction, crack growth, component geometry and load time history all play a role. Thus, the prediction of fatigue failure must be treated as a probabilistic problem [62, 115, 101, 81, 14, 15, 98].

Early application of probabilistic analysis to fatigue crack growth can be found in the works of Ortiz and Kiremidjian [81], Kozin and Bogdanoff [62], Besterfield et al. [15], Schall et al. [98], Harkness et al. [51] and Zhu et al. [117]. A probabilistic finite element method in conjunction with FORM has been developed by Besterfield et al. [15] and Harkness et al. [51] for the reliability analysis of the fatigue crack growth. Meanwhile, Schall et al. [98] have linked a finite element analysis with the reliability calculation through a response surface program using Hermite polynomials for the fatigue reliability of marine structures. Zhu

et al. [117] simulated the material resistance to fatigue crack growth and the time-history of the stress randomly to obtain the analytical expressions for a randomized Paris-Erdogan law. Peng et al. [84] combined the stochastic finite element method with second-order three-moment reliability analytical model to investigate the fatigue strength reliability of a gear teeth subjected to bending.

The application of the BEM to fatigue crack growth is widely used since the early 90s. Portela et al. [87] and Mi and Aliabadi [77] presented an application of the Dual Boundary Element Method to the analysis of mixed-mode crack growth in 2D, where the crack growth processes were simulated with an incremental crack extension analysis based on the maximum principal stress criterion for 2D. Lua et al. [70] and Liu et al. [68] both combined the mixed boundary integral equations with first order reliability method for probabilistic crack growth analysis. In their study, the least-squares fitting routine was used to obtain the first-order response-surface model of the random parameters.

In this chapter, the method proposed by Portela et al. [86] will be implemented for stochastic fatigue crack growth analysis. Each new crack growth is treated as an incremental crack growth, and modelled with new boundary elements. For every crack growth, since the crack increment size is predefined in this work, the number of elements added on each crack face will be defined by the increment size; the assumption is to keep the size of the new elements equal to the last element used in crack mesh model which is based on the study by Portela et al. [86]. The new elements will generate new equations to be added to existing ones. The derivatives of the dual boundary integral equations will be formulated to compute the derivatives of boundary responses. The derivatives of the fracture parameter with respect to random parameters, required for probabilistic analysis, will be calculated at each crack increment, as implemented in Chapter 5.

With the evaluation of derivatives of fracture parameter with respect to random parameters accurately, the derivatives of fatigue life with respect to random parameters can be calculated at each crack increment by the total derivative method [88, 68, 70]. Finally, the first order reliability method will be used to evaluate the reliability index. The randomness in the initial crack length, final crack length, fatigue crack growth parameters and the applied stress will be considered in this work. Numerical examples will be presented to validate the method developed here; comparison will be made with Monte Carlo simulations to demonstrate the accuracy of the numerical algorithm.

6.2 Stochastic process in fatigue crack growth

In the numerical simulation of fatigue crack growth, both crack growth direction and crack growth laws are required. The rate of fatigue crack growth, da/dN, can be determined from experiments [7, 21]. This fatigue crack growth law can be used to predict the fatigue life of a component and create a mapping from the fatigue life to the crack growth. While the problem can be formulated under this mapping, the fatigue process is inherently a stochastic process.

The most common law for fatigue crack growth is the Paris-Erdogan model [83] given in equation (3.110), and it can be written as

$$N = \int_{a_0}^{a_f} \frac{1}{C(\triangle K_{eq})^m} da \tag{6.1}$$

where a_0 and a_f are the initial and final crack lengths, respectively; da is the crack increment size; C and m are fatigue crack growth parameters but can also depend on the loading and environmental effects; and ΔK_{eq} is the range of the

equivalent stress intensity factor K_{eq} which is based on the maximum principal stress theory defined in equation (3.109).

6.2.1 Random parameters in fatigue crack growth

For simplicity, only the initial and final crack lengths, applied load and the fatigue crack growth parameters in the Paris law will be treated as random variables in this work, but the analysis can be extended to include randomness in other aspects of crack geometry, material properties and component geometry.

To characterize random crack growth, all random variables characterizing the fatigue crack propagation are classified into two groups: independent random variables and dependent random variables. The independent random variables are given by a vector, i.e.

$$\mathbf{Z} = [a_0 \quad a_f \quad C \quad m \quad \sigma] \tag{6.2}$$

where a_0 and a_f are the initial and final crack lengths measured along the random crack path, respectively; C and m are parameters in the crack growth law, and σ is the applied stress. The joint probability distribution function for the random variables given by $\mathbf{Z}$ is assumed to exist. The dependent random variables are the combination of stress intensity factors K_I and K_{II}; crack length a_i and the angle of the crack tip with respect to the previous crack line θ_t.

6.2.2 Randomness of crack propagation

Since the limits on the integration in equation (6.1) for the fatigue life are random, the crack path mapping is introduced in order to shift the randomness into the local coordinate system. At each crack growth step, the randomness in crack

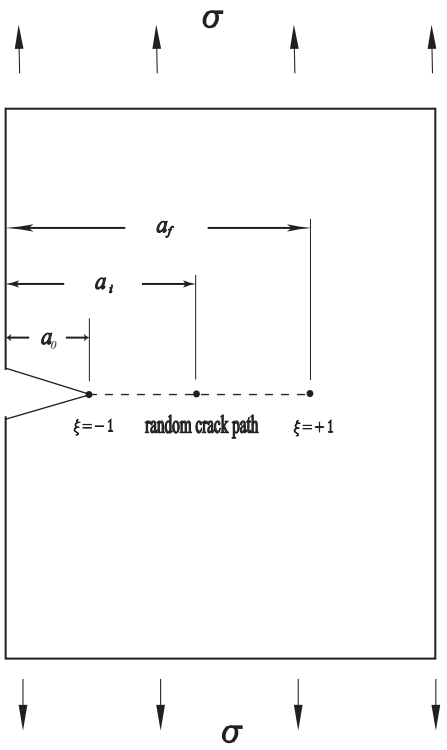

Figure 6.1: Random crack path

growth is characterized by two random functions: the crack growth rate and crack growth direction.

Figure 6.1 shows the random crack path is mapped to a local coordinate system ξ via a transformation, where $\xi \in [-1, +1]$. For a straight or curved crack, the linear interpolation from ξ to a is given by [15]:

$$a(\xi, Z) = \frac{1}{2}\left[(a_f - a_0)\xi + (a_f + a_0)\right] \tag{6.3}$$

and the crack length at each crack increment is given by

$$a_i(\xi, \mathbf{Z}) = \frac{1}{2}\left[(a_f - a_0)\xi_i + (a_f + a_0)\right], \qquad i = 1, 2, \ldots N_{CP} \tag{6.4}$$

where N_{CP} is the number of crack increment for the length of the crack during fatigue crack growth.

6.3 Formulation of fatigue crack growth reliability

6.3.1 Explicit expressions for derivatives of the crack growth law

Since the limits on the integration in equation (6.1) for the fatigue life are random, the crack path mapping in equation (6.3) is used to transform the randomness into the Jacobian $\mathrm{J_{cp}}$. Based on equation (6.1), the fatigue life is then given by [7, 83]:

$$N = \int_{-1}^{+1} f\left[\mathbf{Z}, K_{eq}(\mathbf{Z}, \xi)\right] d\xi \tag{6.5}$$

where

$$f\left[Z, K_{eq}(\mathbf{Z}, \xi)\right] = \frac{\mathrm{J_{cp}}(\mathbf{Z})}{C\left[K_{eq}(\mathbf{Z}, \xi)\right]^m} \tag{6.6}$$

The Jacobian $\mathrm{J_{cp}}$ is given by

$$\mathrm{J_{cp}}(\mathbf{Z}) = \frac{1}{2}(a_f - a_0) \tag{6.7}$$

and its derivative with respect to random vector $\mathbf{Z}$ can be summarized in vector form as

$$\frac{\partial \mathrm{J_{cp}}}{\partial \mathbf{Z}} = \begin{bmatrix} -\frac{1}{2} & \frac{1}{2} & 0 & 0 & 0 \end{bmatrix} \tag{6.8}$$

respectively. If any other parameters are random in addition to those given by equation (6.2), they can be included in the differentiation given by equation (6.11).

The important step in reliability analysis is the determination of the design point, which is the point in the random variable space with the greatest probabil-

ity of failure. The design point is obtained by an iterative optimization algorithm, involving repeated computation of the limit-state function and its gradient. The total derivative method has been employed to calculate the response gradient. The total derivative of fatigue life N with respect to the random vector $\mathbf{Z}$ can be written as [68, 70, 114]:

$$\frac{dN}{d\mathbf{Z}} = \int_{-1}^{+1} \left\{ f_{,\mathbf{Z}} + f_{,K_{eq}} \left[K_{eq,K_I} \frac{\partial K_I(\mathbf{Z},\xi)}{\partial \mathbf{Z}} + K_{eq,K_{II}} \frac{\partial K_{II}(\mathbf{Z},\xi)}{\partial \mathbf{Z}} + K_{eq,\theta_t} \frac{\partial \theta_t(\mathbf{Z},\xi)}{\partial \mathbf{Z}} \right] \right\} d\xi \tag{6.9}$$

where $f_{,\mathbf{Z}}$; $f_{,K_{eq}}$; K_{eq,K_I}; $K_{eq,K_{II}}$ and K_{eq,θ_t} can be determined explicitly and are given as [68, 70, 114]:

$$f_{,\mathbf{Z}} = \frac{1}{C(K_{eq})^m} \left(\frac{\partial \mathrm{J_{cp}}}{\partial \mathbf{Z}} \right) - \frac{1}{C^2(K_{eq})^m} \left(\frac{\partial C}{\partial \mathbf{Z}} \right) - \frac{\mathrm{J_{cp}} \ln(K_{eq})}{C(K_{eq})^m} \left(\frac{\partial m}{\partial \mathbf{Z}} \right) \tag{6.10}$$

where $\frac{\partial \mathrm{J_{cp}}}{\partial \mathbf{Z}}$ is the derivatives of Jacobian with respect to random vector given in equation (6.11), the derivatives of fatigue crack growth parameters with respect to random vector $\frac{\partial C}{\partial \mathbf{Z}}$ and $\frac{\partial m}{\partial \mathbf{Z}}$ are given as [68, 70, 114]:

$$\frac{\partial \mathrm{C}}{\partial \mathbf{Z}} = [0 \quad 0 \quad 1 \quad 0 \quad 0] \tag{6.11}$$

and

$$\frac{\partial m}{\partial \mathbf{Z}} = [0 \quad 0 \quad 0 \quad 1 \quad 0] \tag{6.12}$$

To obtain the derivative of fatigue life with respect to the equivalent stress intensity factor $f_{,K_{eq}}$, the derivatives of fatigue life with respect to each fracture mode

is needed, which can be obtained by differentiating equation (6.6) with respect to K_I and K_{II}, giving

$$f_{,K_I} = -\frac{m\mathrm{J_{cp}}}{C(K_{eq})^{m+1}}\left(\frac{\partial K_{eq}}{\partial K_I}\right) \tag{6.13}$$

and

$$f_{,K_{II}} = -\frac{m\mathrm{J_{cp}}}{C(K_{eq})^{m+1}}\left(\frac{\partial K_{eq}}{\partial K_{II}}\right) \tag{6.14}$$

The derivative of the equivalent stress intensity factor with respect to each fracture mode can be obtained by direct differentiation of equation (3.109) with respect to K_I and K_{II}, giving

$$K_{eq,K_I} = \cos^3\left(\frac{\theta_t}{2}\right) \tag{6.15}$$

and

$$K_{eq,K_{II}} = -3\cos^2\left(\frac{\theta_t}{2}\right)\sin\left(\frac{\theta_t}{2}\right) \tag{6.16}$$

Because of the dependence of K_{eq,K_I}, $K_{eq,K_{II}}$ and K_{eq,θ_t} on both $\mathbf{Z}$ and ξ, $\frac{\partial K_I(\mathbf{Z},\xi)}{\partial \mathbf{Z}}$ and $\frac{\partial K_{II}(\mathbf{Z},\xi)}{\partial \mathbf{Z}}$ can be directly obtained using DBEM with IDM. K_{eq,θ_t} is the derivative of K_{eq} with respect to local crack growth direction θ_t along the crack path, which can be obtained by differentiating equation (3.109) with respect to θ_t, giving

$$K_{eq,\theta_t} = -\frac{3}{2}\cos^2\frac{\theta_t}{2}\sin\frac{\theta_t}{2}K_I + \left[3\cos\frac{\theta_t}{2}\sin^2\frac{\theta_t}{2} - \frac{3}{2}\cos^3\frac{\theta_t}{2}\right]K_{II} \tag{6.17}$$

From the crack growth direction defined in equation (3.112), we have

$$K_I = -\frac{3\cos\theta_t - 1}{\sin\theta_t} K_{II} \tag{6.18}$$

Substituting the above definition of K_I into equation (6.17) gives:

$$K_{eq,\theta_t} = 0 \tag{6.19}$$

Based on above expressions, all the terms in equation (6.9) can be computed either implicitly or explicitly, the derivative of fatigue life with respect to random parameter $\frac{dN}{d\mathbf{Z}}$ can then be obtained.

6.3.2 Approximation formula for fatigue life and its derivative

Equation (6.5) can be numerically integrated by Gaussian integration, Trapezoidal rule or Simpson's rule. The Trapezoidal rule is used in this work for the numerical integration of equation (6.5) which is expressed in a general form by

$$N = \sum_{i=1}^{N_{CP}} \frac{\Delta a_i}{C(\Delta K_{eq})_i^m} W_i \tag{6.20}$$

where N_{CP} is the total number of crack increments for the length of the crack during fatigue crack growth, and W_i are the integration weights evaluated at the crack increment step $\xi = \xi_i$.

The same approach can then be applied to obtain the derivatives of fatigue life with respect to random variables, given as:

$$N_{,\mathbf{Z}} = \sum_{i=1}^{N_{CP}} (f_{,\mathbf{Z}})_i W_i \tag{6.21}$$

$$N_{,K_{eq}} = \sum_{i=1}^{N_{CP}} (f_{,K_{eq}})_i W_i \tag{6.22}$$

6.4 Analytical gradient for fatigue crack growth

The performance function for probabilistic fatigue crack growth analysis can be defined as:

$$g(\mathbf{Z}) = N - N_s \tag{6.23}$$

where N_s is the service life. Although service life can be a random parameter, it is assumed to be a deterministic value in the present work.

Recalling the formula in equation (4.32), sensitivities are evaluated analytically to compute the probability of failure. The performance function for fatigue crack growth (6.23) in the $\mathbf{\Psi}$ space can be expressed as

$$g_{_\Psi}(\mathbf{\Psi}) = g(Z(\mathbf{\Psi})) = N(\mathbf{Z}(\mathbf{\Psi})) - N_s(\mathbf{Z}(\mathbf{\Psi})) \tag{6.24}$$

The derivative of $g_{_\Psi}(\mathbf{\Psi})$ with respect to $\mathbf{Z}$ is given as

$$\frac{\partial g_{_\Psi}(\mathbf{\Psi})}{\partial \Psi_k} = \sum_{m=1}^{N_v} \frac{\partial g}{\partial Z_m} \frac{\partial Z_m}{\partial \Psi_k} = \sum_{m=1}^{N_v} \frac{\partial g}{\partial Z_m} R_{mk} \tag{6.25}$$

where N_v is the number of random variables, $R_{mk} = \frac{\partial Z_m}{\partial \Psi_k}$ can be obtained from equation (4.36). The partial derivatives in the $\mathbf{Z}$ space are

$$\frac{\partial g}{\partial \mathbf{Z}} = \frac{\partial N}{\partial \mathbf{Z}} \tag{6.26}$$

and

$$\frac{\partial g}{\partial N_s} = -1 \tag{6.27}$$

Using the proposed method, the partial derivative of fatigue life with respect to random variables can be easily calculated. Hence, for a given Ψ or Z_m, all gradients of $g_\Psi(\mathbf{\Psi})$ can be evaluated analytically. Therefore, probabilistic analysis can be performed exactly the same way as the algorithm proposed in Chapter 4.

6.5 Examples

6.5.1 Fatigue crack growth reliability analysis of double edge crack specimen

Consider a double edge crack specimen with width $2W$, length $L = 3W$ as shown in Figure 6.2. The initial crack length a_0, final crack length a_f, fatigue parameters C, m and far-field tensile stress σ were treated as statistically independent random variables. Table 6.1 presents the mean, standard deviation and probability distribution for each of these random parameters. The Young's modulus E and Poisson's ratio of $\nu = 0.3$ were assumed to be deterministic. The stress ratio $R = 0.1$ and the plane strain condition is assumed. Various values of the service life are assumed to be known and used in the probabilistic analysis.

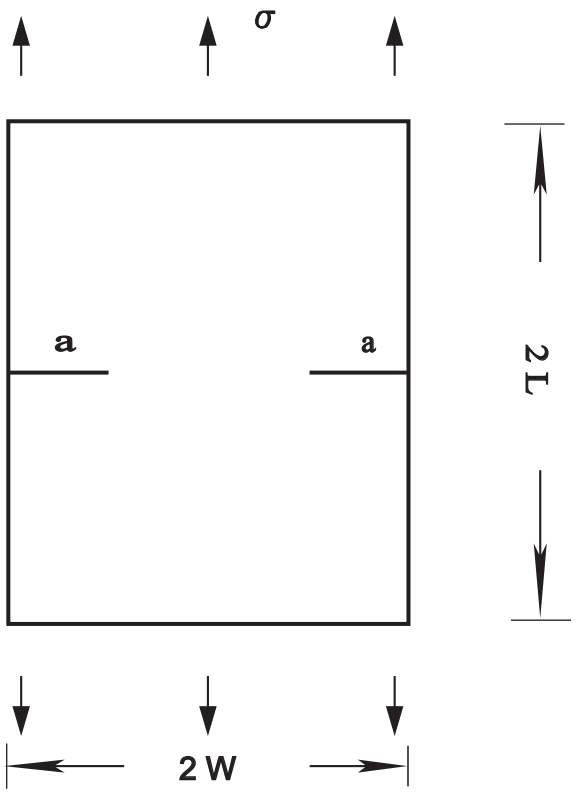

Figure 6.2: Geometry and loads of double edge crack specimen

Table 6.1: Statistical properties of random parameters

Parameters	Mean	Standard deviation	Probability distribution
Normalised initial crack length $\frac{a_0}{W}$	0.1	0.25	Normal
Normalised final crack length $\frac{a_f}{W}$	0.4	0.1	Normal
Fatigue parameter C	1.0×10^{-10}	3.0×10^{-11}	Normal
Fatigue parameter m	3.25	0.08	Normal
Normalised far-field tensile stress $\frac{\sigma}{E}$	4.0×10^{-4}	1.0×10^{-4}	Normal

The crack was assumed to be grown in 4 different increments with 5, 10, 15 and 20 propagation steps. For a known final crack size the normalised crack increment length $\frac{\triangle a}{W}$ are equal to 0.06, 0.03, 0.02 and 0.015, respectively. Half of the plate is modelled due to symmetry. Figure 6.3 shows the boundary conditions and the discretisation using 46 quadratic elements. The BEM model employed 30 continuous elements on the external boundary, while the each crack face is discretised using 8 quadratic discontinuous elements. In the model with 96 quadratic elements, 18 quadratic discontinuous elements were used on each crack face, while the external boundary is modelled with 60 elements.

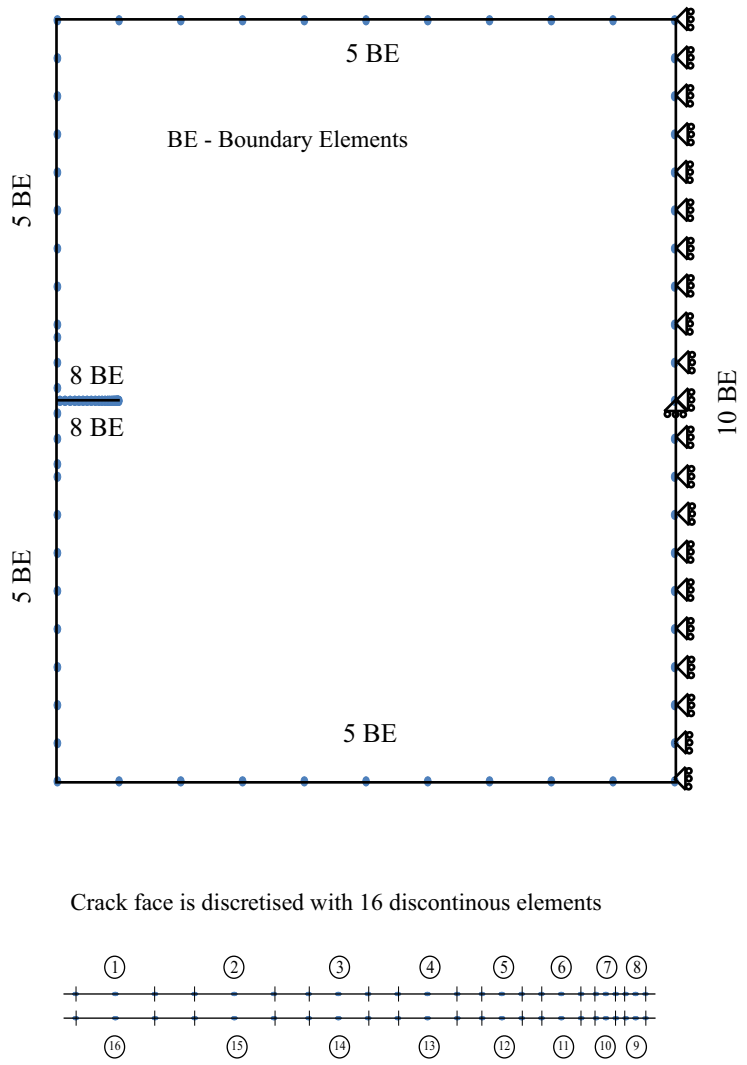

Figure 6.3: Boundary conditions and discretisation of double edge crack specimen

Figures 6.4 to 6.11 show the normalised value of stress intensity factors and its derivative value with respect to crack size for different crack growth sizes. Figures 6.4 to 6.7 show the stress intensity factors obtained by different boundary modelling. As those graphs illustrated, the stress intensity factor increases with each crack growth, the maximum difference between the computational result from DBEM and analytical solutions provided by Tada et al. [105] is less than 0.14%. Figures 6.8 to 6.11 show the normalised value of derivatives of stress intensity

factor with respect to crack size computed for different crack growth increment. As can be seen in those figures the results obtained by the DBEM agree well with deviation from the analytical solution, with a maximum difference of 2.32%. The model with more boundary elements gives better evaluation of the derivatives of stress intensity factor with respect to crack size at each crack growth, although there are no such differences for the calculation of stress intensity factor.

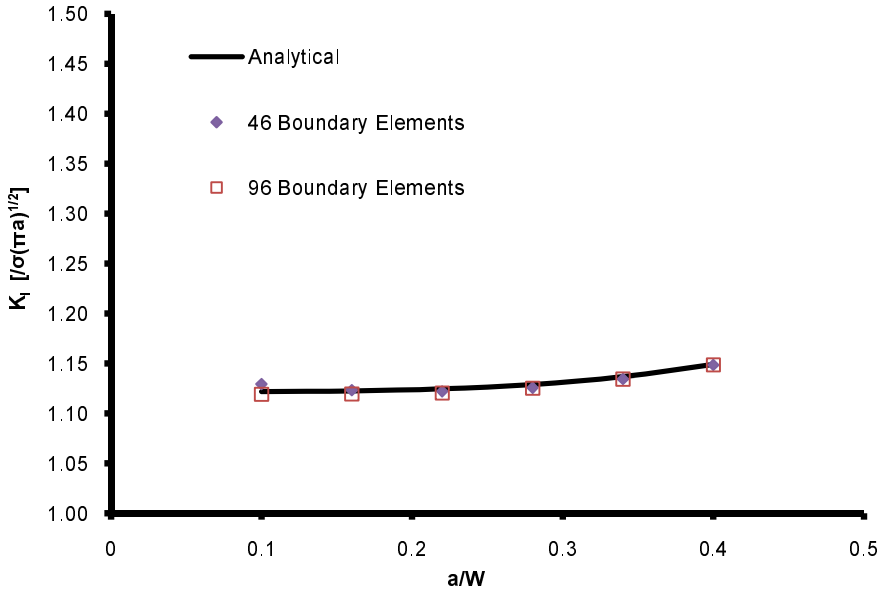

Figure 6.4: Normalised K_I with crack growth size $\frac{\triangle a}{W} = 0.06$

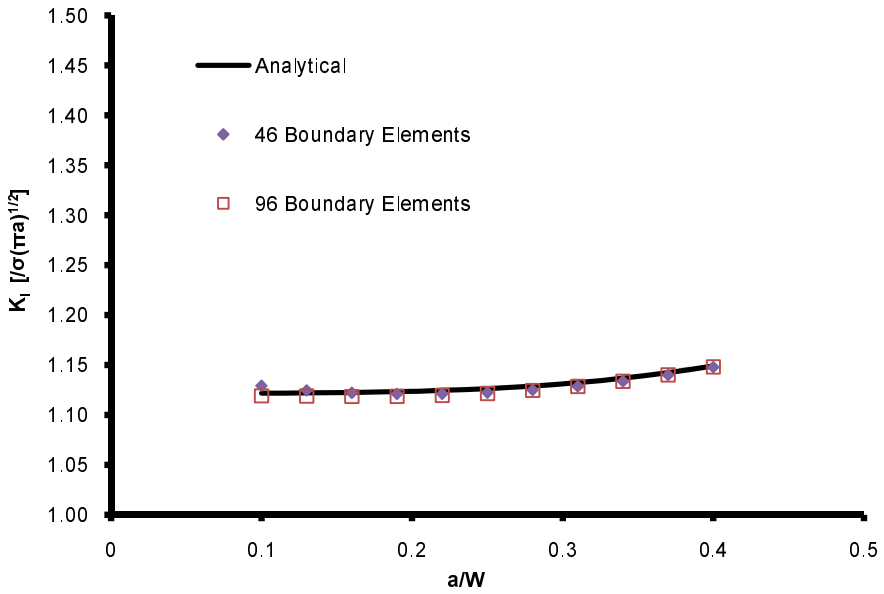

Figure 6.5: Normalised K_I with crack growth size $\frac{\triangle a}{W} = 0.03$

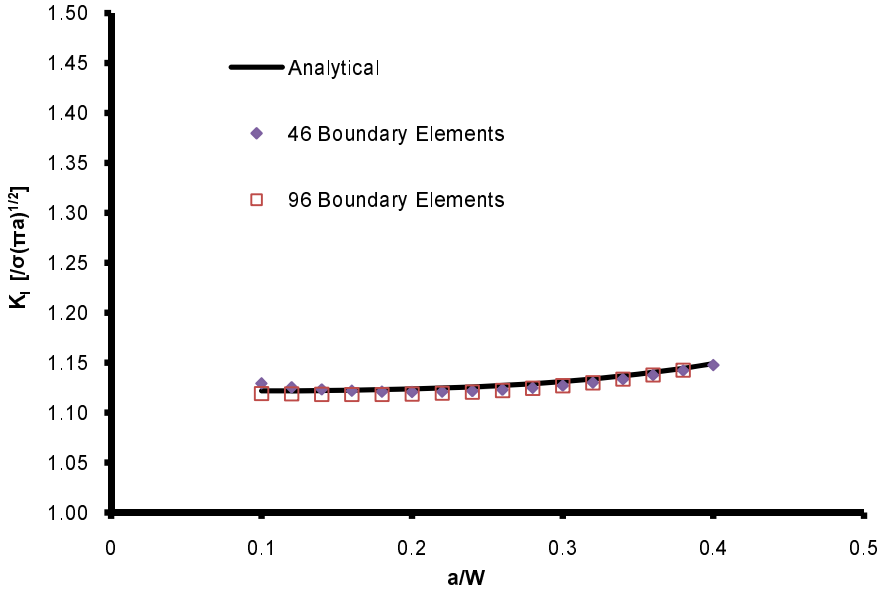

Figure 6.6: Normalised K_I with crack growth size $\frac{\triangle a}{W} = 0.02$

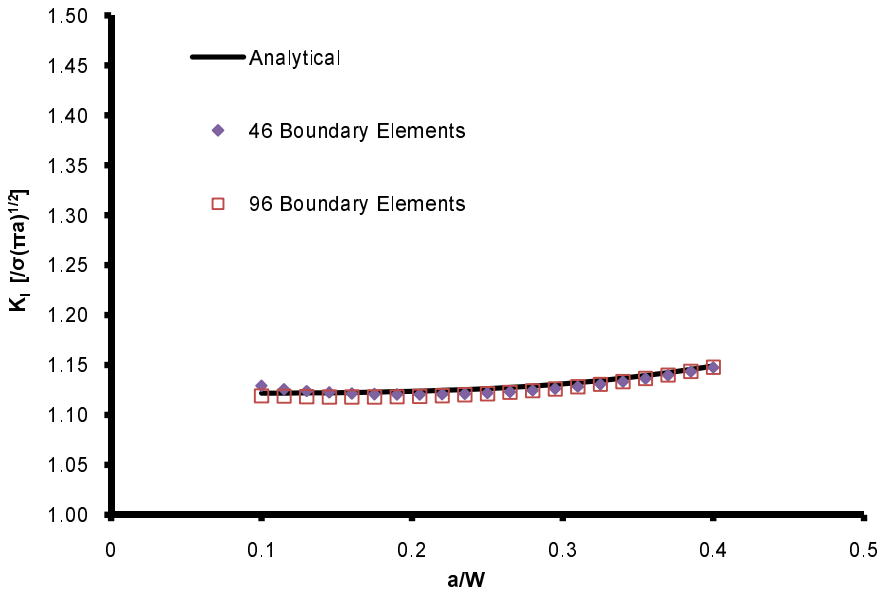

Figure 6.7: Normalised K_I with crack growth size $\frac{\triangle a}{W} = 0.015$

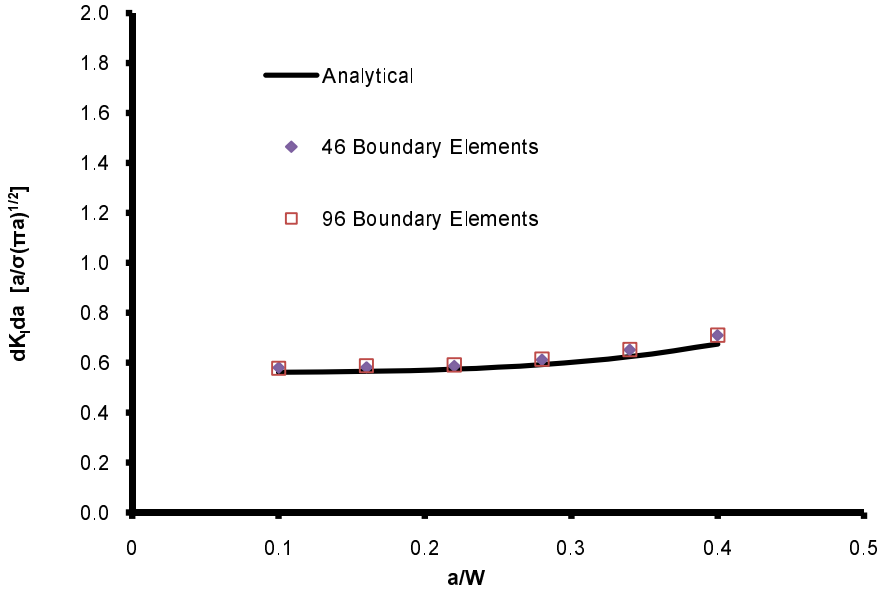

Figure 6.8: Normalised $\frac{\partial K_I}{\partial a}$ with crack growth size $\frac{\triangle a}{W} = 0.06$

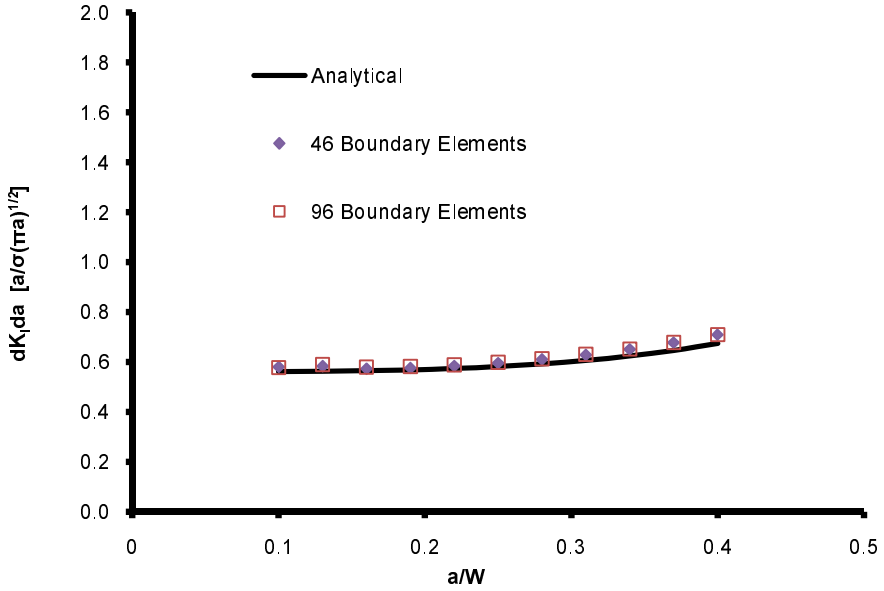

Figure 6.9: Normalised $\frac{\partial K_I}{\partial a}$ with crack growth size $\frac{\triangle a}{W} = 0.03$

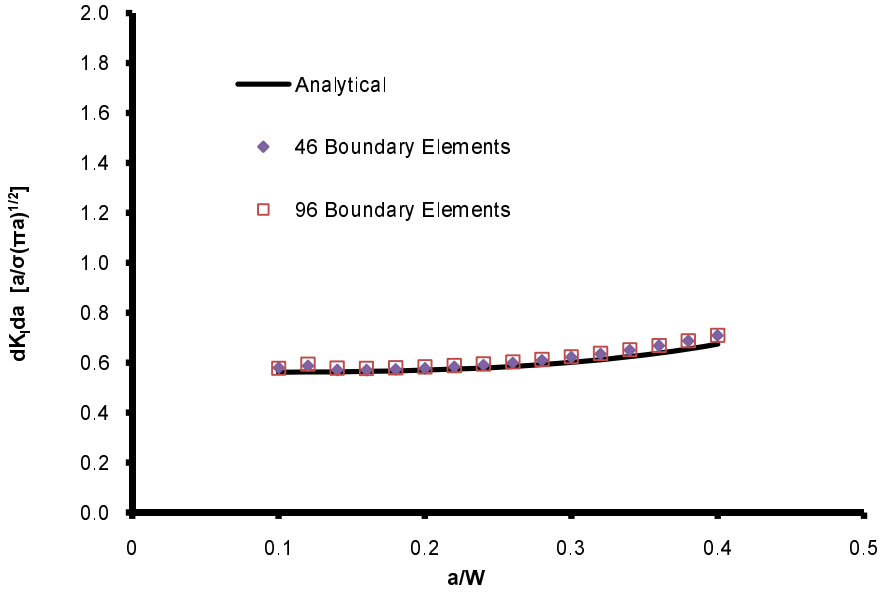

Figure 6.10: Normalised $\frac{\partial K_I}{\partial a}$ with crack growth size with IDM $\frac{\triangle a}{W} = 0.02$

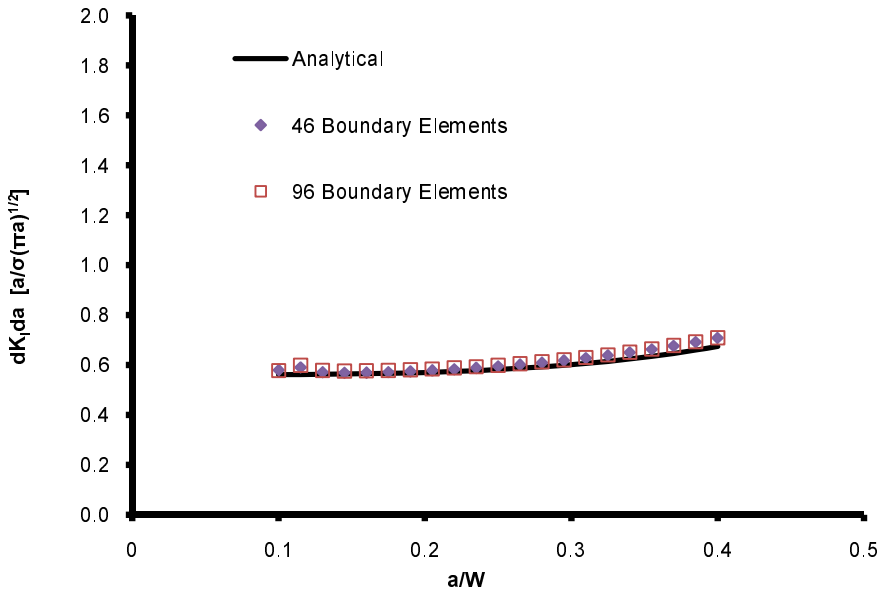

Figure 6.11: Normalised $\frac{\partial K_I}{\partial a}$ with crack growth size $\frac{\triangle a}{W} = 0.015$

The bigger difference in derivatives value is due to new boundary elements introduced at each increment, and the analytical solution in Tada et al. [105] is based on an infinite plate which could also induce the bigger difference in derivative analysis. The new assumption has to be made at each increment to define the new random variable, as the analytical integration has to be performed based on the new crack tip element illustrated in Section (5.2.2). It is well recognized that any small difference between the calculation of the stress intensity factor by the reference solution and the BEM solution will give a larger error in the fatigue life; also the bigger difference in the calculation of the derivatives of stress intensity factor with respect to crack size could induce an even larger difference in the reliability index.

The effect of different crack increment sizes on the K_I and its derivatives was also investigated. Figure 6.12 to 6.15 show BEM solutions for the same number of boundary elements used with different crack increment sizes compared with the analytical solution. The results in those Figures illustrated the normalised crack

increment sizes $\frac{\triangle a}{W}$ equal to 0.06, 0.03, 0.02 and 0.015 all have good evaluation of stress intensity factor and its derivatives. The model with more boundary elements gives better evaluation of the derivatives of stress intensity factor with respect to crack size at each crack growth, although there are no such difference for the calculation of stress intensity factor.

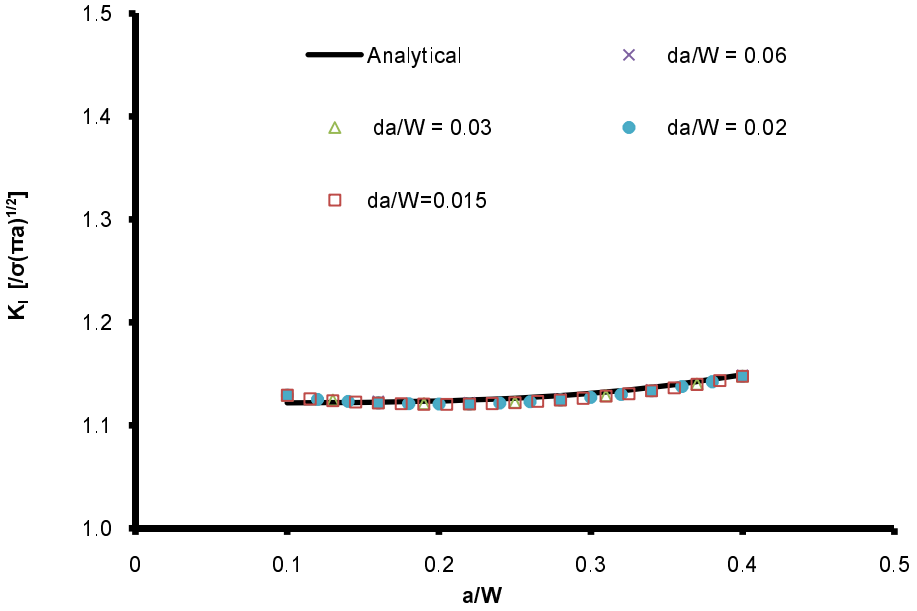

Figure 6.12: Normalised K_I with different crack increment sizes for total 46 boundary elements

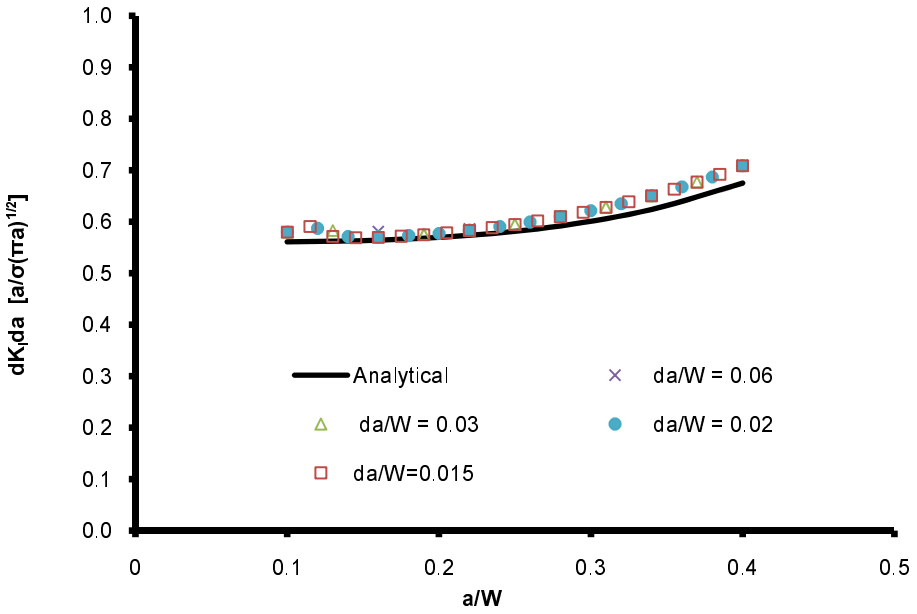

Figure 6.13: Normalised $\frac{\partial K_I}{\partial a}$ with different crack increment sizes for total 46 boundary elements

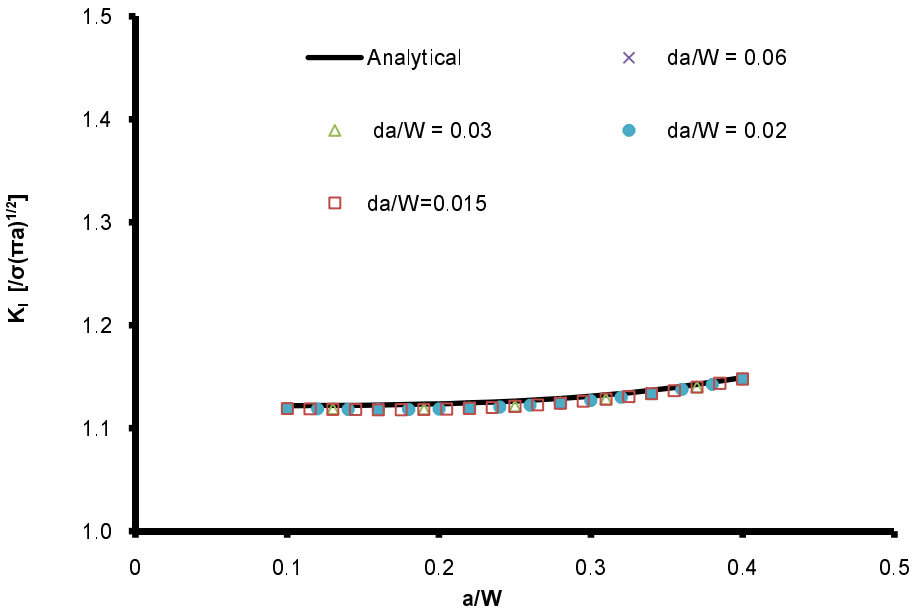

Figure 6.14: Normalised K_I with different crack increment sizes for total 96 boundary elements

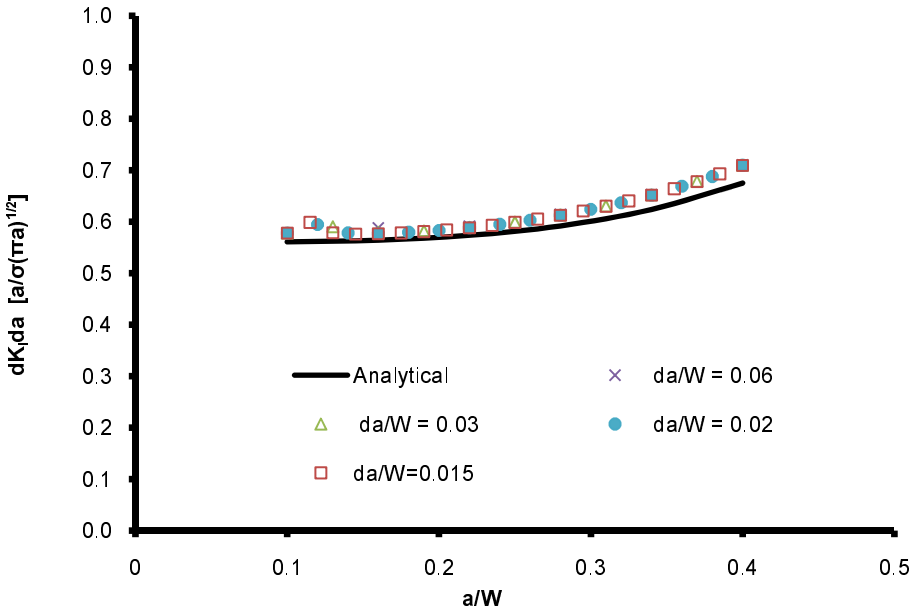

Figure 6.15: Normalised $\frac{\partial K_I}{\partial a}$ with different crack increment sizes for total 96 boundary elements

The reliability index β is plotted as a function of the service life under the various types of uncertainties in Figures 6.16 to 6.21, respectively. The model with 96 boundary elements is used, the crack is assumed to grow in 10 propagation steps. The Monte Carlo simulation with deterministic solution of Paris law is used to validate the result obtained by the proposed method. Three different number of simulations are used to study the accuracy and efficiency of the Monte Carlo simulation. In this particular example, 100000, 500000 and one million simulations are used. As can be seen in Figures 6.16 to 6.21, with the increase of the number of simulation, the reliability index is converge to the numerical result. The results in those Figures demonstrated that in order to obtain the higher reliability index, meaning probability of failures equal to 1×10^{-6} would require one million simulation, although it is computational expensive to perform such task.

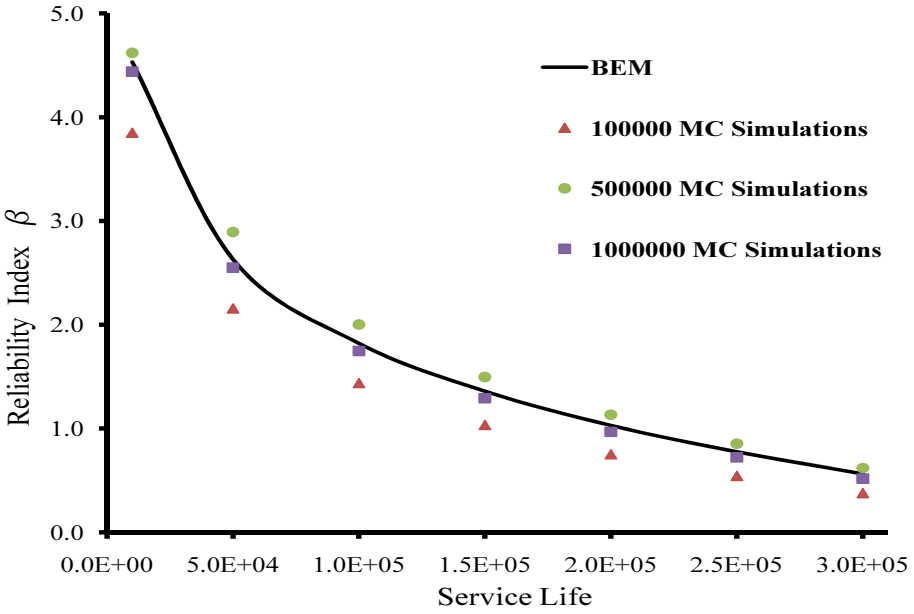

Figure 6.16: Reliability index with various uncertainty

Figure 6.16 showed the combination effect of all those random parameters. In Figures 6.17 to 6.21, the initial crack length a_0, final crack length a_f, fatigue parameter C, fatigue parameter m and far-field tensile stress σ each has been modelled as single random parameter separately, with each one of them being modelled as the only random parameter with the rest remain deterministic. As can be seen in those graphs, all the numerical results agreed well with the simulations. As expected, one million simulation yields the best result compare with 100000 and 500000 simulations. In Figure 6.22 all the numerical results for each random parameters are plotted in the same scales, the combination effect of all random parameters gives the smallest reliability index for a given service life which is expected. For a given reliability index (assuming $\beta = 4$), final crack length a_f modelled as the only random variable yields the highest service life.

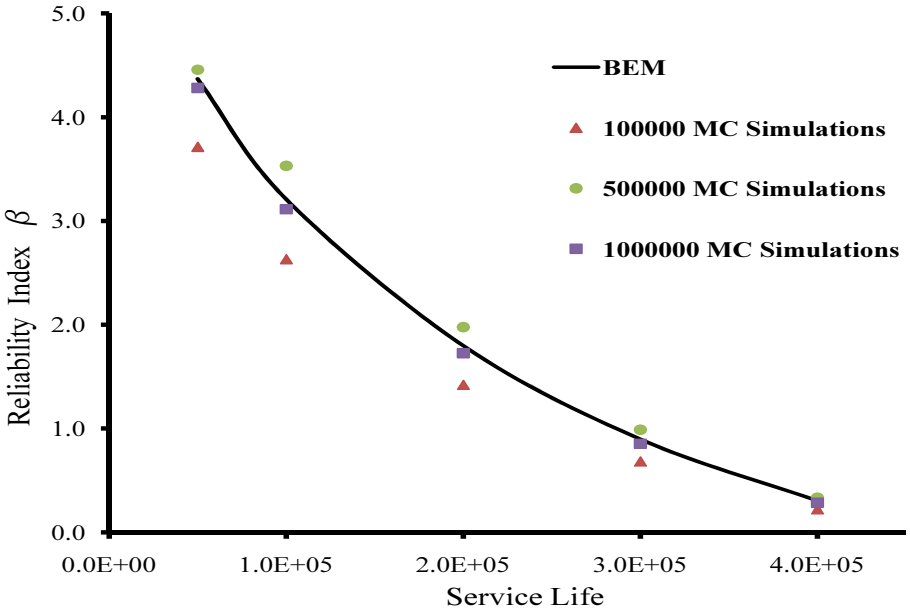

Figure 6.17: Reliability index with random initial crack length

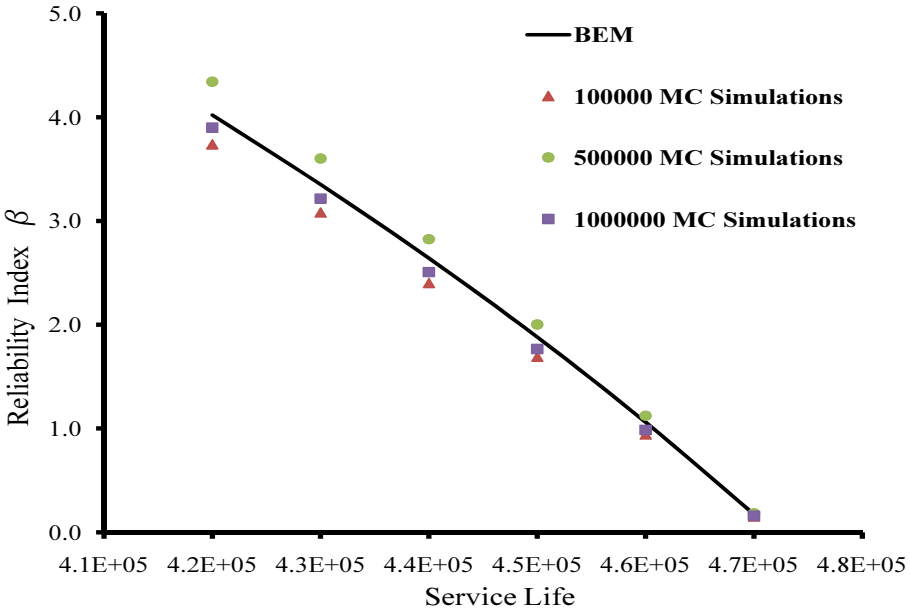

Figure 6.18: Reliability index with random final crack length

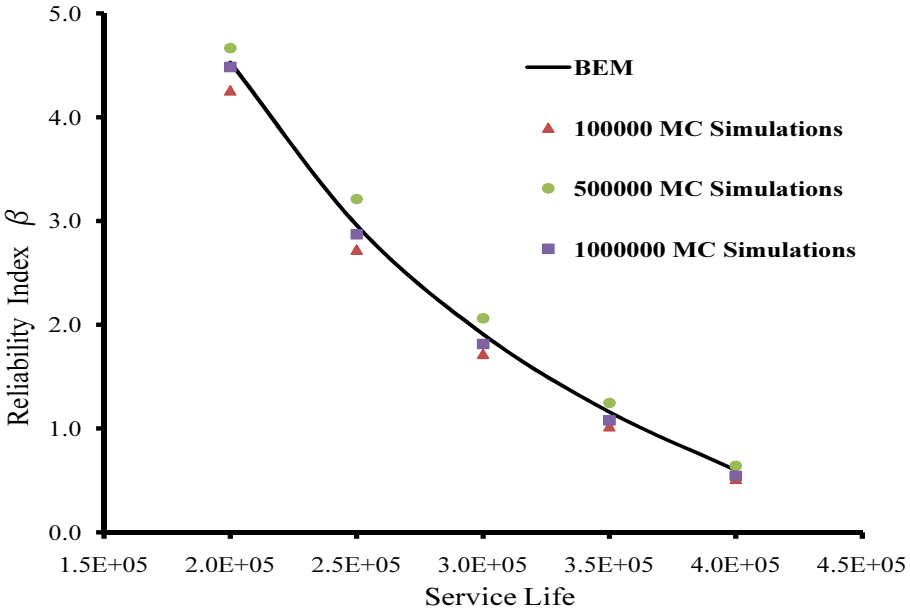

Figure 6.19: Reliability index with random fatigue parameter C

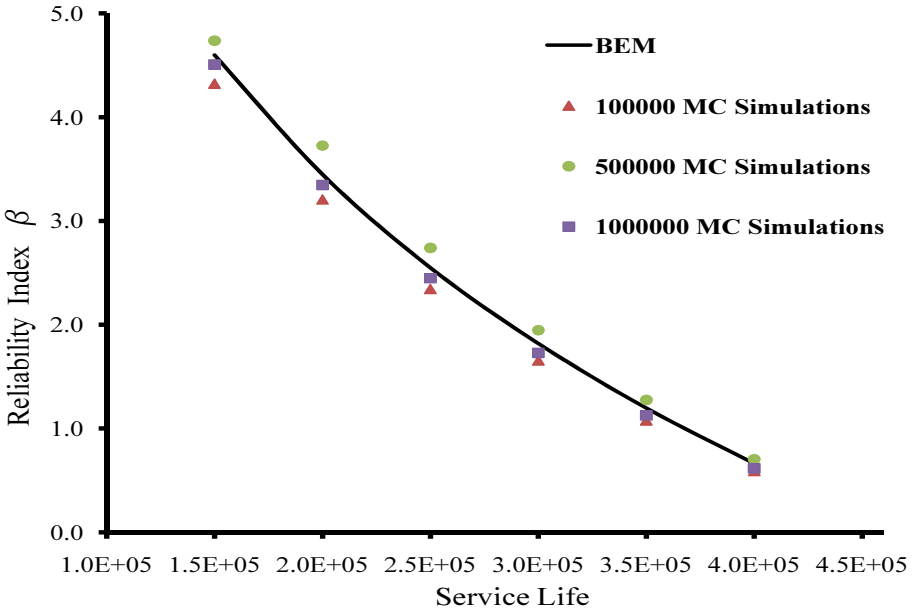

Figure 6.20: Reliability index with random fatigue parameter m

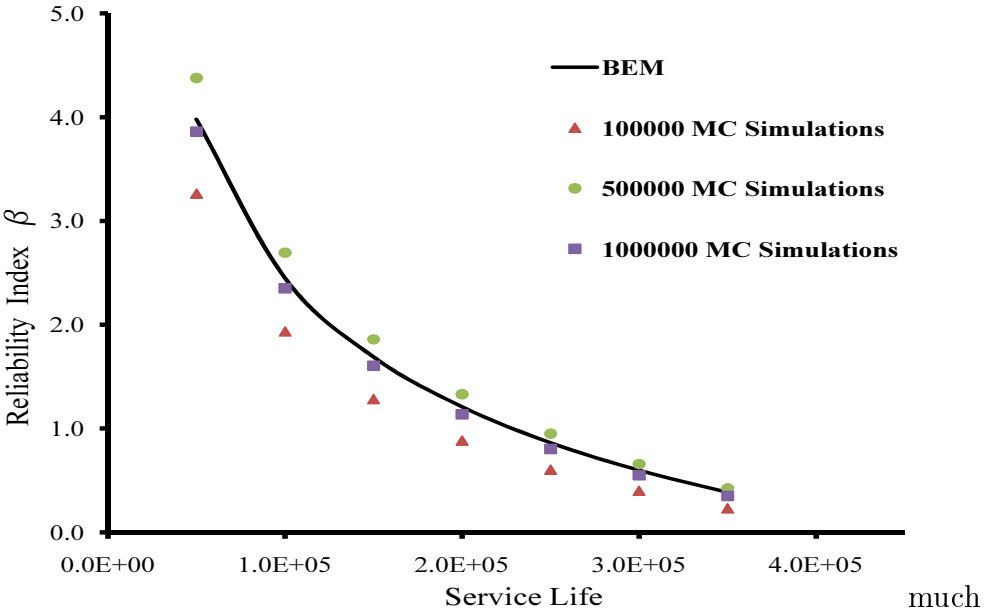

much

Figure 6.21: Reliability index with random stress

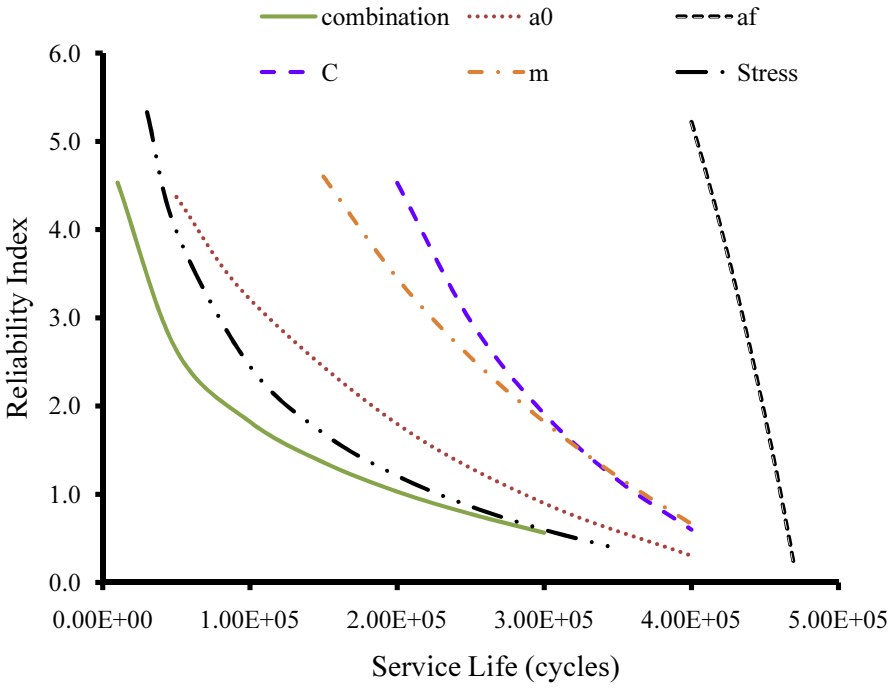

Figure 6.22: Comparison of random parameters

6.5.2 Fatigue crack growth reliability analysis of single edge crack specimen

Consider a single edge crack specimen with width W, length $L = 3W$ as shown in Figure 6.23. The initial crack length a_0, final crack length a_f, fatigue parameters C , m and far-field tensile stress σ were treated as statistically independent random variables. The mean, standard deviation and probability distribution for each of these random parameters are assumed to be the same as those given in Table 6.1. The Young's modulus E and Poisson's ratio of $\nu = 0.3$ were assumed to be deterministic. The stress ratio $R = 0.1$ and the plane stress condition is assumed.

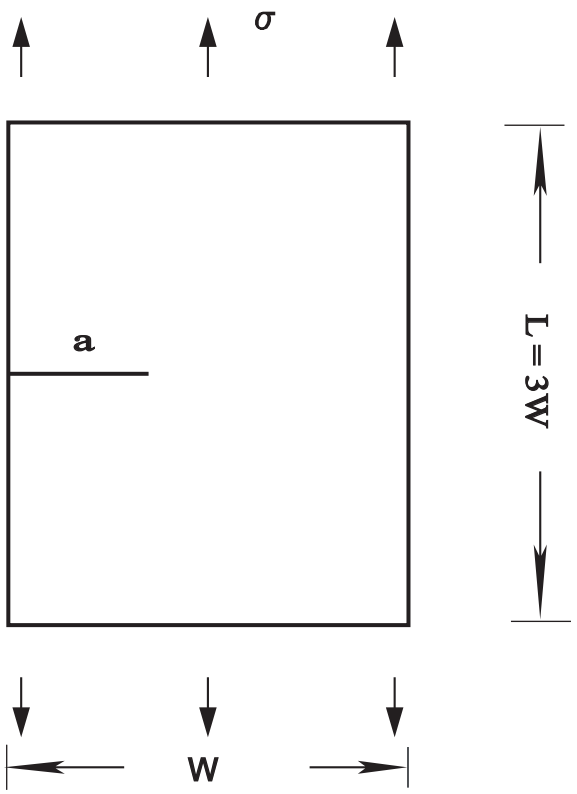

Figure 6.23: Geometry and loads of single edge crack specimen

A total of 96 boundary elements with 18 discontinuous elements on each of

the crack face is used to model the specimen. The crack was assumed to be grown in 4 different increments with 5, 10, 15 and 20 propagation steps. For a known final crack size the normalised crack increment sizes $\frac{\triangle a}{W}$ are equal to 0.06, 0.03, 0.02 and 0.015, respectively.

Figure 6.24 shows the boundary conditions and the discretisation using 96 quadratic elements. The BEM model employed 60 continuous elements on the external boundary, while the each crack face is discretised using 18 quadratic discontinuous elements. In the model with 46 quadratic elements, 8 quadratic discontinuous elements were used on each crack face, while the external boundary is modelled with 30 elements.

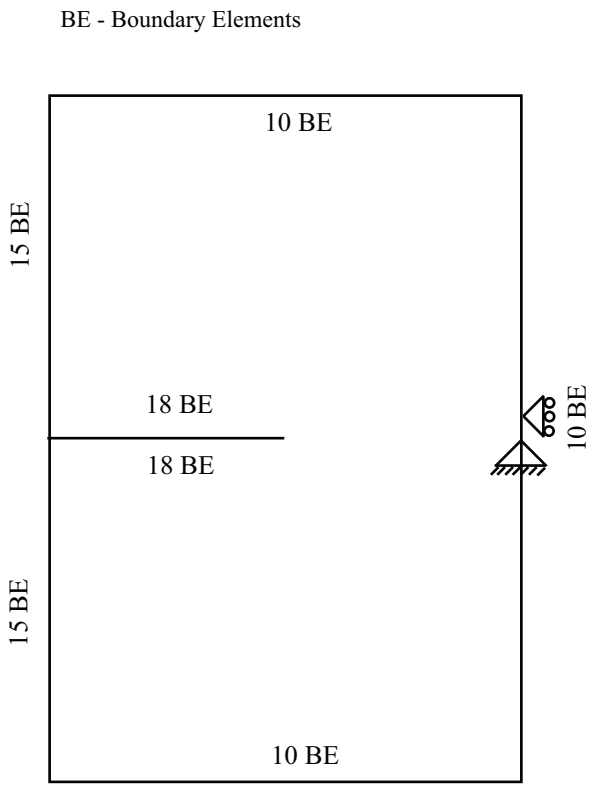

Figure 6.24: Boundary conditions and discretisation of single edge crack specimen

Figures 6.25 to 6.28 shows the stress intensity factor and its derivatives with

respect to crack size at each crack growth. The stress intensity factor increases with each crack growth, the maximum difference between the BEM and analytical solutions provided by Tada et al. [105] is less than 1%. The derivatives of stress intensity factor with respect to crack size at each crack growth are obtained by the BEM with IDM. As can be seen in Figures 6.26 and 6.28, the results agreed well with deviation of the analytical solution, with a maximum difference of 9%.

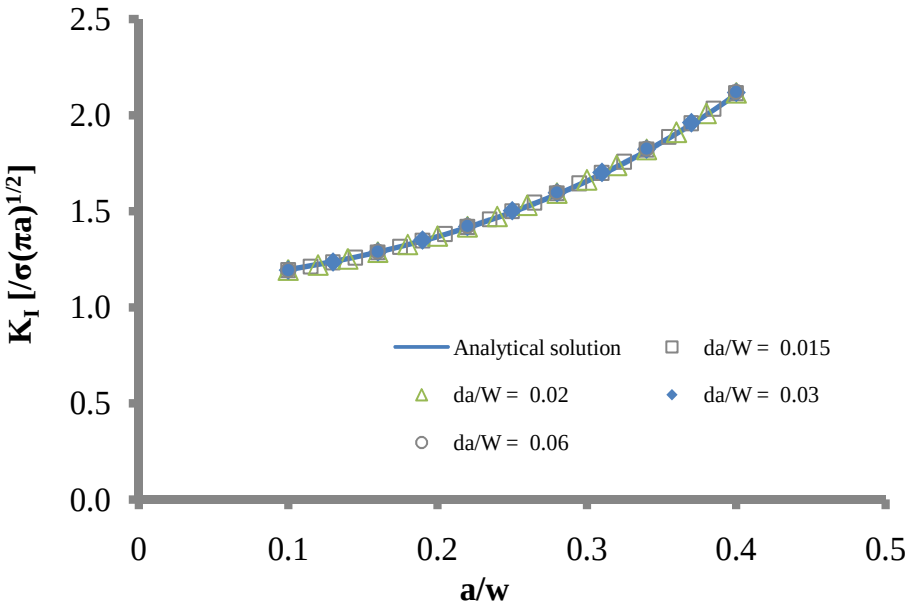

Figure 6.25: Normalised K_I with different crack increment sizes

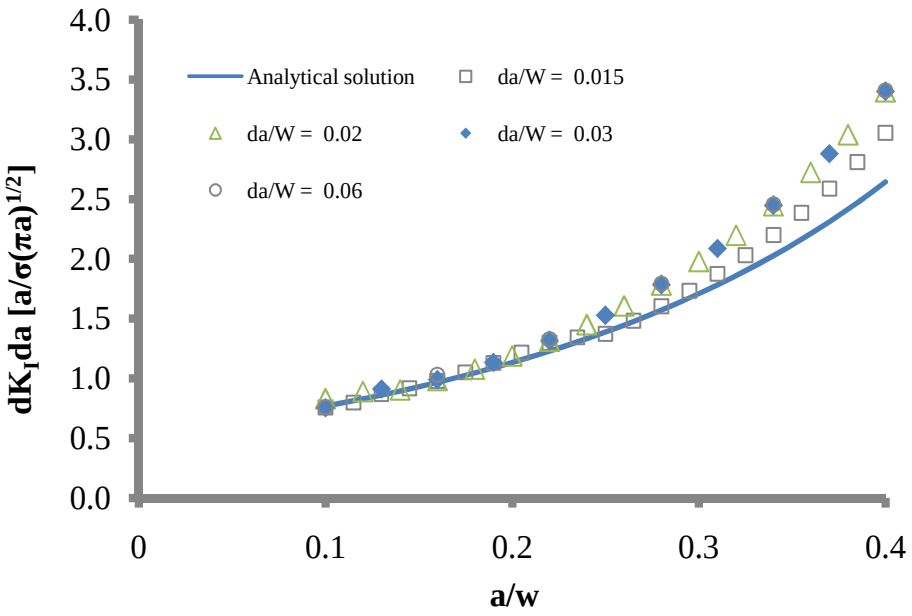

Figure 6.26: Normalised $\frac{\partial K_I}{\partial a}$ with different crack increment sizes

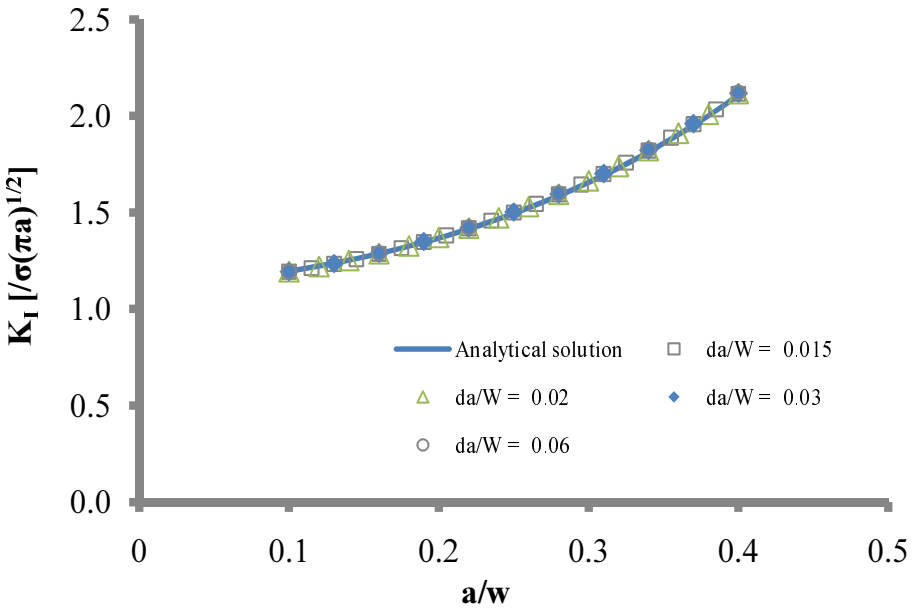

Figure 6.27: Normalised K_I with different crack increment sizes

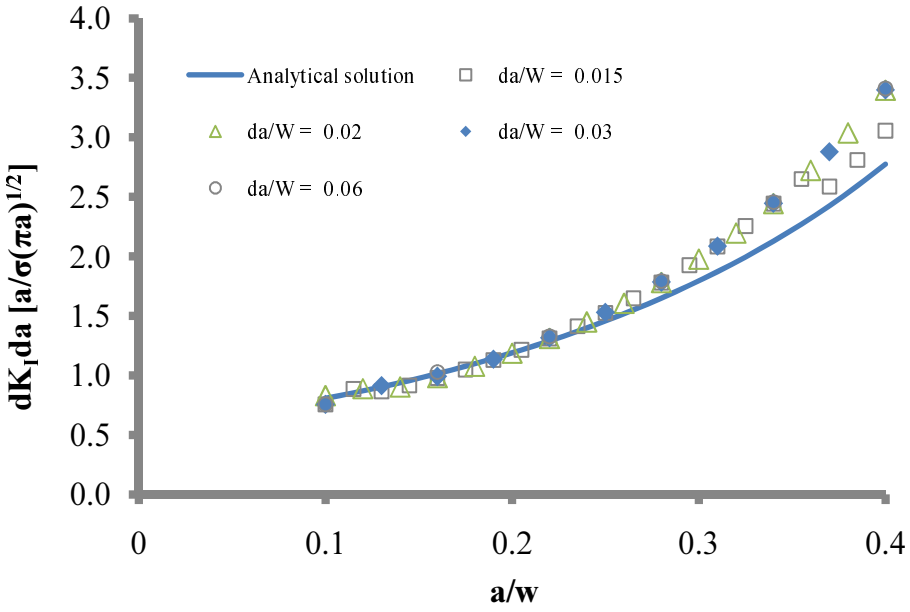

Figure 6.28: Normalised $\frac{\partial K_I}{\partial a}$ with different crack increment sizes

The reliability index is plotted as a function of the service life under the various types of uncertainties in Figures 6.29 to 6.34. One million of Monte Carlo simulations with deterministic solution of Paris law are used in this example. In Figures 6.30 to 6.34 the initial crack length a_0, final crack length a_f, fatigue parameter C, fatigue parameter m, far-field tensile stress σ each has been modelled as a single random parameter, while Figure 6.29 plotted the combination effect of all those random parameters. As can be seen in those graphs, all the numerical results agreed well with the simulations.

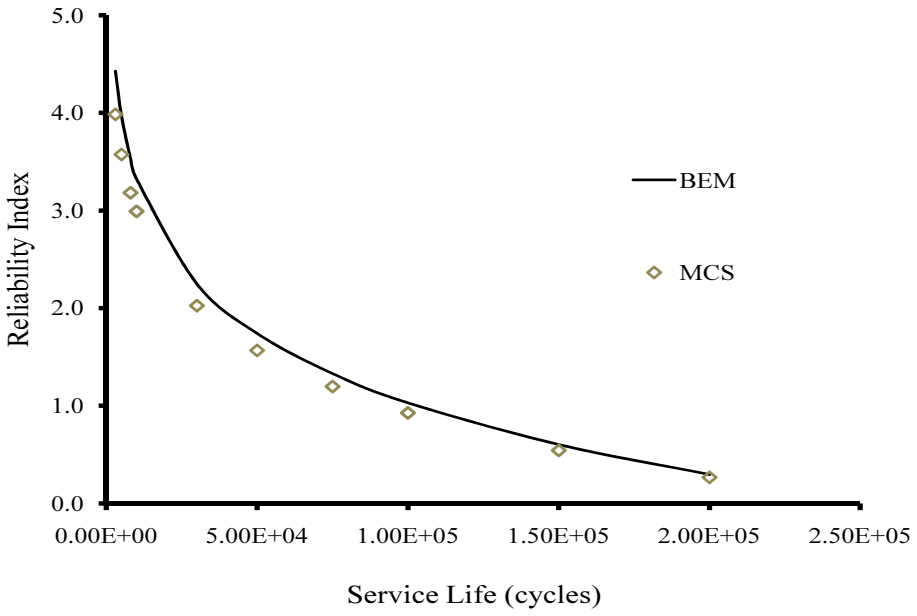

Figure 6.29: Reliability index with various uncertainty

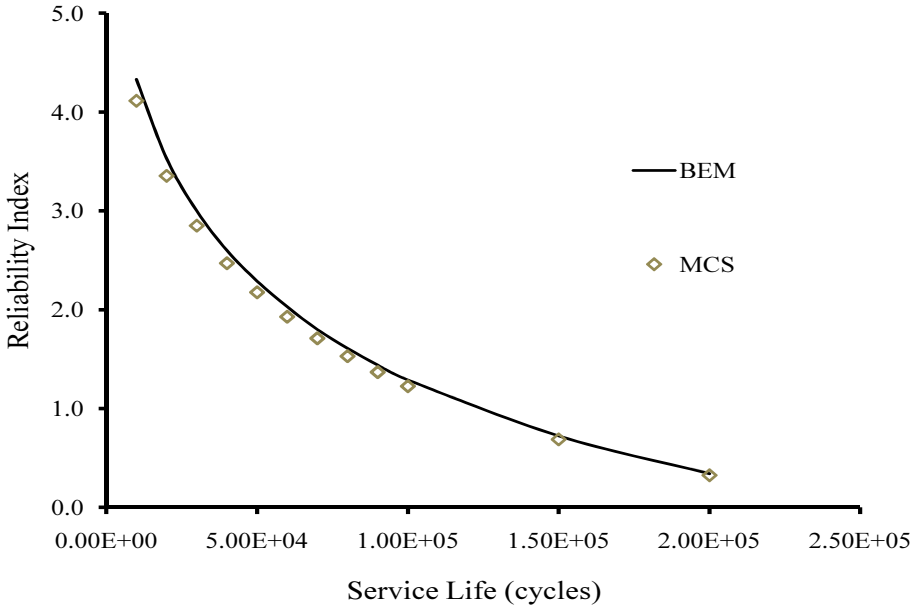

Figure 6.30: Reliability index with random initial crack length

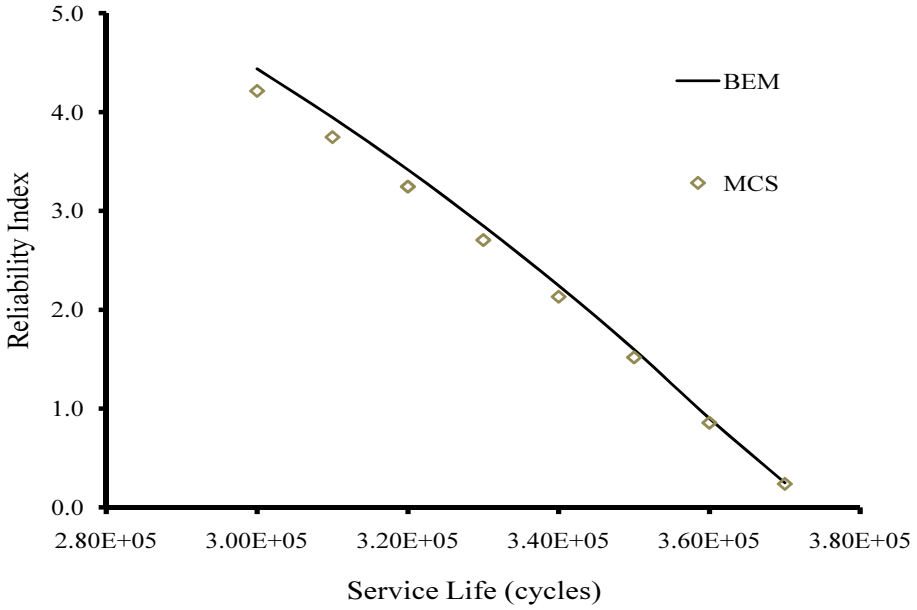

Figure 6.31: Reliability index with random final crack length

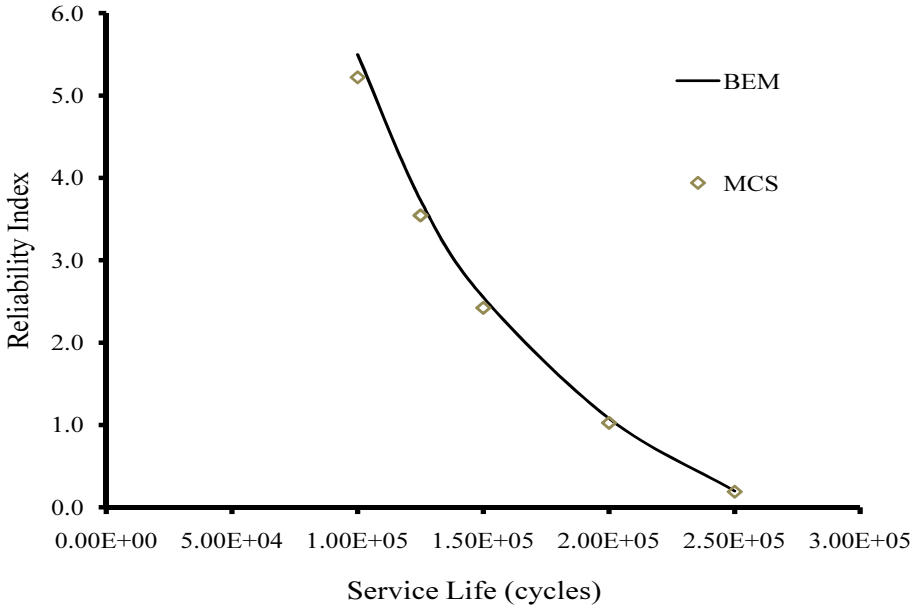

Figure 6.32: Reliability index with random fatigue parameter C

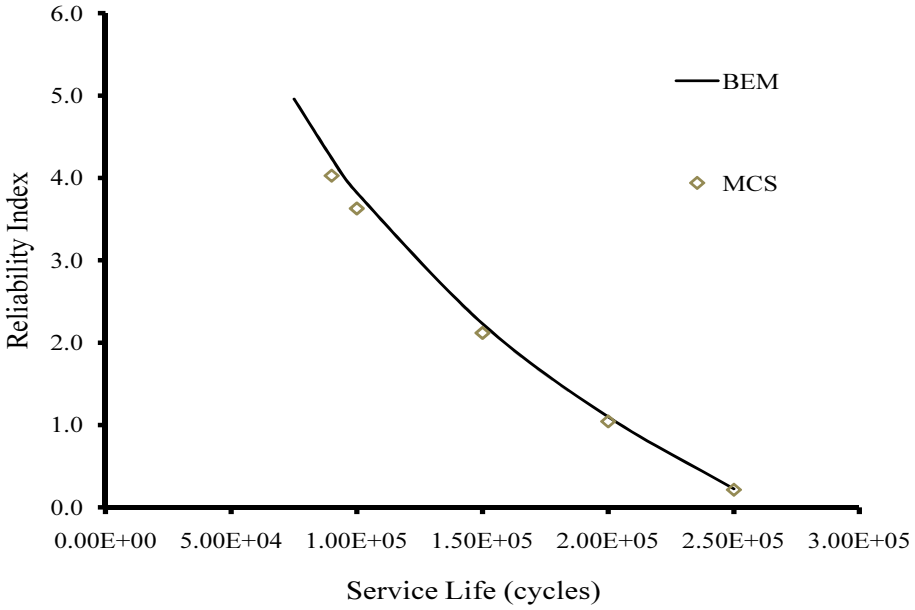

Figure 6.33: Reliability index with random fatigue parameter m

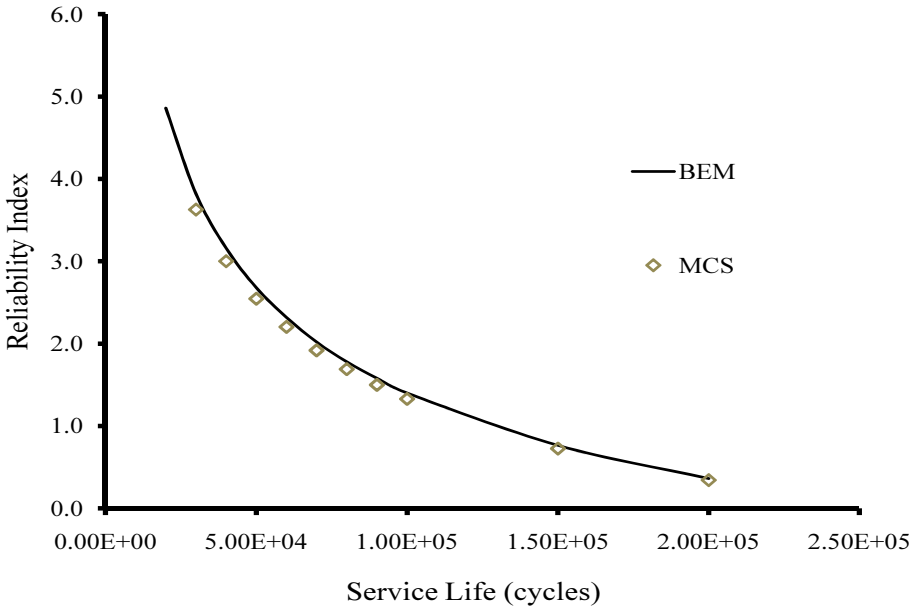

Figure 6.34: Reliability index with random stress

It is essential to study the effect of different probability distribution functions on the reliability of the structure. Figure 6.35 shows the probability of failure P_f of the single edge crack specimen, as a function of service life. The initial crack

length a_0 is treated as the only random variable with a mean value equal to 0.5 and standard deviation equal to 0.1, different probability distribution functions are considered for the analysis. The probability of failure P_f obtained with Log-normal distribution has higher value than the one with Normal distribution in the tail region, while the Normal distribution yields higher probability of failure P_f around its mean value. Figure 6.35 also characterises the CDF of Normal and Lognormal distribution for the function of service life.

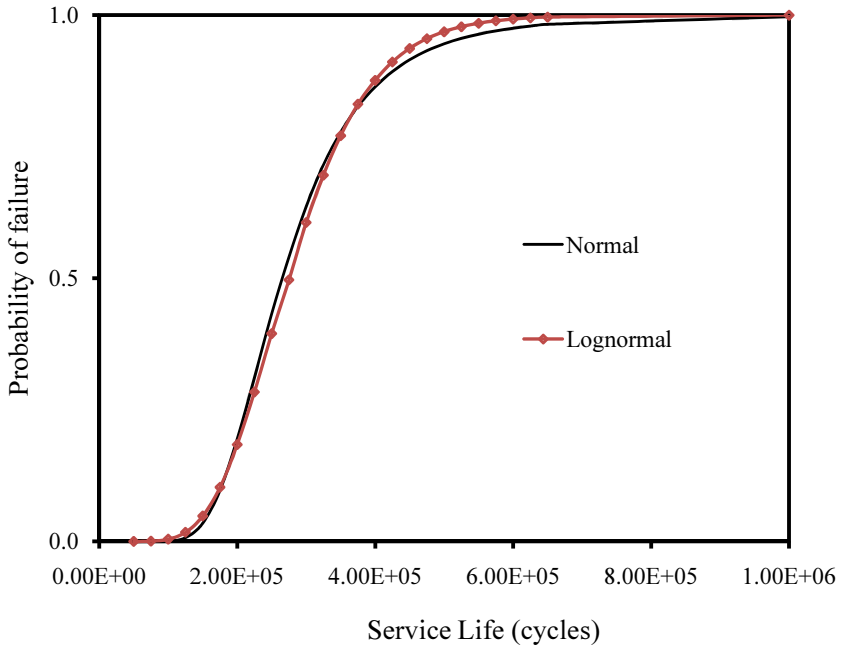

Figure 6.35: Comparison with different distribution

Throughout this work, only the Normal and Lognormal probability distributions have been used to characterize the random parameters. However, various probability distributions presented in Section (2.3) can be applied to evaluate the reliability in the illustrated examples.

6.6 Summary

A method consisting of the DBEM coupled with FORM was developed for determine the reliability of fatigue crack growth. The method involves a total derivatives method for calculating the fatigue parameter derivatives with respect to random parameters. The results obtained from the proposed method demonstrated good agreement with the Monte Carlo simulations, as DBEM provides very accurate calculation of the stress intensity factors and its derivatives which lead to a good accuracy for the reliability index. Since all gradients are calculated analytically, the reliability analysis of fatigue crack growth can be performed efficiently using the proposed method.

Chapter 7

Conclusions and future research

7.1 Introduction

This chapter describes the work of this thesis and recommendations for future research. These conclusions and recommendations are based on the results obtained in the previous chapters, by which the main objectives outlined in Chapter 1 are achieved.

7.2 Summary and Conclusions

The main objective of this thesis was the development of numerical tools based on the dual boundary element method for the probabilistic analysis in fracture mechanics. A summary of the work carried out to reach the objectives is listed below.

In Chapter 4, the first and second order derivatives formulations were successfully implemented to analyse 2-D elastostatics problems. The derivative boundary integral equations were formulated to compute the derivatives of boundary response. The results obtained in Section 4.5.1 showed the accuracy of the proposed

formulation compared with analytical methods. With the successful evaluation of design sensitivities, the first order reliability method was then implemented for probabilistic analysis. The results were compared with Monte Carlo simulations also developed in the Chapter.

In Chapter 5, the derivatives of dual boundary element equations were formulated to compute the derivatives of boundary response for the LEFM problems. Fracture parameters and their derivatives with respect to random parameters were evaluated with the *J-integral* and its derivatives. A convergence study was carried out to access the accuracy of the derivatives of fracture parameter with respect to crack size for different types of boundary meshes. The results obtained in Subsections 5.5.1 to 5.5.3 demonstrated that the derivatives of stress-intensity factors with respect to crack size calculated using the sensitivity BEM for the crack geometry agree favorably with reference solutions obtained either analytically (mode I) or using finite-difference (mixed mode) method. Probabilistic analysis for the simple example in Subsection 5.5.4 shows excellent agreements with available references and the Monte Carlo simulation results.

In Chapter 6, the DBEM is extended to fatigue crack growth problems. A new model was developed to map the random fatigue crack growth to a local coordinate system using linear interpolation functions. The total derivative method was used to obtain the derivative of fatigue life with respect to random parameters. The numerical examples presented in Subsections 6.5.1 and 6.5.2 demonstrated the accuracy of the proposed method where the randomness in initial and final crack size; material property and loading were considered.

Based on the results from each chapter, and particularly from comparisons with equivalent Monte Carlo Simulations, the main conclusions from the present work are listed below:

- Stochastic boundary-value problems can be formulated in terms of stochastic boundary integral equations.

- The boundary mesh size play a significant role in the derivatives BEM formulation because stochastic character of the boundary element values are highly dependent on the chosen mesh geometry.

- The randomness of the boundary and its effect on the stresses, strains and displacements can be treated efficiently by implicit differentiation of the boundary and dual boundary element equations. The results obtained agree well with the analytical solutions , with a maximum difference of 0.027% for the first order derivatives; and with a maximum difference of 1.36% for the second order derivatives.

- The first-order derivatives of stress-intensity factors with respect to random crack size can be calculated by path-independent integrals along fixed contours, far from singularities. The result calculated using the proposed method agrees well with either the analytical solutions (mode I) or the finite-difference method (mixed mode). The maximum difference between the proposed method and the analytical solutions for mode I is less than 2%. The maximum difference between the proposed method and finite-difference method for mixed mode is less than 3.15%

- The derivative of fatigue life with respect to random parameters can be evaluated by the total derivative method. The definition of random crack path and crack growth size is important for the evaluation of the derivative of fatigue life.

- DBEM can be an effective tool for the probabilistic analysis of 2-D fracture mechanics problems.

7.3 Future research

Applications of the boundary element method for the probabilistic analysis of fracture mechanics can be further extended in several areas:

1. To improve the accuracy of FORM calculations, the second order reliability method can be applied. The development of second order derivatives of fracture parameters (J integral) with respect to random parameters in DBEM will be needed. The main curvatures of the hyper-surface at the design point can be evaluated.

2. It is recognized that the randomness of crack size are restricted to the coordinates of the end points of the crack elements in this work. The sensitivity of stress intensity factor based on this assumption can be studied in more detail.

3. More study is needed for the unknown functional relationship between variables; the regression analysis technique can be used to develop a statistical relationship.

4. It is possible that the Rackwitz-Fiessler algorithm may not converge to the most probable point of failure in some cases. It may converge very slowly, or oscillate about the solution without convergence, or diverge away from the solution. Other optimization algorithms such as Sequential quadratic programming or the BFGS (Broyden-Fletcher-Goldfarb-Shanno) method may be used in that case.

5. The curvature of the nonlinear limit state is ignored in the FORM used in present work, which uses only a first-order approximation at the minimum distance point. The curvature of any equation is related to the second-

order derivatives with respect to the basic variables. Thus, the second order reliability method (SORM) is needed to improve the evaluation of probability of failure domain.

6. Development of the probabilistic analysis method coupled with the derivatives dual boundary element formulations for three dimensional problems.

7. The development of probabilistic analysis with DBEM in the study of anisotropic composite laminates with crack problem.

Bibliography

[1] M. Abramowitz and I.A. Stegun. *Handbook of mathematical functions with formulas, graphs, and mathematical tables.* Dover publications, 1964.

[2] M.H. Aliabadi. Evaluation of mixed mode stress intensity factors using path independent integral. *Proceedings of 12th Int. Conf. on Boundary Element Methods*, pages 281–292, 1990.

[3] M.H. Aliabadi. Boundary element formulations in fracture mechanics. *Applied Mechanics Reviews*, 50:83, 1997.

[4] M.H. Aliabadi. A new generation of boundary element methods in fracture mechanics. *International Journal of Fracture*, 86(1):91–125, 1997.

[5] M.H. Aliabadi. *The boundary element method, applications in solids and structures*, volume 2. John Wiley & Sons Inc, 2002.

[6] M.H. Aliabadi and D.P. Rooke. *Numerical fracture mechanics.* Kluwer Academic Pub, 1991.

[7] T.L. Anderson. *Fracture mechanics: fundamentals and applications.* CRC press, 2005.

[8] A.H.S. Ang and W.H. Tang. *Probability Concepts in Engineering Planning and Design, Volume I: Basic Principles.* John Wiley & Sons, 1975.

[9] A.H.S. Ang and W.H. Tang. *Probability concepts in engineering planning and design, vol. 2: Decision, risk, and reliability.* 1984.

[10] G. Augusti, A. Baratta, and F. Casciati. *Probabilistic methods in structural engineering.* Routledge, 1984.

[11] AP Basu. Estimates of reliability for some distributions useful in life testing. *Technometrics*, 6(2):215–219, 1964.

[12] A.A. Becker. *The boundary element method in engineering: a complete course.* McGraw-Hill London, 1992.

[13] A.A. Becker and R.T. Fenner. Axisymmetric fracture mechanics analysis by the boundary integral equation method. *Int. J. Pressure Vessels Piping*, 18(1):55–75, 1985.

[14] G.H. Besterfield, W.K. Liu, M.A. Lawrence, and T.B. Belytschko. Brittle fracture reliability by probabilistic finite elements. *Journal of Engineering Mechanics*, 116(3):642–659, 1990.

[15] G.H. Besterfield, W.K. Liu, M.A. Lawrence, and T. Belytschko. Fatigue crack growth reliability by probabilistic finite elements. *Computer methods in applied mechanics and engineering*, 86(3):297–320, 1991.

[16] E. Betti. Teoria della elasticita¡¯. *Il Nuovo Cimento (1869-1876)*, 7(1): 69–97, 1872.

[17] G.E. Blandford, A.R. Ingraffea, and J.A. Liggett. Two-dimensional stress intensity factor computations using the boundary element method. *International Journal for Numerical Methods in Engineering*, 17(2):387–404, 1981.

[18] J.M. Bloom and J.C. Ekvall. Probabilistic fracture mechanics and fatigue methods: applications for structural design and maintenance. *St. Louis*, page 1983, 1981.

[19] C.A. Brebbia. The Boundary Element for Engineers. *UK Pentech, London*, 1978.

[20] C.A. Brebbia and J. Dominguez. Boundary Elements An Introductory Course. 1992. *Comp. Mech. Pub. McGraw-Hill Book Company.*

[21] D. Broek. *Elementary engineering fracture mechanics.* Kluwer Academic Pub, 1986.

[22] T. Burczynski. The boundary element method for stochastic potential problems. *Applied Mathematical Modelling*, 9:189–194, 1985.

[23] T. burczynski. Applications of BEM in sensitivity analysis and optimization. *Computational Mechanics*, 13(1):29–44, 1993.

[24] T. Burczynski and A. John. Stochastic dynamic analysis of elastic and viscoelastic systems by means of the boundary element method. *Boundary Elements VII*, pages 53–6.

[25] T. Burczynski and J. Skrzypczyk. Theoretical and computational aspects of the stochastic boundary element method. *Computer Methods in Applied Mechanics and Engineering*, 168(1-4):321–344, 1999.

[26] T. Burczynski, JH Kane, and C. Balakrisna. Shape design sensitivity analysis via material derivative-adjoint variable technique for 3-D and 2-D curved boundary elements. *International journal for numerical methods in engineering*, 38(17):2839–2866, 1995.

[27] N.P. Buslenko and J.A. Šrejder. *The Monte Carlo Method*. Pergamon Oxford, London, Edinburg, 1966.

[28] G. Chen, S. Rahman, and Y.H. Park. Shape sensitivity and reliability analyses of linear-elastic cracked structures. *International Journal of Fracture*, 112(3):223–246, 2001.

[29] A.H.D. Cheng and O.E. Lafe. Boundary element solution for stochastic groundwater flow: Random boundary condition and recharge. *Water Resources Research*, 27(2):231–242, 1991.

[30] KK Choi and EJ Haug. Shape design sensitivity analysis of elastic structures. *Journal of Structural Mechanics*, 11(2):231–269, 1983.

[31] C.A. Cornell. Bounds on the reliability of structural systems. *Journal of Structural Division, ASCE*, 93(1):171–200, 1967.

[32] C. Croarkin and P. Tobias. *Engineering statistics handbook*. NIST iTL, 2002.

[33] T.A. Cruse. Numerical solutions in three dimensional elastostatics. *International Journal of Solids and Structures*, 5:1259–1274, 1969.

[34] T.A. Cruse. Numerical evaluation of elastic stress intensity factors by the boundary-integral equation method. In *The surface crack: physical problems and computational solutions*, pages 153–170, 1972.

[35] T.A. Cruse and W. Vanburen. Three-dimensional elastic stress analysis of a fracture specimen with an edge crack. *International Journal of Fracture*, 7(1):1–15, 1971.

[36] A. Der Kiureghian and J.B. Ke. The stochastic finite element method in structural reliability. *Probabilistic Engineering Mechanics*, 3(2):83–91, 1988.

[37] J. Drewniak. Research communication: boundary elements for random heat conduction problems. *Engineering analysis*, 2(3):168–170, 1985.

[38] K. El Harrouni, D. Ouazar, L.C. Wrobel, and A.H.D. Cheng. Uncertainty analysis of groundwater flow with DRBEM. *Engineering analysis with boundary elements*, 19(3):217–221, 1997.

[39] F. Erdogan and G.C. Sih. On the crack extension in plates under plane loading and plane shear. *Journal of Basic Engineering*, 85, 1963.

[40] M. Ettouney, H. Benaroya, and J. Wright. Boundary element methods in probabilistic structural analysis (pbem). *Applied Mathematical Modelling*, 13(7):432 – 441, 1989.

[41] M. Evans, N. Hastings, and B. Peacock. *Statistical distributions*. John Wiley & Sons Inc, 1993.

[42] R.T. Fenner. *Engineering elasticity: application of numerical and analytical techniques*. Ellis Horwood Chichester, UK, 1986.

[43] A.M. Freudenthal. Safety and the probability of structural failure. *Transaction, ASCE*, 121:1337–1397, 1956.

[44] A.M. Freudenthal, J.M. Garrelts, and M. Shinozuka. The analysis of structural safety. *Journal of the structural Division, ASCE*, 92:267–325, 1966.

[45] A.A. Griffith. The phenomena of rupture and flowing solids. *Phil. Trans. R. Soc. A*, 221:163–198, 1920.

[46] M. Grigoriu, MTA Saif, S. El Borgi, and AR Ingraffea. Mixed mode fracture initiation and trajectory prediction under random stresses. *International Journal of Fracture*, 45(1):19–34, 1990.

[47] E.J. Gumbel. *Statistical theory of extreme values and some practical applications: a series of lectures*. US Govt. Print. Office, 1954.

[48] E.J. Gumbel. Statistics of Extremes. *Columbia University Press, NewYork*, 375, 1958.

[49] R.T. Haftka and H.M. Adelman. Recent developments in structural sensitivity analysis. *Structural and Multidisciplinary Optimization*, 1(3):137–151, 1989.

[50] A. Haldar and S. Mahadevan. *Probability, reliability and statistical methods in engineering design*. Wiley New York, 2000.

[51] H.H. Harkness, T. Belytschko, and W.K. Liu. Finite element reliability analysis of fatigue life. *Nuclear engineering and design*, 133(2):209–224, 1992.

[52] R.J. Hartranft and G.C. Sih. An approximate three-dimensional theory of plates with application to crack problems* 1. *International Journal of Engineering Science*, 8(8):711–729, 1970.

[53] A.M. Hasofer and N.C. Lind. Exact and invariant second-moment code format. *Journal of the Engineering Mechanics Division*, 100(1):111–121, 1974.

[54] R. Honda. Stochastic BEM with spectral approach in elastostatic and elastodynamic problems with geometrical uncertainty. *Engineering Analysis with Boundary Elements*, 29(5):415–427, 2005.

[55] G.R. Irwin. Onset of fast crack propagation in high strength steel and aluminum alloys. In *Sagamore research conference proceedings*, volume 2, pages 289–305, 1956.

[56] G.R. Irwin. Analysis of stresses and strains near the end of a crack traversing a plate, 1957.

[57] M.A. Jaswon. Integral equation methods in potential theory. I. *Proceedings of the Royal Society of London. Series A, Mathematical and Physical Sciences*, 275(1360):23–32, 1963.

[58] I. Kaljevic and S. Saigal. Stochastic boundary elements in elastostatics. *Computer methods in applied mechanics and engineering*, 109(3-4):259–280, 1993.

[59] I. Kaljević and S. Saigal. Stochastic boundary elements for two-dimensional potential flow in non-homogeneous media. *Computer Methods in Applied Mechanics and Engineering*, 121(1-4):211–230, 1995.

[60] G. Karami and RT Fenner. Analysis of mixed mode fracture and crack closure using the boundary integral equation method. *International Journal of Fracture*, 30(1):13–29, 1986.

[61] K. Kishitani, T. Hirai, and K. Murakami. J-integral calculations with boundary elements. pages 481–493, 1983.

[62] F. Kozin and JL Bogdanoff. A critical analysis of some probabilistic models of fatigue crack growth. *Engineering Fracture Mechanics*, 14(1):59–89, 1981.

[63] JC Lachat and JO Watson. Effective numerical treatment of boundary integral equations: a formulation for three-dimensional elastostatics. *Inter-*

national Journal for Numerical Methods in Engineering, 10(5):991–1005, 1976.

[64] A.G. Laurent. Conditional distribution of order statistics and distribution of the reduced ith order statistic of the exponential model. *The Annals of Mathematical Statistics*, 34(2):652–657, 1963.

[65] J. Lieblein and M. Zelen. Statistical investigation of the fatigue life of deep-groove ball bearings. *Journal of Research of the National Bureau of Standards*, 57(5):273–316, 1956.

[66] S.C. Lin and J.F. Abel. Variational approach for a new direct-integration form of the virtual crack extension method. *International Journal of Fracture*, 38(3):217–235, 1988.

[67] N.C. Lind. The design of structural design norms. *Mechanics Based Design of Structures and Machines*, 1(3):357–370, 1972.

[68] W.K. Liu, Y. Chen, T. Belytschko, and Y.J. Lua. Three reliability methods for fatigue crack growth. *Engineering fracture mechanics*, 53(5):733–752, 1996.

[69] A. Longo, J. Unzueta, E. Schaeidt, A. Alvarez, and JJ Anza. A general related variational approach to shape optimum design. *Advances in engineering software(1992)*, 16(2):135–142, 1993.

[70] Y.J. Lua, W.K. Liu, and T. Belytschko. Curvilinear fatigue crack reliability analysis by stochastic boundary element method. *International Journal for Numerical Methods in Engineering*, 36(22), 1993.

[71] H.O. Madsen, S. Krenk, N.C. Lind, et al. *Methods of structural safety*. Prentice-Hall Englewood Cliffs, NJ, 1986.

[72] R.E. Melchers. Search-based importance sampling. *Structural Safety*, 9(2): 117–128, 1990.

[73] R.E. Melchers. Structural reliability analysis and prediction. 1999.

[74] S.C. Mellings. *Flaw Identification Using the Inverse Dual Boundary Element Method*. PhD thesis, Wessex Institute of Technology– Universidade of Portsmouth, 1994.

[75] S.C. Mellings and M.H. Aliabadi. Flaw identification using the boundary element method. *International Journal for Numerical Methods in Engineering*, 38(3), 1995.

[76] N. Metropolis and S. Ulam. The monte carlo method. *Journal of the American Statistical Association*, 44(247):335–341, 1949.

[77] Y. Mi and M.H. Aliabadi. Three-dimensional crack growth simulation using BEM. *Computers & Structures*, 52(5):871–878, 1994.

[78] Y. Mi and M.H. Aliabadi. An automatic procedure for mixed-mode crack growth analysis. *Communications in Numerical Methods in Engineering*, 11(2), 1995.

[79] H.R. Millwater. Probabilistic fracture mechanics analysis using the boundary element method. *Uncertainty Modeling and Analysis, 1990. Proceedings., First International Symposium on*, 1990.

[80] A. Moghaddasi-Tafreshi and R.T. Fenner. Design optimization using the boundary element method. *The Journal of Strain Analysis for Engineering Design*, 26(4):231–241, 1991.

[81] K. Ortiz and A.S. Kiremidjian. Stochastic modeling of fatigue crack growth. *Engineering Fracture Mechanics*, 29(3):317–334, 1988.

[82] A. Papoulis, S.U. Pillai, Papoulis A, and Pillai SU. *Probability, random variables, and stochastic processes*. McGraw-Hill New York, 1965.

[83] PC Paris and F. Erdogan. A critical analysis of crack propagation. *J. Bas. Engng*, 85:528–534, 1963.

[84] XQ Peng, L. Geng, W. Liyan, GR Liu, and KY Lam. A stochastic finite element method for fatigue reliability analysis of gear teeth subjected to bending. *Computational Mechanics*, 21(3):253–261, 1998.

[85] R.P. Perry. The cellular sites of synthesis of ribosomal and 4S RNA. *Proceedings of the National Academy of Sciences of the United States of America*, 48(12):2179–2186, 1962.

[86] A. Portela, M.H. Aliabadi, and D.P. Rooke. The dual boundary element method: effective implementation for crack problems. *International Journal for Numerical Methods in Engineering*, 33(6), 1992.

[87] A. Portela, MH Aliabadi, and DP Rooke. Dual boundary element incremental analysis of crack propagation. *Computers and Structures*, 46(2): 237–247, 1993.

[88] HJ Pradlwarter. A selective MC simulation technique for nonlinear structural reliability assessment. 1992.

[89] W.H. Press, S.A. Teukolsky, W.T. Vetterling, and B.P. Flannery. *Numerical recipes in FORTRAN: the art of scientific computing*. Cambridge Univ Pr, 1992.

[90] J.W. Provan. Probabilistic fracture mechanics and reliability. *Martinus Nijhoff Publishers, P. O. Box 163, 3300 AD Dordrecht, The Netherlands, 1987. 467*, 1987.

[91] R. Rackwitz and B. Fiessler. Structural reliability under combined random load sequences. *Computers and structures*, 9(5):489–494, 1978.

[92] BN Rao and S. Rahman. Probabilistic fracture mechanics by Galerkin meshless methods–part I: rates of stress intensity factors. *Computational Mechanics*, 28(5):351–364, 2002.

[93] J.R. Rice. A Path Independent Integral and the Approximate Analysis of Strain Concentration by Notches and Cracks. *Journal of Applied Mechanics*, 35:379–386, 1968.

[94] F.J. Rizzo. An integral equation approach to boundary value problems of classical elastostatics. *Q. appl. Math*, 25:83–95, 1967.

[95] M. Rosenblatt. Remarks on a multivariate transformation. *The Annals of Mathematical Statistics*, pages 470–472, 1952.

[96] R.V. Roy and S.T. Grilli. Probabilistic analysis of flow in random porous media by stochastic boundary elements. *Engineering analysis with boundary elements*, 19(3):239–255, 1997.

[97] J.Z.M.G. Satish. A boundary element method for stochastic flow problems in a semiconfined aquifer with random boundary conditions. *Engineering analysis with boundary elements*, 19(3), 1997.

[98] G. Schall, R. Rackwitz, M. Scharrer, and C. Ostergaard. Fatigue reliability investigation for marine structures using a response surface method. *Offshore Mechanics and Arctic Engineering–1991.*, 2:247–254, 1991.

[99] G.K. Sfantos and M.H. Aliabadi. A boundary element sensitivity formulation for contact problems using the implicit differentiation method. *Engineering Analysis with Boundary Elements*, 30(1):22 – 30, 2006.

[100] M.L. Shooman. *Probabilistic reliability: an engineering approach.* RE Krieger Pub. Co, 1990.

[101] K. Sobczyk. Modelling of random fatigue crack growth. *Engineering Fracture Mechanics*, 24(4):609–623, 1986.

[102] I.M. Sobol. *A primer for the Monte Carlo method.* CRC, 1994.

[103] C. Somigliana. Sopra l'equilibrio di un corpo elastico isotropo. *Il Nuovo Cimento (1877-1894)*, 17(1):140–148, 1885.

[104] G.T. Symm. Integral equation methods in potential theory. II. *Proceedings of the Royal Society of London. Series A, Mathematical and Physical Sciences*, 275(1360):33–46, 1963.

[105] H. Tada, P.C. Paris, and G.R. Irwin. The stress analysis of cracks handbook. *American Society of Mechanical Engineers, 3 Park Avenue, New York, NY 10016-5990, USA, 2000.*, pages 1–677, 2000.

[106] C.L. Tan and R.T. Fenner. Elastic fracture mechanics analysis by the boundary integral equation method. *Proceedings of the Royal Society of London. Series A, Mathematical and Physical Sciences*, 369(1737):243–260, 1979.

[107] K. Tanaka. Fatigue-Crack Propagation From a Crack Inclined to the Cyclic Tensile Axis. *Engineering Fracture Mechanics*, 6(3):493–507, 1974.

[108] RF Tate. Unbiased estimation: functions of location and scale parameters. *The Annals of Mathematical Statistics*, 30(2):341–366, 1959.

[109] S.P. Timoshenko and J.N. Goodier. *Theory of elasticity*. New York: McGraw Hill;, 1970.

[110] DA Tortorelli and P. Michaleris. Design sensitivity analysis: overview and review. *Inverse Problems in Science and Engineering*, 1(1):71–105, 1994.

[111] W. Weibull. A statistical representation of fatigue failures in solids. 1949.

[112] W. Weibull. A statistical distribution function of wide applicability. *Journal of applied mechanics*, 18(3):293–297, 1951.

[113] L.C. Wrobel. *The Boundary Element Method: Applications in Thermo-Fluids and Acoustics*, volume 1. John Wiley & Sons Inc, 2002.

[114] Y.T. Wu. Computational methods for efficient structural reliability and reliability sensitivity analysis. *AIAA journal*, 32(8):1717–1723, 1994.

[115] Y.T. Wu and P.H. Wirsching. Advanced reliability method for fatigue analysis. *Journal of Engineering Mechanics*, 110(4):536–553, 1984.

[116] Q. Zhang and S. Mukherjee. Second-order design sensitivity analysis for linear elastic problems by the derivative boundary element method. *Comp. Methods Appl. Mech. Eng.*, 86(3):321–335, 1991.

[117] W.Q. Zhu, Y.K. Lin, and Y. Lei. On fatigue crack growth under random loading. *Engineering Fracture Mechanics*, 43(1):1–12, 1992.

Appendix A

Table of the CDF of the standard normal distribution

$$\Phi(Z) = \frac{1}{\sqrt{2\pi}} \int_{-\infty}^{Z} e^{-(s^2/2)} ds \tag{A.1}$$

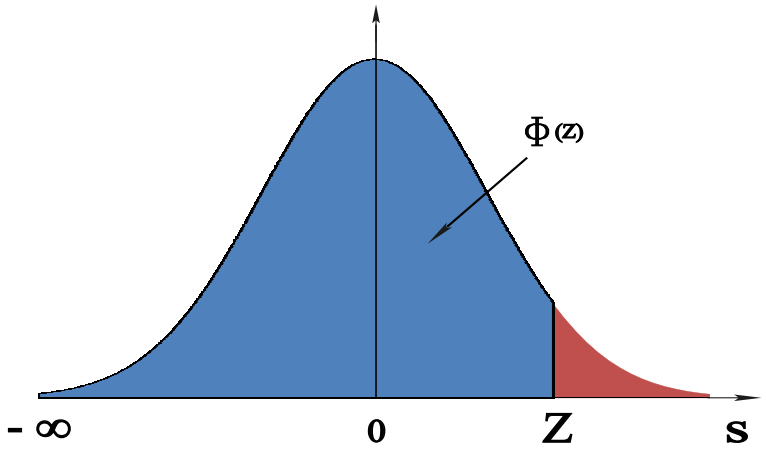

Figure A.1: Standard normal distribution

Z	φ(z)	Z	φ(z)	Z	φ(z)	Z	φ(z)
0	5.0000E-01	0.51	6.9497E-01	1.02	8.4614E-01	1.53	9.3699E-01
0.01	5.0399E-01	0.52	6.9847E-01	1.03	8.4849E-01	1.54	9.3822E-01
0.02	5.0798E-01	0.53	7.0194E-01	1.04	8.5083E-01	1.55	9.3943E-01
0.03	5.1197E-01	0.54	7.0540E-01	1.05	8.5314E-01	1.56	9.4062E-01
0.04	5.1595E-01	0.55	7.0884E-01	1.06	8.5543E-01	1.57	9.4179E-01
0.05	5.1994E-01	0.56	7.1226E-01	1.07	8.5769E-01	1.58	9.4295E-01
0.06	5.2392E-01	0.57	7.1566E-01	1.08	8.5993E-01	1.59	9.4408E-01
0.07	5.2790E-01	0.58	7.1904E-01	1.09	8.6214E-01	1.6	9.4520E-01
0.08	5.3188E-01	0.59	7.2240E-01	1.1	8.6433E-01	1.61	9.4630E-01
0.09	5.3586E-01	0.6	7.2575E-01	1.11	8.6650E-01	1.62	9.4738E-01
0.1	5.3983E-01	0.61	7.2907E-01	1.12	8.6864E-01	1.63	9.4845E-01
0.11	5.4380E-01	0.62	7.3237E-01	1.13	8.7076E-01	1.64	9.4950E-01
0.12	5.4776E-01	0.63	7.3565E-01	1.14	8.7286E-01	1.65	9.5053E-01
0.13	5.5172E-01	0.64	7.3891E-01	1.15	8.7493E-01	1.66	9.5154E-01
0.14	5.5567E-01	0.65	7.4215E-01	1.16	8.7698E-01	1.67	9.5254E-01
0.15	5.5962E-01	0.66	7.4537E-01	1.17	8.7900E-01	1.68	9.5352E-01
0.16	5.6356E-01	0.67	7.4857E-01	1.18	8.8100E-01	1.69	9.5449E-01
0.17	5.6749E-01	0.68	7.5175E-01	1.19	8.8298E-01	1.7	9.5543E-01
0.18	5.7142E-01	0.69	7.5490E-01	1.2	8.8493E-01	1.71	9.5637E-01
0.19	5.7535E-01	0.7	7.5804E-01	1.21	8.8686E-01	1.72	9.5728E-01
0.2	5.7926E-01	0.71	7.6115E-01	1.22	8.8877E-01	1.73	9.5818E-01
0.21	5.8317E-01	0.72	7.6424E-01	1.23	8.9065E-01	1.74	9.5907E-01
0.22	5.8706E-01	0.73	7.6730E-01	1.24	8.9251E-01	1.75	9.5994E-01
0.23	5.9095E-01	0.74	7.7035E-01	1.25	8.9435E-01	1.76	9.6080E-01
0.24	5.9483E-01	0.75	7.7337E-01	1.26	8.9617E-01	1.77	9.6164E-01
0.25	5.9871E-01	0.76	7.7637E-01	1.27	8.9796E-01	1.78	9.6246E-01
0.26	6.0257E-01	0.77	7.7935E-01	1.28	8.9973E-01	1.79	9.6327E-01
0.27	6.0642E-01	0.78	7.8230E-01	1.29	9.0147E-01	1.8	9.6407E-01
0.28	6.1026E-01	0.79	7.8524E-01	1.3	9.0320E-01	1.81	9.6485E-01
0.29	6.1409E-01	0.8	7.8814E-01	1.31	9.0490E-01	1.82	9.6562E-01
0.3	6.1791E-01	0.81	7.9103E-01	1.32	9.0658E-01	1.83	9.6638E-01
0.31	6.2172E-01	0.82	7.9389E-01	1.33	9.0824E-01	1.84	9.6712E-01
0.32	6.2552E-01	0.83	7.9673E-01	1.34	9.0988E-01	1.85	9.6784E-01
0.33	6.2930E-01	0.84	7.9955E-01	1.35	9.1149E-01	1.86	9.6856E-01
0.34	6.3307E-01	0.85	8.0234E-01	1.36	9.1309E-01	1.87	9.6926E-01
0.35	6.3683E-01	0.86	8.0511E-01	1.37	9.1466E-01	1.88	9.6995E-01
0.36	6.4058E-01	0.87	8.0785E-01	1.38	9.1621E-01	1.89	9.7062E-01
0.37	6.4431E-01	0.88	8.1057E-01	1.39	9.1774E-01	1.9	9.7128E-01
0.38	6.4803E-01	0.89	8.1327E-01	1.4	9.1924E-01	1.91	9.7193E-01
0.39	6.5173E-01	0.9	8.1594E-01	1.41	9.2073E-01	1.92	9.7257E-01
0.4	6.5542E-01	0.91	8.1859E-01	1.42	9.2220E-01	1.93	9.7320E-01
0.41	6.5910E-01	0.92	8.2121E-01	1.43	9.2364E-01	1.94	9.7381E-01
0.42	6.6276E-01	0.93	8.2381E-01	1.44	9.2507E-01	1.95	9.7441E-01
0.43	6.6640E-01	0.94	8.2639E-01	1.45	9.2647E-01	1.96	9.7500E-01
0.44	6.7003E-01	0.95	8.2894E-01	1.46	9.2785E-01	1.97	9.7558E-01
0.45	6.7364E-01	0.96	8.3147E-01	1.47	9.2922E-01	1.98	9.7615E-01
0.46	6.7724E-01	0.97	8.3398E-01	1.48	9.3056E-01	1.99	9.7670E-01
0.47	6.8082E-01	0.98	8.3646E-01	1.49	9.3189E-01	2	9.7725E-01
0.48	6.8439E-01	0.99	8.3891E-01	1.5	9.3319E-01	2.01	9.7778E-01
0.49	6.8793E-01	1	8.4134E-01	1.51	9.3448E-01	2.02	9.7831E-01
0.5	6.9146E-01	1.01	8.4375E-01	1.52	9.3574E-01	2.03	9.7882E-01

Z	φ(z)	Z	φ(z)	Z	φ(z)	Z	φ(z)
2.04	9.7932E-01	2.55	9.9461E-01	3.06	9.9889E-01	3.57	9.99822E-01
2.05	9.7982E-01	2.56	9.9477E-01	3.07	9.9893E-01	3.58	9.99828E-01
2.06	9.8030E-01	2.57	9.9492E-01	3.08	9.9896E-01	3.59	9.99835E-01
2.07	9.8077E-01	2.58	9.9506E-01	3.09	9.9900E-01	3.6	9.99841E-01
2.08	9.8124E-01	2.59	9.9520E-01	3.1	9.9903E-01	3.61	9.99847E-01
2.09	9.8169E-01	2.6	9.9534E-01	3.11	9.9906E-01	3.62	9.99853E-01
2.1	9.8214E-01	2.61	9.9547E-01	3.12	9.9910E-01	3.63	9.99858E-01
2.11	9.8257E-01	2.62	9.9560E-01	3.13	9.9913E-01	3.64	9.99864E-01
2.12	9.8300E-01	2.63	9.9573E-01	3.14	9.9916E-01	3.65	9.99869E-01
2.13	9.8341E-01	2.64	9.9585E-01	3.15	9.9918E-01	3.66	9.99874E-01
2.14	9.8382E-01	2.65	9.9598E-01	3.16	9.9921E-01	3.67	9.99879E-01
2.15	9.8422E-01	2.66	9.9609E-01	3.17	9.9924E-01	3.68	9.99883E-01
2.16	9.8461E-01	2.67	9.9621E-01	3.18	9.9926E-01	3.69	9.99888E-01
2.17	9.8500E-01	2.68	9.9632E-01	3.19	9.9929E-01	3.7	9.99892E-01
2.18	9.8537E-01	2.69	9.9643E-01	3.2	9.9931E-01	3.71	9.99896E-01
2.19	9.8574E-01	2.7	9.9653E-01	3.21	9.9934E-01	3.72	9.99900E-01
2.2	9.8610E-01	2.71	9.9664E-01	3.22	9.9936E-01	3.73	9.99904E-01
2.21	9.8645E-01	2.72	9.9674E-01	3.23	9.9938E-01	3.74	9.99908E-01
2.22	9.8679E-01	2.73	9.9683E-01	3.24	9.9940E-01	3.75	9.99912E-01
2.23	9.8713E-01	2.74	9.9693E-01	3.25	9.9942E-01	3.76	9.99915E-01
2.24	9.8745E-01	2.75	9.9702E-01	3.26	9.9944E-01	3.77	9.99918E-01
2.25	9.8778E-01	2.76	9.9711E-01	3.27	9.9946E-01	3.78	9.99922E-01
2.26	9.8809E-01	2.77	9.9720E-01	3.28	9.9948E-01	3.79	9.99925E-01
2.27	9.8840E-01	2.78	9.9728E-01	3.29	9.9950E-01	3.8	9.99928E-01
2.28	9.8870E-01	2.79	9.9736E-01	3.3	9.9952E-01	3.81	9.99931E-01
2.29	9.8899E-01	2.8	9.9744E-01	3.31	9.9953E-01	3.82	9.99933E-01
2.3	9.8928E-01	2.81	9.9752E-01	3.32	9.9955E-01	3.83	9.99936E-01
2.31	9.8956E-01	2.82	9.9760E-01	3.33	9.9957E-01	3.84	9.99938E-01
2.32	9.8983E-01	2.83	9.9767E-01	3.34	9.9958E-01	3.85	9.99941E-01
2.33	9.9010E-01	2.84	9.9774E-01	3.35	9.9960E-01	3.86	9.99943E-01
2.34	9.9036E-01	2.85	9.9781E-01	3.36	9.9961E-01	3.87	9.99946E-01
2.35	9.9061E-01	2.86	9.9788E-01	3.37	9.9962E-01	3.88	9.99948E-01
2.36	9.9086E-01	2.87	9.9795E-01	3.38	9.9964E-01	3.89	9.99950E-01
2.37	9.9111E-01	2.88	9.9801E-01	3.39	9.9965E-01	3.9	9.99952E-01
2.38	9.9134E-01	2.89	9.9807E-01	3.4	9.9966E-01	3.95	9.99961E-01
2.39	9.9158E-01	2.9	9.9813E-01	3.41	9.9968E-01	4	9.99968E-01
2.4	9.9180E-01	2.91	9.9819E-01	3.42	9.9969E-01	4.05	9.99974E-01
2.41	9.9202E-01	2.92	9.9825E-01	3.43	9.9970E-01	4.1	9.99979E-01
2.42	9.9224E-01	2.93	9.9831E-01	3.44	9.9971E-01	4.15	9.99983E-01
2.43	9.9245E-01	2.94	9.9836E-01	3.45	9.9972E-01	4.2	9.99987E-01
2.44	9.9266E-01	2.95	9.9841E-01	3.46	9.9973E-01	4.25	9.99989E-01
2.45	9.9286E-01	2.96	9.9846E-01	3.47	9.9974E-01	4.3	9.99991E-01
2.46	9.9305E-01	2.97	9.9851E-01	3.48	9.9975E-01	4.35	9.99993E-01
2.47	9.9324E-01	2.98	9.9856E-01	3.49	9.9976E-01	4.4	9.99995E-01
2.48	9.9343E-01	2.99	9.9861E-01	3.5	9.9977E-01	4.45	9.99996E-01
2.49	9.9361E-01	3	9.9865E-01	3.51	9.9978E-01	4.5	9.99997E-01
2.5	9.9379E-01	3.01	9.9869E-01	3.52	9.9978E-01	4.55	9.99997E-01
2.51	9.9396E-01	3.02	9.9874E-01	3.53	9.9979E-01	4.6	9.99998E-01
2.52	9.9413E-01	3.03	9.9878E-01	3.54	9.9980E-01	4.65	9.99998E-01
2.53	9.9430E-01	3.04	9.9882E-01	3.55	9.9981E-01	4.7	9.99999E-01
2.54	9.9446E-01	3.05	9.9886E-01	3.56	9.9981E-01	4.75	9.99999E-01

Appendix B

Rosenblatt Transformation

The advanced feature of FORM is a technique for transforming the original, non-Gaussian, dependent random variables into a set of independent, standardized Gaussian random variables. This feature is based on the general transformation method developed by *Rosenblatt [95]*. In the interests of completeness, the following discussion outlines the fundamental approach of the transformation method.

Consider a vector of dependent random variables, denoted $\mathbf{X} = \{X_1, X_2, \ldots, X_n\}$ may be transformed to the independent uniformly distributed random vector $\mathbf{Z} = \{Z_1, Z_2, \ldots, Z_n\}$ through the *Rosenblatt [95]* transformation $\mathbf{Z} = \mathbf{TX}$ given by

$$\begin{aligned} Z_1 =& P(X_1 \leq x_1) = F_1(x_1) \\ Z_2 =& P(X_2 \leq x_2 \mid X_1 = x_1) = F_2(x_2 \mid x_1) \\ &\vdots \\ Z_n =& P(X_n \leq x_n \mid X_1 = x_1, \ldots, X_{n-1} = x_{n-1}) = F_n(x_n \mid x_1, \ldots, x_{n-1}) \end{aligned} \tag{B.1}$$

where $F_i()$ is shorthand for the conditional cumulative distribution function $F_{x_i|x_{i-1},\ldots,x_1}()$.

If the joint probability density function $f_{\mathbf{X}}()$ is known then $F_i()$ can be determined as follows. The conditional probability density function $f_i()$ is given by

$$f_i(x_i \mid x_1, \ldots, x_{n-1}) = \frac{f_{X_i}(x_1, \ldots, x_i)}{f_{X_{i-1}}(x_1, \ldots, x_{i-1})} \tag{B.2}$$

where $f_{X_i}(x_1, \ldots, x_i)$ is a marginal probability density function obtained from

$$f_{X_i}(x_1, \ldots, x_i) = \int_{-\infty}^{\infty} \ldots \int_{-\infty}^{\infty} f_{\mathbf{X}}(x_1, \ldots, x_n) dx_{i+1}, \ldots, dx_n \tag{B.3}$$

$F_i()$ is then obtained by integrating $f_i()$ given by equation (B.2) over x_i:

$$F_i(x_i \mid x_1, \ldots, x_{n-1}) = \frac{\int_{-\infty}^{\infty} f_{X_i}(x_1, \ldots, x_{i-1}, t) dt}{f_{X_{i-1}}(x_1, \ldots, x_{i-1})} \tag{B.4}$$

with all the conditional cumulative distribution functions $F_i()$ determined in this way, equation (B.5) may be inverted successively to obtain

$$\begin{aligned} x_1 &= F_1^{-1}(Z_1) \\ x_2 &= F_2^{-1}(Z_2 \mid x_1) \\ &\vdots \\ x_n &= F_n^{-1}(Z_n \mid x_1, \ldots, x_{n-1}) \end{aligned} \tag{B.5}$$

It follows immediately that equation (B.5) can be used to generate the random vector $\mathbf{X}$ with probability density function $f_{\mathbf{X}}()$ from $\mathbf{Z}$. A practical difficulty is that, unless $F_i()$ is simple in form, the inversion will need to be done numerically.

As noted by Rosenblatt [95], there are $n!$ possible ways in which expressions

(B.1) can be written, depending on the numbering adopted for the variables in $\mathbf{X}$. Equally, of course, there are $n!$ possible ways of conditioning the X_i in expression (B.1), as seen for the simple case $n = 2$ [95]:

$$F_{x_1,x_2}(x_1, x_2) = F_{x_1}(x_1) f_{x_2|x_1}(x_2 \mid x_1) = F_{x_2}(x_2) f_{x_1|x_2}(x_1 \mid x_2) \tag{B.6}$$

It is probably obvious that this freedom can lead to considerable differences in the difficulty of solving for $\mathbf{X}$, i.e. in solving equation (B.5).

Unfortunately, the above method is not always useful for practical problems since $F_{\mathbf{X}}()$, or the conditional probability density functions $f_i()$ which characterize the dependence structure of the problem, are not always known. A special case arises when the X_i are independent. All the conditional requirements in equation (B.5) then disappear and each transformation takes the form $x_i = F_i^{-1}(z_i)$ independent of all other $x_j (j \neq i)$.

The Rosenblatt transformation may be used to transform from one distribution to another by applying equation (B.1) twice, using $\mathbf{Z}$ as a transmitter, e.g.

$$\begin{aligned} F_1(\Psi_1) = Z_1 &= F_1(\Psi_1) \\ F_2(\Psi_2 \mid \Psi_1) = Z_2 &= F_2(\Psi_2 \mid \Psi_1) \\ &.etc. \end{aligned} \tag{B.7}$$

A particular case of interest is where $\mathbf{\Psi}$ in equation (B.6) is standard normal distributed, with $\mathbf{X}$, say, a vector of correlated random variables and $\mathbf{\Psi}$ uncorrelated. Then equation (B.5) may be written as

$$\begin{aligned} x_1 =& F_1^{-1}\left[\Phi(\Psi_1)\right] \\ x_2 =& F_2^{-1}\left[\Phi(\Psi_2) \mid x_1\right] \\ & .etc. \end{aligned} \tag{B.8}$$

In practice solution of equation (B.8) requires multiple integration. This technique is used to convert non-normal distributed random variables to equivalent normal random variables, where both $\mathbf{\Psi}$ and $\mathbf{X}$ are normal vectors, an easier approach to finding the transformation implied by equation (B.8) is to make direct use of the special properties of the Normal distribution.

Appendix C

Treatment of singularity

As it has been mentioned before, each singular integral is treated separately based on its order of singularity and location. On the boundary, near singular integrals (when the collocation node is close to the integration element) are treated with the element subdivision technique Aliabadi [5]. Weakly singular integrals $O(\ln \frac{1}{\eta})$ are treated using a special logarithmic Gaussian quadrature scheme. Strong singular integrals $O(1/\eta)$ on the main diagonal are computed indirectly by considering the generalized rigid body motion. Strong $O(1/\eta)$ singular and the hyper singular integrals $O(1/\eta^2)$ outside the main diagonal are evaluated using a singularity subtraction technique based on the Taylor series expansion around the singular point, as reported by Portela et al. [86].

C.1 Weakly singular integration

In the BE formulations for two-dimensional problems, some of the kernal functions contain a singular term of the form $\ln(\frac{1}{\eta})$ as η approaches zero. For such integrals,

there is a suitable logarithmic form of Gaussian quadrature as follows:

$$\int_0^1 f(\eta)\ln(\frac{1}{\eta})d\eta = \sum_{gl=1}^{G_t} f(\eta_{gl})w_{gl} \tag{C.1}$$

where G_t is the total number of logarithmic Gaussian integration points and η_{gl} and w_{gl} are the logarithmic Gaussian coordinates and weight functions, respectively. A simple linear transormation can be used to transform the integral variable from ξ to η as follow:

1. If the collocation point is the first node of the element, $\eta = 0.5(1+\xi)$.

2. If the collocation point is the second node of the element, the element is divided into two sub-elements: $\eta = -\xi$ (for $-1 < \xi < 0$) and $\eta = \xi$ (for $0 < \xi < 1$).

3. If the collocation point is the third node of the element, $\eta = 0.5(1-\xi)$.

C.2 Strong singular integration

Using a singularity subtraction technique based on a Taylor series expansion around the singular point [86] the strong singular integrals $O(1/\eta)$ can be regularized. Let's consider for example, the integral containing the $U^*_{\alpha\beta\gamma}$ kernel as follows:

$$\int_{\Gamma_e} T_{ij}(x', x)u_j^n(x)d\Gamma(\mathbf{x}) = u_j^n(x)\int_{-1}^{+1}\frac{f_{ij}^n(\xi)}{\xi - \xi'}d\xi \tag{C.2}$$

where $f_{ij}^n(\xi) = T_{ij}(x', x(\xi))M^n(\xi)J^\gamma(\xi)(\xi - \xi')$; Γ_e denotes the boundary of the singular element, M^n is the element shape function corresponding to the node n in the element under consideration and J is the Jacobian of the transformation

from x_i coordinate system to the local coordinate system ξ (i.e., $d\Gamma = J(\xi)d\xi$). Now the term $f_{ij}^n(\xi)$ is a regular function.

The integral in the right hand side of equation (C.2) can be regularized with the aid of a Taylor series expansion of the function $f_{ij}^n(\xi)$ about the singular point ξ' in the local coordinate system, as follows:

$$f_{ij}^n(\xi) = f_{ij}^n(\xi') + f_{ij}^{n\prime}(\xi')(\xi - \xi') + \frac{1}{2}f_{ij}^{n\prime\prime}(\xi')(\xi - \xi')^2 + ... \tag{C.3}$$

By subtracting the first term of the Taylor expansion of the function $f_{ij}^n(\xi)$ and then adding it again, equation (C.2) can be written as:

$$\int_{-1}^{+1} \frac{f_{ij}^n(\xi)}{\xi - \xi'} d\xi = \int_{-1}^{+1} \frac{f_{ij}^n(\xi) - f_{ij}^n(\xi')}{\xi - \xi'} d\xi + f_{ij}^n(\xi') \int_{-1}^{+1} \frac{d\xi}{\xi - \xi'} \tag{C.4}$$

The first integral in the right hand side is now regular and the second integral which is strongly singular can be integrated analytically to give:

$$\int_{-1}^{+1} \frac{d\xi}{\xi - \xi'} = \ln\left|\frac{1 - \xi'}{1 + \xi'}\right| \tag{C.5}$$

C.3 Hyper singular integration

Hypersingular integrals $O(1/\eta^2)$ can be treated in a similar way as strong singular integrals. In this case lets consider the integral containing the $S_{kij}^{(i)*}$ kernel as follows:

$$\int_{\Gamma_e} S_{kij}(\mathbf{x}', \mathbf{x}) u_j^n(\mathbf{x}) d\Gamma(\mathbf{x}) = u_j^n \int_{-1}^{+1} \frac{g_{kij}^n(\xi)}{(\xi - \xi')^2} d\xi \tag{C.6}$$

where $g_{kij}^n(\xi) = S_{kij}^{(i)*}(\xi', \xi) M^n(\xi) J(\xi)(\xi - \xi')^2$ is a regular function.

Now, the integral on the right hand side of equation (C.6) can be regularized with the aid of the first and second term of a Taylor series expansion of the function

$g^n_{kij}(\xi)$ about the singular point ξ' in the local coordinate system, as follows:

$$g^n_{kij}(\xi) = g^n_{kij}(\xi') + g^n_{kij}{}'(\xi')\,(\xi - \xi') + \frac{1}{2} g^n_{kij}{}''(\xi')\,(\xi - \xi')^2 + ... \tag{C.7}$$

By subtracting the first and the second terms of the Taylor expansion of the function $g^n_{kij}(\xi)$ and then adding it again, equation (C.6) can be written as:

$$\int_{-1}^{+1} \frac{g^n_{kij}(\xi)}{(\xi - \xi')^2} d\xi = \int_{-1}^{+1} \frac{g^n_{kij}(\xi) - g^n_{kij}(\xi') - g^n_{kij}{}'(\xi')\,(\xi - \xi')}{(\xi - \xi')^2} d\xi \tag{C.8}$$

$$g^n_{kij}(\xi') = \int_{-1}^{+1} \frac{d\xi}{(\xi - \xi')^2} + g^n_{kij}{}'(\xi') \int_{-1}^{+1} \frac{d\xi}{\xi - \xi'}$$

where $g^n_{kij}{}'$ denotes the first derivatives of g^n_{kij}.

At the collocation point the function g^n_{kij} is required to have continuity of its second derivatives. The requirement is automatically satisfied by the use of discontinuous elements, since the nodes are internal to the element. In equation (C.8) the first integral on the right hand side is now regular, and the third integral is identical with the one given in equation (C.4). The second integral on the right hand side is hyper singular and can be integrated analytically to give,

$$\int_{-1}^{+1} \frac{d\xi}{(\xi - \xi')^2} = -\frac{1}{(1 + \xi')} - \frac{1}{(1 - \xi')} \tag{C.9}$$